Metal-NHC complexes for anti-cancer applications : gold(I) for antimitochondrial activity and iridium(III) for photodynamic therapy

Chen Zhang

Université de Toulouse

THÈSE

En vue de l'obtention du

DOCTORAT DE L'UNIVERSITÉ DE TOULOUSE

Délivré par :
Université Toulouse III Paul Sabatier (UT3 Paul Sabatier)

Discipline ou spécialité :

Chimie Organométallique et de Coordination

Présentée et soutenue par :
Chen ZHANG

le : mercredi 26 septembre 2018

Titre :

Metal-NHC Complexes for Anti-Cancer Applications:
Gold(I) for Antimitochondrial Activity and Iridium(III) for Photodynamic Therapy

---

Ecole doctorale :
Sciences de la Matière (SDM)

Unité de recherche :
Laboratoire de Chimie de Coordination (UPR 8241)

Directeur(s) de Thèse :

M. Heinz GORNITZKA et Mme. Catherine HEMMERT

Rapporteurs :

M. Miguel A. SIERRA et M. Gilles GASSER

Membre(s) du jury :

M. Gilles GASSER	Professeur d'Université	Rapporteur
M. Miguel A. SIERRA	Professeur d'Université	Rapporteur
M. Heinz GORNITZKA	Professeur d'Université	Directeur de thèse
Mme. Maëlle CARRAZ	Chargée de Recherche	Examinatrice
Mme. Catherine HEMMERT	Chargée de Recherche	Membre invité
M. Olivier CUVILLIER	Directeur de Recherche	Membre invité

“The Chinese people are a great people; they are industrious and brave, and they never pause in pursuit of progress.”

“The Chinese nation is a great nation; it has been through hardships and adversity but remains indomitable.”

Xi Jinping (President of People's Republic of China)

Acknowledgement

The work presented in this thesis was carried out at the Laboratoire de Chimie de Coordination (LCC) du CNRS de Toulouse. I would like to thank Dr. Azzedine Bousseksou, Director of this laboratory, for having welcomed me.

Thanks to Gilles GASSER, professor at Chimie ParisTech; Miguel A.SIERRA, rofessor at Universidad Complutense and Maëlle CARRAZ, researcher at Université Paul Sabatier Toulouse III, for being my jury members to judge my work.

I would like to express my sincere gratitude to my supervisors Prof. Heinz Gornitzka and Dr. Catherine Hemmert for the continuous support of my Ph.D study and related research, for their patience, motivation, and immense knowledge. Their guidance has helped me in all the time of research and writing of this thesis.

Thanks to Dr. Olivier Cuvillier at the Institut de Pharmacologie et de Biologie Structurale (IPBS, CNRS, UPS) for supervising me in my first experience in biology.

Thanks to all the collaborators who made the biological measurements of the synthesized molecules in this manuscript: Prof. Raymond Wai-Yin Sun (University of Hong Kong) for anti-cancer tests; Prof. Alexis Valentin and Dr Sandra Bougeade Delmas (IRD-Pharma-DEV, Toulouse) for anti-leishmanial tests and Dr. Serge Mazères (IPBS, CNRS, UPS) for confocal microscopy studies.

I also express my gratitude to the administrative and scientific services of LCC, in particular, the NMR service and the mass spectrometry service of Université Paul Sabatier.

Thanks to all the group members in Team V (Team of Dr. Françoise Benoit-Vical) for all the moments together.

Thanks to my wife Mengyun Pan for supporting me spiritually throughout PhD studies. Thanks to my elder brothers Changlong Wang, Chongwei Zhu, my friends Qiuming Ma, Xinda Wu, Tianyi Zhang, Tianyi Liu, Jieru Qiu, Liang Chen, Xudong lin, Roberto Gonzalez, Alvaro Fernandez and so on.

非常感谢我的两位导师对我科研以及生活中的帮助，非常感谢我的老婆以及球友们给我生活中带来的快乐！有了你们，我的博士生涯才如此幸福！

Metal-NHC Complexes for Anti-Cancer Applications: Gold(I) for Antimitochondrial Activity and Iridium(III) for Photodynamic Therapy

In this work of thesis, several groups of novel NHC-based gold(I) complexes containing aliphatic and aromatic amino-side arms with interesting potential in biomedical applications have been synthesized and fully characterized. Also, a series of iridium(III) complexes containing NHC ligands with pronounced PDT anticancer activities has been prepared and fully characterized.

The first group represents a family of cationic bis(NHC)-gold(I) complexes containing aliphatic amino-side arms. These complexes have been synthesized and investigated for their antiproliferative activities towards four human cancer cell lines and the non-cancerous MDCK cell line. In this series, the lipophilicity correlates directly with the cytotoxic activity against cancer cells.

The second family of compounds concerns cationic gold(I) bis(NHC) complexes containing aromatic amino-side arms. The *in vitro* cytotoxicity of these complexes and proligands on the representative PC-3 prostate and T24 bladder cancer cell lines has been evaluated. All these complexes show higher Log P values (lipophilicity) than the first series of complexes, and in line with this higher cytotoxicity, nevertheless too high lipophilicity can also lead to lower selectivity.

In order to develop a drug candidate with optimized activity and selectivity, we designed and synthesized the third family of cationic gold(I) bis(NHC) complexes. The Log P values of this series were between the first series and the second series. The lower cytotoxicity towards non-cancerous NIH3T3 cells was found for this series of complexes whereas they also displayed less activities towards cancer cells than the second series.

The mechanistic studies on two gold complexes by monitoring the cellular uptake showed the rapid cellular accumulation of the intact gold bis(NHC) and a good bioavailability, in good agreement with the antiproliferative activity of these two

complexes. Moreover, both complexes inhibit TrxR, a common target for gold(I) complexes. The cell death induced by these two complexes was ROS-dependent.

Besides anticancer activities, we also tested gold(I) mono-NHC complexes for other biomedical applications in parasite disease Leishmaniasis. They were screened *in vitro* against both promastigote and axenic amastigote forms of *L. infantum*. Moreover, their cytotoxicity was evaluated on the murine J774A.1 macrophages in order to determine their selectivity of action.

Another topic of this thesis concerns iridium(III)-NHC complexes. Three families of theranostic iridium(III)-NHC complexes were prepared and characterized. The *in vitro* cytotoxicity of all the complexes against PC-3 prostate, T24 bladder cancer cells and non-cancerous NIH3T3 cells was evaluated. Moreover, all complexes are theranostic agents, and the confocal microscopy experiments of one complex showed that it can be quickly and effectively taken up into PC-3 cells and specifically localize into mitochondria. Interestingly, these complexes can act as efficient photosensitizers. The cytotoxicity of these complexes was increased substantially upon 365 nm light irradiation, which suggested the high potential to be mitochondria-targeting theranostic anticancer agents for photodynamic therapy.

Complexes métalliques à ligands NHC pour des applications anticancer: Or(I) pour l'activité antimitochondriale et Iridium(III) pour la thérapie photodynamique

Dans ce travail de thèse, plusieurs groupes de nouveaux complexes d'or(I) à base de carbènes N-hétérocyclique (NHC) contenant des bras amino-aliphatiques et aromatiques avec un potentiel intéressant dans des applications biomédicales ont été synthétisés et entièrement caractérisés. En outre, une série de complexes d'iridium(III) contenant des ligands NHC avec des activités anticancéreuses prononcées pour une application en thérapie photodynamique, a été préparée et entièrement caractérisée.

Le premier groupe représente une famille de complexes cationiques or(I) bis(NHC) contenant des bras latéraux amino-aliphatiques. Ces complexes ont été synthétisés et étudiés pour leurs activités antiprolifératives vis-à-vis de quatre lignées cellulaires cancéreuses humaines et de la lignée cellulaire non cancéreuse MDCK. Dans cette série, la lipophilie est directement liée à l'activité cytotoxique contre les cellules cancéreuses.

La deuxième famille de composés concerne les complexes cationiques or(I) bis(NHC) contenant des bras latéraux amino-aromatiques. La cytotoxicité in vitro de ces complexes et de leurs proligands sur les lignées cellulaires représentatives du cancer de la prostate PC-3 et de la vessie T24 a été évaluée. Tous ces complexes présentent des valeurs de Log P (lipophilie) supérieures à celles de la première série de complexes en accord avec leur cytotoxicité plus élevée, mais une lipophilie trop élevée peut également conduire à une sélectivité plus faible.

Afin de développer un candidat-médicament avec une activité et une sélectivité optimisées, nous avons conçu et synthétisé la troisième famille de complexes cationiques or(I) bis(NHC). Les valeurs de log P de cette série se situent entre la première série et la deuxième série. Ces complexes moins lipophiles sont moins cytotoxiques envers les lignées cellulaires saines (NIH3T3) et montre des activités anticancéreuses un peu plus faibles sur les cellules PC-3 que la deuxième série, avec néanmoins des valeurs de GI50 dans la gamme du nanomolaire.

Les études mécanistiques sur deux complexes d'or(I) ont été réalisées. Les mesures d'absorption cellulaire ont montré une accumulation cellulaire rapide et une bonne biodisponibilité des complexes, en accord avec l'activité antiproliférative de ces deux complexes. De plus, les deux complexes inhibent la thiorédoxine reductase (TrxR), une cible commune pour les complexes d'or(I). La mort cellulaire induite par ces deux complexes est dépendante des espèces réactives de l'oxygène.

En plus des activités anticancéreuses, nous avons également testé des complexes d'or(I) mono-NHC pour une autre application biomédicale, la leishmaniose, maladie parsitaire. Ils ont été testés in vitro sur les formes promastigotes et amastigotes axéniques de L. infantum. De plus, leur cytotoxicité a été évaluée sur les macrophages murins J774A.1 afin de déterminer leur sélectivité d'action.

Un autre sujet de cette thèse concerne les complexes d'iridium(III)-NHC. Trois familles de complexes ont été préparées et caractérisées. La cytotoxicité in vitro de tous les complexes sur les cellules cancéreuses de la prostate PC-3 et de la vessie T24, et les cellules non cancéreuses NIH3T3 a été évaluée. De plus, tous les complexes sont des agents théranostiques, et les expériences de microscopie confocale d'un complexe ont montré qu'il pouvait être rapidement et efficacement absorbé dans les cellules PC-3 et se localiser spécifiquement dans les mitochondries. De manière intéressante, ces complexes peuvent agir comme des photosensibilisateurs efficaces. La cytotoxicité de ces complexes a été augmentée substantiellement après une irradiation lumineuse de 365 nm, ce qui suggère le potentiel élevé de ces agents anticancéreux théranostiques ciblant les mitochondries pour la thérapie photodynamique.

Table of contents

List of abbreviations

AIE = aggregation-induced emission

Ama = amastigote

ANT = adenine nucleotide translocator

Bak = Bcl-2-antogonist/killer

Bax = Bcl-2-associated X protein

Bcl-2 = B-cell lymphoma-2

Bn = benzyl

BODIPY = boron-dipyrromethene

Bpy = 2,2'-bipyridine

CA-4 = Combretastatin A-4

Cat B = cathepsin B

CC_{50} = cytotoxic concentration

CCDC = Cambridge crystallographic data center

Ce6 = Chlorin e6

COD = cyclooctadiene

COSY = correlation spectroscopy

COX = Cyclooxygenase

DAB = 3,3'-diaminobenzidine

DAPI = 4',6-diamidino-2-phenylindole

DCA = Dichloroacetic acid

DCF = 2',7'-dichlorofluorescein

DCFDA = 2',7'-dichlorofluorescin diacetate

DFT = density functional theory

DLC = delocalized lipophilic cations

DMF = dimethylformamide

DMSO = dimethyl sulfoxide

DNA = deoxyribonucleic acid

DTNB = 5,5'-Dithiobis(2-nitrobenzoic acid)

EC_{50} = Half maximal effective concentration

EDTA = Ethylenediaminetetraacetic acid

ELISA = enzyme-linked immunosorbent assay

ER = Endoplasmic reticulum

ERK = extracellular signal-regulated kinases

ESI = electrospray ionization

Et = ethyl

FAD = Flavin adenine dinucleotide

FDA = Food and Drug Administration

5-FU = Fluorouracil

GC-MS = Gas chromatography-mass spectrometry

GI_{50} = concentration causing 50% decrease in cell growth

GPx = gluotathione peroxidase

GR = gluotathione reductase

GSH = gluothione reduced

HMBC = Heteronuclear multiple-bond correlation spectroscopy

HOMO = highest occupied molecule orbital

HRMS = high resolution mass spectrometry

HSP60 = Heat shock proteins

HSQC = Heteronuclear single quantum correlation

HT-DNA = human telomeric deoxyribonucleic acid

H_2TPP = Tetraphenylporphyrin

IC_{50} = half maximal inhibitory concentration

ICP-AES = Inductively coupled plasma-atomic emission spectroscopy

ICP-MS = Inductively coupled plasma-mass spectrometry

JNK = c-Jun N-terminal kinases

LC = ligand centered

LC_{50} = lethal concentration, 50%

LC-MS = liquid chromatography-mass spectrometry

LED = light-emitting diodes

LLCT = ligand-to-ligand charge transfer

LUMO = lowest unoccupied molecular orbital

MCSs = multicellular spheroids

MCTS = multicellular tumor spheroids

Me = methyl

MIC = minimum inhibitory concentration

MLCT = metal-to-ligand charge transfer

MMP = mitochondrial membrane permeability

MNBA = meta-nitrobenzylalcohol

MOF = Metal-organic framework

MOMP = mitochondrial outer membrane permeability

MPT = mitochondrial permeability transition

MTD = maximum tolerated dose

MTT = 3-(4,5-Dimethylthiazolyl-2-yl)-2,5-diphenyltetrazolium bromide

NAC = N-Acetylcysteine

NAPD = nicotinamide adenine dinucleotide

NADPH = nicotinamide adnine dinucleotide phosphate

NBT = Nitro blue tetrazolium

NHC = *N*-heterocyclic carbene

NIR = Near-infrared

NMR = nuclear magnetic resonance

NPM = nucleophosmin

OD = optical density

OP = one photon

PARP = Poly (ADP-ribose) polymerase

PBS = Phosphate buffered saline

PDT = photodynamic therapy

PI = phototoxicity index

POPOP = 1,4-bis(5-phenyloxazol-2-yl) benzene

Ppy = 2-phenylpyridine

Pro = promastigote

Prx = peroxiredoxin

PS = photosensitizers

RNA = ribonucleic acid

ROS = reactive oxygen species

RT = room temperature

SAR = structure-activity relationship

SEM = standard error of mean

SI = selectivity index

SRB = Sulforhodamine B

TBAB = Tetrabutylammonium bromide

TMS = Tetramethylsilane

TNB = 5-thio-2-nitrobenzoic acid

TP = two photon

TrxR = thioredoxin reductase

TrxR1 = cytosolic TrxR

TrxR2 = mitochondrial TrxR

VDAC = voltage dependent anion channel

YB-1 = Y-box-binding protein 1

Cell lines

A2780 = human ovarian cancer cells

A375 = human melanoma cells

A549 = human lung cancer cells

B16F10 = mouse melanoma cells

Caki-1 = human renal cancer cells

CCD-18Co = human normal colon fibroblast cells

CCRF-CEM = human Caucasian acute lymphoblastic leukaemia cells

EC109 = human esophageal squamous cell carcinoma cells

HEK-293 = human embryonic kidney normal cells

HeLa = human cervical cancer cells

Hep3B = human black hepatocyte carcinoma cells

HepAD38 = human hepatoblastoma cells

HepG-2 = human liver cancer cells

HL60 = human promyelocytic leukemia cells

HMEC = human mammalian epithelial cells

HT29 = human colon cancer cells

HUVEC = primary human umbilical vein endothelial cells

LO2 = human normal liver cells

MB157 = human breast cancer cells

MC3T3 = mouse osteoblast precursor cells

MCF-7 = human breast cancer cells

MCF-10A = human mammary epithelial cells

MDA-MB-231 = human breast cancer cells

MDA-MB-468 = human breast cancer cells

MDCK = Madin-Darby Canine Kidney cells

Miapaca-2 = human pancreas carcinoma cells

NCI-H460 = human lung cancer cells

NCI-H1666 = human non-small lung cancer cells

NCI-H1975 = human adenocarcinoma cells

NIH3T3 = mouse embryo fibroblast cells

OVCAR-3 = human ovarian cancer cells

PC-3 = human prostate cancer cells

RC-124 = human kidney primary cells

RAW264.7 = mouse leukemic monocyte-macrophage cells

SKOV-3 = human ovarian cancer cells

SUNE-1 = human nasopharyngeal cancer cells

T24 = human bladder cancer cells

4T1 = mouse breast cancer cells

U-2 OS = human bone osteosarcoma cells

U87 = human primary glioblastoma cells

U937 = human monocyte-macrophage cells

1. Introduction

1.1. Metals in medicine

Medicinal inorganic chemistry is a developing field, and novel therapeutic and diagnostic metal complexes have a great impact on medical treatment.

Metal complexes are very important for our health both endogenously and exogenously. Exogenous metal complexes can be administrated to our body in a controlled way, as the case of therapeutic agents, or in an uncontrolled way, as by air or pollutants. It is remarkable that the therapeutic agents or pollutants are directed towards the endogenous metal targets or require metal coordination to act. The biological activity of pharmaceuticals depends on the nature and oxidation state of metal and its ligands. Two main factors, thermodynamic stability and selectivity, are very important in the design of metal complexes for medical applications.[1]

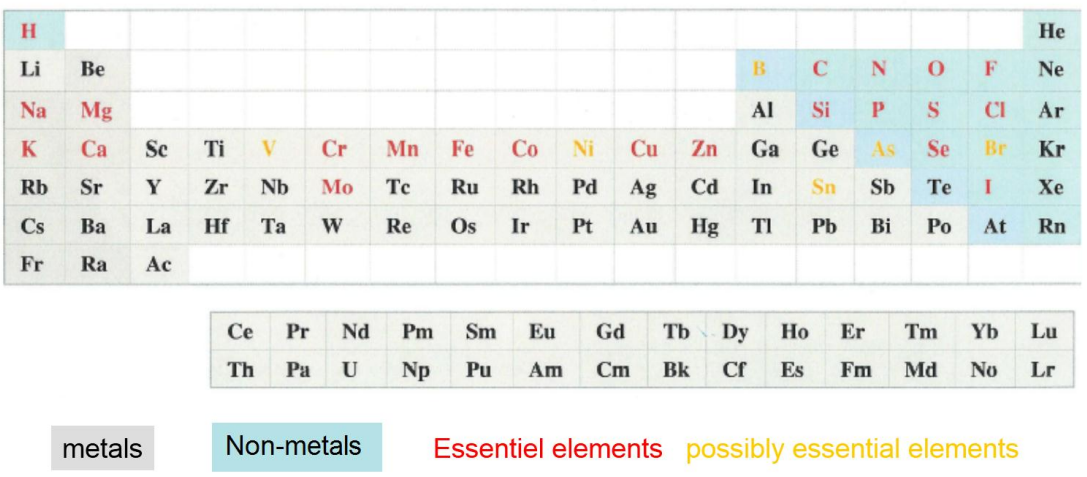

Fig 1.1.1 Essential elements.

A wide variety of metal compounds are already in clinical use. These include mineral supplements containing metals essential for mammalian life, e.g. Ca, Mg, Cr, Mn, Fe, Co, Cu and Zn (Fig 1.1.1). Vitamin B_{12}, which contains colbalt positioned in the center of a planar tetra-pyrrole, shows physiological activity. Most of them are used as antacids, many of which are simple inorganic salts from group I, II and XIII metals, such as sodium bicarbonate, magnesium oxide or carbonate and aluminium

hydroxide.[2]

In 1890, the first well-defined metal-based drug potassium dicyanoaurate with formula $K[Au(CN)_2]$ as antibacterial was discovered. Since 1940, gold complexes have been used for the treatment of arthritic disorder in humans. At the end of last century, gold complexes such as gold sodium thiomalate and gold thioglucose used to treat arthritis were administered by injection. It was discovered, however, that orally-administered auranofin (Fig.1.1.2) was equally effective against rheumatoid arthritis. It is notable that the coordination of gold by thiolate appears to be a natural process in the body.[2-3]

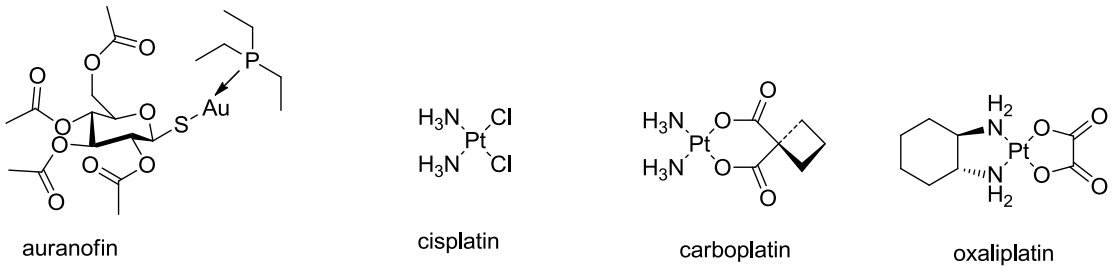

Fig 1.1.2 Structures and names of some metal-based drugs.

The cytotoxicity of cisplatin has drastically promoted the development of treatment of certain types of cancer.[4] Cisplatin and carboplatin (Fig 1.1.2) are used to treat various types of cancers such as testicular, ovarian, lung and bladder cancer. Oxaliplatin (Fig 1.1.2) was the first drug which could avoid the cisplatin resistance of colon carcinoma.[5] The ultimate target for Pt(II) drugs is DNA and certain platinated DNA adducts trigger conformational change of DNA structure, leading to DNA repair response and then to cell death (Fig 1.1.3).[6]

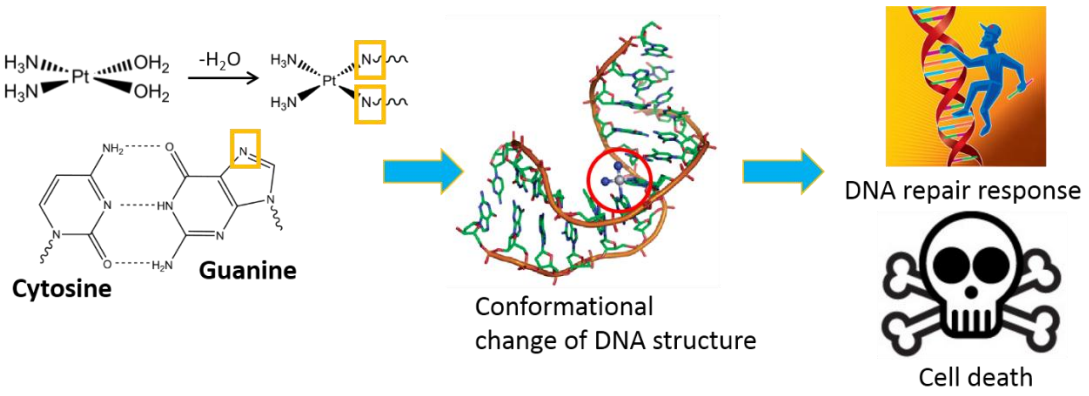

Fig 1.1.3 Mechanism of cisplatin.

However, the use of cisplatin in clinic trials is limited by 1) the resistance observed in several types of cancer cells, 2) the increase of resistance after continuous treatment and 3) the high toxicity against normal cells, which means strong side effects.[7] Therefore, there are more interests in the development of platinum drugs against a wide range of types of cancer cells, especially cisplatin-resistant cancer cells. Although platinum complexes have been the most detailedly investigated, research has been extended to other metal-based drugs, such as gold, silver, copper, palladium, rhodium, iridium and ruthenium.

1.2. *N*-heterocyclic carbene metal complexes in medicine

The last decade has witnessed the dramatic development in the field of metal complexes of *N*-heterocyclic carbenes (NHCs).[8] NHCs are a class of electron donating ligand, which form strong σ bonds to metal ions in both high and low oxidation states. Some similarities between NHC and phosphine ligands have been noted and NHCs have been used to replace phosphines, which are sensitive to oxygen, to prepare catalysts.[9] Nowadays, metal-NHC complexes appear to be a more and more popular field of research in the development of metal-based drugs because of their high stability and the ease of NHC derivatization (Fig 1.2.1).[8b, 8d, 10] At the beginning, most of the researchers focused on the 1,3-nitrogen substituents to do modulations.[11] Then substituents at 4- and 5-positions started to draw the attention of some researchers. Recently, benzimidazole, pyrazole, triazole, tetrazole and caffeine-based NHC gold complexes were designed and synthesized to enlarge the families of NHC ligands for biomedical applications.[10]

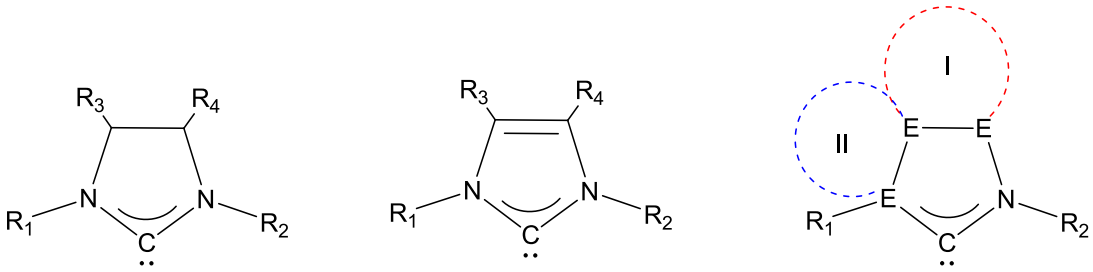

R_1, R_2 = alkyl or aryl
R_3, R_4 = alkyl, aryl or halogen
E = N, C or S
Ring I = benzene, acenaphthene
or 1,3-dimethylpyrimidine-2,4(1*H*,3*H*)-dione
Ring II = pyridine or cyclohexene

Fig 1.2.1 Scheme of different types of NHC ligands.

Various metal-NHC complexes have been shown to possess biological activities like anti-infective, anti-bacterial and anti-cancer. The main results reported in the literature for biomedical NHC compounds are related to Au, Ag, Ru, Rh and Cu complexes.[8b, 12]

Here, we will talk about Ag, Ru, Rh and Cu complexes bearing NHC ligands, and then introduction of gold NHC complexes will be presented in a special section.

Silver complexes: Silver complexes have been noted as antimicrobial agents for many years and nowadays they also display anti-cancer activity.[13] The first Ag(I)-NHC complexes with antimicrobial activity was published by Youngs' group. In this report by Youngs and co-workers,[14] the synthesis of two pyridine-linked pincer silver NHC complexes **1a** and **1b** (Fig 1.2.2) is presented. **1a** and **1b** were active against *E. coli*, *S. aureus* and *P. aeruginosa*, showing minimum inhibitor concentration (MIC) values much lower than that of silver nitrate, which is the appropriate reference for this type of application.

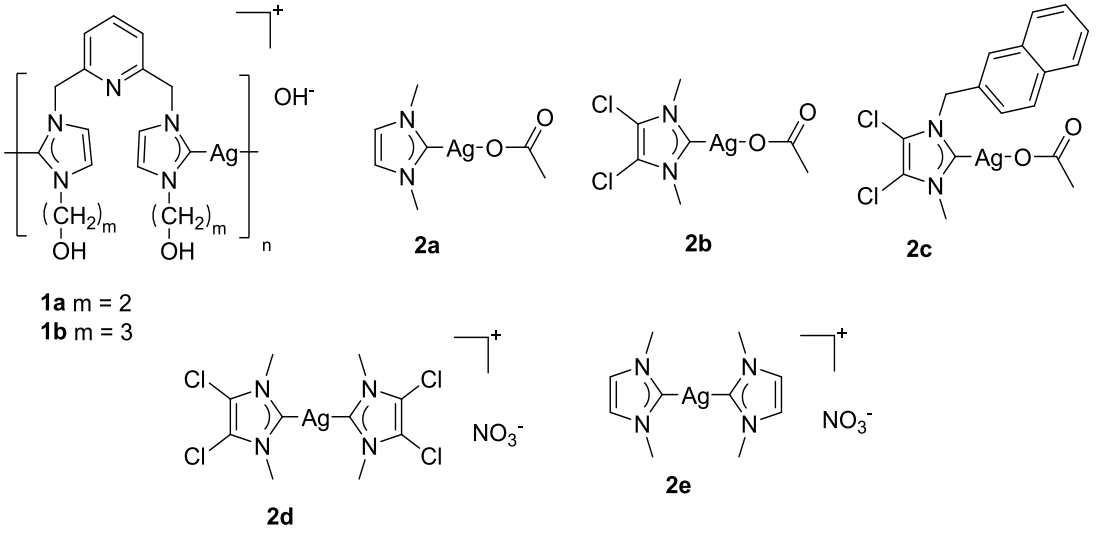

Fig 1.2.2 NHC-Ag(I) silver complexes as antimicrobial (**1a** and **1b**) and anticancer (**2a-2e**) agents reported by Youngs and co-workers.

Besides the antimicrobial activity of silver, these years more and more attentions are focused on the research of anticancer activity of silver complexes.[8d] Youngs' group reported the anticancer activity of several monomeric and dimeric imidazol-2-ylidene and 4,5-dichloroimidazol-2-ylidene silver acetate complexes (**2a-2e**, Fig 1.2.2). Complex **2a** is not stable enough to study its activity, but the IC_{50} values of complexes **2b** and **2c** were in the same range as cisplatin against ovarian (OVCAR-3) and breast (MB157) cancer cell *in vitro*.[15] On the other hand, dimeric complexes **2d** and **2e** just showed 10-fold less activity than cisplatin against lung (H460) cancer cell and no significant effect against cervical (HeLa) cancer cell.[16]

Ruthenium complexes: Group 8 metal complexes based on ruthenium have arisen interest in the research of metal-based anticancer agents. Two ruthenium complexes NAMI-A and KP1019 (Fig 1.2.3) have entered phase II clinical trials, and the former as an antimetastatic agent.[17] They are less toxic than platinum-based drugs and capable of overcoming the resistance of cisplatin-resistant cancer cells.

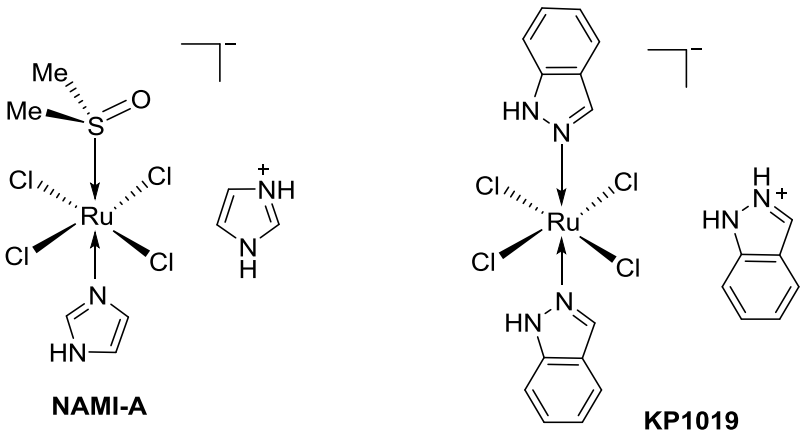

Fig 1.2.3 Chemical structure of NAMI-A and KP1019.

Ott and co-workers reported a series of ruthenium complexes (**3a-3d**, Fig 1.2.4) of the type (*p*-cymene)(NHC)$RuCl_2$ and studied their behavior in biological tests.[18] These compounds interact with biologically relevant thiols and selenols, which lead to the inhibition of enzymes like thioredoxin reductase (TrxR) and cathepsin B (catB). One of the complexes (**3d**) showed pronounced antiproliferative effects with low IC_{50} values against breast cancer cells (MCF-7, 2.07 μM) and colon adenocarcinoma cells (HT-29, 2.40 μM). The inhibition of tumor cell growth was accompanied by a perturbation of metabolic parameters such as cellular respiration.

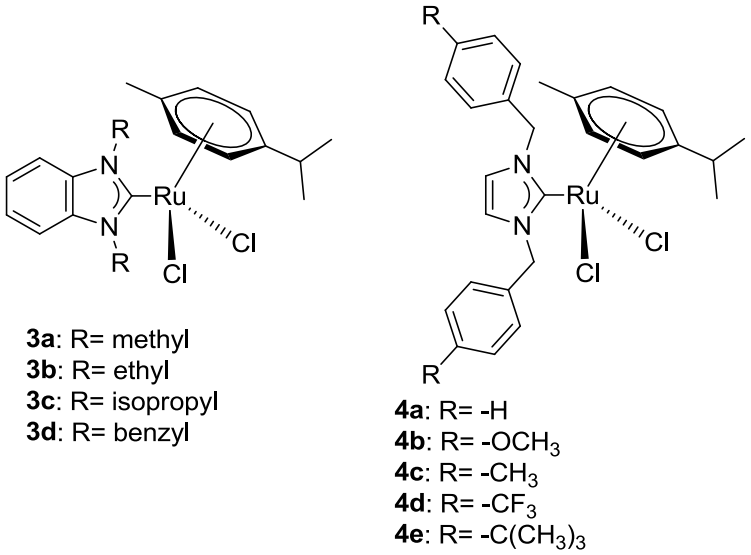

Fig 1.2.4 Structure of NHC-Ru complexes as anticancer agents.

Similarly, five Ru(II)-NHC complexes **4a-4e** (Fig 1.2.4) were synthesized, characterized and tested by MTT (3-(4,5-dimethylthiazol-2-yl)-2,5-diphenyl

tetrazolium bromide) assay on four different human cancer cell lines by Qiu, Lin and co-workers.[19] The cytotoxicity of these complexes enhanced with the increase of the lipophilicity. The most lipophilic complex **4e** (Log P = 2.62) showed the best activity with IC_{50} values of 10.3 μM for SKOV-3 (ovarian), 2.9 μM for PC-3 (prostate), 8.2 μM for MDA-MB (breast) and 6.4 μM for EC109 (esophagus) cancer cell lines. Moreover, **4e** can inhibit PC-3 cell lines by inducing cell cycle arrest at G2/M phase.

Rhodium complexes: With the development of ruthenium complexes as potential chemotherapeutic agents, the neighboring group 9 rhodium complexes have drawn lots of attention. Because of the controllable reactivity, good solubility and relative accessibility, rhodium complexes have become potential alternatives to palladium and ruthenium metallodrugs.

Ott and co-workers developed a series of Rd(I)-NHC complexes **5a-5h** (Fig 1.2.5) with cyclooctadiene (COD) as secondary ligands with pronounced antiproliferative effects against HT-29 (colon carcinoma) and MDA-MB-231 (human breast adenocarcinoma) cells.[20] The most active complex **5g** triggered IC_{50} values of 1.5 μM in both cancer cell lines. Structure-activity relationship for cytotoxicity indicated that the biological properties of rhodium complexes could be modulated by changing the substituents on the NHC ligands and the nature of the secondary halide ligand. In terms of their mode of action, effects on cellular signal of certain targets such as p38 (a class of mitogen activated protein kinases) and ERK1/2 (extracellular signal-regulated kinases) have to be taken into account.

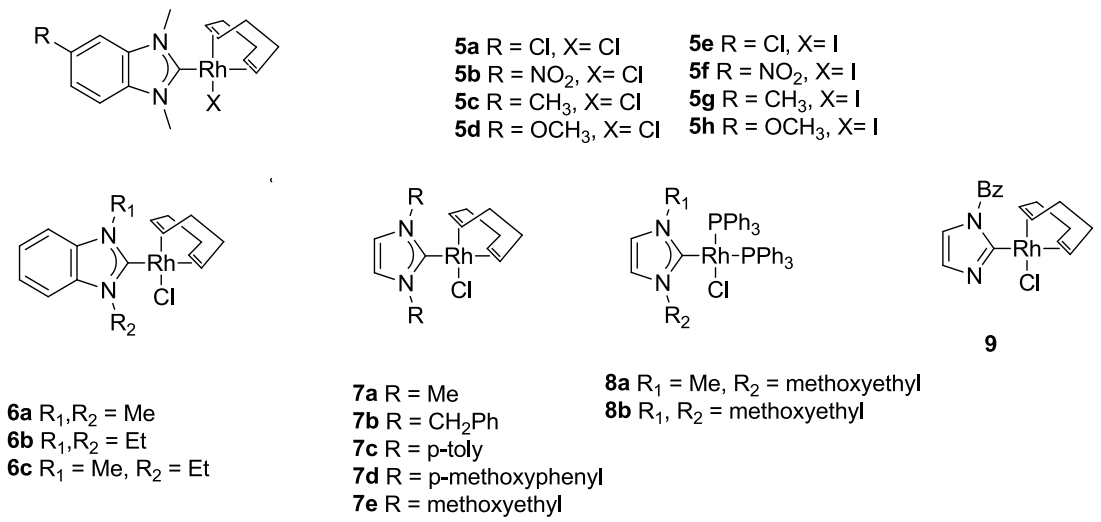

Fig 1.2.5 Structure of NHC-Rh complexes as anticancer **(5a-5h**) and antimicrobial (**6-9**) agents.

Besides anticancer activity, rhodium complexes can also be taken as antimicrobial agents. Cetinkaya and co-workers were the first to investigate the *in vitro* antimicrobial activities of Rh(I)-NHC complexes.[21] The rhodium complexes **6-9** (Fig 1.2.5) were evaluated against *E. coli, S. aureus, Enterococcus faecalis and P. aeruginosa*. Of all these compounds, **6a** and **6c** were found to be the most effective against both Gram-positive bacteria with MIC values of 5 μg/ml. No significant inhibition was observed against Gram-negative bacteria.

Copper complexes: Copper is an essential element for most aerobic organisms, and it has a long history for medical applications. Copper, which is important for the function of several enzymes and proteins and is involved in many biological pathways, is maybe less toxic than non-essential elements.[22]

Two types of novel NHC-copper(I) bromide derivatives **10a-10j** (Fig 1.2.6) have been synthesized *via* silver oxide pathway by Tacke and co-workers.[23] The copper(I)-NHC complexes **10a-10e** showed high cytotoxicity against breast carcinoma (MCF-7) and renal cell carcinoma (Caki-1) with low IC_{50} values in the micromolar and sub-micromolar range. With IC_{50} value of 0.60 μM against MCF-7 and 0.65 μM against Caki-1, the most active compound **10c** has been selected as a

promising candidate for future biological studies.

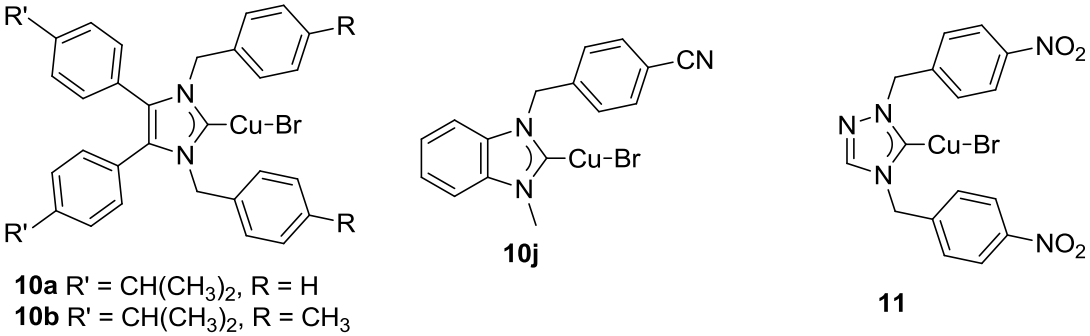

10a R' = $CH(CH_3)_2$, R = H
10b R' = $CH(CH_3)_2$, R = CH_3
10c R' = $CH(CH_3)_2$, R = OCH_3
10d R' = $CH(CH_3)_2$, R = $COOCH_3$
10e R' = $CH(CH_3)_2$, R = CN
10f R' = H, R = H
10g R' = CH_3, R = CH_3
10h R' = OCH_3, R = CH_3
10i R' = Cl, R = OCH_3

Fig 1.2.6 Structure of NHC-Cu complexes as anticancer agents.

The newly-designed Cu(I) 1,2,4-triazole based NHC complex **11** (Fig 1.2.6) was synthesized and assessed for its cytotoxic properties in various human cancer cell lines, including cisplatin sensitive and resistant cells.[24] Compared with corresponding Ag(I)-NHC and Au(I)-NHC complexes, Cu(I)-NHC complex **11** was the most efficacious antiproliferative compound, and it was able to promote a growth inhibitory effect up to 7-times higher than that triggered by cisplatin. It was shown that copper complexes can enter and accumulate into cancer cells leading to cell death through the impairment of ubiquitin-proteasome degradation pathway (ubiquitin-proteasome pathway is the principle catabolism in the mammalian cytosol and nucleus).

1.3. *N*-heterocyclic carbene gold complexes as potential anticancer metallodrugs

Among the non-platinum anti-cancer drugs, gold complexes with metal center in the oxidation states +1 and +3 have drawn considerable attentions because of their strong cytotoxic activity in various cancer cells.[8d] Based on the great structural variety of the ligands, the detailed mechanisms of action of gold complexes remain unclear. Among the numerous hypothesis in terms of mechanism of action, inhibition

of enzyme TrxR seems to play an important role in pharmacology of gold complexes as gold displays a high affinity to selenol group.[8d]

Thioredoxin reductase targeting mode of action:

Thioredoxin reductase (TrxR), a homodimeric protein containing one selenocysteine and one FAD, catalyses the NADPH-dependent reduction of thioredoxin disulfide and numerous other oxidized cell constituents (Fig 1.3.1). As a general reducing enzyme with little substrate specificity, it also contributes to redox homeostasis and is involved in prevention, intervention and repair of damage caused by H_2O_2-based oxidative stress.[25]

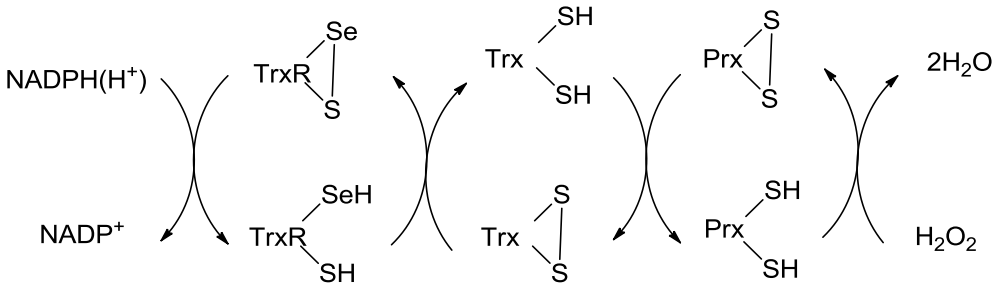

Fig 1.3.1 The thioredoxin reductase/thioredoxin system.

In cancer cells, although many different targets are available for gold complexes, the observed inhibition of TrxR seems to play a main role. Humans express mainly two TrxR isoenzymes: TrxR1 (cytosolic) and TrxR2 (mitochondrial). The mechanism of action of cell death induced by gold complexes is shown below in Fig 1.3.2.[26] The mitochondrial respiratory chain produces superoxide anion that becomes hydrogen peroxide and oxidizes thioredoxin in a reaction mediated by peroxiredoxin (Prx). However, TrxR, inhibited by gold complexes, is no longer able to reduce back the oxidized thioredoxin that accumulates together with hydrogen peroxide and both act on several different mitochondrial targets leading to the opening of the mitochondrial permeability transition pore or an increase of the permeability of outer membrane, and therefore causing the release of proapoptotic factors.

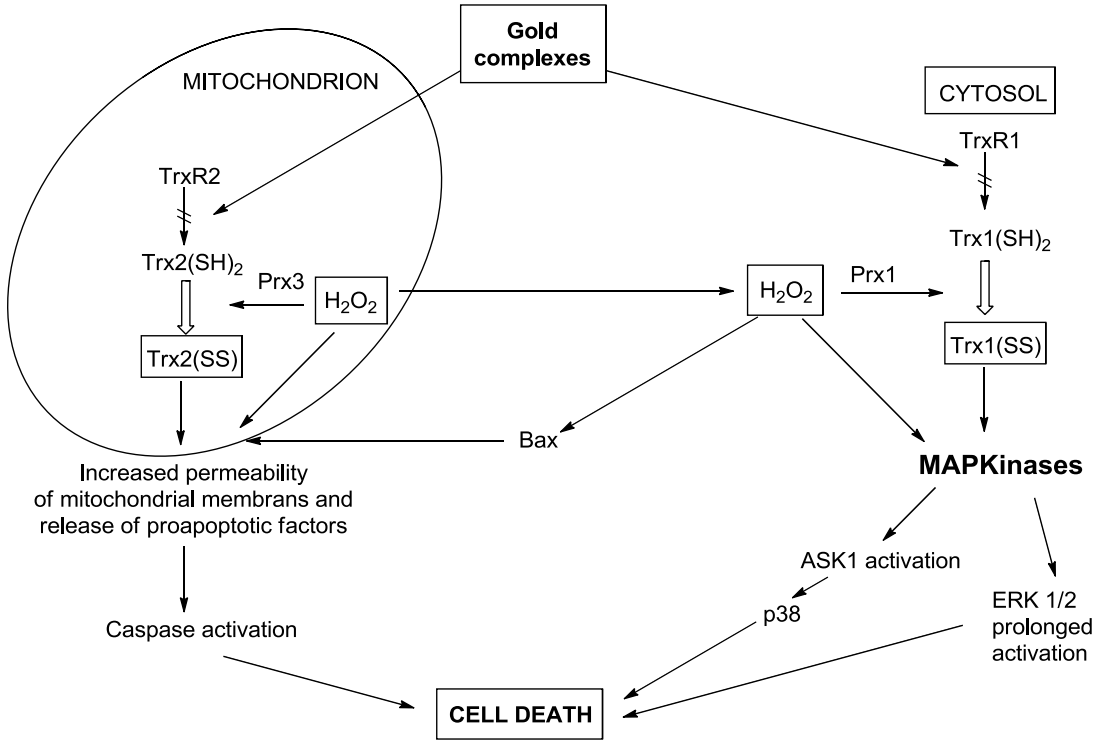

Fig 1.3.2 Model depicting the mechanism of action of cell death induced by gold complexes as proposed by Bindoli and co-workers.[26]

Mitochondria targeting mode of action:

Mitochondria play a major role in the regulation of apoptosis (cell death) and in diseases characterized by abnormal apoptotic responses such as cancer. Apoptosis is a form of cell death characterized by activation of caspases that cleave multiple targets in the cell.[27] In vertebrate cells, the main form of apoptosis proceeds through the mitochondrial pathway, and the critical event in the process is mitochondrial outer membrane permeabilization (MOMP), which represents the "point of no return" of cell death.[28] The mechanisms responsible for MOMP during apoptosis remain controversial, but there are two classes of mechanism that have been described, and each of them may function under different circumstances (Fig 1.3.3).[29] On one hand, MOMP can occur as a consequence of the mitochondrial permeability transition (MPT).[30] The opening of MPT involves the adenosine nuclear transporter (ANT) in the inner mitochondrial membrane, and the voltage-dependent anion channels (VDACs) in the outer membrane. On the other hand, MOMP appears to be mediated

by members of the Bcl-2 family of apoptosis-regulating proteins acting directly on the outer mitochondrial membrane.[31] The proapoptotic multidomain member Bax or Bak, leading to the release of cytochrome c from mitochondria, are vital for MOMP to occur during apoptosis.

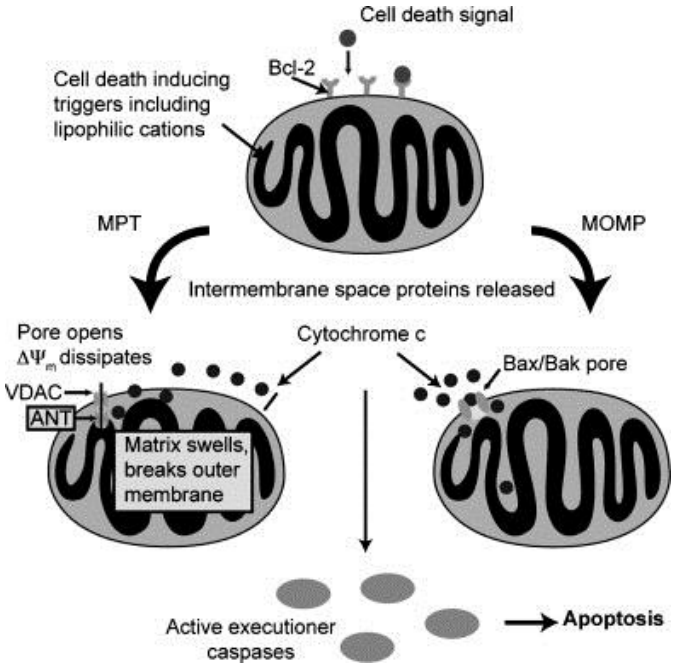

Fig 1.3.3 Mechanism for MOMP during apoptosis.[27]

Chen and co-workers found that compared with living cells, carcinoma cells have higher mitochondrial membrane potential ($\Delta\Psi m$).[32] Recent researches in mitochondria result in the elevated interest in the development of delocalized lipophilic cations (DLCs). They can readily pass through the lipid bilayer and selectively accumulate in mitochondria of carcinoma cells as the consequence of elevated $\Delta\Psi m$ in tumor cells. A huge variety of DLCs have shown pronounced anti-tumor activities, and the selectivity of cancer cells over normal cells can be modulated by changing the lipophilicity of DLCs.[33]

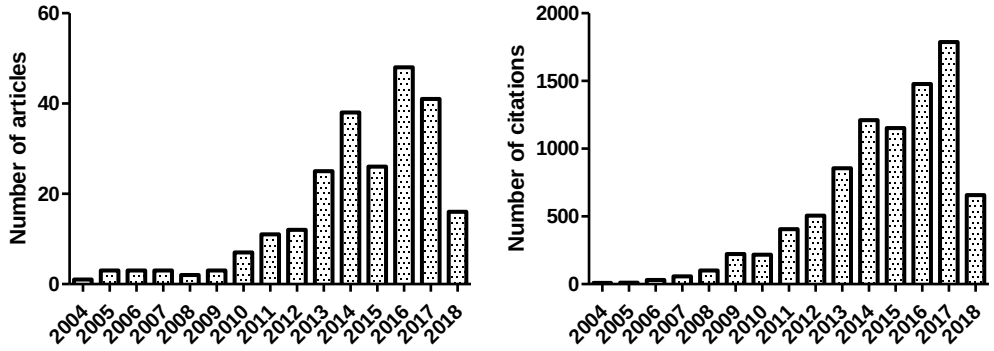

Fig 1.3.4 Number of articles (left) and citations (right) per year on the topic of "gold + anticancer + NHC or carbene". Data were obtained from Web of Science.

As shown in Fig 1.3.4, which reports the number of articles and citations in Web of science on the topics "gold, anticancer, NHC or carbene" from 2004 to May 2018, the field has rapidly grown in the past few years. This introduction will focus on Au(III)-NHC and Au(I)-NHC complexes, highlighting the potential of using gold NHC complexes in the development of new anticancer drugs.

1.3.1. Gold(III)-NHC complexes as anticancer agents

Organometallic complexes of gold are found increasing usage in biomedical application. Many complexes with anticancer activity use the metal gold in the oxidation state +1 or +3, which can be stabilized by NHC-based ligands.[8d, 10] While majority of researches focus on the NHC complexes of gold in +1 oxidation state, the gold(III)-NHC complexes have drawn lots of attention recently.

It has been previously reported that gold(III) complexes are not very stable under physiological environments, and Au(III) can be reduced to Au(I) by thiols and thioethers containing cysteine residues in proteins and peptides.[34] However, by taking advantage of the donating property of NHC ligands and the ease of pharmaco-modulation, Che's group previously reported a panel of stable cyclometalated gold(III) complexes **12a-g** containing NHC ligands (Fig 1.3.5).[35] These complexes show potent and selective cytotoxicity against cancer cells and *in vivo* anti-tumor activities in mice bearing xenografts of HeLa (cervical) and

NCI-H460 (lung) cancer cells. Furthermore, they studied about the mechanism of action, and they found the specific engagement of Au(III) NHC complexes with various cellular targets, such as heat shock proteins (HSP60), vimentin, nucleophosmin (NPM) and Y-box binding protein 1 (YB-1).

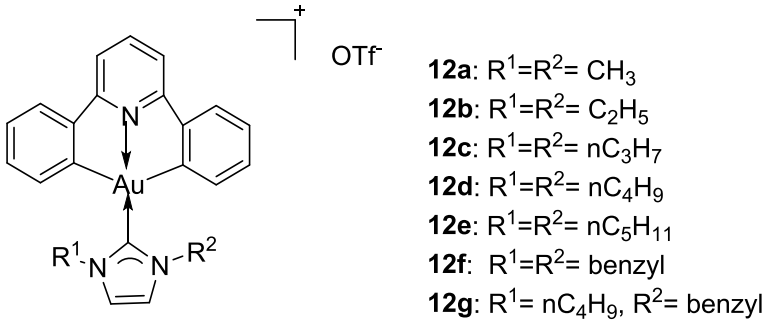

Fig 1.3.5 Au(III)- NHC complexes reported by Che and co-workers.

Bochmann and co-workers reported a series of cyclometalated gold(III) complexes **13a-13c** containing pyrazine-based (C^N^C)-type pincer ligand (Fig 1.3.6).[36] These complexes afford a new platform for the study of antiproliferative activities of gold(III) complexes. Of the whole series, complex **13a** had the most effective activity against HL60 (leukemia), A549 (lung cancer) and MCF-7 (breast cancer), which gave IC_{50} values in submicromolar range, accompanied by low cytotoxicity against healthy human lung fibroblast cells. Complex **13a** proved to be not affected by glutathione under physiological conditions, and it could stabilize the DNA G-quadruplex and i-motif structures, which was firstly reported in gold complexes.

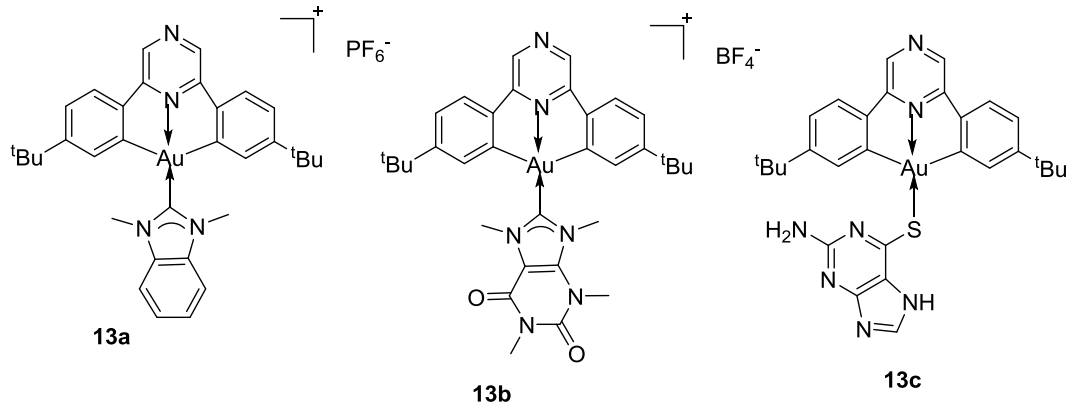

Fig 1.3.6 Pyrazine-based (C^N^C) Au(III) complexes reported by Bochmann and co-workers.

The gold(III) NHC complex (**14**, Fig 1.3.7) was prepared by Haque and co-workers.[37] Complex **14** displayed remarkable antiproliferative activities against MCF-7 (breast carcinoma), PC-3 (prostate carcinoma) and U937 (histiocytic leukemia) cells in the nanomolar range with IC_{50} values of 0.31 nM, 0.34 nM and 190 nM, respectively. Moreover, human colorectal normal cells (CCD-18Co) were used to determine the cytotoxic selectivity of the compound towards cancer cells and its safety towards normal cells. Selectivity index (SI) results revealed that complex **14** exhibited high selectivity towards all tested cancer cells with SI values of 57096, 52095 and 93 for MCF-7, PC-3 and U937, respectively.

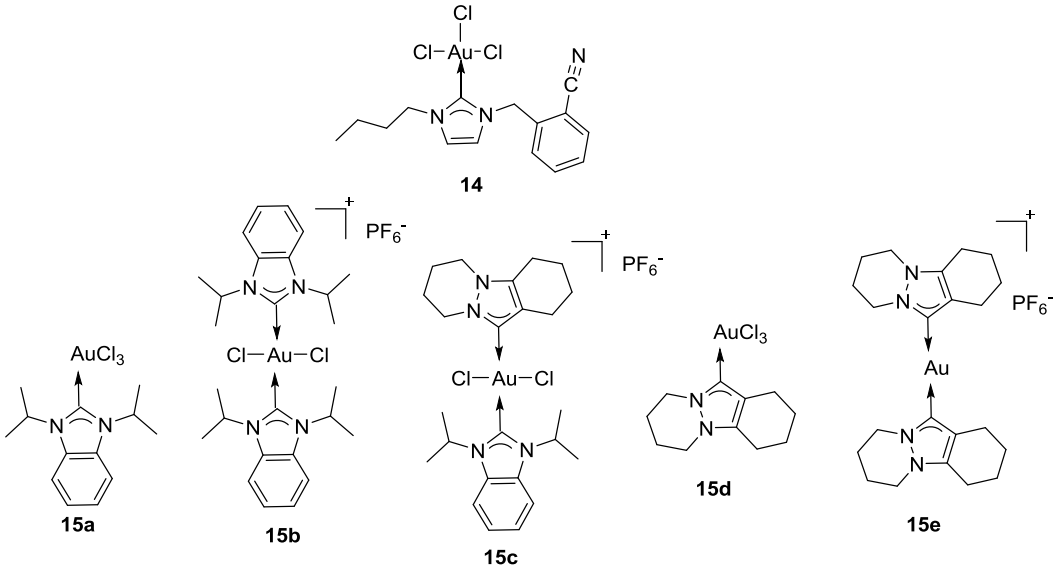

Fig 1.3.7 Au(III) complexes reported by Haque and co-workers (**14**) and by Huynh and co-workers (**15a-15e**).

Huynh and co-workers reported a series of Au(III) mono-, homobis- and heterobis-(NHC) complexes (**15a-15e**, Fig 1.3.7).[38] The cytotoxic activities of these complexes against NCI-H1666 (non-small cell lung cancer) cells were tested using cisplatin as a reference drug (IC_{50} = 2.51 μM). In terms of benzimidazole moiety, the neutral monocarbene complex **15a** (IC_{50} > 10 μM) was found to be less active than cisplatin, and displayed much lower activities as compared to the cationic homo- and heterobis-(carbene) complexes **15b** and **15c** with IC_{50} values of 0.536 μM and 0.210 μM, respectively. Concerning the pyrazole moiety, complex **15d** (IC_{50} > 10 μM) and

15e (IC_{50} = 1.46 μM) displayed lower cytotoxicity than analogue **15c** towards NCI-H1666 cells.

1.3.2. Dinuclear gold(I)-NHC complexes as anticancer agents

The group of Berners-Price was a pioneer in the research of gold(I) complexes containing NHC ligands as anticancer agents. They reported a series of dinuclear Au(I)-NHC complexes (**16a-16g**, Fig 1.3.8).[39] These complexes were studied for their ability to induce mitochondrial membrane permeability (MMP) in isolated rat liver mitochondria. The rates and levels of uptake of these complexes into mitochondria were evaluated by measuring mitochondrial gold levels using inductively coupled plasma optical emission spectroscopy. The mechanism by which MMP is induced by these Au(I)-NHC complexes was not a purely function of the level of gold accumulation, but it may involve disruption of the function of a specific enzyme or interaction with a mitochondrial permeability transition pore (MPT) component.

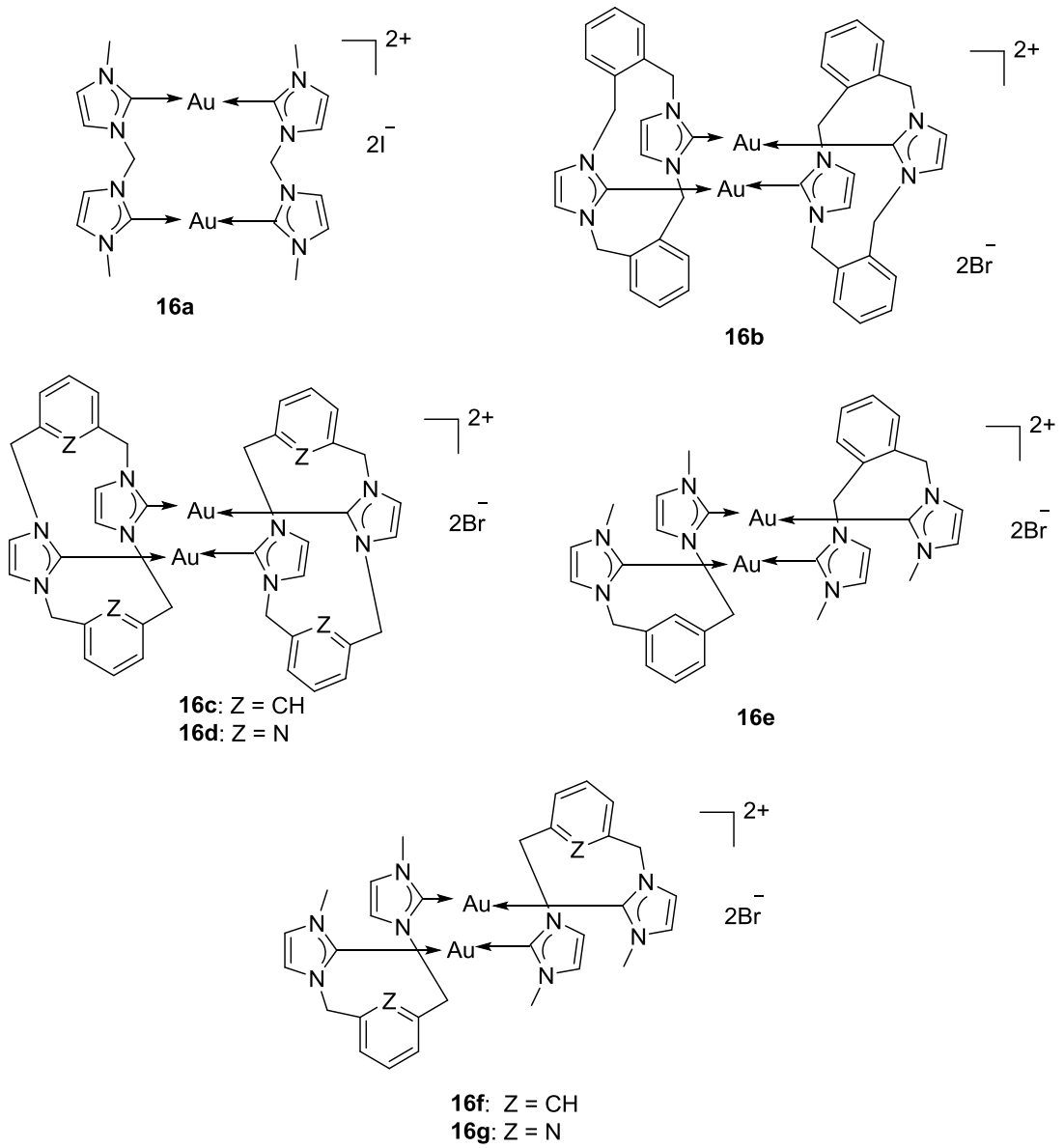

Fig 1.3.8 Dinuclear gold(I)-NHC complexes reported by Berners-Price and co-workers (**16a-16g**).

Another dinuclear NHC complex (**17**, Fig 1.3.9) was obtained through a transmetalation route by Goite, Castro and co-workers.[40] Complex **17** was found to interact with DNA mainly through noncovalent interaction as π-π stacking and produced conformational changes in the structure of DNA. Sulphorhodamine-B (SRB) assay was used to distinguish between a cytostatic effect (reduction in cell proliferation) and a cytotoxic effect (decrease of the number of viable cells). Complex **17** displayed a good cytostatic activity against MCF-7 (breast carcinoma), PC-3

(prostate carcinoma) and HT29 (colon carcinoma) cell lines (GI_{50} = 0.6, 1.3 and 2.3 μM, respectively), while it showed a low cytotoxic effect on all cancer cell lines with a LC_{50} (50 % cytotoxicity) lower than 30 μM.

Che and co-workers reported three dinuclear complexes (**18a-18c**, Fig 1.3.9) with mixed bridging diphosphine and bis(NHC) ligands. Complex **18a** exhibited a favorable stability that enabled it to inhibit TrxR activity without being attacked by blood thiols. Complex **18a** was found to be cytotoxic against breast carcinoma (MCF-7), nasopharyngeal carcinoma (SUNE-1), lung adenocarcinoma (NCI-H1975) and mouse melanoma (B16-F10) with IC_{50} values ranging from 1.3 to 3.2 μM, higher than those of cisplatin. Furthermore, this complex was found to inhibit tumor growth in mice bearing HeLa xenografts and highly aggressive mouse B16-F10 melanoma without observation of side effects under *in vivo* conditions.[41]

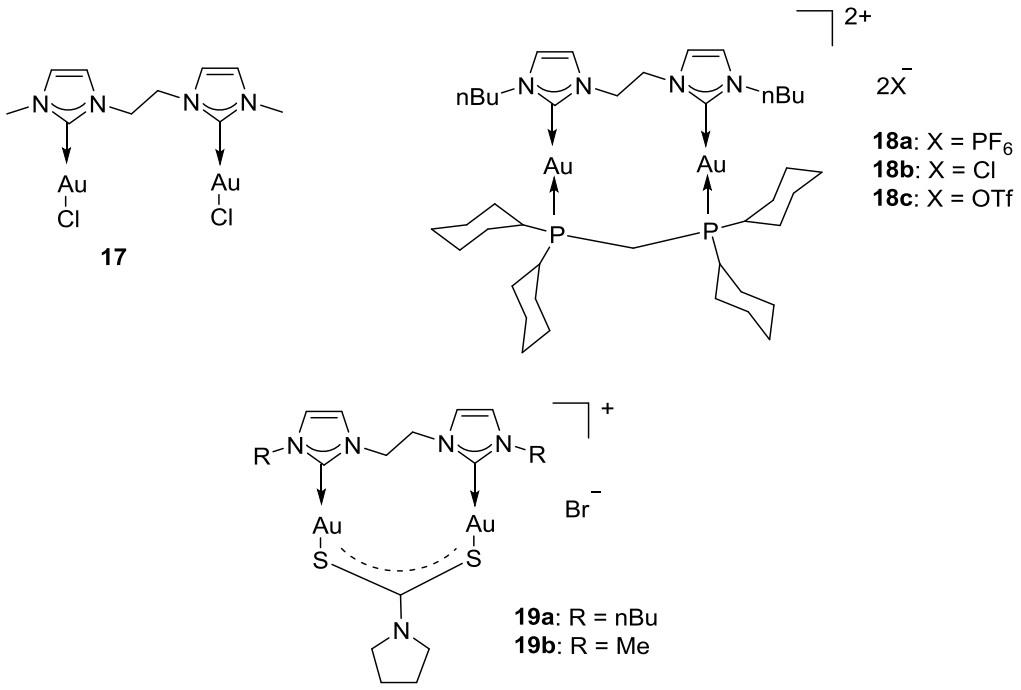

Fig 1.3.9 Dinuclear Au(I)-NHC complexes reported by Castro and co-workers (**17**), by Che and co-workers (**18a-18c**), and by Sun and co-workers (**19a-19b**).

Various new gold(I) pyrrolidinedithiocarbamato complexes (**19a-19b**, Fig 1.3.9) bearing NHC ligands were prepared by Sun and co-workers. A dinuclear gold(I) complex **19a** with a bidentate carbene ligand displayed a potent cytotoxic (IC_{50} value

of 0.83 μM) and antimigratory activity *in vitro* towards cisplatin-resistant ovarian cancer cells A2780cis. Due to the rigid scaffold, the complex **19a** enabled zinc(II)-based metal-organic framework (Zn-MOF) to be used as a carrier to improve its cellular uptake and release under physiological conditions. Notably, the biocompatible Zn-MOF didn't exhibit cytotoxicity to the cancer cells, whereas the survival percentage of A2780cis cancer cells decreased significantly with increasing incubation time of **19a**@Zn-MOF.[42]

1.3.3. Mononuclear gold(I) mono-NHC complexes as anticancer agents

After the development of auranofin (Fig 1.3.10) as an antirheumatic drug and the discovery of its antiproliferative activity, gold(I) complexes start to play a vital role in metal-based anticancer drugs. Ott and co-workers previously reported a series of gold(I) NHC complexes (**20a-20c**, Fig 1.3.10) with 1,3-diethybenzimidazol-2-ylidene NHC ligands. These complexes of type NHC-Au-L (L= Cl, NHC, PPh_3) were evaluated as potent TrxR inhibitors with remarkable antiproliferative activities *in vitro* against a wide range of tumor cells. Of the entire series, complex **20a** with chloride substituent showed a strong and selective inhibition of TrxR, similar to auranofin. Moreover, this selective inhibition of TrxR over structural related enzymes like glutathione reductase (GR) and glutathione peroxidase (GPx) indicated that covalent interaction with selenium was relevant for the mechanism of drug action.[43]

To study the mechanism of cell death induced by gold(I) NHC complexes, Wölfl and co-workers reported an organometallic complex of Au(I)(NHC)(phosphane) type (**21**, Fig 1.3.10). Strong cytotoxicity *in vitro* was found in various cancer cells, associated with irreversible loss of mitochondrial membrane potential as well as oxidative stress due to the inhibition of TrxR, leading to apoptotic cell death. Moreover, ELISA analysis of signal transduction pathway revealed the cleavage of poly-ADP-ribose polymerase (PARP), the decrease of anti-apoptotic Bcl-2 (B-cell lymphoma 2) and the activation of apoptotic signaling proteins like p38 (mitogen-activated protein kinases) and JNK (c-Jun N-terminal kinases) during cell death. Further results showed that cell damage triggered by gold(I) complexes was

significantly different from other DNA damage agents due to the lack of p53 phosphorylation.[44]

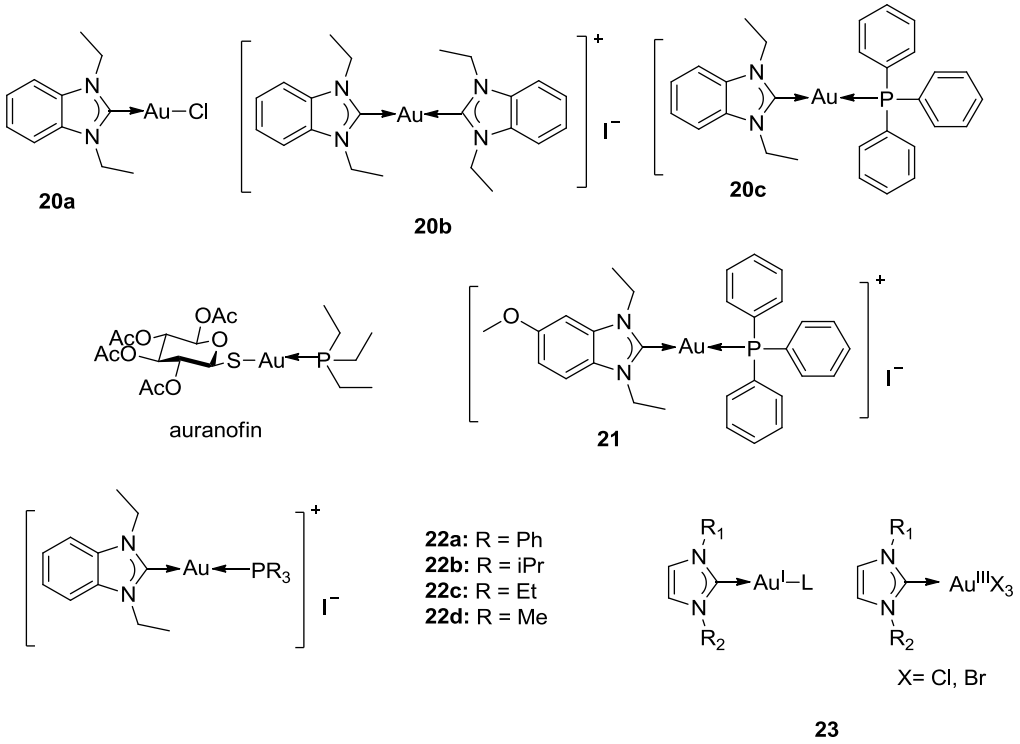

Fig 1.3.10 Gold(I) mono-NHC complexes reported by Ott and co-workers (**20**, **22**, **23**) and reported by Wölfl and co-workers (**21**).

Since phosphine group is one of the most detailed studied ligand in gold complexes and exists in the lead complex auranofin, Ott and co-workers reported a series of organometallic complexes with NHC ligands containing different phosphanes as secondary ligands (**22a-22d** in Fig 1.3.10).[45] All these complexes induced cytotoxicity *in vitro* against HT-29 (colon carcinoma) and MCF-7 (breast carcinoma) cells with IC_{50} values ranging from 0.41 μM to 8.85 μM. Moreover, these complexes can significantly inhibit the seleno-enzyme TrxR and zinc-finger enzyme PARP-1. In terms of the inhibition of TrxR, the activity depends on the size of the substituents of phosphane. Density functional theory (DFT) calculation showed that [Au(NHC)(PPh_3)]I had the lowest binding energy for Au-PR_3 bond, leading to the highest activity of PARP-1.

To study about structure-activity relationship (SAR) of Au-NHC complexes, Ott and co-workers also reported a series of 20 Au-NHC complexes (general structure: **23**,

Fig 1.3.10) with the aim of finding a correlation between TrxR inhibition, cytotoxicity and structures of the compounds. These complexes consisted of compounds with Au(I) and Au(III) atom containing coordinated halides, thiolates and diverse NHC ligands. From the data of TrxR inhibition, gold(I) NHC complexes were stronger TrxR inhibitors than gold(III) with IC_{50} values in the submicromolar or micromolar range, thiophenolate ligands afforded strong TrxR inhibition with IC_{50} values ranging from 0.32 μM to 1.1 μM, and the insertion of amino acid into side chains of NHC nitrogens led to increased TrxR inhibition. Although a direct relationship between TrxR inhibition and cytotoxicity cannot be reached, the data indicated that TrxR played a vital role in the mechanism of action of gold complexes.[46]

With the aim of enlarging SAR studies for the Au-NHC complexes, Gantin, Santini and co-workers designed 1,2,4-triazole based Group 11 NHC complexes (**24**, Fig 1.3.11) and the antiproliferative activities of these complexes were evaluated *in vitro* towards various human cancer cell lines including cisplatin-sensitive and resistant cells. Among the entire series of complexes, the Cu(I)-NHC complex gave the most cytotoxic activity, which was a non-apoptotic cell death pathway, and Au(I) and Ag(I) NHC complexes were able to inhibit the activity of TrxR with IC_{50} values in the nanomolar range (10.1 nM and 7.2 nM, respectively), leading to oxidative stress followed by cell death *via* apoptosis.[24]

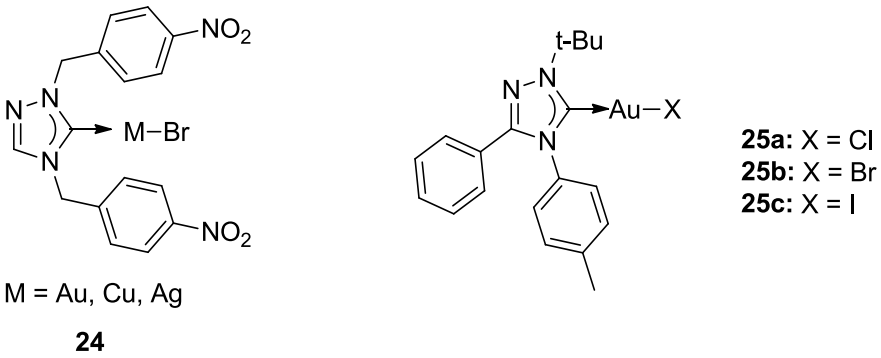

Fig 1.3.11 Gold triazole-based NHC complexes reported by Gantin and co-workers (**24**) and reported by Růžička and co-workers (**25a-25c**).

Three gold(I) complexes (**25a-c**, Fig 1.3.11) of type Au(NHC)X containing triazole-based NHC ligands and diverse halido ligands (X= Cl, Br, I) were reported by

Růžička and co-workers.[47] The antiproliferative activities of these complexes were screened *in vitro* against various cancer cell lines, such as HepG-2 (liver cancer), HeLa S3 (cervical cancer), HL-60 and CCRF-CEM (leukemia) as compared to cisplatin and auranofin. It was shown that complexes **25a** and **25b** with chloride and bromide were more active than the complex **25c** with iodide and cisplatin, and slightly less active than auranofin against HeLa S3 and HL-60 cell lines, but more effective than auranofin against HepG-2. In addition, the apoptotic properties of these complexes were confirmed using cell cycle analysis where they induced an obvious increase in sub-G1 population by around 50% compared to the non-treated control. All complexes also had some effects on cell cycle distribution by slightly increasing the percentage of G2/M phase, suggesting the mechanism of antiproliferative activities of the tested complexes may differ from that of auranofin.

Mohr, Casini, Rigobello and co-workers reported a gold-NHC complex bearing fluorescent anthracenyl group (**26**, Fig 1.3.12).[48] Complex **26** was evaluated for the cytotoxic activity *in vitro* against cancer and normal cells. It showed no selectivity between cancer cells (A2780s and A2780R) and normal cell (HEK-293T). Both on isolated enzyme and in cell extracts, this complex exhibited a pronounced TrxR inhibition compared with related enzyme GR. From the fluorescence microscopy experiments, the cellular distribution displayed a larger diffusion of these molecules in tumor cells when compared to normal cells.

Similarly, Au(I)-NHC complex **27** (Fig 1.3.12) with a fluorescent coumarin group was evaluated for its cellular uptake and subcellular localization in the PC-3 human prostate cancer cell line by Gautier and co-workers. This complex was obtained by the combination of "auto-click" reaction with the transmetallation route. After incubation with complex **27**, the fluorescence was found in the cytoplasm, not in the nucleus. Moreover, it could be specifically localized in mitochondria.[49]

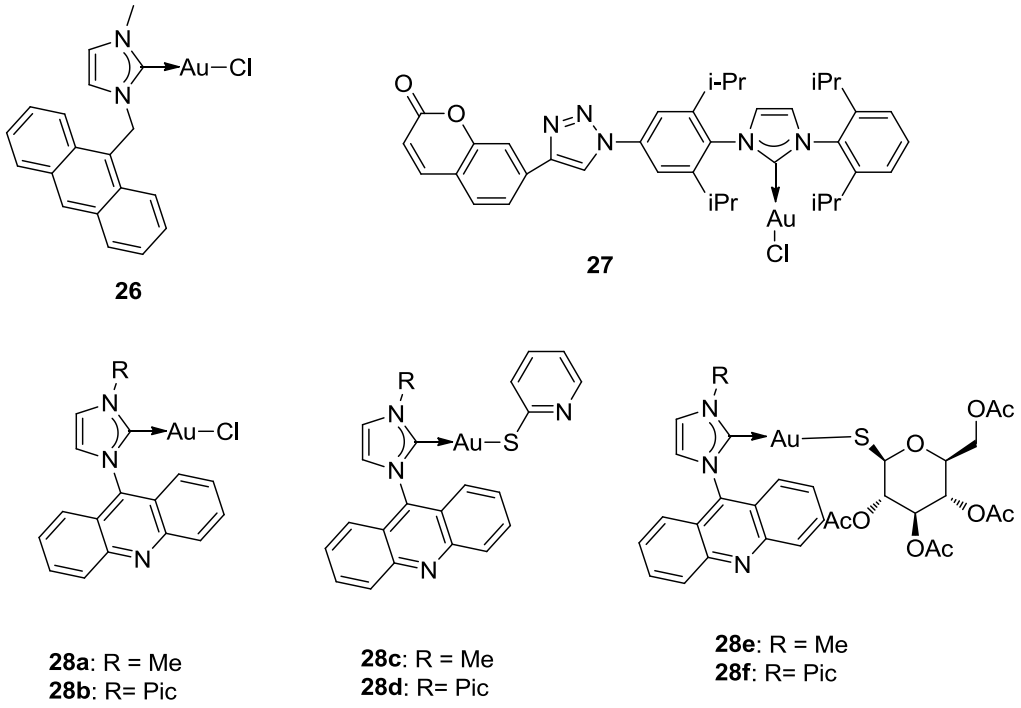

Fig 1.3.12 Gold NHC complexes bearing chromophores reported by Casini and co-workers (**26**), Gautier and co-workers (**27**) and Gimeno and co-workers (**28a-28f**).

Gimeno and co-workers reported a series of gold(I)-NHC complexes bearing a fluorescent acridine group (**28a-28f**, Fig 1.3.12).[50] Their cytotoxicity against A549 (human liver cancer) and Miapaca2 (pancreatic carcinoma) revealed thiolate-Au-NHCs had higher antiproliferative activities *in vitro* as compared to the corresponding chloride derivatives. In particular, complexes **28e** and **28f** with the tetra-*O*-acetyl-1-thio-β-D-glucopyranoside ligand displayed even better anticancer activities, especially in Miapaca2 cells reaching IC_{50} values of 2.8 μM and 3.4 μM, respectively. Furthermore, flow cytometry assay showed that apoptotic pathway was the main mechanism for cell death. From the fluorescent microscopy experiments, it was shown that these complexes were mainly located into lysosomes, and small amout of them have been accumulated in the nucleus.

A series of gold(I) complexes bearing a glucopyranoside-incorporated NHC ligand were reported by D'Amora and co-workers (**29a-29c**, Fig 1.3.13).[51] Different secondary ligands (chloride and phosphane) were coordinated to the gold atom, and these complexes were evaluated for their cytotoxicity *in vitro* against various cancer

cell lines, such as PC-3 (prostate cancer), A375 (malignant melanoma), U-2 OS (osteoblast) and MCF-7 (breast carcinoma) as compared to cisplatin. Among the entire series, complex **29a** and **29b** showed an EC_{50} (half maximal effective concentration) against PC-3 comparable with cisplatin, nevertheless, the complex **29c** was inactive.

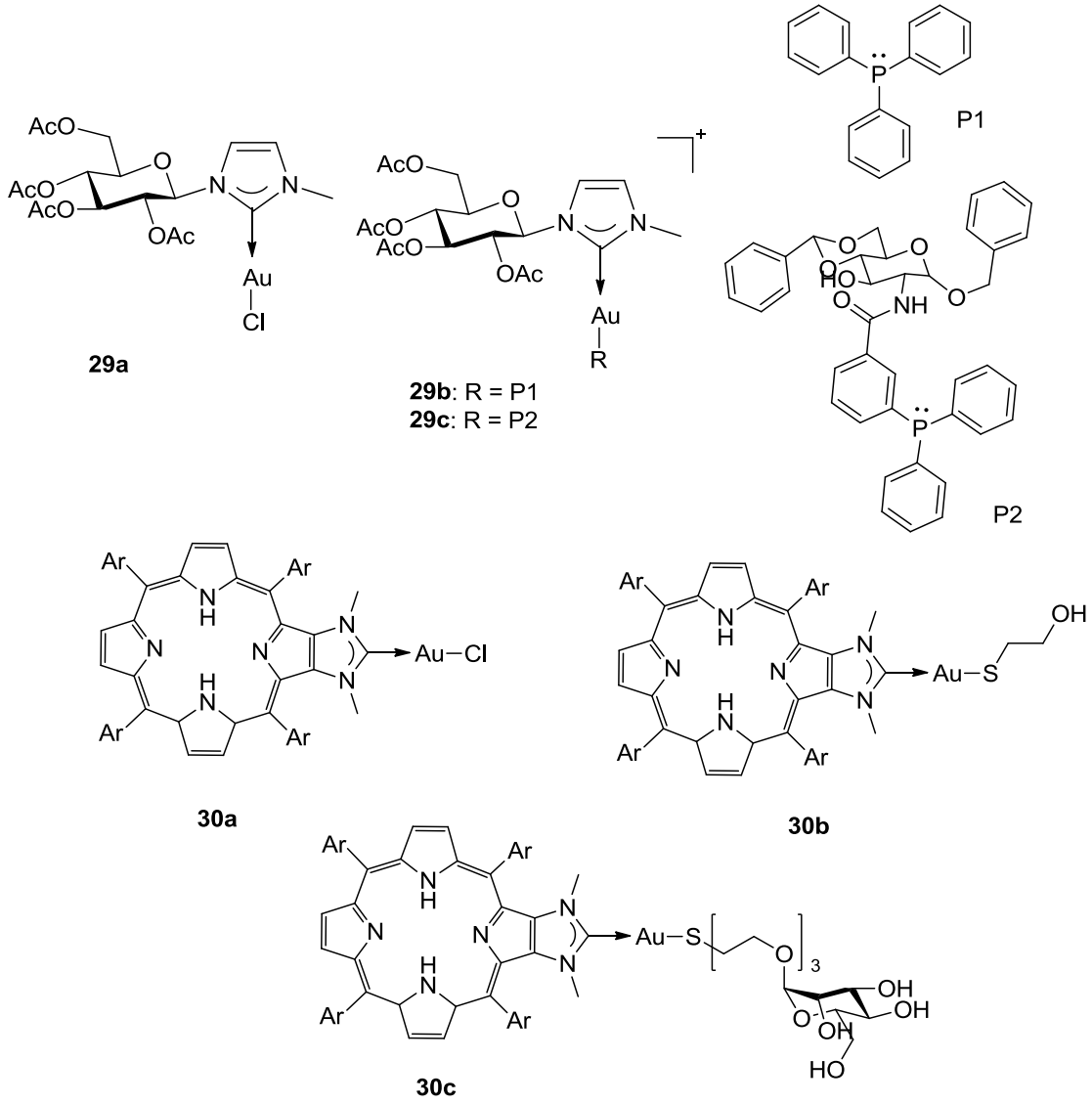

Fig 1.3.13 Gold NHC complexes reported by Amora and co-workers (**29a-29c**) and reported by Richeter and co-workers (**30a-30c**).

Richeter and co-workers reported several Au(I) complexes bearing porphyrins-incorporated NHC ligands (**30a-30c**, Fig 1.3.13). Photodynamic properties of these complexes to kill MCF-7 (human breast cancer) were investigated. The

results showed that these complexes **30a-30c** were not effective in the dark whereas upon irradiation photocytotoxicity was observed, not only due to the photodynamic properties of porphyrin but also due to the peripheral Au(I) complex losing its thiolato ligand upon irradiation.[52]

1.3.4. Bis-NHC gold(I) complexes as anticancer agents

The first discovery of mitochondria targeting property of bis-NHC gold(I) complexes was made by Berners-Price and co-workers. A series of Au(I) bis-NHC complexes functionalized with different alkyl substituents (**31a-31d**, Fig 1.3.14) was investigated about their cytotoxicity *in vitro* against two tumorigenic breast cell lines (MDA-MB-231, MDA-MB-468) and normal human mammary epithelial cells (HMEC). These complexes showed the selectivity between cancer cells and normal cells, and the degree of selectivity was related with the lipophilicity of these complexes. Furthermore, it was shown that complex **31a** induced selective cell death through a mitochondrial apoptotic pathway. TrxR activity was inhibited by 50 % with 5 μM of complex **31a**, whereas no inhibition of glutaredoxin (GR) activity was found. Therefore, TrxR plays an important role in cytotoxicity and its inhibition may lead to the apoptosis in breast cancer cells.[33]

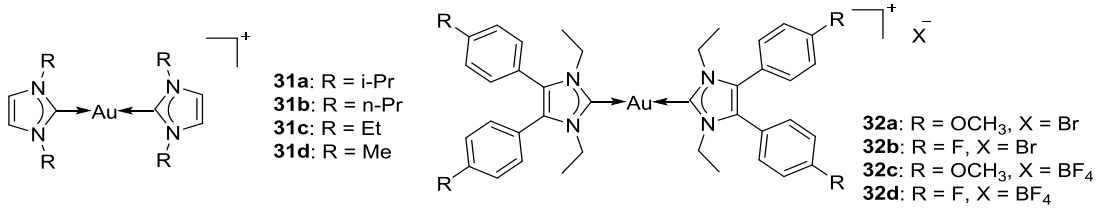

Fig 1.3.14 Bis-NHC Au(I) complexes reported by Berner-Price and co-workers (**31a-31d**) and by Gust and co-workers (**32a-32d**).

Gust and co-workers reported a series of cationic bis[1,3-diethyl-4,5-diarylimidazol-2-ylidene] gold(I) complexes (**32a-32d**, Fig 1.3.14).[53] The antiproliferative activities *in vitro* against MCF-7 (breast carcinoma), MDA-MB-231 (breast carcinoma) and HT-29 (colon carcinoma) cells were evaluated as compared to

cisplatin and fluorouracil (5-FU). Among all the complexes, **32b** being the most cytotoxic compound, gave a pronounced IC_{50} value of 0.1 μM, which was 10-fold higher than that of cisplatin and 5-FU. However, the mode of action remained unclear. Thioredoxin reductase (TrxR), the estrogen receptor (ER) and the cyclooxygenase enzymes (COX), which may be considered as targets for the drug design, can be excluded.

In the past few years, gold complexes bearing NHC ligands have drawn more and more attention. However, only gold mono(NHC) and homo-bis(NHC) complexes have been reported, whereas gold complexes with different kinds of NHC ligands were barely investigated. Triggered by the interest on heteroleptic complexes, Huynh and co-workers reported a series of cationic gold(I) complexes bearing pyrazole-derived NHC and 1,3-disubstitued benzimidazole-derived NHC ligands (**33a-33h**, Fig 1.3.15). The cytotoxicity of complexes **33a-33h** was evaluated *in vitro* against NCI-H1666 (non-small cell lung cancer cell line) as compared with cisplatin. Among the entire series, complex **33a** showed the best effective antiproliferative activity against NCI-H1666, with an IC_{50} value of 0.241 μM, and most of the complexes were more active than cisplatin.[54]

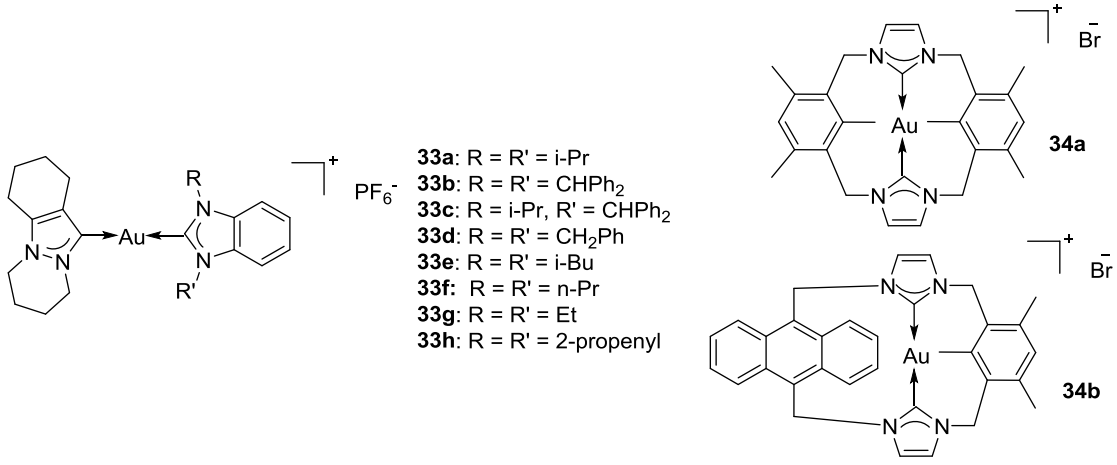

Fig 1.3.15 Bis-NHC Au(I) complexes reported by Huynh and co-workers (**33a-33h**) and by Mao and co-workers (**34a, 34b**).

Mao and co-workers reported two gold(I) complexes bearing NHCs derived from cyclophanes as potential anticancer agents (**34a** and **34b**, Fig 1.3.15).[55] They showed

better antiproliferative activities than cisplatin *in vitro* against human breast carcinoma (MDA-MB-231), human cervical carcinoma (HeLa), human lung adenocarcinoma cisplatin-sensitive A549 and cisplatin-resistant A549R cell lines. In addition, these two complexes were less cytotoxic than cisplatin against normal human liver cell line LO2. In terms of the study of mechanism of action, complex **34a** and **34b** induced apoptosis through mitochondria pathway since they could significantly reduce the mitochondrial membrane potential (MMP). Furthermore, they could stimulate the activation of caspase-3/7 and trigger apoptosis through caspase-dependent pathway.

Since gold carbene complexes are considered to act on some protein targets but not on DNA, Gabbiani and co-worker designed two novel gold(I)-NHC complexes (**35a** and **35b**, Fig 1.3.16) to study their reactivity with different kinds of proteins. Both complexes possessed pronounced cytotoxic activities *in vitro* against A2780 human ovarian carcinoma cells with IC_{50} values of 1.98 μM and 1.68 μM, respectively, and surprisingly showed even better cytotoxicity against the corresponding cisplatin-resistant A2780R cells with IC_{50} values of 0.68 μM and 0.75 μM, respectively. Binding with proteins was monitored through ESI-MS and UV-vis spectrophotometry: no adduct formation was found when reacted with cytochrome c and lysozyme, whereas copper chaperone Atox-1 bearing a characteristic CXXC motif displayed a potent affinity for gold complexes, which suggested that gold-NHC complexes were very selective in metalating proteins, and they could only form adducts with those proteins bearing specific structural motifs for metal recognition.[56]

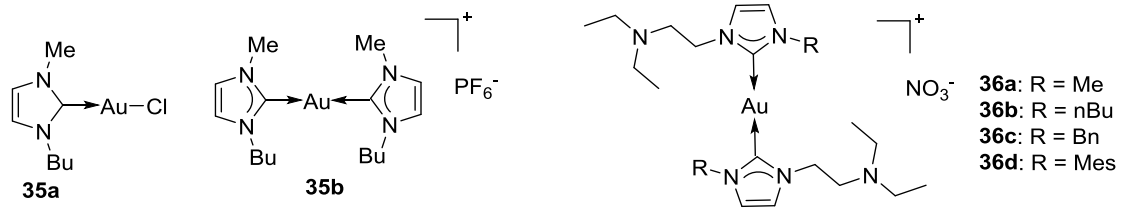

Fig 1.3.16 Au(I) NHC complexes reported by Gabbiani and co-workers (**35a, 35b**) and by Gornitzka, Hemmert and co-workers (**36a-36d**).

Four novel gold(I) complexes bearing aliphatic amino-functionalized NHC ligands

(**36a-36d**, Fig 1.3.16) were synthesized, characterized and evaluated for their cytotoxicity *in vitro* on PC-3 prostate cancer cell line by Gornitzka, Hemmert and co-workers. The lipophilicity (log P) of these complexes was in good agreement with the antiproliferative activities. The most active complex **36d** exhibited pronounced cytotoxicity against five different kinds of cell lines (PC-3 prostate cancer, MCF-7 breast cancer, U87 brain cancer, A549 lung cancer and Hep3B liver cancer) with GI_{50} values ranging from 400 nM to 1 μM, whereas it was insensitive to normal primary human umbilical vein endothelial cells (HUVECs) with an GI_{50} value over 5 μM, suggesting a selectivity between cancer cells and healthy cells.[57]

In order to extend the structural diversity of coordinated NHC ligands, Ott and co-workers prepared gold(I) complex **37 (**Fig 1.3.17) bearing an aminotriazole-based NHC ligand *via* silver(I) oxide route. The complex **37** displayed pronounced cytotoxic activities *in vitro* against HT-29 (colon carcinoma) and MDA-MB-231 (breast carcinoma) cells with IC_{50} values in the low micromolar range (2.1 μM and 1.0 μM, respectively), which is comparable with imidazole and benzimidazole-based $[Au(NHC)_2]^+$ complexes. In addition, it showed moderate TrxR inhibition activity with an IC_{50} value of 1.2 μM. Cellular uptake studies demonstrated a fast accumulation in HT-29 cells, which could be related to cationic charge and lipophilic property of the complex.[58]

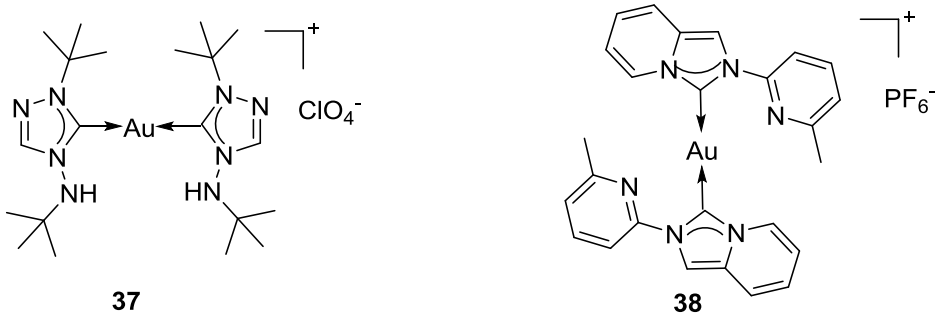

37 **38**

Fig 1.3.17 Bis-NHC Au(I) complexes reported by Ott and co-workers (**37**) and by Saha, Dinda and co-workers (**38**).

A novel Au(I)-NHC complexes (**38**, Fig 1.3.17) derived from 2-pyridin-2-yl-2*H*-imidazo[1,5-α]pyridine-4-ylium salt was synthesized by Saha, Dinda and

co-workers. The cytotoxic activities of complex **38** were carried out *in vitro* on a panel of cancer cells, such as HepG-2 (human hepatocellular carcinoma), HCT-116 (human colorectal carcinoma), MCF-7 (human breast adenocarcinoma) and A549 (human non-small lung carcinoma). In addition, IC_{50} values of **38** were 2-3 times lower than those of cisplatin. Furthermore, **38** could induce apoptotic change in cell morphology (namely, cell shrinkage and rounding, chromatin condensation, and DNA fragmentation), mediate cell cycle arrest at the G2/M phase, and mediate cell death through mitochondrial pathway in HepG-2 cells.[59]

Three gold(I) complexes (**39a-39c**, Fig 1.3.18) of the type $[Au(NHC)_2]^+$ bearing ferrocene-functionalized NHC ligands were prepared by Arambula et al.. From a series of cell proliferation assays, it was shown that their cytotoxic activities *in vitro* were proportional to the amount of ferrocene in the complexes (IC_{50} values of **39a** < **39b** < **39c**). Moreover, complex **39c** (IC_{50} = 0.14 μM) displayed over 10 times higher antiproliferative activity than auranofin (IC_{50} = 1.67 μM) against A549 lung cancer cells. Complexes **39a-39c** were capable of time-dependent TrxR inhibition similar to auranofin as a result of lipoate reduction and intracellular free zinc elevation. Furthermore, RNA microarray gene expression was used to explain the mechanism of action of gold complexes, and it revealed that **39c** can induce oxidative stress in endoplasmic reticulum.[60]

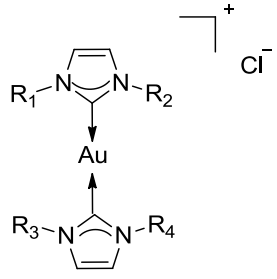

39a: R_1, R_4 = Mes; R_2, R_3 = CH_2-Ph
39b: R_1, R_4 = Mes; R_2, R_3 = CH_2-Fc
39c: R_1, R_2, R_3, R_4 = CH_2-Fc

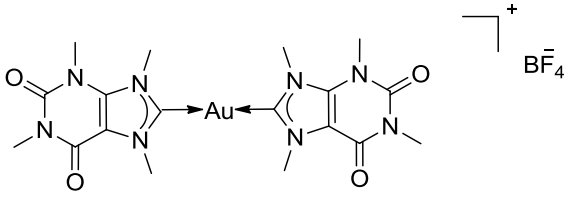

40

Fig 1.3.18 Bis-NHC Au(I) complexes reported by Arambula et al. (**39a-39c**) and by Casini and co-workers (**40**).

To study about the interaction of the biscarbene gold(I) complex and DNA sequence, [Au(9-methylcaffein-8-ylidene)$_2$]BF_4 (**40**, Fig 1.3.18) was investigated through different physio-chemical methods. Complex **40** was recently reported by Casini and co-workers to form stable adducts with human telomeric DNA (HT-DNA) folded into the G-quadruplexes.[61] A few years later, Messori and co-workers reported the identification of conformational changes experienced by Tel23 (5'-TAGGG(TTAGGG)3-3') upon interaction with gold-bis(NHC) complex **40**. A series of computational studies revealed the inherent non-covalent metallodrug/DNA interaction, and it was shown that Au(NHC)$_2$/Tel23 adduct was capable of producing a strong and selective inhibition of telomerase activity in cancer cells, which could be a validated target for new anticancer drug development.[62]

A series of gold-bis(NHC) complexes (**41a-41d**, Fig 1.3.19) were prepared by Ott and co-workers and their antiproliferative activities against cancer cells were evaluated. All these complexes were effective with IC_{50} values in the low micromolar and nanomolar range. Complexes **41c** and **41d** exhibited much higher activities *in vitro* than auranofin against four different kinds of cells (namely, HT-29 colon carcinoma, MCF-7 breast cancer, MDA-MB-231 breast cancer and RC-124 healthy human kidney cells) and reached IC_{50} values in the range of 0.05-0.18 μM. Protein binding and cellular uptake experiments indicated a strong correlation between cellular bioavailability and cytotoxic effects.[63]

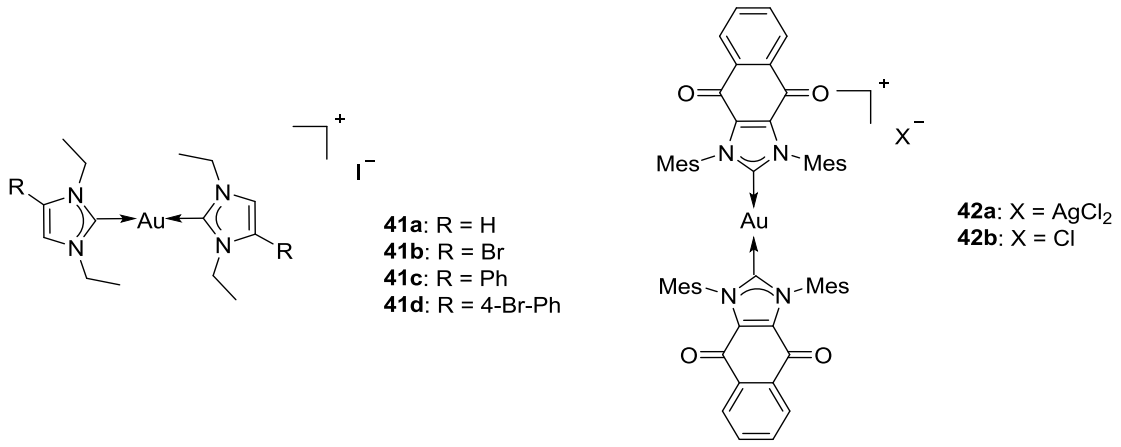

Fig 1.3.19 Bis-NHC Au(I) complexes reported by Ott and co-workers (**41a-41d**) and by Arambula and co-workers (**42a and 42b**).

To achieve an approach of targeting antioxidant pathway, gold(I) complexes bearing 1,4-naphthoquinone-based NHC ligands (**42a** and **42b**, Fig 1.3.19) were designed and synthesized by Arambula and co-workers and their cytotoxic effects were tested *in vitro* against a panel of human cancer cell lines. Complex **42a**, containing two NHC-quinone groups, was found to show much higher antiproliferative activities than the corresponding mono(NHC)-Au complex. In addition, A549 cells treated with complex **42a**, which was found to localize in mitochondria, led to an increase of ROS production. Furthermore, complex **42a** was found to induce cell death via apoptotic pathway, and it was shown to be effective in zebrafish bearing A549 xenografts.[64]

1.3.5. Polynuclear NHC complexes as theranostic agents

The first example concerning the luminescence studies of the intracellular distribution of biologically active NHC complexes was reported by Berners-Price and co-workers in 2006.[65] Two dinuclear gold(I) complexes (**43-cis** and **43-trans**, Fig 1.3.20) bearing bidentate NHC ligands were designed to support Au-Au interactions of a predetermined length, which led to native luminescence of these complexes.

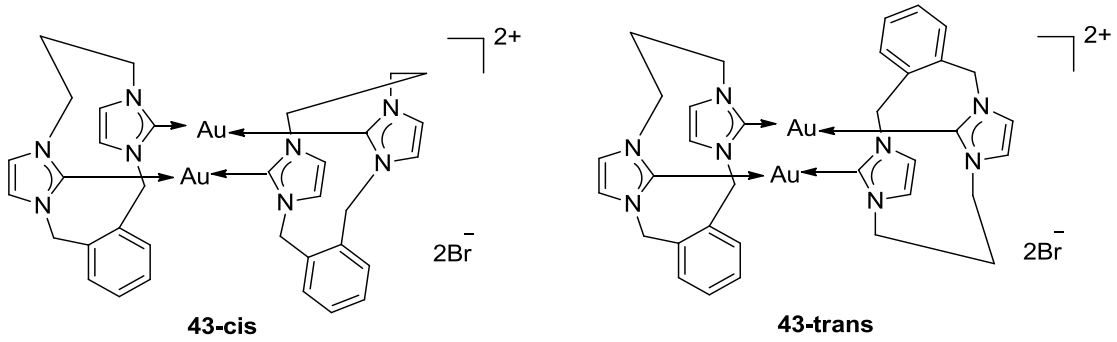

Fig 1.3.20 Polynuclear NHC complexes reported by Berners-Price and co-workers (**43-cis** and **43-trans**).

The cellular uptake and distribution of complex **43-cis** were evaluated in RAW264.7 cells (mouse macrophage cancer cell line) by fluorescence confocal microscopy. Comparison with bright-field images permitted exclusion of cell nuclei as targets. Furthermore, colocalization studies using LysoTracker red and MitoTracker

green manifested the localization of gold complexes in lysosomes rather than mitochondria (Fig 1.3.21).[65]

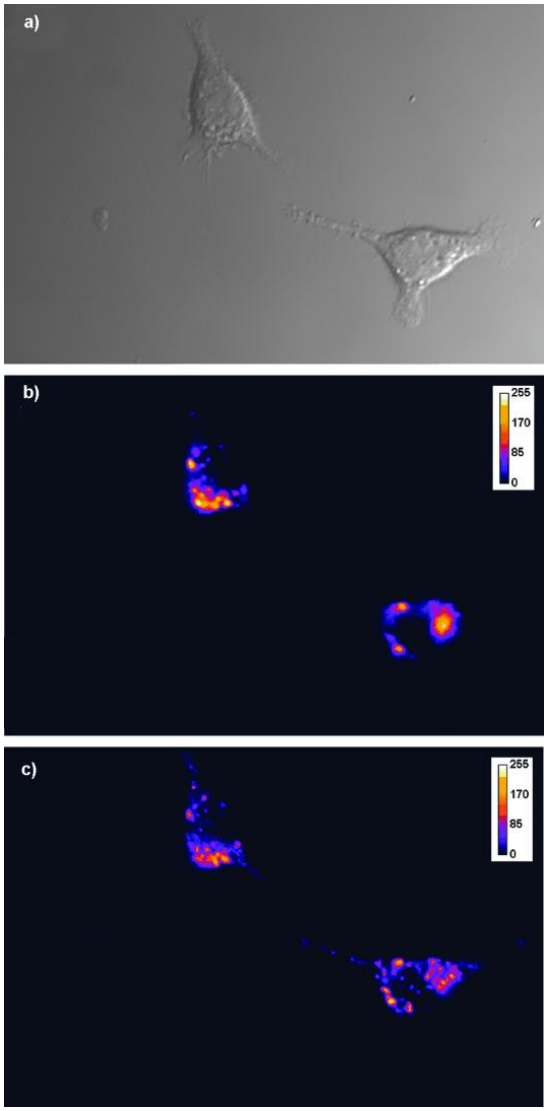

Fig 1.3.21 (a) Bright-field image, (b) luminescence image showing **43-cis** distribution and (c) luminescence image showing LysoTracker red distribution.[65]

Incorporation of organic chromophores within the carbene structure has been a straightforward method in fluorescence confocal microscopy technologies, leading to the development of theranostic agents. In the previous paragraph, several NHC-metal complexes with organic chromophores have been mentioned about their anticancer activities, and additionally, they displayed luminescence that enabled them to study cellular distribution. Complex **34a** and **34b** (Fig 1.3.15) reported by Mao and co-workers contained fluorescent anthracene groups incorporated in the cyclic

bis(NHC) ligands.[55] These complexes were excited at 405 nm and blue emission could be observed on the confocal microscopy. Colocalization assays with organelle-specific stains, such as MitoTracker green, manifested these complexes were localized in mitochondria and not in lysosomes (Fig 1.3.22).

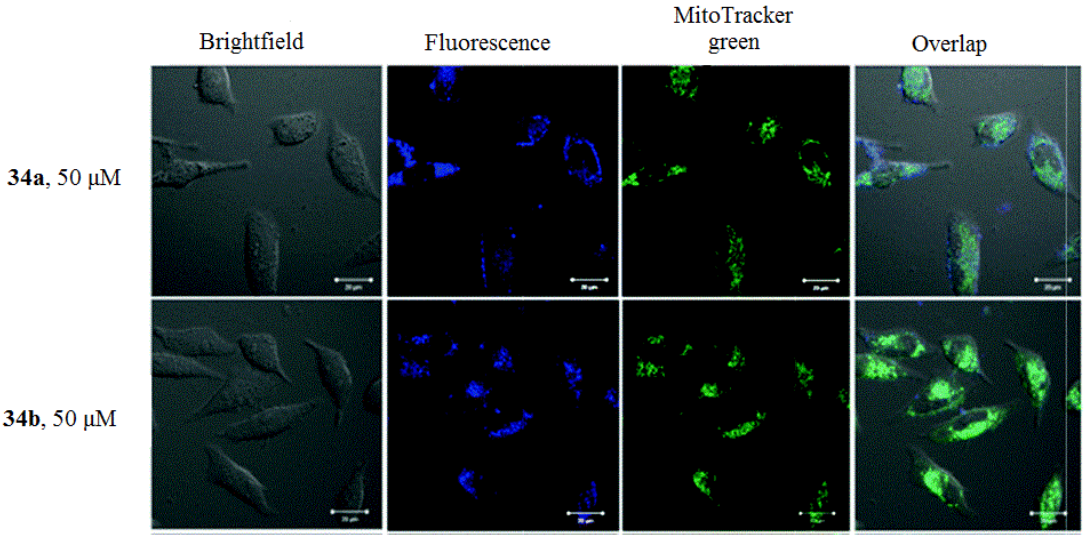

Fig 1.3.22 Determination of intercellular localization of compound by confocal microscopy (63 * oil-immersion objective lens). **34a** and **34b** were excited at 405 nm (blue). MitoTracker green was excited at 488 nm (green).[55]

Other examples like complex **26** (Fig 1.3.12) bearing fluorescent anthracenyl group,[48] complex **27** (Fig 1.3.12) with fluorescent coumarin group[49] and complexes **28a-28f** (Fig 1.3.12) containing fluorescent acridine group[50] could also act as theranostic agents for cellular distribution studies.

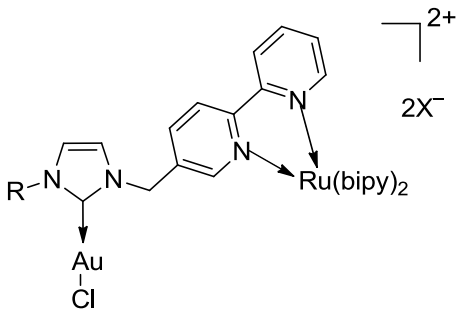

44a: R = Me, X = PF_6
44b: R = nBu, X = Cl, Br
44c: R = Bn, X = PF_6

Fig 1.3.23 Au(I)-Ru(II) NHC complexes reported by Gornitzka, Hemmert and co-workers (**44a-44c**).

Another way to make a bioactive molecule luminescence consists of the attachment of an organometallic dye. Gornitzka, Hemmert and co-workers reported three heterobimetallic gold(I)-ruthenium(II) complexes containing heteroditopic bipyridine-based NHC ligands (**44a-44c**, Fig 1.3.23).[66] Then *in vitro* cytotoxic, antileishmanial and antimalarial activities of these complexes were evaluated, and all these complexes showed moderate effects due to the presence of $Ru(bpy)_3$ moiety. The fluorescent confocal microscopy experiments indicated that **44b** was localized in the cytoplasm. Experiments using MitoTracker green for mitochondria labeling and DAPI for nuclei labeling demonstrated that no colocalization could be found in mitochondria or in nucleus (Fig 1.3.24).

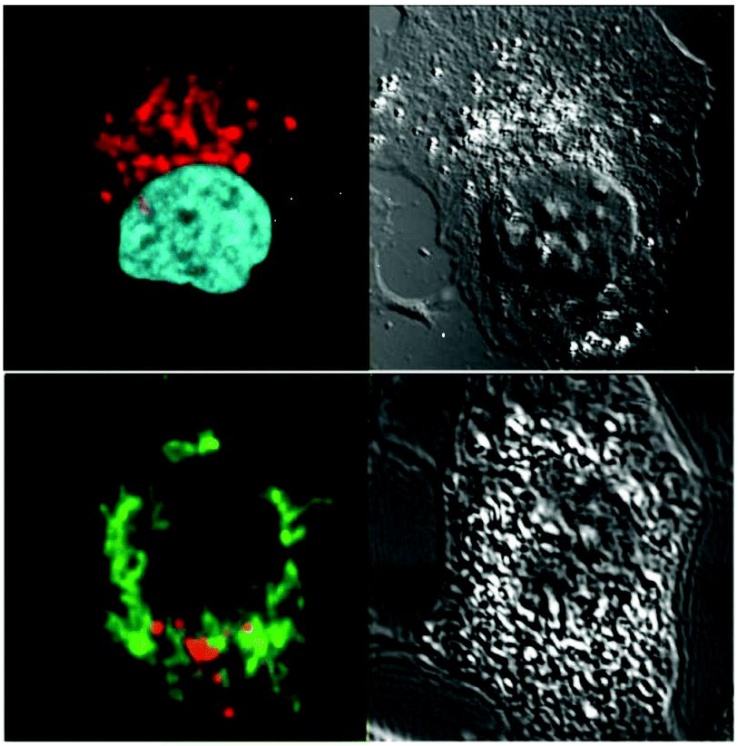

Fig 1.3.24 Fluorescence and transmission images of the cells treated with **44b** (in red) and labeled with MitoTracker (in green, bottom) or DAPI (cyan, top).[66]

1.3.6. *In vivo* anticancer studies of Au(I)-NHC complexes

Despite the general interest in the development of gold-based complexes and the high *in vitro* anticancer activity shown in several gold NHC complexes, there are only few studies to investigate their *in vivo* anticancer activity.

Zou et al. evaluated the *in vivo* anticancer effect of the dinuclear gold(I) complex (**18a**, Fig 1.3.9) bearing a bridging bis(NHC) ligand and a diphosphine ligand. Complex **18a** can significantly inhibit tumor growth in mice bearing HeLa xenograft and mice bearing highly aggressive mouse B16-F10 melanoma, whereas no mouse death or body weight loss were observed. Moreover, toxicity studies suggested that **18a** did not show systematic anaphylaxis on guinea pigs and localized irritation on rabbits.[67]

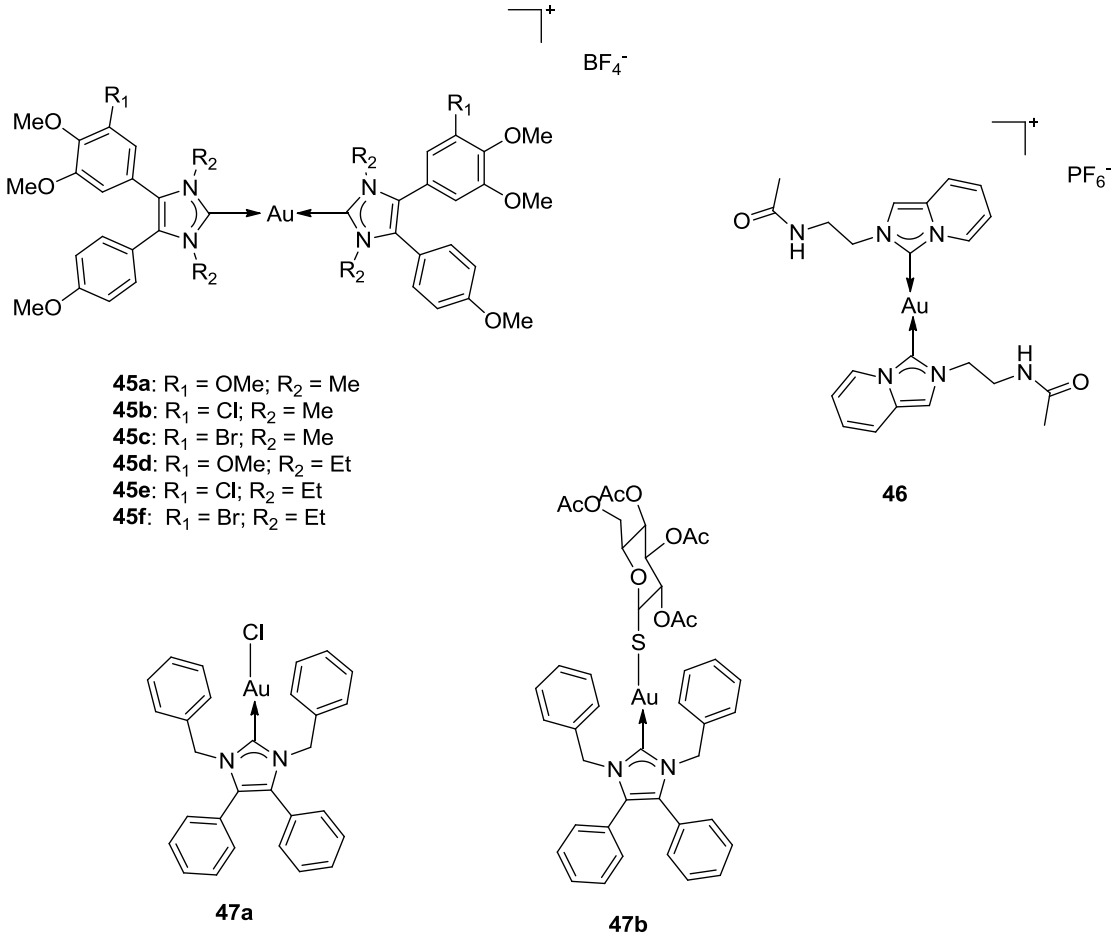

Fig 1.3.25 Au(I)-NHC complexes for *in vivo* studies reported by Schobert and co-workers (**45**), Dinda, Saha and co-workers (**46**) and Tacke and co-workers (**47**).

A series of gold(I) bis-carbene complexes (**45a-45f**, Fig 1.3.25) with NHC ligands derived from the plant metabolite combretastatin A-4 (CA-4) was designed and synthesized by Schobert and co-workers.[68] The *in vivo* anticancer activity and tolerance of gold complexes **45d** and **45f** were investigated in a Balb/c mouse xenograft model of highly metastatic B16-F10 mouse melanoma cells. Two weeks after continuous implantation of 200,000 cells in mice, complexes **45d** and **45f** were repeatedly administered at 15 mg per kg body weight for two consecutive days. The results showed that this treatment was well tolerated by the mice, leading to a slight decrease in body weight, and noticeable tumor regression.

Another gold bis(NHC) complex (**46**, Fig 1.3.25) was tested *in vivo* on mice bearing the B16-F10 mouse melanoma by Dinda, Saha and co-workers.[69] Complex **46**

was administered at the dosages of 5 and 10 mg/kg body weight per day from 15th day onward since the day of injection of B16-F10 cells in the mice till the 23rd day. Dose-dependent decrease in the tumor size was observed following treatment with complex **46**, whereas body weight remained nearly constant.

The two neural Au(I) complexes 1,3-dibenzyl-4,5-diphenyl-imidazol-2-ylidene gold(I) chloride **47a** (Fig 1.3.25) and its 2',3',4',6'-tetra-*O*-acetyl-β-D-glucopyranosyl-1'-thiolate derivative **47b** (Fig 1.3.25) were tested *in vivo* in a Caki-1 xenograft mouse model.[70] Firstly, the maximum toterable dose (MTD) was determined with single injection to groups of two mice, giving values of 10 mg/kg for **47a** and 7.5 mg/kg for **47b**. In tumor xenograft experiments, these complexes were given at MTD in six injections to two cohorts of six Caki-1 tumor-bearing NMRI: nu/nu mice. Complex **47a** at the dose of 10 mg/kg and complex **47b** at the lower dose of 7.5 mg/kg induced both low toxicities in the form of abdominal swelling but no significant body weight loss was found in both groups. Both complexes displayed a significant and identical tumor volume growth reduction, and the optimal T/C values (tumor size in the treated group in relation of non-treated control) of 0.47 were observed on day 19 for **47a** and on day 29 for **47b**.

1.4. Metal complexes for photodynamic therapy application

1.4.1. Mechanism of action of photodynamic therapy

Photodynamic therapy (PDT), an emerging light-activated treatment for cancer, has been successfully used for skin cancer for over 100 years.[71] PDT requires three essential non-toxic components, namely, light, a photosensitizer (PS) and molecular oxygen (Fig 1.4.1). Reactive oxygen species (ROS), such as singlet oxygen and free radicals, are generated by the energy transfer between the excited state of PS and the ground state of molecular oxygen, leading to cellular toxicity.[72]

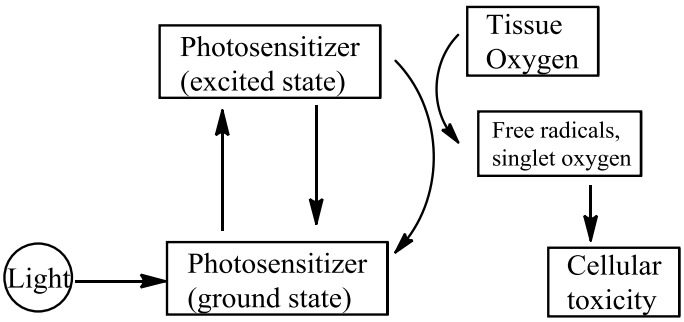

Fig 1.4.1 Mechanism of action of photodynamic therapy (PDT).

Generally, absorption of light (photons) leads to a transform from a ground state (singlet state) of PS into an excited state (triplet state) *via* an excited singlet state. Then two kinds of relaxation reactions can occur (Fig 1.4.2). Firstly, the PS in triplet state can transfer its energy to molecular oxygen ($^3O_2$) leading to singlet oxygen ($^1O_2$), which is the major cytotoxic agent involved in photodynamic therapy (type II process). Alternatively, the triplet state PS can react directly with a substrate, such as the cell membrane or a molecule, and transfer a hydrogen atom or electron to form radicals. These radicals interact with oxygen to produce oxidation products ($^1O_2$), which is a type I process.[73]

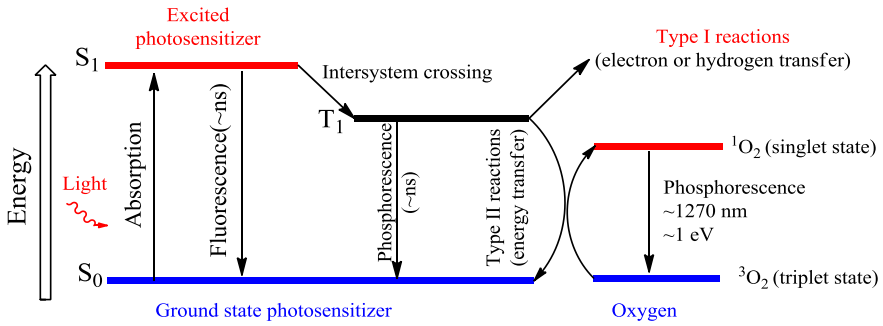

Fig 1.4.2 Photosensitization process illustrated by a modified Jablonski diagram.

1.4.2. Ruthenium(II) complexes as photodynamic anticancer agents

To date, Food and Drug Administration (FDA)-approved sensitizers for PDT were mainly porphyrinoid compounds. The first PS for treatment of different kinds of cancer all over the world including the United State (by FDA in 1995) was photofrin (Fig 1.4.3).[74] However, its clinical trials were hampered by poor solubility of porphyrin derivatives, low quantum yield of singlet oxygen ($^1O_2$) production and lack

of selectivity between normal cells and cancer cells. In 2002, Foscan® (dihydroporphyrin or chlorine, Fig 1.4.3) was granted marketing authorization in several countries for the treatment of neck and head cancers.[75] In urology, the french company Steba-Biotech has developed Tookad®, currently in phase III for the treatment of prostate cancer.[76] Tookad® (Fig 1.4.3) is a palladium-containing lipophilic bacteriochlorophyll; his maximum absorption is at 760 nm which allows light to penetrate deeply into tissue (up to 2 cm instead of 3-5 mm for porphyrins), and its low distribution in tissue allows rapid clearance. These three PDT agents are based on tetrapyrrole or porphyrin derivatives. The phototoxicity induced by these PSs has an absolute dependence on oxygen, which excludes activity in hypoxic tissues and compromises clinical dosimetry *in vivo*.

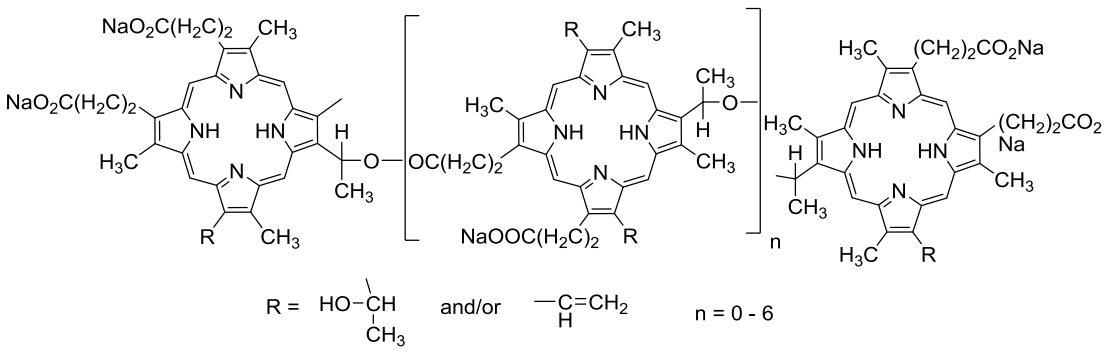

Photofrin (porfimer sodium)

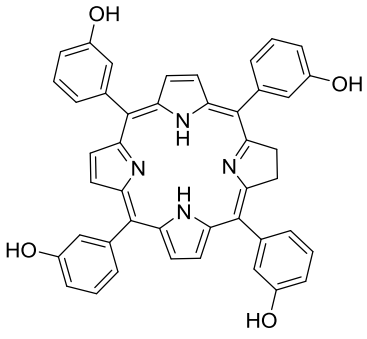

Foscan (temoporfin)

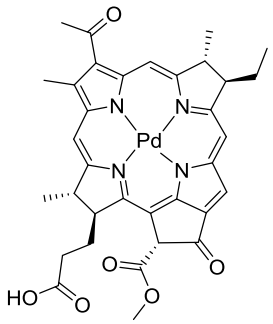

Tookad (padoporfin)

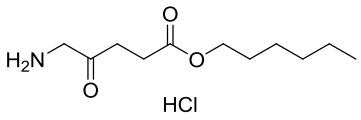

Hexvix (hexaminolevulinate)

Fig 1.4.3 Photosensitizers in clinical PDT.

With regard to bladder cancer, Hexvix® (hexaminolevulinate, Fig 1.4.3), which induces fluorescence by cystoscopy in blue light, is a pro-drug indicated in addition to conventional cystoscopy in white light, to aid diagnosis and treatment in patients with

known or strongly suspected bladder carcinoma.[77] It is a pro-drug with no photochemical activity that will enter the body and initiate a series of biochemical reaction in the cells after irradiation leading to the formation of PS drug, hypericin, a powerful PS. This is a polycyclic aromatic compound belonging to the class of quinone derivatives used for fluorescence diagnosis of bladder carcinoma.[78] Hypericin has drawn a lot of attention in its possible use in the treatment of bladder cancer. It causes damage to the urothelial tumor, however, there are 2 to 5% of tumor cells that can survive after photodynamic treatment, which leads to the regrowth of tumors after a prolonged period of time.

Various researchers in the field of coordination chemistry have recognized the importance of metals in medicine and have made significant progress towards the development of unique organometallic PSs.[79] Most of the metal complexes proposed as PSs are ruthenium polypyridyl complexes, the Ru(II) complex TLD1433 (a Ru(II) Dyad derived from 2-(1-pyrenyl)-1*H*-imidazo[4,5-f][1,10]phenanthroline, Fig 1.4.4) being approved to enter phase Ib clinical trials for non-muscle invasive bladder cancer in Canada (Parenteral, NCT03053635).[80]

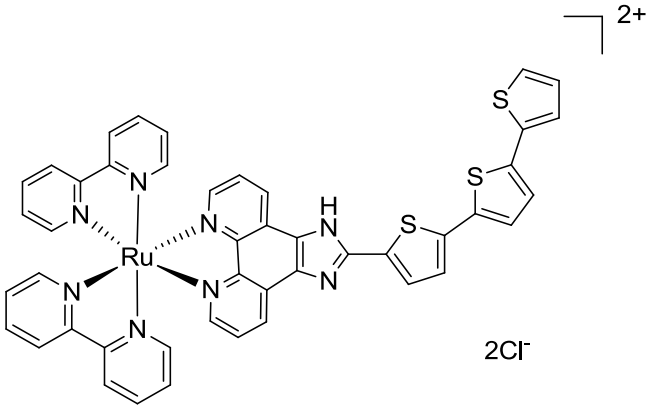

TLD1433

Fig 1.4.4 Structure of TLD1433.

Gasser and co-workers reported two Ru(II) polypyridyl complexes (**48a** and **48b**, Fig 1.4.5) as PSs for PDT. Complex **48b** displayed moderate phototoxicity against HeLa (human cervical cancer cells) in micromolar range with an IC_{50} value of 25.3 μM, and more importantly, no dark toxicity was found for this compound. Complex

48a manifested phototoxicity in the nanomolar range with an IC_{50} value of 0.6 μM against HeLa cells, and phototoxic index (PI) was 80 relative to the dark experiments. From the confocal microscopy experiments, it was shown that complex **48a** accumulated in the cytoplasm, particularly in mitochondria. The results confirmed by ICP-MS showed an accumulation of 67% of Ru taken up into mitochondria for complex **48a**, and by comparison, the cellular uptake for complex **48b** was more diffuse. Therefore, improving the cellular uptake of the complexes may help to increase the photodynamic activity and selectivity against cancer cells.[81]

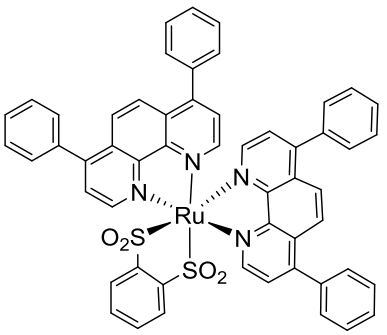

48a

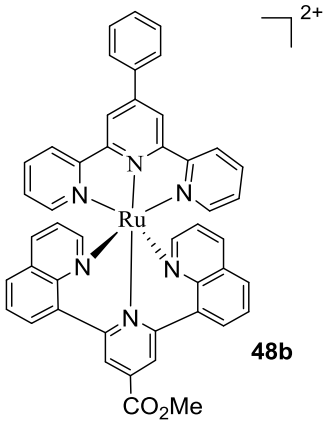

48b

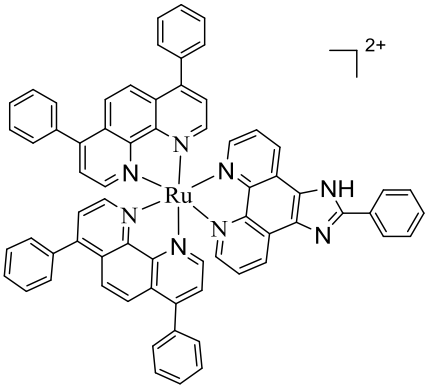

49a

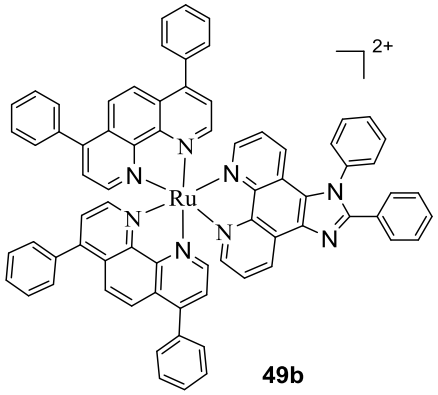

49b

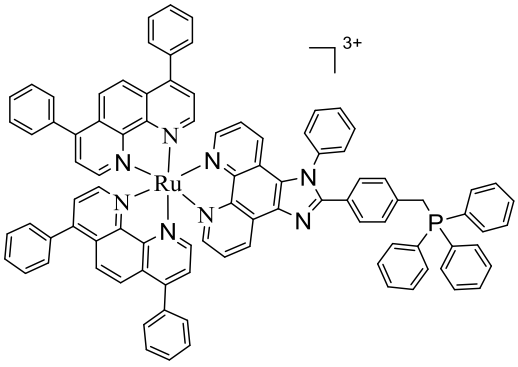

49c

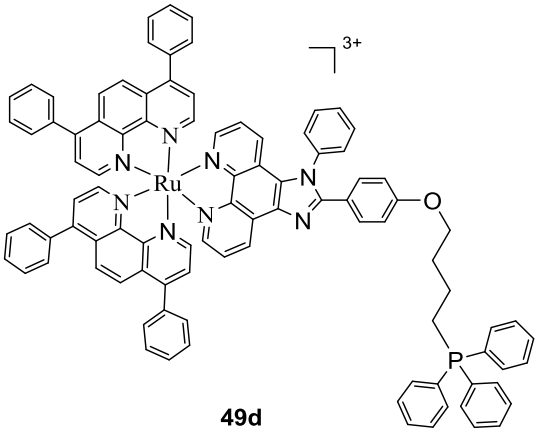

49d

Fig 1.4.5 Ruthenium(II) complexes as PSs reported by Gasser and co-workers (**48a** and **48b**) and by Chao and co-workers (**49a-49d**).

Since the irradiation wavelength of the one-photon (OP) PSs for PDT was visible light, which had limited tissue penetration, further work was done to develop novel ruthenium two-photon (TP) PSs that were active in the red-to-NIR region. Chao and co-workers developed four ruthenium(II) polypyridyl complexes (**49a-49d**, Fig 1.4.5), which acted as mitochondria-targeting TP PDT agents. These complexes **49a-49d** displayed remarkable singlet oxygen quantum yield (0.74-0.81) and two-photon absorption cross section (σ2) values were ranged from 124 to 198 GM (1 GM = 10^{-50} cm^4 s $photon^{-1}$), which were much larger than that of tetraphenylporphyrin (H_2TPP, σ = 2.2 GM). In addition, OP photocytotoxicity of these complexes towards HeLa monolayer cells was evaluated. Complexes **49a-49c** exhibited similar phototoxic activity with IC_{50} values of 12.4-15.5 μM, whereas **49d** displayed the lowest IC_{50} value of 3.5 μM, having a PI value of over 28. Furthermore, two-photon photocytotoxicity against 3D multicellular spheroids (MCSs) was assessed. After laser irradiation, complex **49a-49d** displayed a very effective inhibition of MCSs growth. Remarkably, complex **49d** demonstrated the lowest IC_{50} value of 1.9 μM in TP PDT (λ_{irr} = 830 nm) for 3D MCSs, suggesting this cationic ruthenium(II) complex as a mitochondria-targeting TP PDT agent.[82]

1.4.3. Iridium(III) complexes as photodynamic anticancer agents

Iridium(III) complexes as PSs were studied due to their easy synthesis, air and moisture stability. Furthermore, heteroleptic Ir(III) complexes with bipyridyl and cyclometalated ligands have displayed high photostability due to high metal-centered state and ease of modulation of HOMO and LUMO energy levels.[79b]

Four cyclometalated iridium(III) complexes bearing β-carboline (a kind of biologically active alkaloid) ligands (**50a-50d**, Fig 1.4.6) was designed and synthesized by Mao and co-workers. Upon visible light (425 nm) irradiation, they displayed strong photocytotoxicity against cancer cells. Remarkably, complex **50b** showed the most effective phototoxic activity with a PI value of over 833 against

A549 cells (human lung carcinoma) and high selectivity between cancer cells (A549) and normal cells (LO2). Further mechanism studies demonstrated that **50b**-mediated PDT triggered caspase- and ROS-dependent apoptotic cell death through lysosomal damage and cathepsin B release. In addition, this compound could be used to monitor real-time lysosomal integrity during PDT.[83]

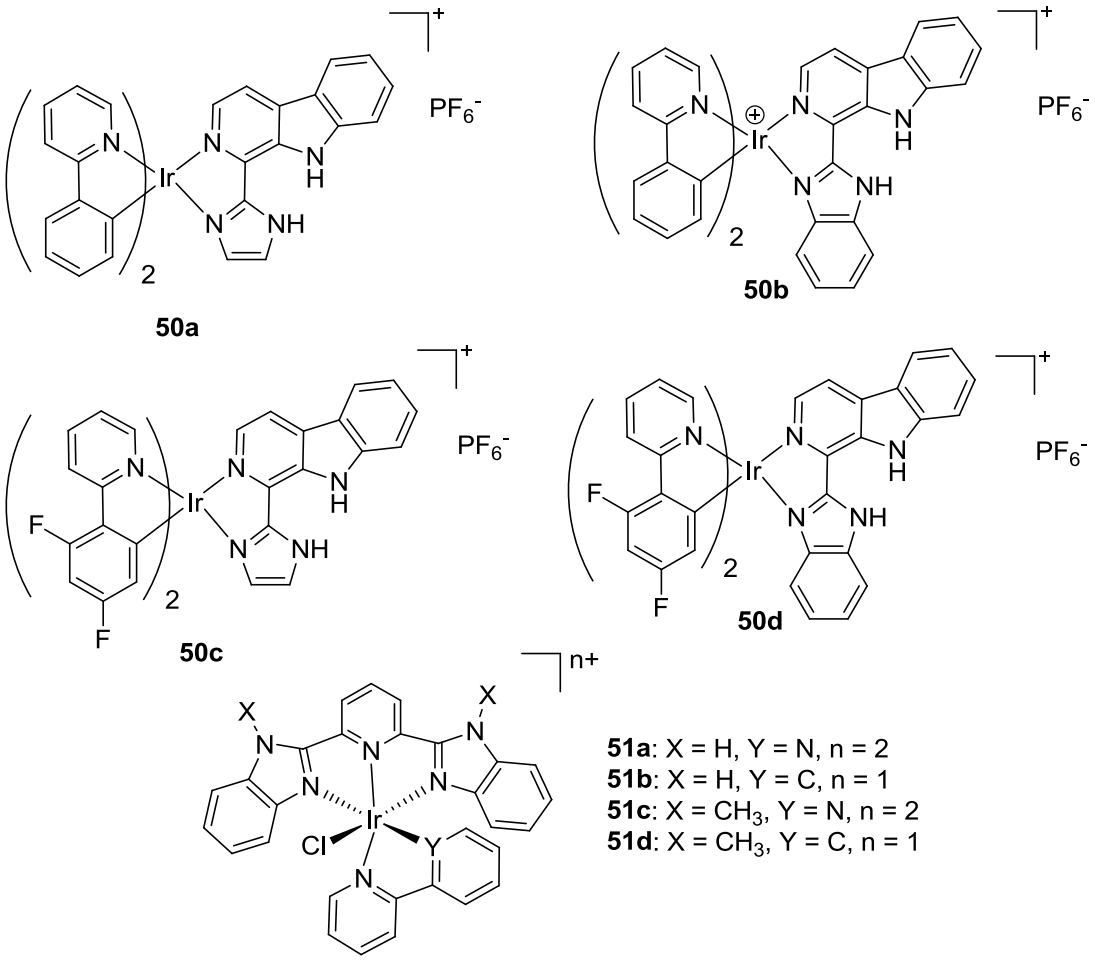

Fig 1.4.6 Iridium(III) complexes as PSs reported by Mao and co-workers (**50a-50d**, **51a-51d**).

Based on this work, Mao and co-workers reported a second generation of mixed-ligand phosphorescent iridium complexes (**51a-51d**, Fig 1.4.6).[84] These complexes showed high luminescence quantum yields, long lifetimes and high aqueous photostability. Since complexes **51b** and **51d** with phenyl-pyridine (ppy) ligands were more lipophilic than **51a** and **51c** with bipyridine (bpy) ligands, they can be taken up into A549 (lung carcinoma) cells more effectively. The intracellular

phosphorescence intensity of **51b** at pH roughly mimicking the lysosomal environment (5.0) was much stronger than that at pH in the physiological condition (7.4). This result manifested that the selective lysosomal targeting property of **51b** originated from its pH-dependent emission. However, **51d** showed similar phosphorescence intensity both in acidic and physiological condition, and it can specifically target mitochondria. Notably, complex **51b** displayed the best PDT activity against various cell lines with a photocytotoxicity index (PI) ranging from 12.7 to 54.1. From the study of mechanism, it was shown that **51b** and **51d** induced apoptotic cell death through caspase- and ROS-dependent pathways. The results revealed the potential of these iridium(III) complexes as novel photodynamic anticancer agents.

Zhao and co-workers developed two PSs based on iridium(III) complexes (**52a** and **52b**, Fig 1.4.7), which specifically target the mitochondria and lysosomes. The singlet oxygen quantum yields (Φ_Δ) of **52a** and **52b** were 0.17 and 0.21, respectively, which revealed their potentials as PDT agents. The phototoxic activities of these complexes under normoxia (normal oxygen condition) and hypoxia (low oxygen condition) were evaluated. The results indicated that mitochondria-targeting complex **52a** had a better PDT activity than lysosome-targeted complex **52b**, especially under hypoxia condition, which was an advantage for PDT applications in hypoxic solid tumors. One explanation was that the complex **52a** displayed a more efficient inhibition of mitochondrial respiration leading to a higher mitochondria oxygen concentration.[85]

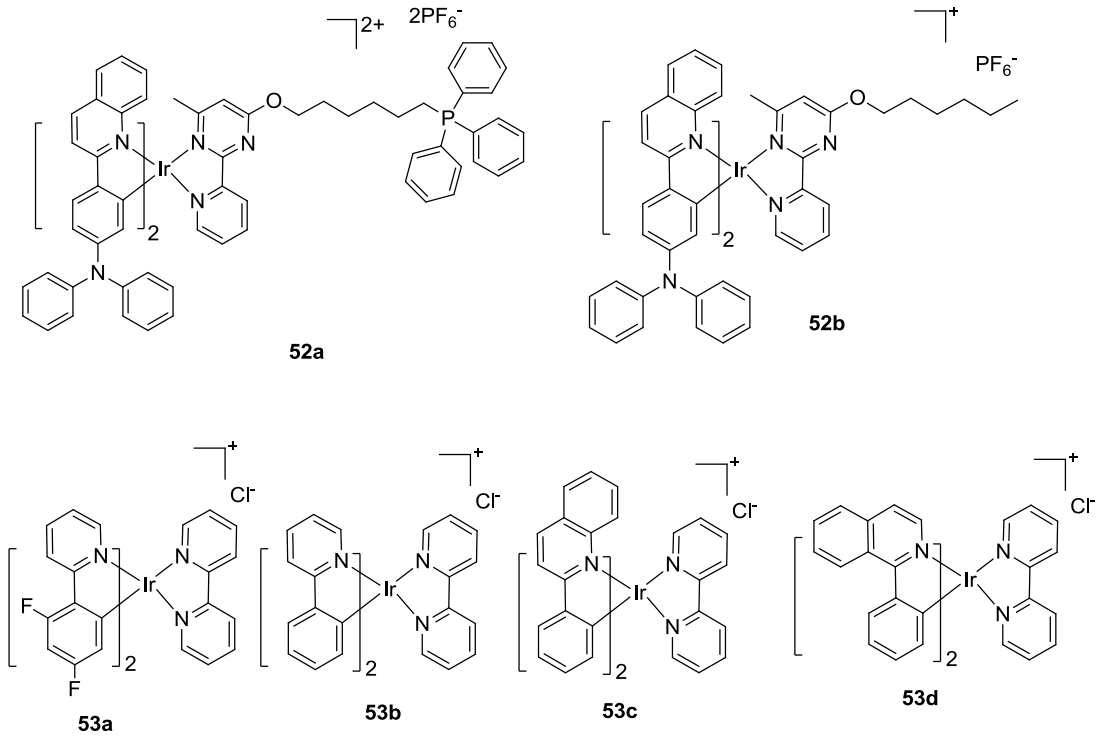

Fig 1.4.7 Iridium(III) complexes as PSs reported by Zhao and co-workers (**52a** and **52b**) and by Kwon and co-workers (**53a-53d**).

To study the detailed mechanism of protein inactivation triggered by ROS, Kwon and co-workers reported four Ir(III) complexes (**53a-53d**, Fig 1.4.7).[86] From MTT tests, it was shown that the complexes **53c** and **53d** had potentials to be PDT agents at low concentration upon low-energy light irradiation (1 J cm^{-2}), due to their relatively high ROS generation ability. In addition, **53c** could induce cell death upon TP irradiation (860 nm). Furthermore, two kinds of protein modifications (protein-protein cross-linking and protein oxidation) were verified by mass spectrometry (MS). In living cells, these modifications induced by these Ir(III) complexes were found at both endoplasmic reticulum and mitochondria, leading to an obvious effect for cancer cell death.

To avoid the problem of aggregation-induced fluorescence quenching and reduced photocytotoxicity, the group of Chao designed a series of iridium(III) complexes (**54a-54c**, Fig 1.4.8) which had aggregation-induced emission (AIE) properties. As an AIE-active agent, the phosphorescence quantum yields (Φ_{PL}) of complex **54a** increased from 0.001 in DMSO to 0.044 in 90% water-DMSO. All these complexes

exhibited more efficient ROS generation in a 90% water-DMSO mixture. The cellular uptake and intracellular distribution experiments revealed that iridium complexes selectively accumulated in mitochondria. Furthermore, all the complexes showed low toxicity towards HeLa and LO2 cell lines, whereas after OP-PDT, the cytotoxicity increased drastically. Interestingly, all these complexes were less toxic towards noncancerous LO2 cell lines. Notably, complex **54a** was found to be the most effective against HeLa cells with an IC_{50} value of 0.4 μM and a PI value of 75. Additionally, complex **54a**, which exhibited the highest TP absorbing cross-section (214 GM in 90% DMSO-water), the highest ROS generation ability and the most impressive lethality towards 3D multicellular tumor spheroids (MCTS), was a promising candidate for TP-PDT.[87]

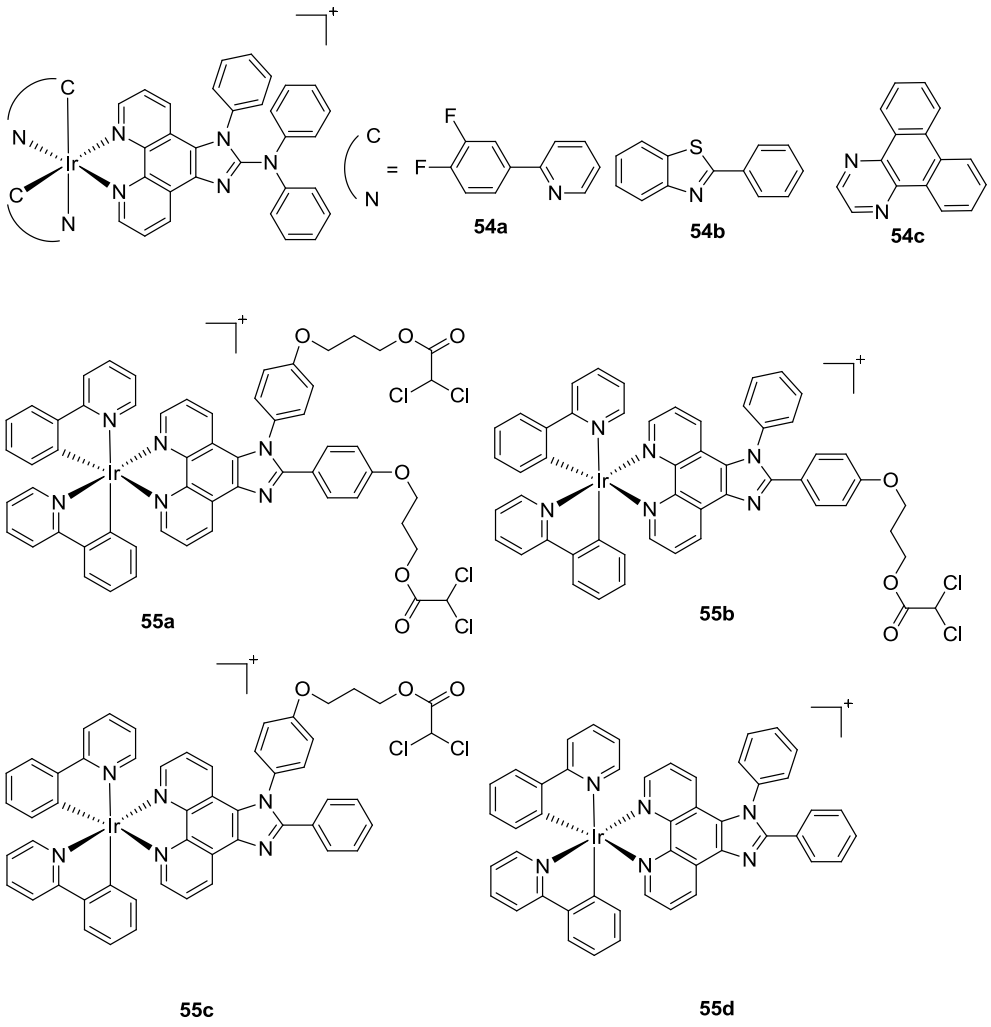

Fig 1.4.8 Iridium(III) complexes as PSs reported by Chao and co-workers (**54a-54c**, **55a-55d**).

In the same group, they reported a series of novel cyclometalated iridium(III) complexes acting as co-drugs (**55a-55d**, Fig 1.4.8) with dichloroacetate (DCA) to obtain enhanced PDT anticancer activities. The $^1O_2$ quantum yield values of these Ir(III) complexes were ranging from 0.53 to 0.74, comparable to that of H_2TPP. The confocal imaging experiments displayed that all these complexes could accumulate in mitochondria to a high degree. Complexes **55a-55c** including DCA moiety induced obvious decrease of mitochondrial membrane potential (MMP) as a result of efficient cellular uptake and successful release of DCA, while **55d** and DCA caused slight changes. It was shown that obvious enhancement of anticancer activities was found for **55a-55c** after OP irradiation, and they manifested lower toxicity against LO2 than other cancerous cells, whereas for DCA monotherapy and **55d** without DCA moiety, no discrepancy occurred. Furthermore, after TP irradiation, complexes **55a-55c** displayed significant inhibition of MCTSs growth. In particular, **55a** was found to be the most potent towards both monolayer cells and hypoxia MCTSs, being a promising candidate for TP-PDT.[88]

Weinstein, Bryant and coworkers reported two cationic iridium(III) complexes bearing bisbenzimidazole ligands (**56a** and **56b**, Fig 1.4.9).[89] The emission quantum yields of complexes **56a** and **56b** were 0.33 and 0.24, respectively, and complex **56a** had a remarkable TP cross section of 112 GM at 760 nm. Clonogenic assay in HeLa cells was made to evaluate the cytotoxicity of these complexes. Both complexes displayed high photocytotoxicity, with LC_{50} (50 % lethal concentration) values of 0.3 and 0.5 μM, respectively. Notably, complex **56a** exhibited low dark cytotoxicity, with a phototoxic index (PI) value of over 333, suggesting its potential as a PDT agent. The mechanistic studies revealed that ROS production and apoptosis were the mode of action of cell death. Furthermore, TP excitation at 760 nm in **56a**-treated HeLa cells showed high photocytotoxicity with light power of 25 mW (2720 J cm^{-2}) whereas no cell death was found without the complex.

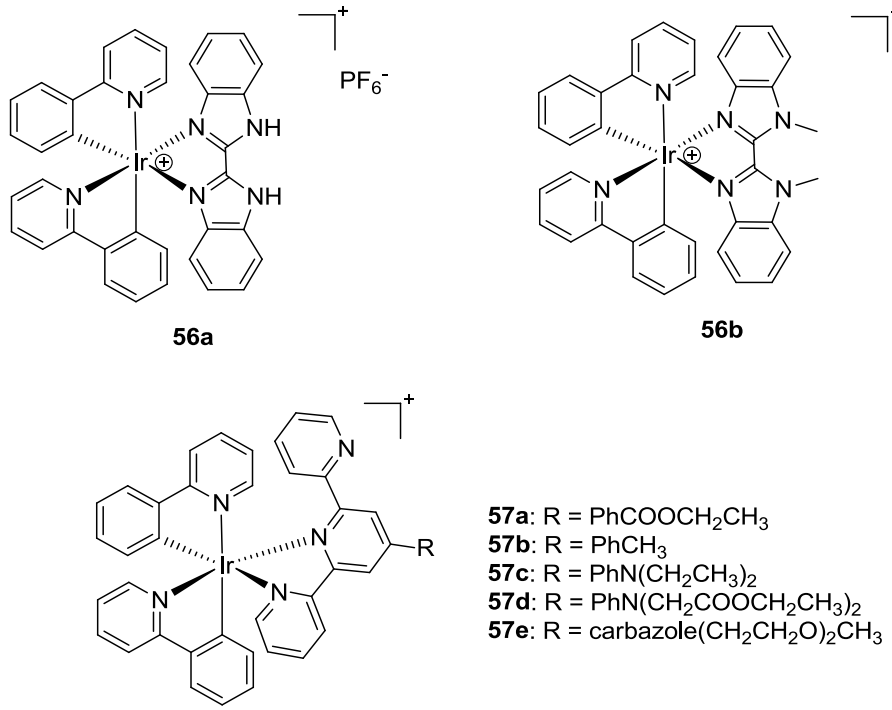

Fig 1.4.9 Iridium(III) complexes as PSs reported by Weinstein, Bryant and co-workers (**56a** and **56b**) and by Tian et al. (**57a**-**57e**).

Tian et al. developed a series of terpyridine-based cyclometalated Ir(III) complexes with TP-PDT anticancer activity (**57a**-**57e**, Fig 1.4.9).[90] These five complexes showed varied luminescent lifetimes and quantum yields, demonstrating the tunable photophysical properties of iridium(III) complexes. The toxicity against HepG-2 (liver carcinoma) cells under dark and UV light condition was evaluated, and the results revealed **57b** displayed less dark toxicity whereas the obvious decrease of cell viability occurred under UV light irradiation. In addition, from the intracellular distribution experiments, it was shown that complex **57a** was located in nuclear region, while the others accumulated in mitochondria. Furthermore, the potential of **57a** and **57b** as candidates for TP-PDT agents was determined on mice with planted solid tumors (4T1 mammary carcinoma cells). Interestingly, when treated with complex **57a**, the tumor growth was significantly inhibited, comparable with the commercial PDT agent Chlorin e6 (Ce6).

A series of biscyclometalated Ir(III) complexes bearing borondipyrromethene (BODIPY)-based ancillary ligands (**58a**-**58c**, Fig 1.4.10) was designed by Martinez,

Ortiz and co-workers.[91] Complexes **58a** and **58b** with BODIPY groups directly linked to acetylacetonate displayed higher molar absorption coefficient, stronger emission quantum yield and more singlet oxygen production ($\Phi_\Delta = 0.86$ and 0.60, respectively) upon visible light irradiation than **58c** ($\Phi_\Delta = 0.51$, only upon UV light). Additionally, the dark and photocytotoxicity of complexes **58a** and **58b** were tested in HeLa tumor cells. The results revealed that when irradiated by green light (for **58a**) and red light (for **58b**), both complexes induced remarkable photocytotoxicity, whereas no dark toxicity was found for them. Notably, **58a** exhibited much better photocytotoxicity than **58b**, with an IC_{50} value of 50 nM.

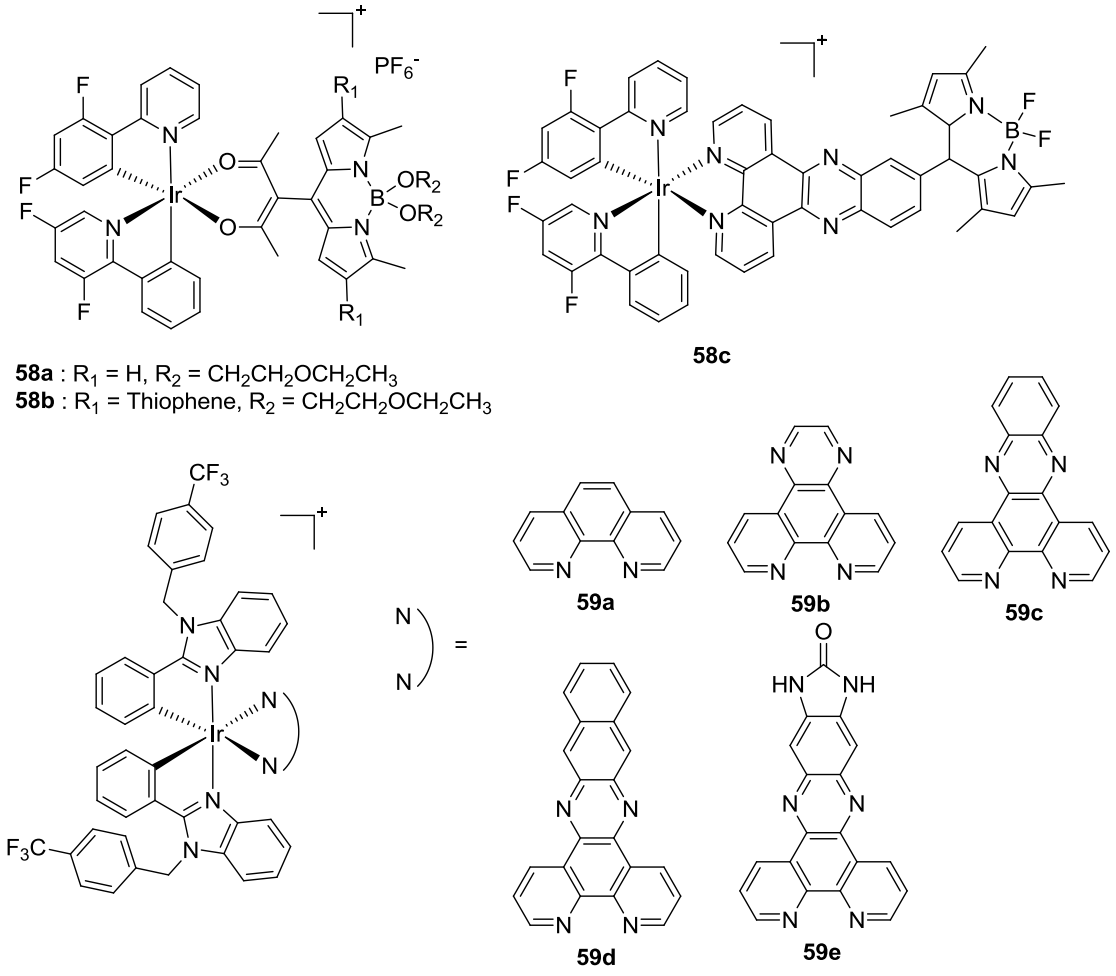

Fig 1.4.10 Iridium(III) complexes as PSs reported by Martinez, Ortiz and co-workers (**58a-58c**) and by Ruiz and coworkers (**59a-59e**).

Ruiz and co-workers reported five novel biscyclometalated iridium(III) complexes of general formula $[Ir(C\hat{}N)_2(N\hat{}N)][PF_6]$ (**59a-59e**, Fig 1.4.10) to study the effect of π

system of the polypyridyl ligand on cytotoxicity against various cancer cells. The less lipophilic complexes **59a** and **59b** with lower cellular uptake displayed higher cytotoxicity than complexes **59c** and **59d** against A2780 (ovarian carcinoma), HeLa (cervical carcinoma) and MCF-7 (breast carcinoma) cell lines with IC_{50} values ranging from 0.5 μM to 1.8 μM. Moreover, **59a** and **59b** were more efficient than cisplatin and showed better selectivity between cancer cells and normal cells (MCF-10A noncancerous breast cells) with SI values of 3.7 and 6.4, respectively. Mechanistic studies revealed that these iridium complexes involved inhibition of protein translation targeting endoplasmic reticulum (ER) and induced cell death through apoptotic pathway. Furthermore, the phototoxic activities against HeLa cells of all these complexes were evaluated, and the results demonstrated that upon visible light (420 nm) irradiation, the toxicity was significantly enhanced with IC_{50} values ranging from 0.044 μM to 0.866 μM due to a remarkable increase of intracellular ROS production.[92]

2. NHC-gold complexes containing aliphatic amino-side arms

2.1. Introduction

In this chapter, the synthesis and the characterization of a family of NHC-gold(I) complexes containing aliphatic amino-side arms and the related anticancer activities will be discussed.

Our group reported the synthesis and the biological investigation of a series of gold(I) complexes (**II-1a** to **II-1d**, Fig 2.1) containing two 1-[2-(diethylamino)ethyl] imidazolydene ligands. These complexes have been tested for their cytotoxic activities against PC-3 cells. It was shown that the lipophilicity of these complexes was in good agreement with the observed biological activities.[57] The most active complex **II-1d** displayed remarkable cytotoxicity against five cancer cell lines (PC-3 prostate cancer, MCF-7 breast cancer, U87 brain cancer, A549 lung cancer and Hep3B liver cancer) with GI_{50} values ranging from 400 nM to 1 μM, whereas for HUVECs (normal primary human umbilical vein endothelial cells), it exhibited low activity even at the highest concentration of 5 μM, which suggested a good selectivity of **II-1d**.

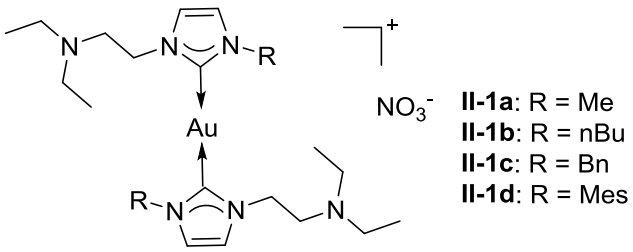

Fig 2.1 Bis-NHC Au(I) complexes reported by our group (**II-1a** to **II-1d**).

The cationic charge and the lipophilic properties of complex **II-1d** are typical characteristic for delocalized lipophilic cations (DLCs). It was previously reported that DLCs can pass through the lipid bilayer and selectively accumulate in mitochondria of carcinoma cells as the consequence of elevated mitochondrial membrane potential ($\Delta\Psi m$) in tumor cells.[33] A huge number of DLCs have shown

remarkable anticancer activities, and the selectivity between cancer cells and normal cells can be modulated by changing the log P values of DLCs.

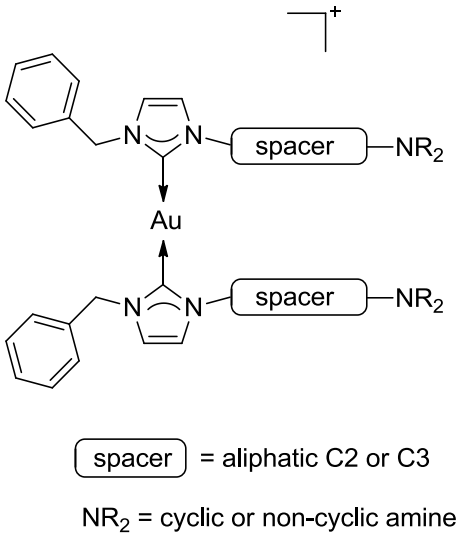

Fig 2.2 Scheme of the NHC gold(I) complexes used in this study.

In the previous work, we fixed the nitrogen-containing side arm but differ in their non-functionalized groups, namely, methyl, butyl, benzyl and mesityl. Based on previous biological activities of gold complexes, we designed a new series of complexes using benzyl group on one side of the azolium ring and varied the amine on the other side (Fig 2.2) in order to extend the SAR study.

2.2. Synthesis and characterization

The carbene precursors (**II-2a** to **II-2d**, Fig 2.3) were readily obtained after a quaternization step of 1-benzylimidazole with 1-(2-chloroethyl) piperidine hydrochloride, 1-(2-bromoethyl)-1*H*-pyrrole, 4-(2-chloroethyl)morpholine hydrochloride and 3-chloro-*N*,*N*-dimethylpropylamine hydrochloride, respectively, in aceronitrile at 80 ^{o}C with moderate yields ranging from 33 to 76%. The most notable features in the ^{1}H and ^{13}C NMR spectra of the imidazolium salts are the resonances for imidazolium protons (H2) located at 8.76-9.51 ppm and the corresponding imidazolium carbons (C2) in the range of 136.89-137.72 ppm. The resonance of the hydrochloride proton is comprised between 11.24 and 11.47 ppm. The high resolution mass spectra of the proligands exhibit the classical peak correponding to

$[M\text{-}Cl^{-}\text{-}HCl]^{+}$ for **II-2a**, **II-2c** and **II-2d**, and $[M\text{-}Br^{-}]^{+}$ for **II-2b**.

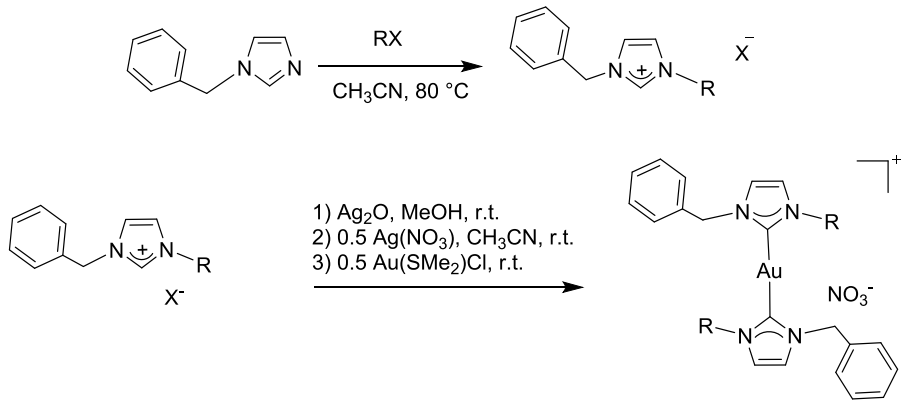

Ligand	R	X	Complex	Yield (%)
II-2a	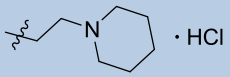	Cl	**II-3a**	40
II-2b	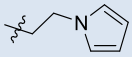	Br	**II-3b**	50
II-2c	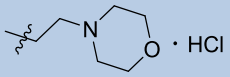	Cl	**II-3c**	84
II-2d	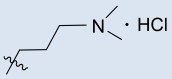	Cl	**II-3d**	84

Fig 2.3 Synthesis of carbene precusors (**II-2a** to **II-2d**) and gold(I) complexes (**II-3a** to **II-3d**).

We have chosen the convenient transmetalation route to prepare the four gold(I) complexes (**II-3a** to **II-3d,** Fig 2.3). Firstly, the silver precursor complexes were prepared by deprotonation of the imidazolium salts **II-2a** to **II-2d**, with an excess of the mild base Ag_2O (1.05 equivalent) in dry methanol at room temperature. An ion exchange with one half equivalent of $AgNO_3$ dissolved in acetonitrile was performed, in order to avoid the formation of insoluble compounds or ionic species of type $[Ag(NHC)_2][AgX_2]$. The carbene transfer reaction was thus carried out *in situ*, by adding one half equivalent of $Au(SMe_2)Cl$, with respect to the ligand. Gold(I) complexes **II-3a** to **II-3d** were isolated as white or grey powders with yields ranging from 40 to 84%; all the synthesized complexes are highly stable towards air and moisture and soluble in CH_3CN, MeOH and DMSO.

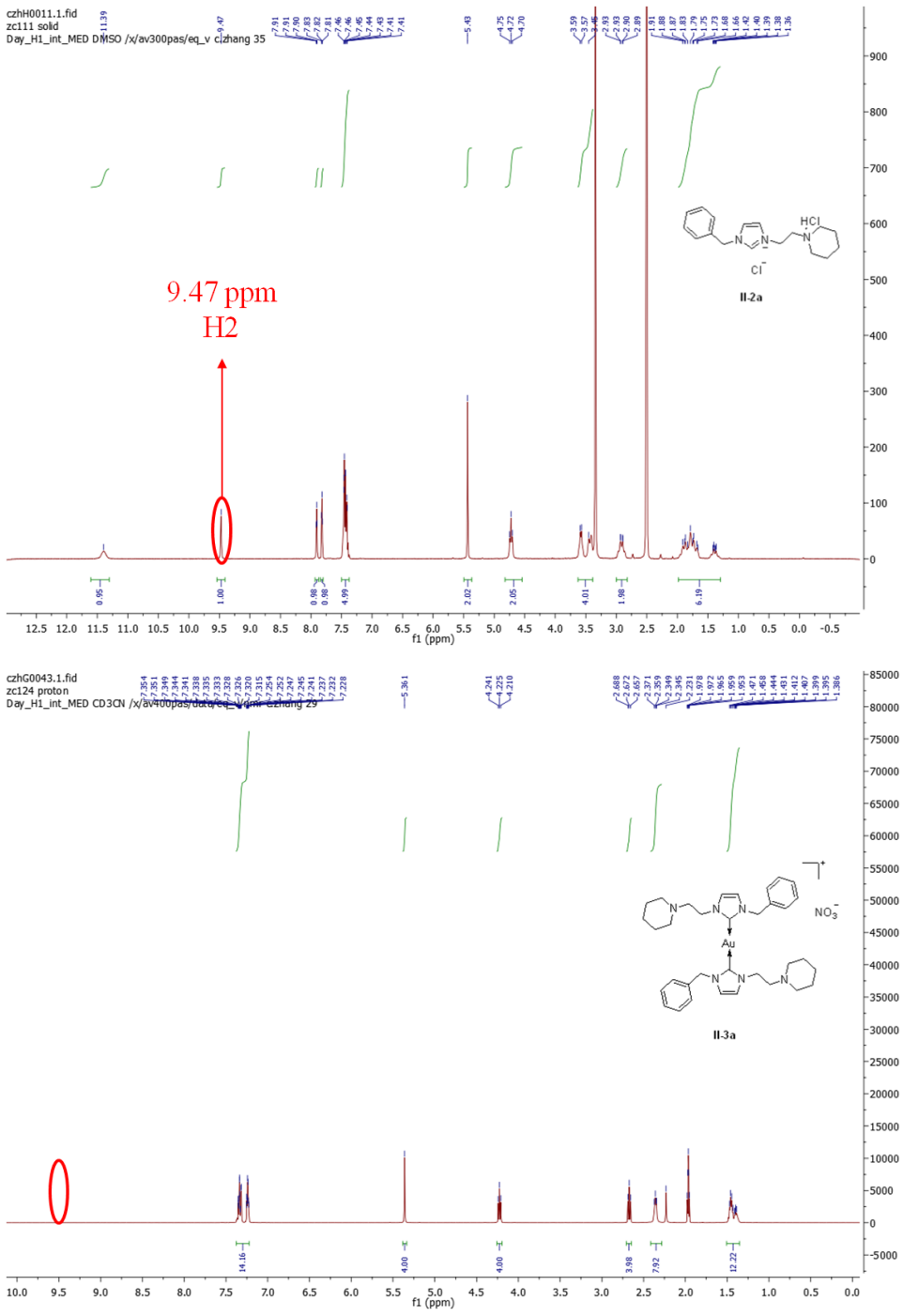

Fig 2.4 ^{1}H NMR spectra of **II-2a** (top) and **II-3a** (down).

From the comparison between the spectra, the success of the reaction can be readily proved (Fig 2.4). The characteristic signal related to H2 proton of the imidazolium salt was absent in the ^{1}H NMR spectrum of the complex accompanied by a significant shift of other peaks. These experimental evidences can be observed for all the other compounds. In all case, the integration fits with the number of protons of the analyzed

compounds.

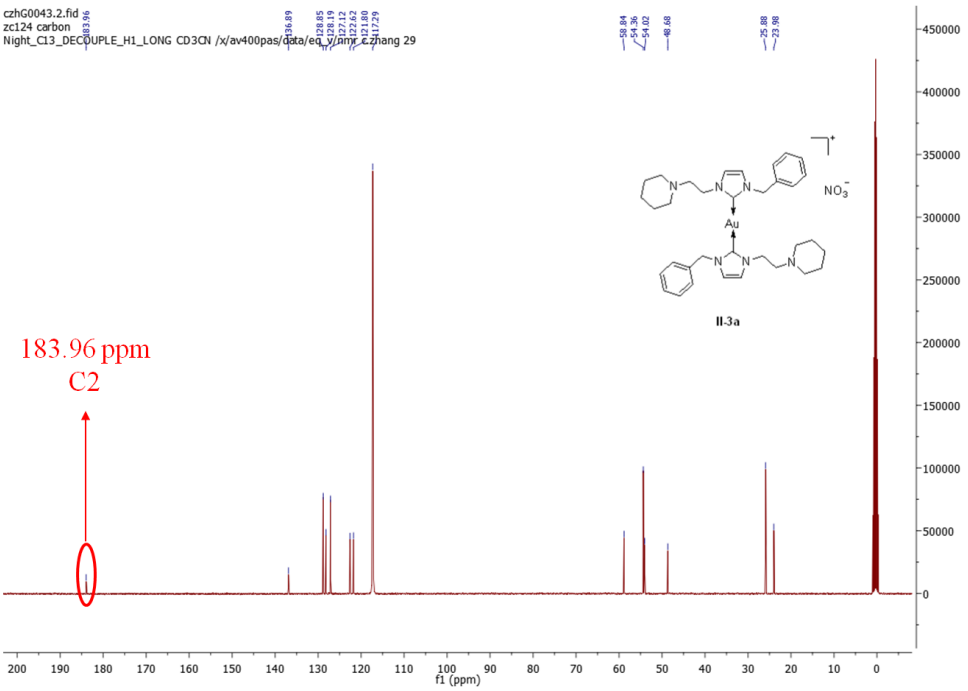

Fig 2.5 ^{13}C NMR spectrum of **II-3a**.

The ^{13}C spectra show the resonance for the carbene carbon atoms at 183.96, 184.45, 183.95 and 183.84 ppm, for **II-3a** to **II-3d**, respectively (spectrum for **II-3a**, see Fig 2.5). The elemental analysis of the gold(I) complexes correspond to the general $[AuL_2][NO_3]$ formula for **II-3a** to **II-3d** and the HRMS exhibit the classical peak corresponding to the cationic fragment $[M\text{-}NO_3^-]^+$ for **II-3a** (m/z = 735.3448), **II-3b** (m/z = 699.2509), **II-3c** (m/z = 739.3036) and **II-3d** (m/z = 683.3130).

2.3. Molecular structures

Crystals of compounds **II-3a** and **II-3c** have been obtained by slow gas-phase diffusion of diethyl ether into a concentrated solution of the complexes in acetonitrile. Crystals of compounds **II-3b** and **II-3d** suitable for X-ray diffraction analysis were obtained by slow evaporation from a methanol solution of these complexes.

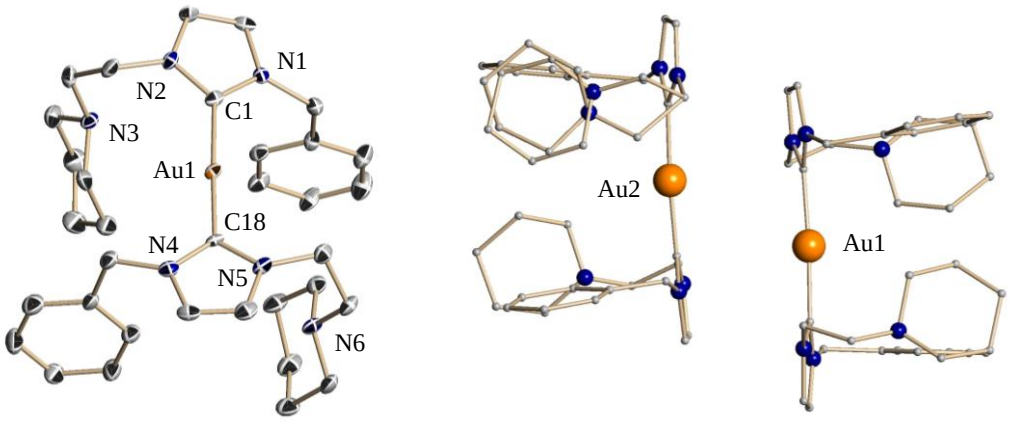

Fig 2.6 Molecular structure of **II-3a** in the solid state. The cationic part is depicted on the left side at a 30% level thermal ellipsoid plot. For clarity only one of two independent cations is shown and H-atoms, non-coordinating anions and a disorder of one piperidine group are omitted. The arrangement of the two independent cations is shown on the right side. Selected bond distances [Å] and angles [°]: Au1-C1 2.020(9), Au1-C18 1.995(9), C1-Au1-C18 176.5(4).

The cations of **II-3a** formed a kind of dimers in the solid state (Fig 2.6) with a distance Au1-Au2 of 4.023 Å which is too long to be considered as an aurophilic interaction. This arrangement explains the fact that the four side-arms of the two NHC ligands are placed on the same side in report to the NHC-Au-NHC plane. The NHC planes in each cation show only slight torsions of 7 ° and 9 °, respectively. The gold atoms are coordinated in a classical nearly linear manner for gold(I). The benzyl groups are in trans position related to the C-Au-C line.

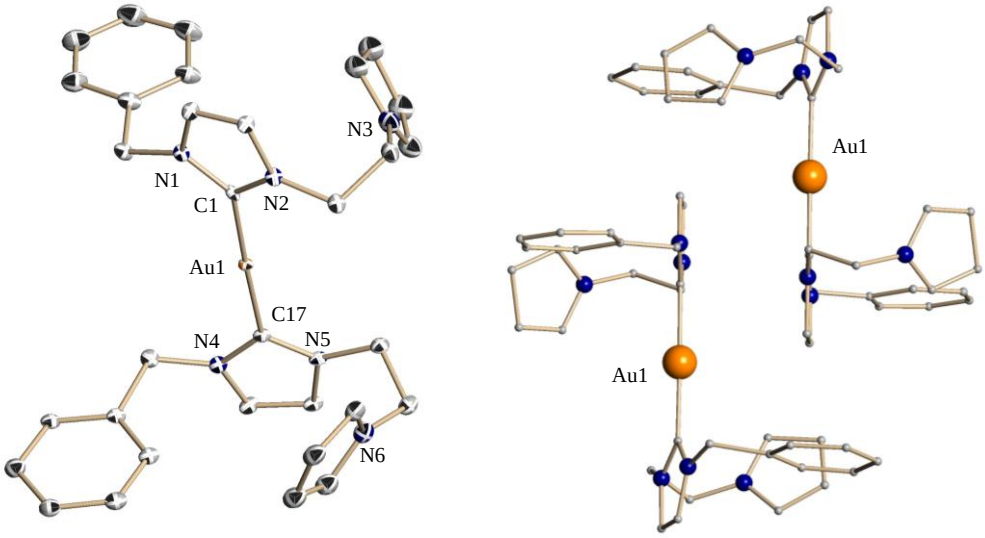

Fig 2.7 Molecular structure of **II-3b** in the solid state. The cationic part is depicted on the left side at a 30% level thermal ellipsoid plot. For clarity H-atoms and non-coordinating anions are omitted. The arrangement of the cations in the solid state is shown on the right side. Selected bond distances [Å] and angles [°]: Au1-C1 2.035(9), Au1-C17 2.034(9), C1-Au1-C17 178.1(4).

The cations of **II-3b** formed also a kind of dimers in the solid state (Fig 2.7) with a distance Au1-Au1 of 5.764 Å which is also too long to be considered as an aurophilic interaction. In this arrangement the two side arms of one NHC ligand are on the same side of the connected NHC plane, but in this case the side arms of the other NHC of the cation are on the other side of the NHC-Au-NHC plane. In **II-3b** the NHC planes show a rotation of about 20 ° around the C-Au-C axis. The gold atoms are again coordinated in a classical nearly linear manner for gold(I). Fig 2.8 shows that the anions are located in canals between chains of cations.

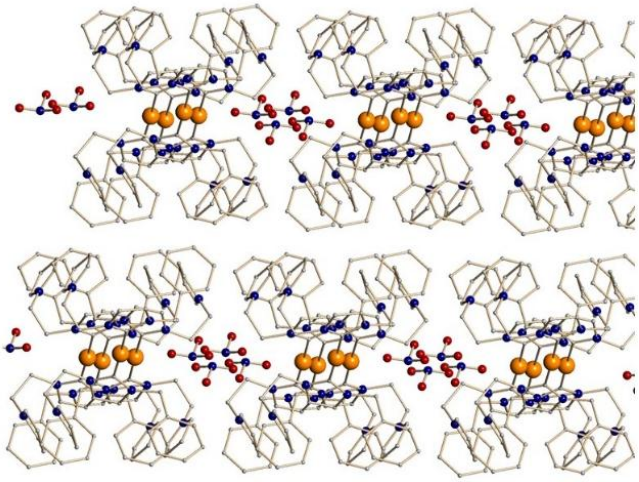

Fig 2.8 Packing of **II-3b** in the solid state.

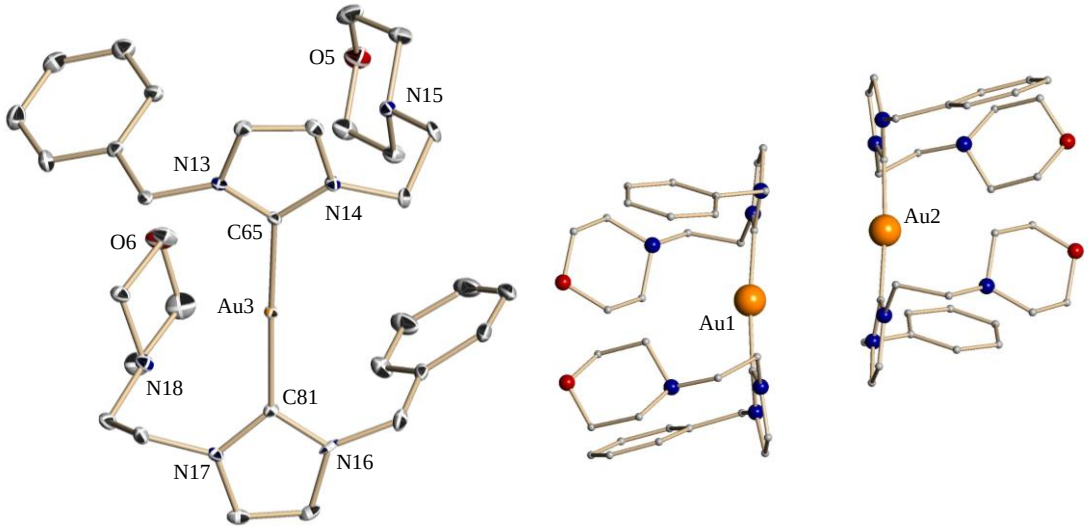

Fig 2.9 Molecular structure of **II-3c** in the solid state. The cationic part is depicted on the left side at a 50% level thermal ellipsoid plot. For clarity only one of four independent cations is shown, H-atoms, non-coordinating anions and a disorder of one morpholine group are omitted. The arrangement of the cations in the solid state is shown on the right side. Selected bond distances [Å] and angles [°]: Au3-C65 2.014(7), Au3-C81 2.015(7), C65-Au3-C81 174.8(3).

Complex **II-3c** crystalized in the monoclinic space group $P2_1$ with four independent molecules in the asymmetric unit. The absolute structure parameter refined to x = 0.245(7) and a disorder present in only one morpholine group has been treated. As in cations **II-3a** and **II-3b**, cations of **II-3c** formed a kind of dimers in the solid state

(Fig 2.9) with gold-gold distances out of range for aurophilic interactions (Au1-Au2 4.136 Å and Au3-Au4 4.228 Å). All four independent cations show the same structural main features. As observed in **II-3a**, the four side-arms of the two NHC ligands of one cation are placed on the same side in report to the NHC-Au-NHC plane. The NHC planes in each cation show only slight torsions between 10 ° and 15 °. The gold atoms are coordinated in a classical nearly linear manner for gold(I). The benzyl groups are in trans position related to the C-Au-C line. In **II-3c** the anions are more like located in wholes as in canals (Fig 2.10).

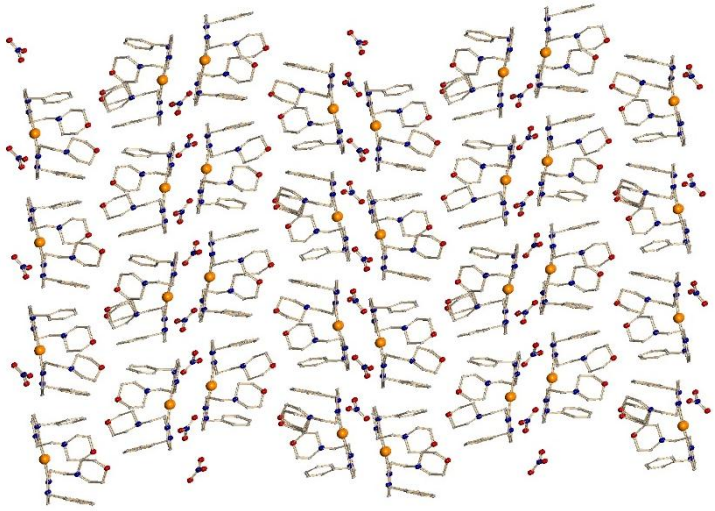

Fig 2.10 Crystal packing of **II-3c**.

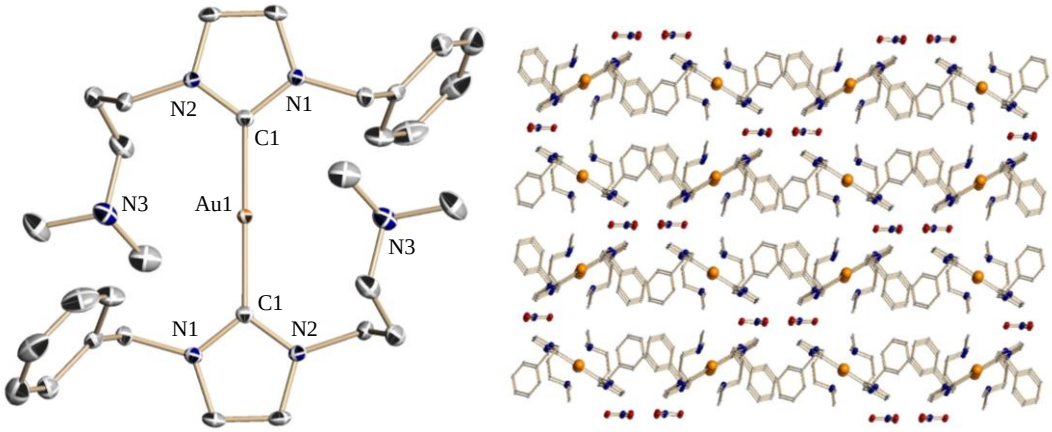

Fig 2.11 Molecular structure of **II-3d** in the solid state. The cationic part is depicted on the left side at a 50% level thermal ellipsoid plot. For clarity H-atoms and non-coordinating anions are omitted. The crystal packing is shown on the right side. Selected bond distances [Å] and angles [°]: Au1-C1 2.012(2), C1-Au1-C1 180.0.

In **II-3d** only half a molecule is present in asymmetric unit with the gold atom located on an inversion center (Fig 2.11). Cations are isolated from each other and the anions are placed in canals. The shortest gold-gold distances are 7.53 Å. The two NHC planes are perfectly coplanar. The side arms of one NHC ligand are placed on the same side of the plane of the corresponding NHC ring. The side arms of the second NHC ligand of one cation are situated on the other side of the NHC-Au-NHC plane. Looking on this plane the benzyl substituents are in trans position to each other.

2.4. Antiproliferative activity

The *in vitro* anticancer activities of these four Au(I)-NHC complexes **II-3a** to **II-3d** against four human cancer cell lines containing ovarian carcinoma (A2780 and its cisplatin-resistant variant A2780cis), hepatocellular carcinoma (HepG-2 and HepAD38) and the non-tumor Madin-Darby canine kidney epithelial (MDCK) cell line were examined by MTT assays[93] (MTT: 3-(4,5-dimethylthiazol-2-yl)-2,5-diphenyltetrazoliam bromide) and compared to the reference drug cisplatin. The cytotoxicity at 72 h against these five cell lines was depicted in terms of GI_{50} values and summarized in Table 2.1. This work has been done in collaboration with Raymond Wai-Yin Sun, Hong Kong.

The cationic gold(I) bis(NHC) complexes **II-3a** and **II-3b** were found to display potent antiproliferative activities against cancer cell lines, with GI_{50} values ranging from 0.91 to 4.8 μM. The most active complex resulted to be **II-3b** with GI_{50} values of around 0.9 μM towards two kinds of ovarian cancer cell lines (A2780 and A2780cis). These results are indicative of a bioactivity of these complexes for cancer cells dependent on the nature of the groups on the NHC ligands. Importantly, this series of cationic gold(I) complexes (**II-3a-II-3d**) showed much higher cytotoxicity to ovarian carcinoma cell lines than to hepatocellular carcinoma ones. However, it should be mentioned that the commercial drug Sorafenib currently used to treat hepatocarcinoma exhibited a high IC_{50} value of 6.4 μM against HepG-2 cell line.[94] Remarkably, complexes **II-3a** and **II-3b** were found to be very effective towards

cisplatin-resistant ovarian cell line A2780cis, suggesting that these complexes are able to overcome the resistance to cisplatin with a resistant ratio of around 10.

Table 2.1 Cytotoxic activity of gold(I) NHC complexes expressed as GI_{50} (μM) values towards selected cancer and normal cell lines as determined by MTT assay (72 h).

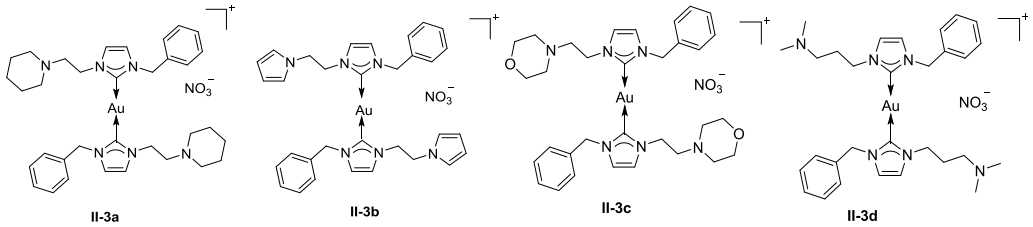

complex	A2780cis	A2780	HepG-2	HepAD38	MDCK	Log P
II-3c	44 ±11	28 ±9	>50	>50	>50	-0.46 ±0.02
II-3d	20 ±3	11 ±2	>50	>50	>50	-0.23 ±0.06
II-3a	2.8 ±0.6	2.1 ±0.4	4.8 ±1.5	4.5 ±1.7	10 ±3	-0.01 ±0.01
II-3b	0.97 ±0.11	0.91 ±0.23	3.1 ±1.1	1.1 ±0.2	5.9 ±1.5	0.29 ±.0.02
cisplatin	34 ±2.40	3.2 ±0.61	4.31 ±1.10	12 ±1.3	27 ±3.8	

The GI_{50} values represent the concentrations of the complexes and compounds causing 50% inhibition of cellular growth. Data are expressed as mean ± standard error μM and are resulted from at least three independent experiments.

In this series of cationic gold(I) bis(NHC) complexes, the two complexes **II-3c** and **II-3d** containing a morpholine moiety and an aliphatic amine, respectively, were found to be inactive against the cancer cell lines. All the complexes **II-3a** to **II-3d** showed a lower cytotoxic activity towards the healthy MDCK cells in comparison to cancer cells. The IC_{50} value of complex **II-3b** against a non-cancerous origin derived cell line MDCK was found to be 5.9 μM. In comparison to the A2780 cell line, **II-3b** exhibited a 6.5-fold selectivity towards cancerous cells than normal cells.

In order to study SAR, lipophilicity of the gold complexes has been determined by using a shake-flask method.[95] Stock solutions of these four compounds (50 μM) were prepared in the aqueous phase (previously saturated with n-octanol) and aliquots (1

mL) of each of these stock solutions were then added to an equal volume of the n-octanol phase (previously saturated with water). The resultant biphasic solutions were mixed for 1 h and then centrifuged (3000 × g, 5 min) to separate the phases. The concentrations of these complexes in the organic and aqueous phases were then determined using UV absorbance spectroscopy (260 nm). Log P was defined as the logarithm of the ratio of the concentrations of the studied complex in the organic and aqueous phases (Log P = Log [Au(org)]/[Au(aq)]). The obtained results are reported in Table 2.1.

The Log P values (-0.01 ± 0.01 for **II-3a**, 0.29 ± 0.02 for **II-3b**, -0.46 ± 0.02 for **II-3c** and -0.23 ± 0.06 for **II-3d**) showed clearly a difference between **II-3b** containing a pyrrole group and the other complexes. In this series, the highest lipophilicity found for the complex **II-3b** correlates with the highest cytotoxic activity against cancer cells. These complexes ordered for cytotoxicity are **II-3c** < **II-3d** < **II-3a** < **II-3b** and exactly the same order was found for the lipophilicity. Moreover, this general trend can be related to an effect commonly known for DLCs.[11a] Due to the electric gradient between membrane's inner and outer layers, DLCs can penetrate the hydrophobic barrier of cellular membranes and accumulate selectively in tumor cell mitochondria, due to a difference of around 60 mV between the mitochondrial membrane potential of cancerous and healthy cells.

In conclusion, these data show that complex **II-3b** is active against a panel of cancer cell lines whereas reduced cytotoxicity is found towards healthy cells, which suggests that this complex is a good candidate as an anticancer agent with good prerequisites for *in vivo* tests.

3. NHC-gold complexes containing aromatic amino-side arms

3.1. Introduction

In this chapter, the synthesis and the characterization of a family of NHC-gold(I) complexes containing amino groups linked to the NHC skeleton by an aromatic spacer and the related anticancer activities will be discussed.

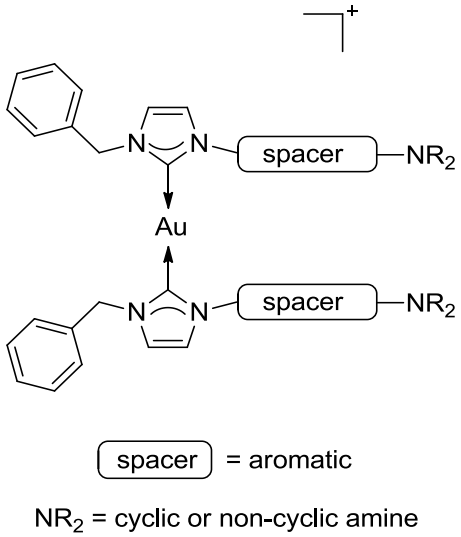

Fig 3.1 Sheme of the NHC gold(I) complexes used in this study.

Recently, we have demonstrated that some mononuclear lipophilic cationic gold(I) bis(NHC) complexes containing aliphatic or aromatic functionalized arms displayed *in vitro* potent and selective anticancer activities on several human cancer cell lines.[57, 96] In chapter 2, we discussed about one class of our ligands characterized by a nitrogen containing group connected by aliphatic linkers to the NHC skeleton. By measuring the Log P values of the complexes **II-3a** to **II-3d**, we confirmed the direct relationship between cytotoxicity and lipophilicity. Herein, we present the synthesis and antiproliferative screening of an optimized series of complexes (Fig 3.1). Our pharmaco-modulation consisted in the replacement of the aliphatic linker by an aromatic linker in order to increase the lipophilicity.

3.2. Synthesis and characterization

Firstly, we wanted to use the same synthetic route presented in chapter 2 to obtain the imidazolium salts. In the case of **III-2a**, we started from 1-benzylimidazole to react with 4-bromo-*N*,*N*-dimethylaniline under different conditions (Fig 3.2). In spite of the high temperature and the addition of catalysts, no formation of the imidazolium salt **III-2a** could be observed.

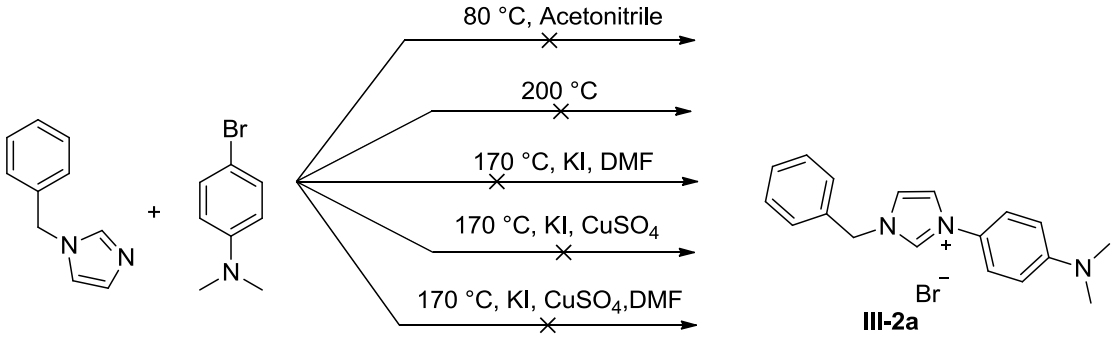

Fig 3.2 Attempts to synthesize the proligand **III-2a**.

Therefore, we changed the sequence of the synthetic route. Prior to the substitution reaction with the benzyl group, a copper-catalyzed *N*-arylation of imidazole with 4-bromo-*N*,*N*-dimethylaniline in the presence of postassium carbonate and copper sulfate at 205 ^{o}C was carried out to achieve 4-(1*H*-imidazol-1-yl)-*N*,*N*-dimethylaniline.

For the synthesis of the substituted imidazoles **III-1c** and **III-1d**, we started from imidazole to react with 1-(4-chlorophenyl)-1*H*-pyrrole and 4-(4-bromophenyl) morpholine, respectively, using the same procedure. Nevertheless, no reaction happened even after 3 days (Fig 3.3). So, we turned to use the stronger base potassium phosphate and copper(I) catalysts to obtain **III-1c** and **III-1d** (Fig 3.4).

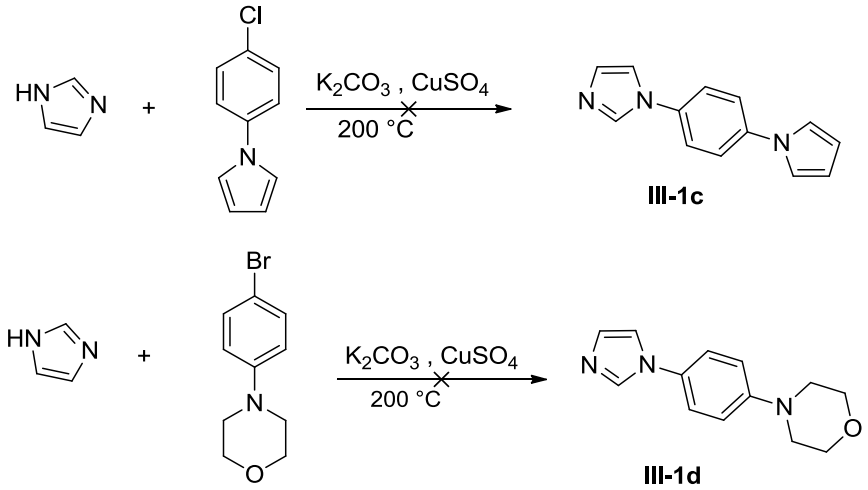

Fig 3.3 Attempts to synthesize the substituted imidazoles **III-1c** and **III-1d**.

In summary, the substituted imidazoles **III-1a** to **III-1d** were readily prepared by a copper-catalyzed *N*-arylation of imidazole with 4-bromo-*N*,*N*-dimethylaniline or 4-bromo-*N*,*N*-diethylaniline in the presence of K_2CO_3 and $CuSO_4$ at 205 ℃ for 10 h in the case of **III-1a** and **III-1b** respectively, and in the presence of K_3PO_4 and CuI at 160 ℃ for 3 days in the case of **III-1c** and **III-1d** respectively (Fig 3.4). 1-Arylimidazoles **III-1a** to **III-1d** were treated with benzyl chloride in dry acetonitrile at 80 ℃ for 10 h. Then the crude products were isolated by column chromatography on silica gel to obtain the four corresponding proligands **III-2a** to **III-2d** with yields ranging from 76 to 95%. They were classically characterized by ^{1}H and ^{13}C NMR spectroscopy, mass spectrometry and elemental analysis. The most notable features in the ^{1}H and ^{13}C NMR spectra of the imidazolium salts are the resonances for imidazolium protons (H2) located at 8.33-10.36 ppm, and the corresponding imidazolium carbons (C2) in the range of 135.22-136.09 ppm.

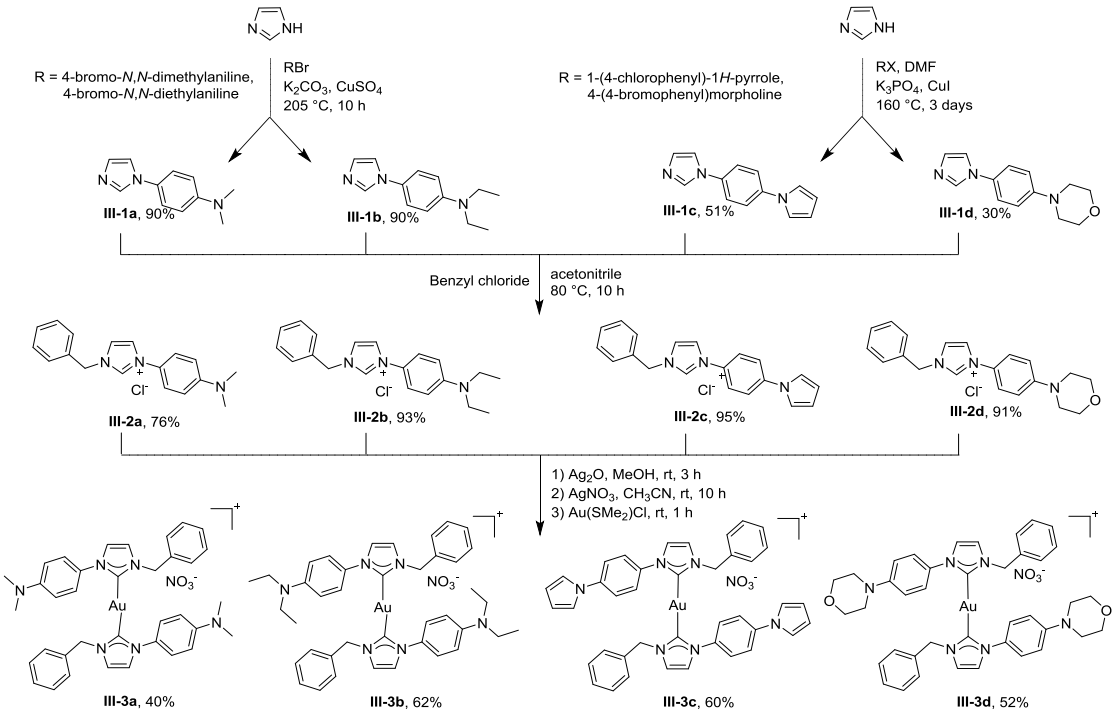

Fig 3.4 Synthesis of imidazolium salts **III-2a** to **III-2d** and gold(I) complexes **III-3a** to **III-3d**.

The target gold(I) complexes **III-3a** to **III-3d** were synthetized according to the transmetalation pathway. Firstly, the silver precursor complexes were prepared by deprotonation of the imidazolium salts **III-2a** to **III-2d**, with an excess of the mild base Ag_2O (1.05 equivalent) in dry methanol at room temperature. An ion exchange with $AgNO_3$ dissolved in acetonitrile was performed, in order to avoid the formation of insoluble compounds or ionic species of type $[Ag(NHC)_2][AgBr_2]$. The carbene transfer reaction was thus carried out *in situ*, by adding one half equivalent of $Au(SMe_2)Cl$, with respect to the ligand. Then the crude products were isolated after column chromatography on silica gel to achieve the gold complexes **III-3a** to **III-3d** as yellow powders with good yields ranging from 40% to 62%; all the synthesized complexes are highly stable towards air and moisture and even in solution. NMR spectroscopy unequivocally demonstrated the formation of the gold(I) complexes with the absence of the proton resonance of the acidic imidazolium and the ^{13}C NMR spectra show the resonance for the carbene carbon atoms at 182.66 to 182.78 ppm, in good agreement with reported values for Au(I) bis(NHC) complexes.[97] Protons 4 and

5 of the imidazole rings in the complexes were shifted upfield when compared to their corresponding proligands. The elemental analysis of the gold(I) complexes correspond to the general $[AuL_2][NO_3]$ formula for **III-3a** to **III-3d**, attesting of their purity and the HRMS exhibit the classical peak corresponding to the cationic fragment $[M\text{-}NO_3^-]^+$ for **III-3a** to **III-3d**.

3.3. Molecular structures

Crystals of **III-3a** have been obtained by gas phase diffusion of diethylether in an acetonitrile solution of **III-3a**.

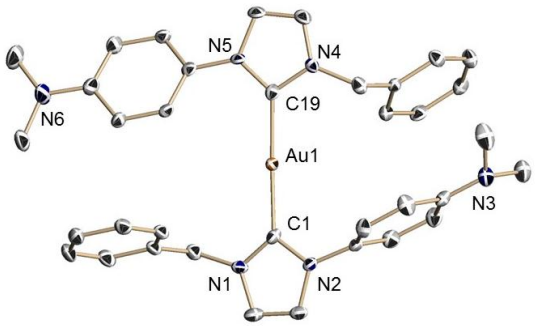

Fig 3.5 Molecular structure of **III-3a** in the solid state. The cationic part is depicted as a 50% level thermal ellipsoid plot. H-atoms and non-coordinating anion are omitted for clarity. Selected bond distances [Å] and angles [°]: Au1-C1 2.012(7), Au1-C19 2.013(8), C1-Au1-C19 177.4(4).

The coordination sphere of the gold(I) cation (Fig 3.5) shows a classical linear geometry and the two NHC ring systems are slightly twisted with a torsion angle of around 8 °. The two benzyl groups are in trans position in relation to the C-Au-C axe and to the NHC-Au-NHC plane. It is remarkable that the geometry around the nitrogen atom N3 is not planar as reflected in the total sum of the C-N-C angles, which is 350.45 °. The crystal packing of **III-3a** presented in Figure 3.5 shows the arrangement of the NO_3^- anions in channels in direction *b*.

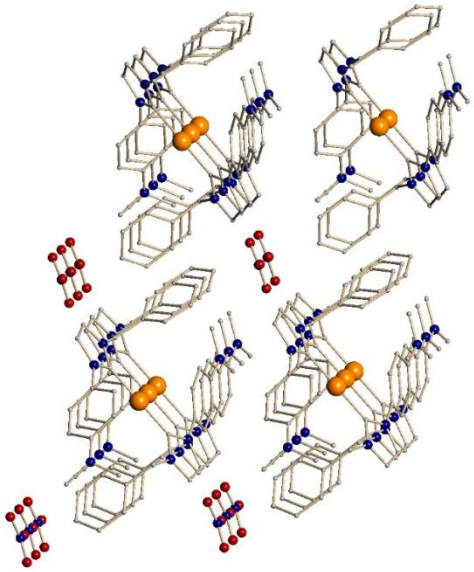

Fig 3.6 Crystal packing of **III-3a** with view along *b*.

Crystals of **III-3b** have been obtained by slow evaporation from methanol solutions of **III-3b**.

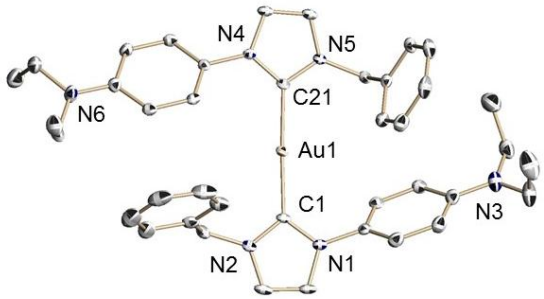

Fig 3.7 Molecular structure of **III-3b** in the solid state. The cationic part is depicted as a 50% level thermal ellipsoid plot. For clarity only one of two independent cations is shown and H-atoms, non-coordinating anions and non-coordinating MeOH are omitted. Selected bond distances [Å] and angles [°]: Au1-C1 2.019(3), Au1-C21 2.024(3), C1-Au1-C21 176.92(9).

In the case of **III-3b** the asymmetric unit contains two cations, two anions and one molecule of MeOH. As visualized in Figure 3.7, in this complex, the benzyl groups are in trans position relative to the C-Au-C axe, but they are on the same side of the NHC-Au-NHC plane. Moreover, the two NHC planes of a cation are coplanar (Fig

3.8).

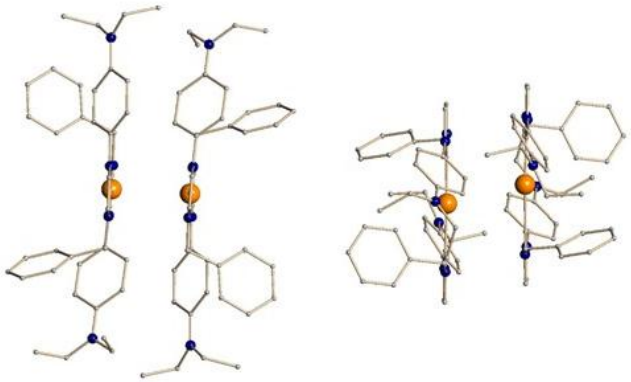

Fig 3.8 Dimeric arrangement of **III-3b** with view along the C-Au-C axe on the left side and perpendicular to this on the right side.

In the solid state, **III-3b** forms dimers with Au-Au distances of 3.45 Å (Au1-Au1) and 3.64 Å (Au2-Au2), respectively. One is in the range for aurophilic interaction (aurophilic interaction can occur when the distance between two gold atoms is less than 3.6 Å, around twice the van der Waals radius of gold atom),[98] the other one not. Also in this case, the anions are located in channels following direction *b*.

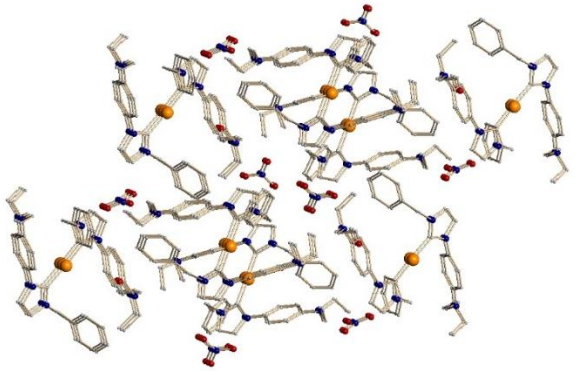

Fig 3.9 Crystal packing of **III-3b** with view along *b*.

Crystals of **III-3c** have been obtained by slow evaporation from acetonitrile solutions of **III-3c**.

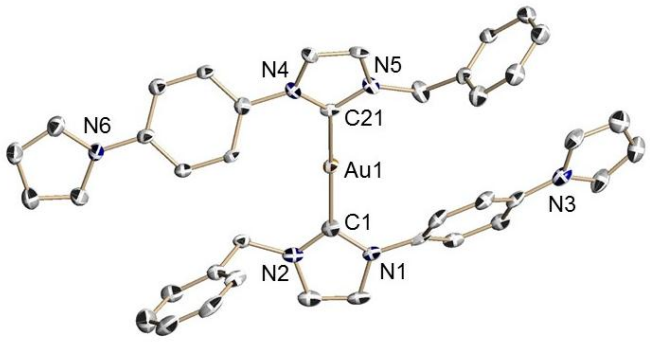

Fig 3.10 Molecular structure of **III-3c** in the solid state. The cationic part is depicted as a 30% level thermal ellipsoid plot. For clarity H-atoms, non-coordinating anions and disorders of one benzyl group are omitted. Selected bond distances [Å] and angles [°]: Au1-C1 2.024(16), Au1-C21 2.018(14), C1-Au1-C21 171.9(6), Au1-Au1 3.309(2).

In **III-3c** the groups show the same arrangement as in **III-3b**, which means that the benzyl groups are in trans relative to the C-Au-C axe and on the same side relative to the best plane formed by the NHC ring systems and the gold cation. In this case, a deformation of the linear geometry of the gold cation is reflected by the C-Au-C angle of 171.9 °, this has also an effect on the co-planarity of the NHC rings, which are twisted by about 10 °. This deformation can be explained by an aurophilic interaction (Fig 3.10) with an Au-Au distance of 3.309 Å.

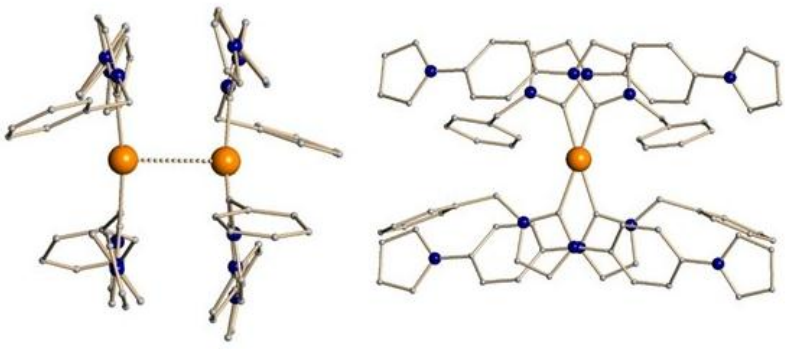

Fig 3.11 Dimeric arrangement of **III-3c** in the solid state. Left side shows the view perpendicular to the Au-Au bond and the on the right the view along the Au-Au bond is depicted.

The dimer shows a rotation of 36.2 ° of the two cations around the Au-Au bond showing a slightly crossed configuration of the two cations relatively to each other (Fig 3.11). Moreover, the anions are not located in channels or layers (Fig 3.12).

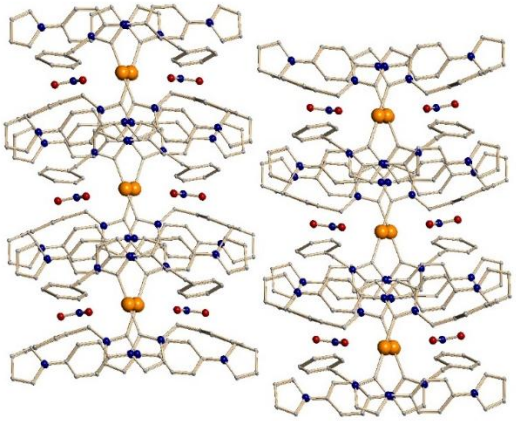

Fig 3.12 Packing of **III-3c** with view along *a*.

3.4. Antiproliferative activities

We firstly evaluated the *in vitro* cytotoxicity of the cationic gold(I) bis(NHC) complexes **III-3a** to **III-3d** and proligands **III-2c** and **III-2d** on the representative PC-3 prostate and T24 bladder cancer cell lines using the colorimetric MTT assays. This work has been done in collaboration with Dr. Olivier Cuvillier (IPBS, France), who supervised me to make the biological measurements. PC-3 and T24 cells (5000 cells/well) were seeded on a 24-well tissue culture plate and allowed to attach overnight. Then, cells were treated with complexes **III-3a** to **III-3d** and incubated for 72 h. Complex-free solvent controls were also included (not shown) to verify the absence of unusual cellular behaviour. The values reported in Fig 3.13 and Fig 3.14 are presented means ± standard error of the mean (SEM) of three independent experiments.

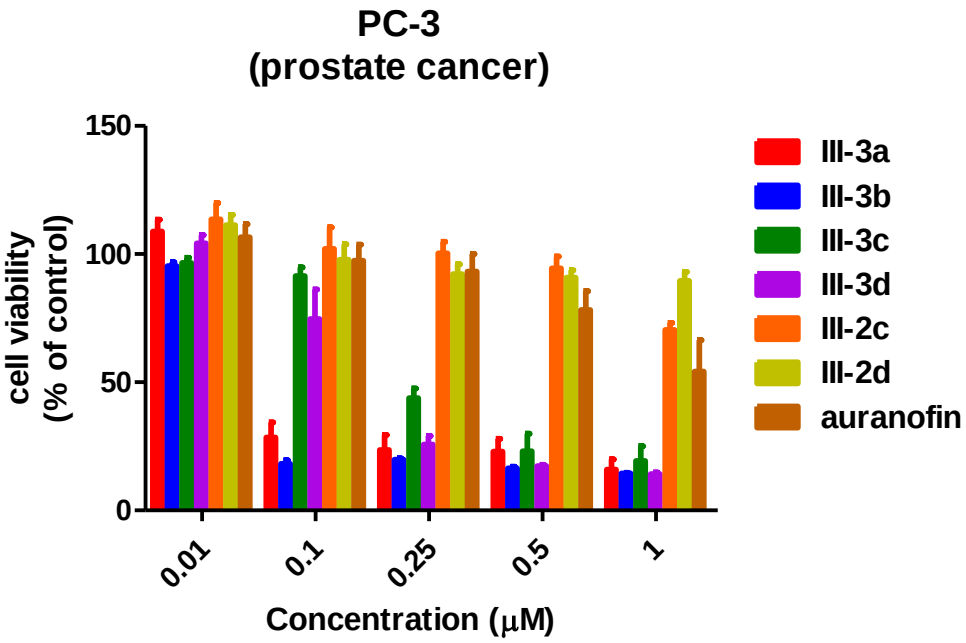

Fig 3.13 Cell viability of PC-3 prostate cancer cells treated for 72 h with increasing concentrations of gold complexes **III-3a** to **III-3d**, proligands **III-2c** and **III-2d** and auranofin.

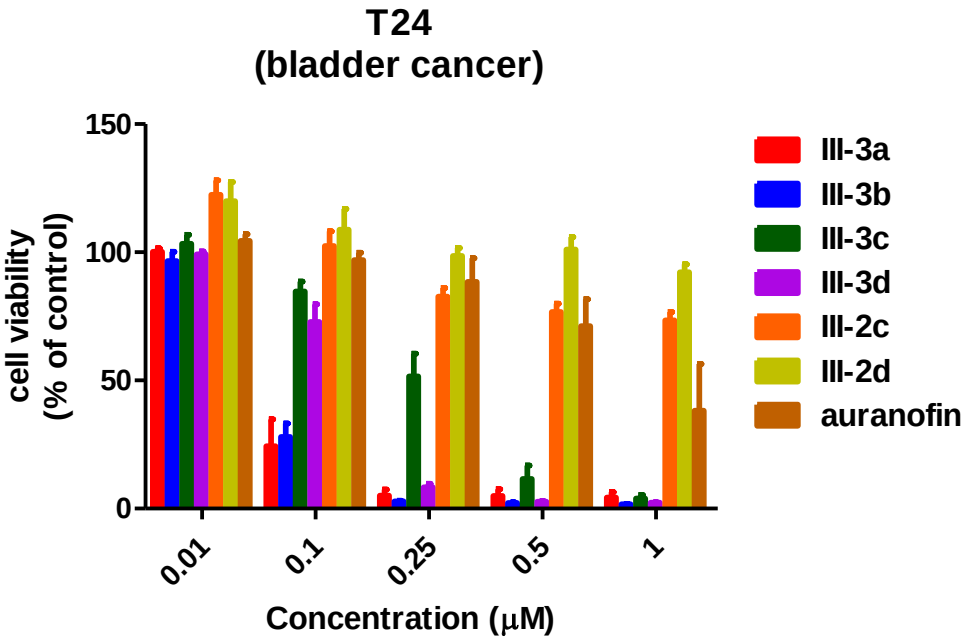

Fig 3.14 Cell viability of T24 bladder cancer cells treated for 72 h with increasing concentrations of gold complexes **III-3a** to **III-3d**, proligands **III-2c** and **III-2d** and auranofin.

As shown in Fig 3.13 and Fig 3.14, the four complexes **III-3a** to **III-3d** induced a pronounced loss of PC-3 and T24 cancer cell viability with GI_{50} values lower than 250 nM with the complex **III-3b** displaying the strongest activity ($GI_{50} \approx 30$ nM). Interestingly, among all the tested complexes, complex **III-3c** was the only one exhibiting a clear dose-dependent effect. Very notably, the proligands **III-2c** and **III-2d** showed no cytotoxic activities against PC-3 and T24 cells. We used the anti-arthritic drug auranofin as a reference for gold complexes given its potential repurposing in cancer as a pro-oxidant therapy with ongoing clinical trials in leukemia and lung cancer alone or in a combined modality. Remarkably, auranofin displayed a weaker efficacy towards prostate and bladder cells ($GI_{50} \approx 1$ μM) as compared to all the tested complexes **III-3a** to **III-3d** (Fig 3.13 and Fig 3.14).

The MC3T3 osteoblast precursor cell line is derived from mouse calveria, and it was used as non-cancerous cell model. Whereas less selectivity between cancer and non-cancerous cells was found for complexes **III-3a**, **III-3b** and **III-3d**, MC3T3 cells showed a pronounced insensitivity to complex **III-3c** up to the concentration of 0.5 μM (GI_{50} value > 0.9 μM, Fig 3.15).

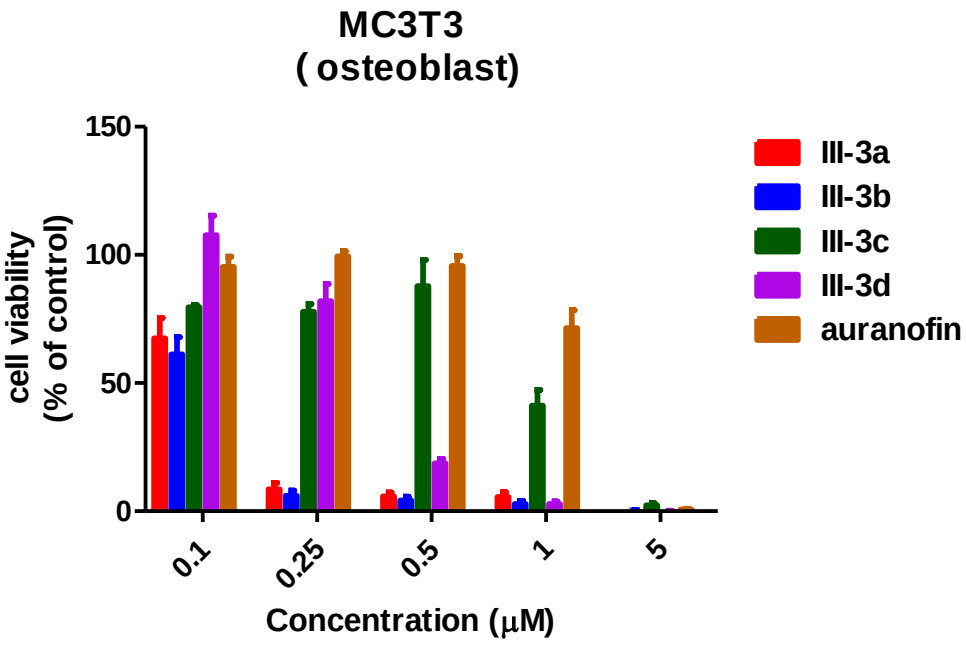

Fig 3.15 Cell viability of MC3T3 osteoblastic cancer cells treated for 72 h with increasing concentrations of gold complexes **III-3a** to **III-3d** and auranofin.

In order to study about the SAR, we have determined the lipophilicity of the gold complexes **III-3a** to **III-3d** using a shake-flask method.[8b] The obtained results were reported in Table 3.1.

Table 3.1 Lipophilicity for complexes **III-3a** to **III-3d** expressed as Log P.

Complex	Log P
III-3a	1.256 ±0.047
III-3b	0.926 ±0.030
III-3c	1.033 ±0.060
III-3d	0.501 ±0.024

In our group, we have previously reported that lipophilic mononuclear cationic gold(I) bis(NHC) complexes containing amino groups on NHC scaffold were highly cytotoxic and selective. For example, a cationic gold(I) bis(NHC) complex involving a 1-[2-(diethylamino)ethyl] group on one side and a mesitylene group on the other side of the NHC ligands, with a Log P value of 1.13, showed GI_{50} values of 400 nM against PC-3 prostate cancer cells and > 5 μM on normal primary human umbilical vein endothelial cells (HUVECs).[57] The corresponding benzyl containing complex had a Log P of 0.3 and showed a GI_{50} value of 1.44 μM on PC-3 prostate cancer cells. By replacing the aliphatic linker of this complex by an aromatic one (complex **III-3b**), the Log P value increased to 0.9 and the GI_{50} value on PC-3 prostate cancer cells decreased to 30 nM. In the case of complex **III-3c**, the log P is about 1 and the GI_{50} value on HepG-2 cells is 640 nM, whereas the corresponding aliphatic connected pyrrole system display a log P value of 0.3 and an GI_{50} value on HepG-2 cells of 3.1 μM.[96] In summary, the Log P values of the tested complexes reflect the high lipophilicity of these complexes in good agreement with the obtained antiproliferative activities, whereas too high lipophilicity may also lead to the loss of selectivity.

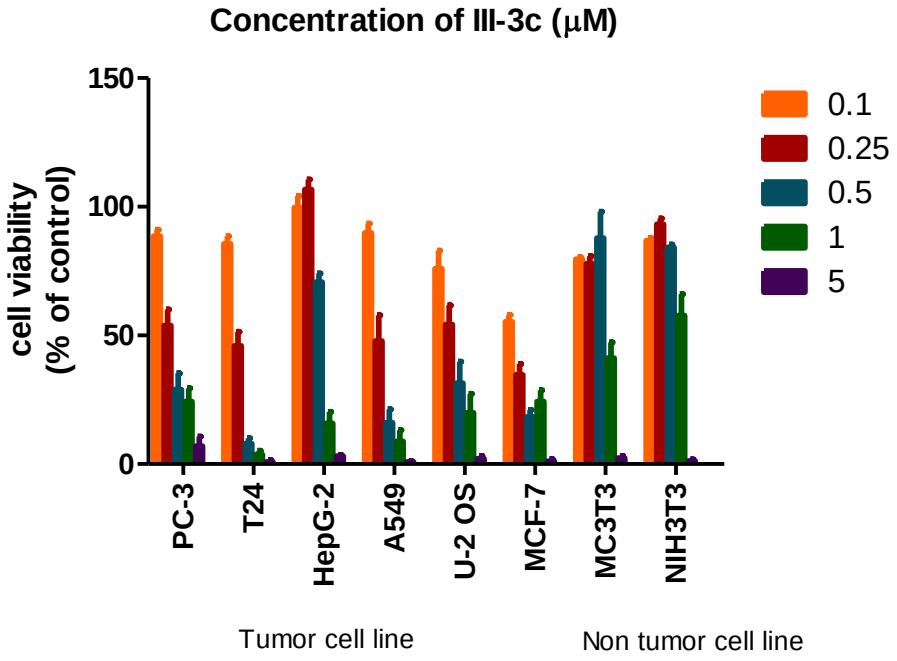

Fig 3.16 Cell viability of PC-3, T24, HepG-2, A549, U-2 OS, MCF-7, MC3T3 and NIH3T3 treated for 72 h with increasing concentrations of gold complex **III-3c**.

Accordingly, complex **III-3c** was selected as the most effective and selective compound for further *in vitro* screening on a representative panel of cancer cells, such as MCF-7 (human breast adenocarcinoma), HepG-2 (human liver cancer), A549 (human lung carcinoma) and U-2 OS (human osteosarcoma) in addition to PC-3 and T24 cancer cell models. Two non-cancerous cell lines (MC3T3 mouse osteoblasts and NIH3T3 murine fibroblasts) were used as controls. All these cell lines were seeded at 5000 cells/well in 24-well tissue culture plates, and allowed to attach overnight and then exposed to the graded concentrations of complex **III-3c** (0.1 μM to 5 μM) for 72 h. The values reported in Fig 3.16 represent as the mean of three independent experiments.

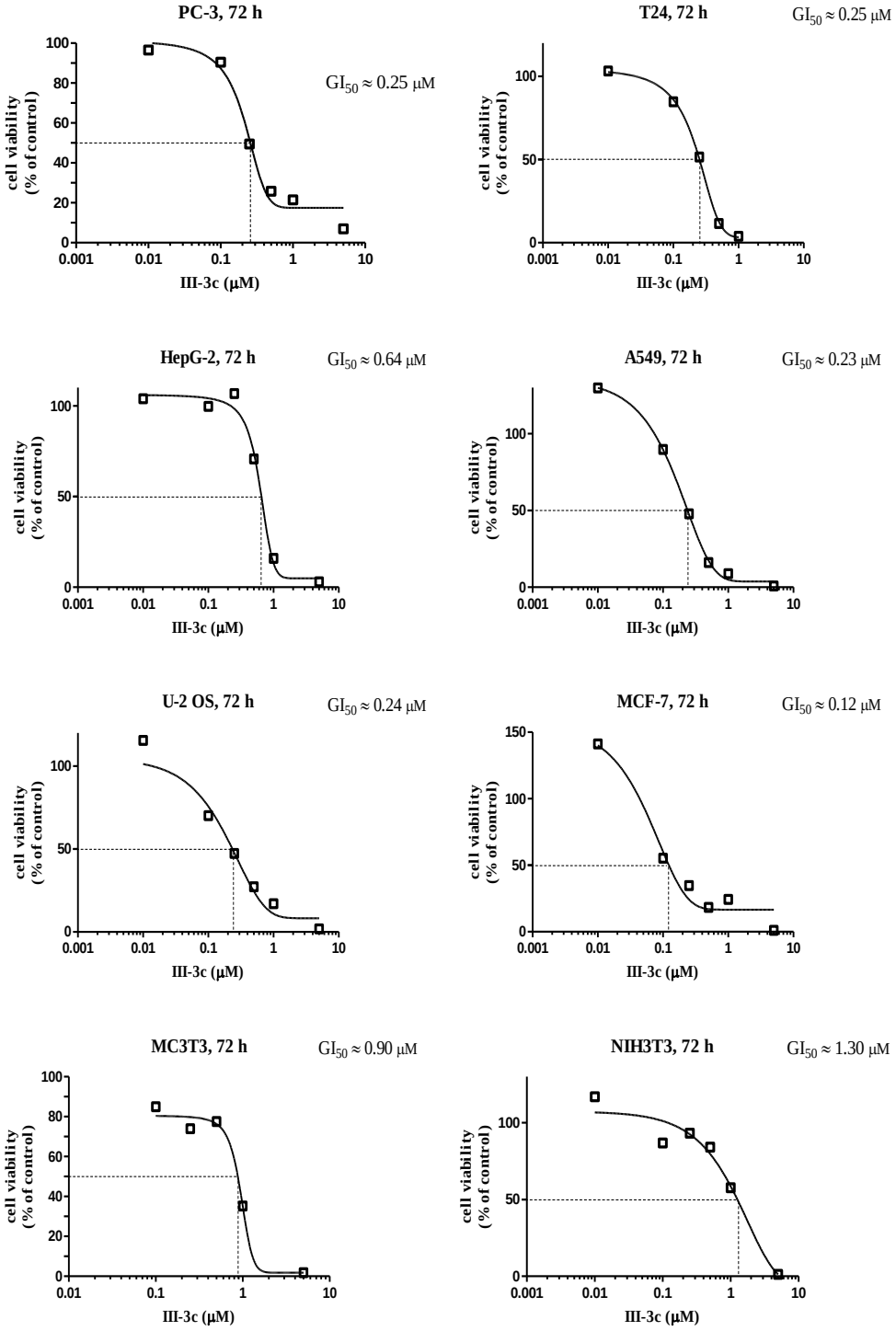

Fig 3.17 Dose- response curves for the *in vitro* tested activity of complex **III-3c** towards PC-3, T24, HepG-2, A549, U-2OS, MCF-7, MC3T3 and NIH3T3 cell lines.

All the viability values, obtained by MTT assay, were used to create log concentration *versus* percentage of cell viability curves (Fig 3.17). The GI_{50} values

were calculated from dose-response curves obtained by nonlinear regression analysis for each cell line (Table 3.2).

Table 3.2 GI_{50} values of complex **III-3c** after 72h.

GI_{50} values of complex **III-3c** after 72h		
Origin	Cell line	GI_{50}
Prostate cancer	PC-3	0.25 μM
Bladder cancer	T24	0.24 μM
Liver cancer	HepG-2	0.64 μM
Lung cancer	A549	0.23 μM
Osteosarcoma	U-2 OS	0.24 μM
Breast cancer	MCF-7	0.12 μM
Osteoblast	MC3T3	0.90 μM
Fibroblast	NIH3T3	1.30 μM

The GI_{50} values of complex **III-3c** were in the range of 0.12 μM to 0.25 μM for all tested cancer cell lines except for HepG-2 with a GI_{50} value of 0.64 μM. It should be pointed out that hepatocarcinoma is notoriously refractory to chemotherapy and even sorafenib, a commercial drug to treat hepotocarcinoma, displays a high GI_{50} value of 6.4 μM on HepG-2 cell line.[94] In contrast, the cytotoxicity of complex **III-3c** towards MC3T3 osteoblasts and NIH3T3 fibroblasts was low with GI_{50} values of 900 nM and 1.3 μM, respectively. Compared with auranofin (GI_{50} value of 1.05 μM for PC-3 and 1.80 μM for NIH3T3), complex **III-3c** displayed better selectivity between cancer cells and healthy cells with SI values of ranging from 2.1 to 10.8. In conclusion, these MTT results suggested that complex **III-3c** was highly active against various cancer cell lines and was selective with limited effects towards non-cancerous cells.

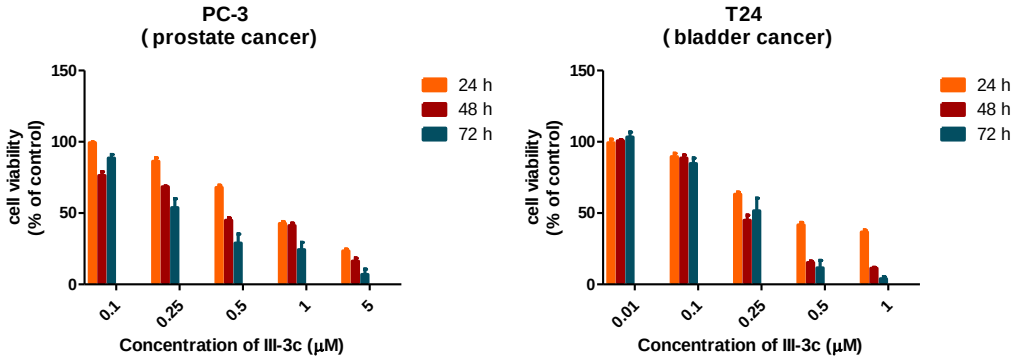

Fig 3.18 Cell viability of PC-3 (left) and T24 (right) cells treated with increasing concentrations of gold complex **III-3c** for the indicated times.

Furthermore, the kinetic effects of gold complex **III-3c** on PC-3 and T24 cancer cell lines have been evaluated. As shown in Fig 3.18, the cell viability after treated with different concentrations of **III-3c** decreases with time, which means the cytotoxic activities of **III-3c** against PC-3 and T24 are enhanced with time. Taking PC-3 as an example, the GI_{50} value of **3c** after 24 h was 810 nM, 550 nM for 48 h, and decreased to 250 nM at 72 h (Fig 3.18). This result displayed clearly the high growth inhibitory ability of **III-3c** against tested cancer cells. Interestingly, a linear increasing of the GI_{50} value over a period of 72 h could be observed. It is important to verify this tendency in order to exclude the possibility of a recovery of cell viability after the complex impact.

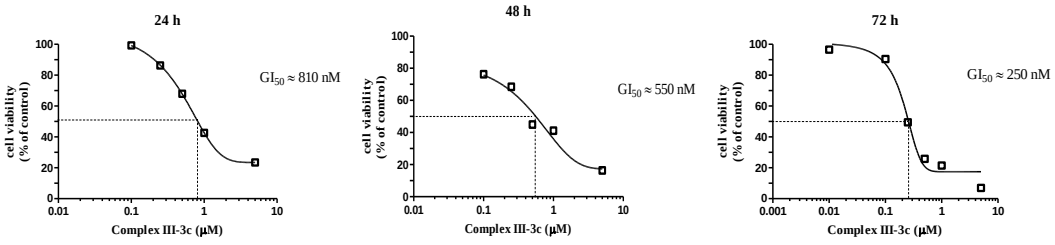

Fig 3.19 GI_{50} values of complex **III-3c** against PC-3 after 24 h, 48 h and 72 h.

Another method to study the cytotoxic effect of gold complexes concerns clonogenic assay. Clonogenic assay or colony formation assay determines the ability of a cell to form a large colony (> 50 cells).[99] It was the method of choice to

determine the effectiveness of radiotherapy or cytotoxic agents. As shown in Fig 3.20, no visible colony formation was observed at concentration of over 0.25 μM for PC-3 cells and over 0.5 μM for T24 cell. This assay manifested the ability of complex **III-3c** to inhibit significantly the number of PC-3 and T24 colonies even at low concentration when compared to the controls. It gave more accurate information about the ability of a single cell to proliferate than MTT tests since it essentially tests every cell in the population for its ability to undergo "unlimited" division.[99]

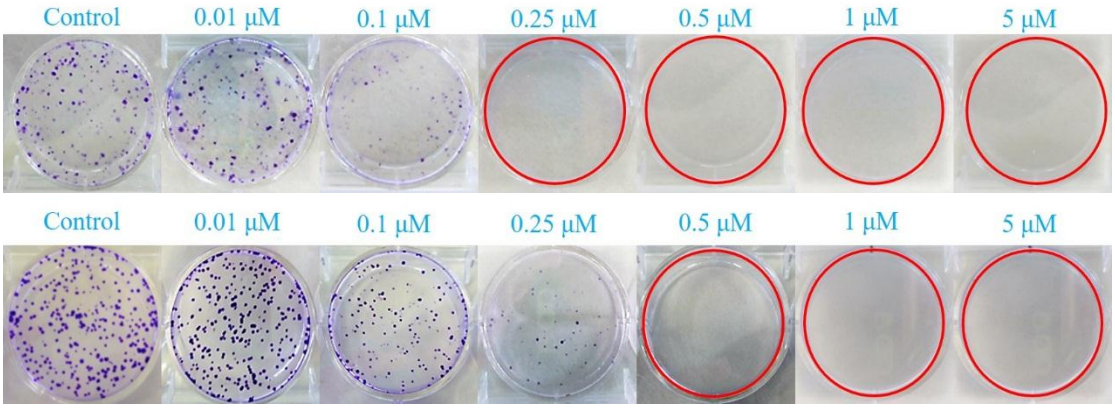

Figure 3.20 Colony formation in PC-3 (top) and T24 (bottom) cells treated with increasing concentrations of complex **III-3c** and stained with crystal violet after 8 days (for PC-3) and 6 days (for T24) of cultivation.

3.5. Optimization of gold(I) bis(NHC) complexes

After increasing the lipophilicity of cationic gold(I) complexes, better anticancer activities were achieved. However, this series of gold complexes containing aromatic side-arms are mainly toxic towards non-cancerous cells, such as MC3T3 and NIH3T3. The lack of selectivity between healthy and cancer cells triggers us to do some pharmaco-modulation to optimize the system for gold(I) complexes.

It has been previously reported by our group that gold(I) NHC complexes containing quinoline and thioanisole functionalized groups displayed better cytotoxicity than the complexes bearing a benzyl moiety against a panel of cancer cell lines with GI_{50} values ranging from 0.11 μM to 0.67 μM.[96] Therefore, we replaced benzyl groups by quinoline and thioanisole groups on one side of the azolium cycle, and used pyrole and piperidine containing side arms on the other side. We designed

and synthesized a novel series of four proligands (**III-5a** to **III-5c**, Fig 3.21) and their corresponding gold(I) complexes (**III-6a** to **III-6d**, Fig 3.21).

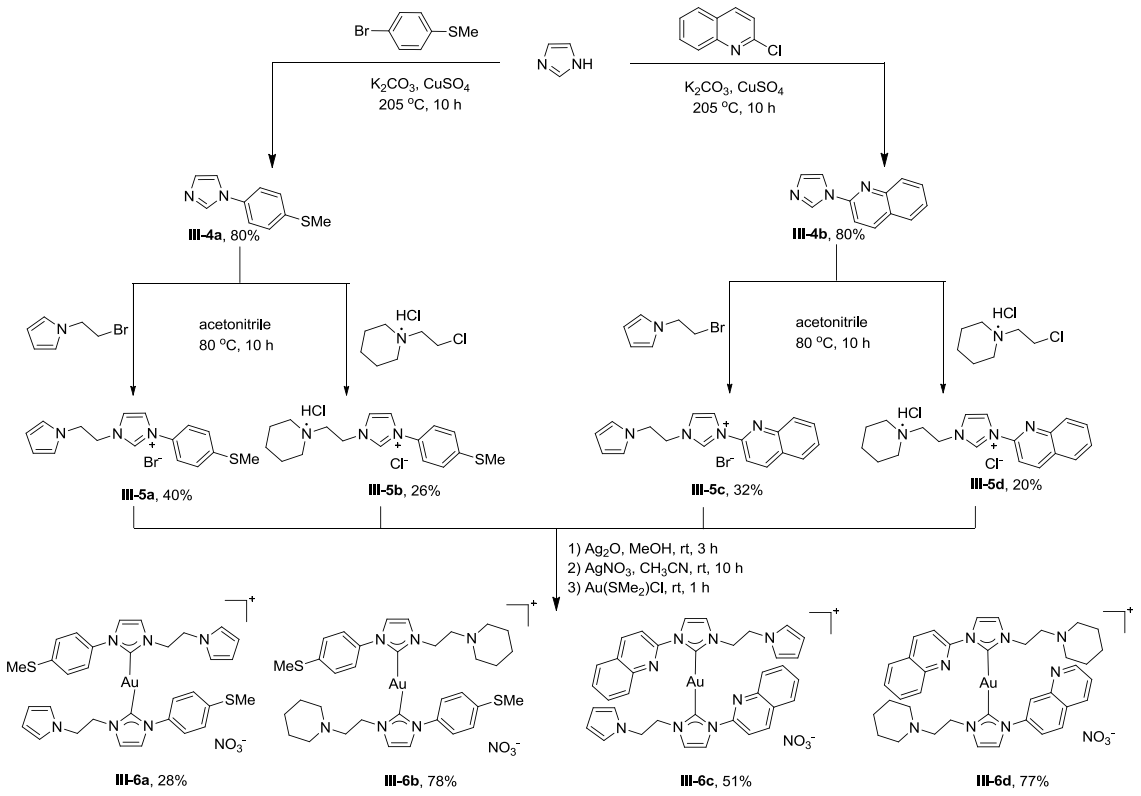

Fig 3.21 Synthesis of imidazolium salts (**III-5a** to **III-5d**) and gold(I) complexes (**III-6a** to **III-6d**).

The substituted imidazoles **III-4a** and **III-4b** were readily prepared with a good yield of 80% by a copper-catalyzed *N*-arylation reaction with 4-bromothioanisole and 2-chloroquinoline, respectively, in the presence of K_2CO_3 and $CuSO_4$ at 205 °C for 10 h. 1-(4-Methylthiophenyl)-1*H*-imidazole (**III-4a**) and 2-(1*H*-imidazol-1-yl)quinoline (**III-4b**) were reacted with 1-(2-bromoethyl)-1*H*-pyrrole in dry acetonitrile at 80 °C for 10 h. Then the crude products were purified by column chromatograpy on silica gel to obtain the proligands **III-5a** and **III-5c** with yields of 40 % and 32 %, respectively. Similarly, the proligands **III-5b** and **III-5d** were achieved by reacting **III-4a** and **III-4b** with 1-(2-chloroethyl)piperidine hydrochloride with yields spanning from 20 % to 26 %. They were classically characterized by ^{1}H and ^{13}C NMR spectroscopy, mass spectrometry and elemental analysis. The most notable features in

the ^{1}H and ^{13}C NMR spectra of the imidazole salts are the resonance for imidazolium protons (H2) located at 9.41 to 10.05 ppm, and the corresponding imidazolium carbons (C2) in the range of 135.81 to 137.33 ppm.

The target gold(I) bis(NHC) complexes **III-6a** to **III-6d** were synthesized according to the transmetalation method. Firstly, the silver precursor complexes were prepared by deprotonation of the imidazolium salts **III-5a** to **III-5d**, with one equivalent of the mild base Ag_2O in dry methanol at room temperature. An ion exchange with $AgNO_3$ dissolved in dry acetonitrile was performed, in order to avoid the formation of insoluble compounds or ionic species of type $[Ag(NHC)_2][AgX_2]$. The carbene transfer reaction was thus carried out *in situ*, by adding one half equivalent of $Au(SMe_2)Cl$, with respect to the proligands. Then the crude products were purified by column chromatography on silica gel to obtain gold(I) bis(NHC) complexes **III-6a** to **III-6d** as pale-yellow powders with moderate to good yields ranging from 30% to 78%, and all the complexes were highly stable towards air, moisture and even in solution. NMR spectroscopy clearly demonstrated the formation of the gold(I) complexes with the disappearance of the proton resonance of the acidic imidazolium and the ^{13}C spectra displayed the resonance for the carbene carbon at 182.43 to 183.13 ppm. The elemental analysis of the gold(I) complexes correspond to the general $[AuL_2][NO_3]$ formula for **III-6a** to **III-6d**, manifesting of their purity and the HRMS exhibit the classical peak corresponding to the cationic fragment $[M\text{-}NO_3^-]^+$ for **III-6a** to **III-6d**.

Molecular structures

Crystals of **III-6c** have been obtained by slow evaporation from an acetonitrile solution of **III-6c**.

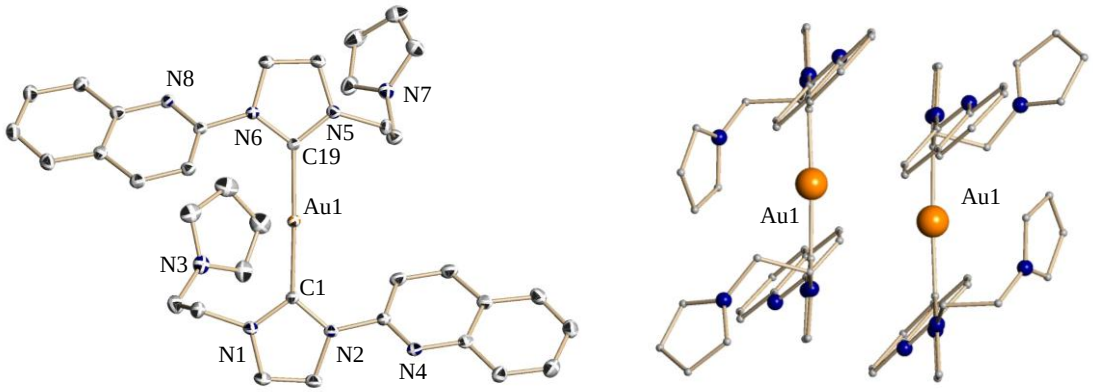

Fig 3.22 Molecule structure of **III-6c** in the solid state. On the left side the cationic part is depicted as a 50% level thermal ellipsoid plot. On the right side the dimeric arrangement is shown. For clarity H-atoms, non-coordinating anion, acetonitrile and disordered water molecules are omitted. Selected bond distances [Å] and angles [°]: Au1-C1 2.023(2), Au1-C19 2.023(2), C1-Au1-C19 177.20(7), Au1-Au1 3.424.

The geometrical environment of Au1 in **III-6c** (see Fig 3.22) is in perfect agreement with other NHC-Au-NHC cations. The atoms forming the NHC-Au-NHC skeleton are coplanar and the pyrrole side arms are situated on the same side of this plane. The short Au-Au distances are in good agreement with aurophilic interactions. As shown in Fig 3.23 the acetonitrile and water molecules are located in channels in the crystal packing, while the anions are more in-between the cations.

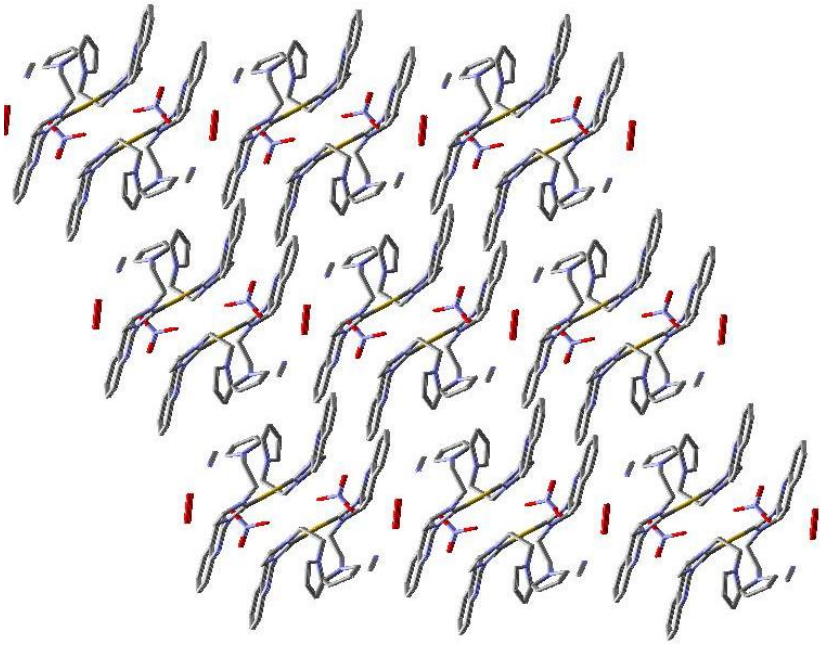

Fig 3.23 Packing of **III-6c** in the solid state with view along *a*.

Crystals of **III-6d** have been obtained by slow evaporation from a methanol solution of **III-6d**.

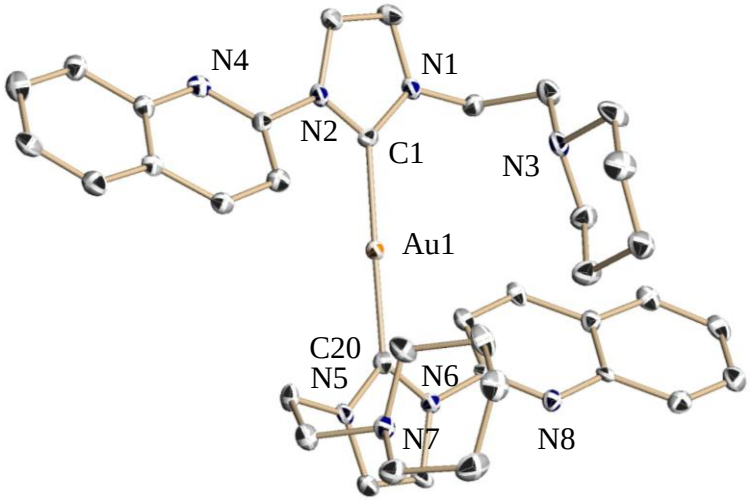

Fig 3.24 Molecule structure of **III-6d** in the solid state. The cationic part is depicted as a 50% level thermal ellipsoid plot. For clarity H-atoms, non-coordinating anion and a disordered methanol molecule are omitted. Selected bond distances [Å] and angles [°]: Au1-C1 2.022(5), Au1-C20 2.018(5), C1-Au1-C20 179.1(2), Au1-Au1 3.715.

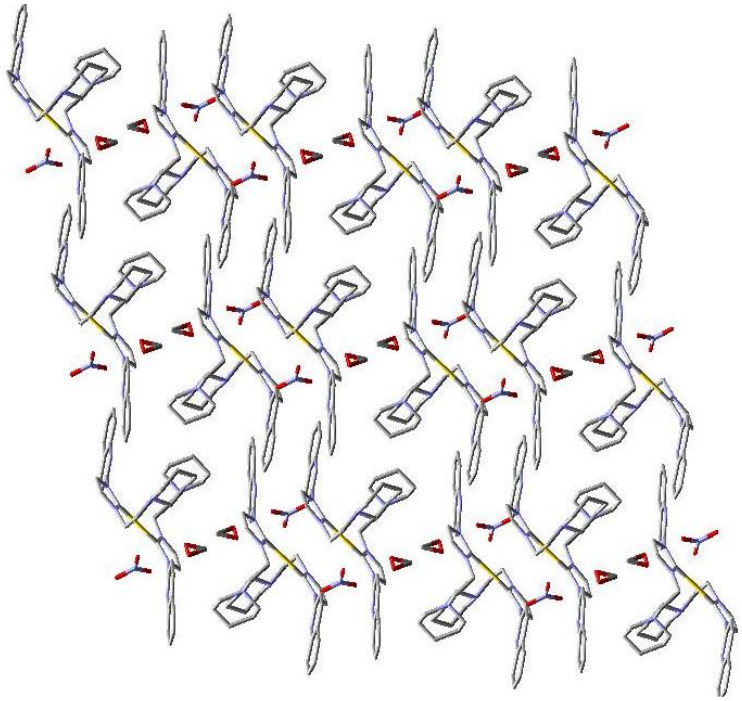

Fig 3.25 Packing of **III-6d** in the solid state with view along *b*.

The geometrical environment of Au1 in **III-6d** (see Fig 3.24) is very similar to other cations of this type. The atoms forming the NHC-Au-NHC skeleton are nearly coplanar with aslight torsan angel of 4 ° of the two NHC planes around the C-Au-C axis. The piperidine side arms are on the same side of the central NHC-Au-NHC plane due to a dimeric arrangement of the cations with long Au-Au distances of of 3.7 Å. As shown in Fig 3.25 the disordered methanol meolecules are located in channels in the crystal packing and the the anions in other channels, separated by the cations from the methanol.

In order to investigate the antiproliferative activities of this novel series of gold(I) cationic bis(NHC) complexes **III-6a** to **III-6d**, they were screened *in vitro* against PC-3 human prostate cancer cells and non-cancerous NIH3T3 murine fibroblast cells. This work has been done in collaboration with Dr. Olivier Cuvillier (IPBS, France), who supervised me to make the biological measurements. Results of the preliminary cytotoxic activities are presented in Table 3.3.

The GI_{50} values reported express the mean of three independent experiments

analyzed 72 h after treatment. Auranofin, a commercial drug for anti-arthritis, was used as a reference. Gold complexes **III-6a** to **III-6c** were more cytotoxic against PC-3 than auranofin with GI_{50} values ranging from 0.53 to 0.71 μM. Interestingly, all the complexes **III-6a** to **III-6c** induced less cytotoxicity than auranofin against non-cancerous NIH3T3 cells, which exhibited a higher selectivity between cancer cells and normal cells than auronofin.

Table 3.3 GI_{50} values of gold (I) complexes **III-6a** to **III-6d** and auronofin against PC-3 and NIH3T3 after 72h.

Complex	PC-3 (μM)	NIH3T3 (μM)	Log P
III-6d	0.55	1.97	0.168 ±0.011
III-6c	0.70	3.00	0.479 ±0.014
III-6a	0.71	2.70	0.549 ±0.009
III-6b	0.53	1.85	0.843 ±0.060
Auranofin	1.05	1.80	

In order to study the SAR of these gold(I) complexes, lipophilicity of this series of gold complexes has been measured. The obtained results are reported in Table 3.3. All the complexes displayed pronounced cytotoxicity with GI_{50} values ranging from 0.53 μM to 0.71 μM. However, no linear correlation between cytotoxic activity and lipophilicity could be observed. Compared with the family of gold(I) complexes containing aromatic amino side-arm (**III-3a** to **III-3d**), this series of compounds **III-6a** to **III-6b** showed less lipophilicity and less cytotoxicity towards healthy cell lines (NIH3T3) although they displayed lower anticancer activities than **III-3a** to **III-3d** against the tested cancer cell lines (PC-3). In addition, all these complexes exhibited higher antiproliferative activities towards cancer cells than the complexes bearing aliphatic amino side-arm (**II-3a** to **II-3d**).

In summary, lipophilicity plays an important role in cytotoxic activity. Nevertheless,

higher lipophilicity may lead to a better anticancer activity, but it can also trigger higher cytotoxicity against healthy cells, resulting in less selectivity. Therefore, the further optimization by pharmaco-modulation will be done to develop some gold complexes with high anticancer activity and low toxicity towards healthy cells.

4. Mechanistic studies of gold(I) complexes (**III-3c** and **IV-1**)

In this chapter, we will discuss about the mechanism of action of Au(I)-NHC complexes, such as cellular uptake, inhibition of isolated TrxR and cellular reducing agents, and reactive oxygen species (ROS) generation.

In chapter 3, the gold complex (**III-3c**, Fig 4.1) was found to be the most effective and selective one among all the tested compounds. In addition, the cationic bis(NHC) complex (**IV-1**, Fig 4.1),[96] which was previously synthesized by Dr. Catherine Hemmert in our group, showed also high cytotoxic potency and selectivity. Therefore, they were chosen for mechanistic studies.

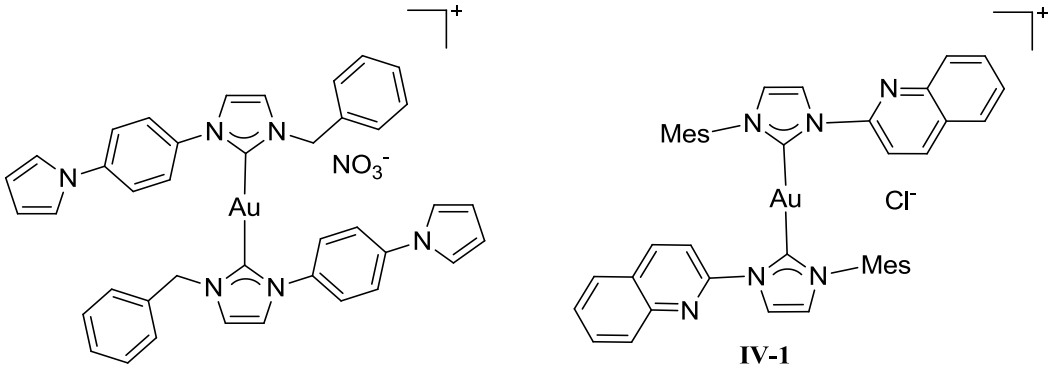

Fig 4.1 Structures of NHC gold(I) complexes **III-3c** and **IV-1** used in this study.

4.1. Cellular uptake

Since both cationic Au-NHC complexes **III-3c** and **IV-1** belong to the class of DLCs, they are expected to easily penetrate the cell membrane and efficiently accumulate in mitochondria of cancer cells due to the 60 mV difference of mitochondrial membrane potential between cancer cells and normal cells. Relationship between high cytotoxicity and intracellular accumulation is reported in previous literature.[100]

Therefore, we evaluate the cellular uptake of complex **III-3c** in PC-3 cells by a method based on gold quantification by inductive coupled plasma atomic emission

spectroscopy (ICP-AES). The measurements were performed under serum-free cell culture medium in order to avoid protein binding. For this purpose, cells were incubated with a 2 μM solution of complex **III-3c** for up to 4 h at 37 ^{o}C and 5 % CO_2, and the gold and protein contents of the cells were determined by ICP-AES and Bradford method, respectively. As shown in Fig 4.2, complex **III-3c** induced a time-dependent gold uptake in PC-3 cells. Additionally, an acute increase of cellular gold content occurred upon treatment with complex **III-3c** culminating a 0.087 μg/mg protein after 4 h of treatment, which corresponds to 0.46 nmol of gold per mg of protein. This result suggests the rapid cellular accumulation of the intact gold bis(NHC) and a good cellular bioavailability, which is in good agreement with the antiproliferative activity of this complex.

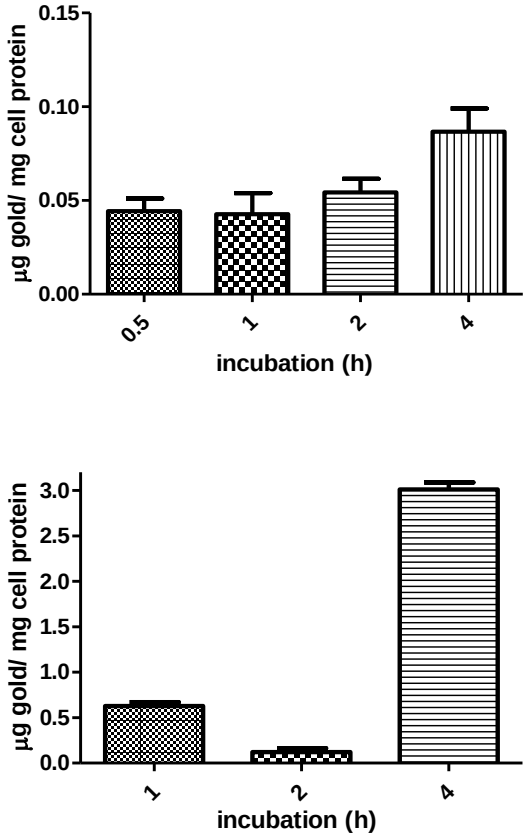

Figure 4.2 Gold uptake by PC-3 cells exposed to 2 μM of **III-3c** (left) and by HepG-2 cells exposed to 2 μM of **IV-1** (right).

For the gold complex **IV-1**, the same method was used. HepG-2 cells were incubated with a 2 μM solution of complex **IV-1** for 1, 2 and 4 h at 37 ºC and 5% CO_2, and the gold and protein levels of the cells were determined by ICP-AES and the Bradford method, respectively. Complex **IV-1** showed a cellular gold level of 0.63 μg/mg protein after 1 h of exposure, which then increased over the total incubation period of 4 h to 3.01 μg/mg protein. This result manifested a fast cellular uptake of complex **IV-1**, in accordance with cytotoxic activity of the complex.

The *in vitro* cytotoxicity of complex **IV-1** towards HepG-2 cells has been tested, giving a GI_{50} value of 0.46 μM. In addition, it has been discussed in chapter 3 that complex **III-3c** induces an anticancer activity on HepG-2 cells with a GI_{50} value of 0.64 μM. From the Fig 4.2, it is shown that complex **IV-1** induces more cellular uptake than complex **III-3c**. Therefore, there is a certain correlation between cellular uptake and *in vitro* cytotoxic activity. Higher cellular uptake may lead to better cytotoxicity.

4.2. Inhibition of mammalian TrxR

The ubiquitous selenoenzyme TrxR is considered as one of the common targets for gold complexes, as gold displays a high infinity to selenol groups.[26, 101] TrxR is a NADPH-dependent flavoprotein responsible for cell homeostasis regulation and inhibition of TrxR could lead to apoptosis through a mitochondrial pathway.[8d, 102] However, if gold displays a high affinity towards thiol and selenol groups, the inhibition potency of TrxR is influenced by the *N*-substituted groups of the NHC ligands and cannot be always correlated to the *in vitro* cytotoxicity. For example, Ott and co-workers reported a series of 20 structural diverse Au-NHC complexes (general structure: **IV-2**, Fig 4.3) with the aim of identifying the relationship between TrxR inhibition, antiproliferative activity and structural features of compounds.[46] Most of the tested complexes displayed cytotoxic activity towards HT-29 colon adenocarcinoma cells with GI_{50} values in the low micromolar range. The most active complex was **IV-2a** with a GI_{50} value of 2.8 μM. However, the IC_{50} value of this

complex towards isolated TrxR was just 5.08 μM. Therefore, a direct correlation between the cytotoxicity of complexes and the inhibition of TrxR could not be reached.

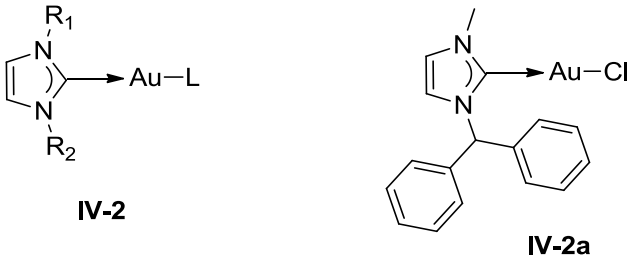

Figure 4.3 Structures of gold(I) NHC complexes (**IV-2**) reported by Ott and co-workers.

The potential of complex **III-3c** to inhibit the target enzyme TrxR was studied *in vitro* on purified rat liver TrxR. Moreover, inhibition of reducing agents present in cell extracts has been tested *in vitro*. Both tests used a previously reported assay based on the NADPH dependent reduction of the sulfide bond of the substrate 5,5'-dithiobis-2-nitrobenzoic acid (DTNB) by the isolate enzyme.[103] Complex **III-3c** was able to inhibit isolated TrxR in the low micromolar range with an IC_{50} value of 2.2 μM (Fig 4.4). In order to evaluate the inhibition of cellular reducing agents, PC-3 cells were exposed to complex **III-3c** in graded concentrations for 1 h and after treatment, the cells were monitored colorimetrically for their ability to reduce DTNB. The IC_{50} value for cellular reducing agents was 7.0 μM, which is in the same level as the isolated TrxR one (Fig 4.3).

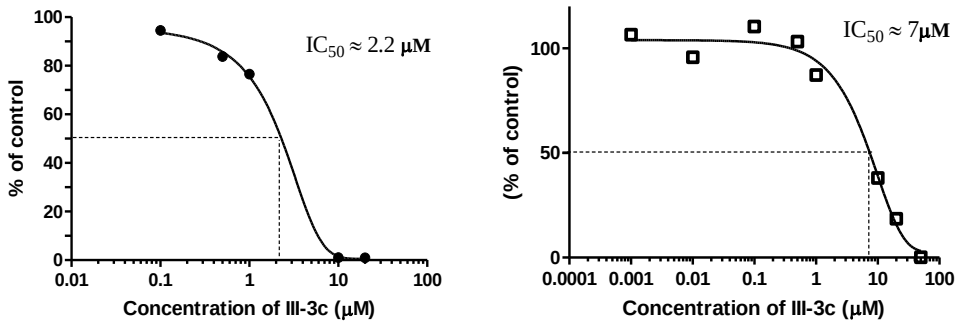

Figure 4.4 IC_{50} values of complex **III-3c** towards isolated TrxR (left) and reducing agents in PC-3 cells (right).

In addition, the inhibition of isolated rat liver TrxR and reducing agents present in cell extracts for complex **IV-1** was tested *in vitro*. Complex **IV-1** was able to inhibit isolated TrxR in the low micromolar range with an IC_{50} value of 2.1 μM (Fig 4.5). In order to evaluate the inhibition of cellular reducing agents, HepG-2 cells were exposed to complex **IV-1** in graded concentrations for 1 h and after treatment, the cell extracts were monitored colorimetrically for their ability to reduce DTNB. The IC_{50} value for cellular reducing agents was 2.0 μM, which is very close to the isolated TrxR one (Fig 4.5).

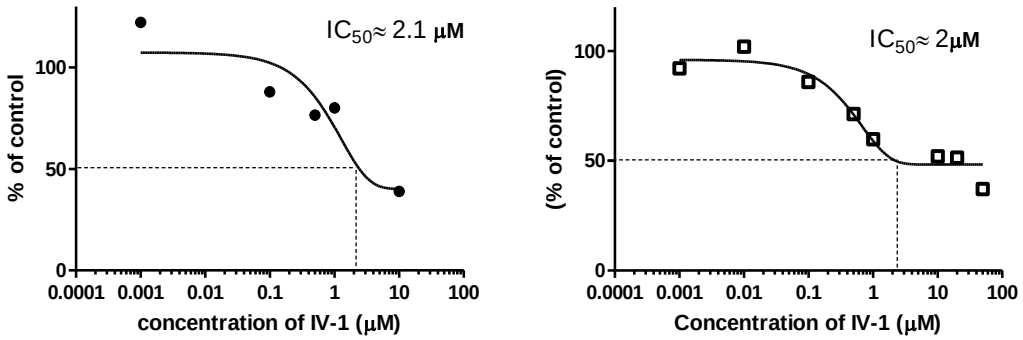

Figure 4.5 IC_{50} values of complex **IV-1** towards isolated TrxR (left) and reducing agents in HepG-2 cells (right).

Recently, a novel series of cationic gold(I) bis(NHC) complexes (**IV-3a** to **IV-3d**, Fig 4.6) designed by Ott and co-workers displayed high cytotoxicity against cancer cells, whereas they just showed moderate to low inhibitory activities towards isolated mammalian TrxR enzyme with IC_{50} values ranging from 16.3 to 127.8 μM.[63] It has been previously reported that neutral mono(NHC) gold(I) complexes were more effective TrxR inhibitors than their cationic bis(NHC) analogues, which can be illustrated in the case of 1,3-diethlbenzimidazol-2-ylidene NHC ligand.[43] The Au(I) bis(NHC) complex **IV-4b** (IC_{50} = 4.89 μM) was found to be less active compared with the mono(NHC) complex **IV-4a** (IC_{50} = 0.36 μM) towards isolated TrxR. Generally, the neutral complexes are less stable in solution and particularly in physiological medium because of the lability of the halide, which generates a vacant site on the gold and allow a fast coordination with selenocysteine residue of the TrxR. Overall, as

discussed in the introduction section, the TrxR appears to be a common relevant target among others shared for this kind of gold complexes.

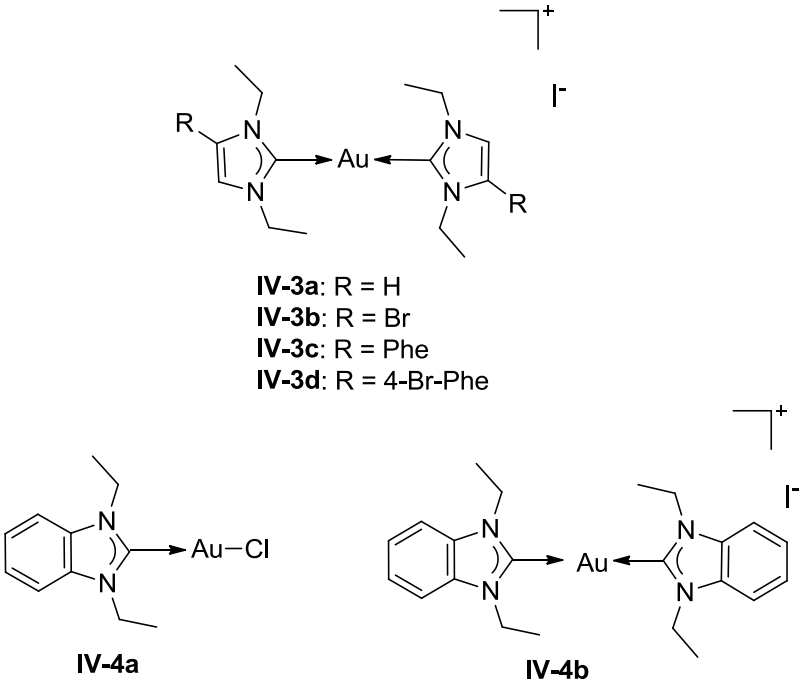

Figure 4.6 Structures of gold(I) NHC complexes (**IV-3** and **IV-4**) reported by Ott and co-workers.

4.3. Effects on intracellular ROS levels

Generation of reactive oxygen species (ROS) is a key characteristic of apoptotic cell death. ROS are mostly the products of the physiological mitochondrial cell metabolism and are involved in cellular redox homeostasis. Their formation may perturb the cellular antioxidant defense system. Au(I)-NHC complexes have been reported to generate ROS, which may be due to the inhibition of the TrxR, one of the antioxidant enzymes present in the mammalian cell together with catalase, glutathione peroxidase and superoxide dismutase that carry out the removal of ROS from the cells.[43, 104]

In order to examine whether ROS played a role in cytotoxicity induced by complex **IV-1**, we used *N*-acetylcysteine (NAC), a ROS scavenger, to study its effect on cell viability. For this purpose, HepG-2 cells were pretreated with NAC at different concentrations (2 mM, 5 mM and 10 mM) for 1 h before the gold complex (1 μM)

was added. After treatment, the results showed that NAC substantially dose-dependently reduced the ROS accumulation and cytotoxicity of complex **IV-1** in HepG-2 cells (Fig 4.7). These data suggested cytotoxicity induced by **IV-1** was ROS-dependent, which is in line with other previously reported gold complexes.

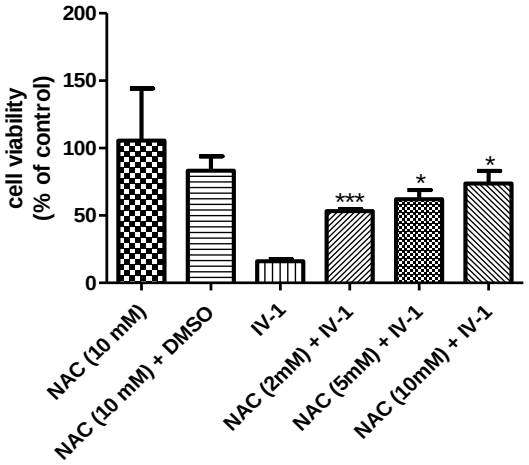

Figure 4.7 Effects of NAC at different concentrations on **IV-1**–induced cytotoxicity. Data are presented as means ± SEM of three independent experiments. *p<0.05, **p<0.005, ***p<0.001, compared with the cell viability of complex **IV-1** alone.

Similarly, PC-3, T24 and HepG-2 cells were pretreated with NAC or gluotathione reduced (GSH) at different concentrations (2 mM, 5 mM and 10 mM) for 1 h prior to the addition of the gold complex **III-3c** (1 μM). As shown in Fig 4.8, in case of HepG-2 cells, without treatment of NAC and GSH, the cell viability was around 30%. After treated with 10 mM of NAC and GSH, the cell viability increased sharply to approximately 70%, which suggests that both NAC and GSH substantially reduced cytotoxic activity of complex **III-3c** in HepG-2 cells. In addition, this tendency was dose-dependent since the cell viability treated with 2 mM and 5 mM of NAC and GSH was around 45% and 60%, respectively. The same results can be also observed in PC-3 and T24 cells. Therefore, both NAC and GSH can dose-dependently reduced ROS production and cytotoxicity of complexes **III-3c** in various cancer cells, suggesting that cell death triggered by comlex **III-3c** was ROS-dependent.

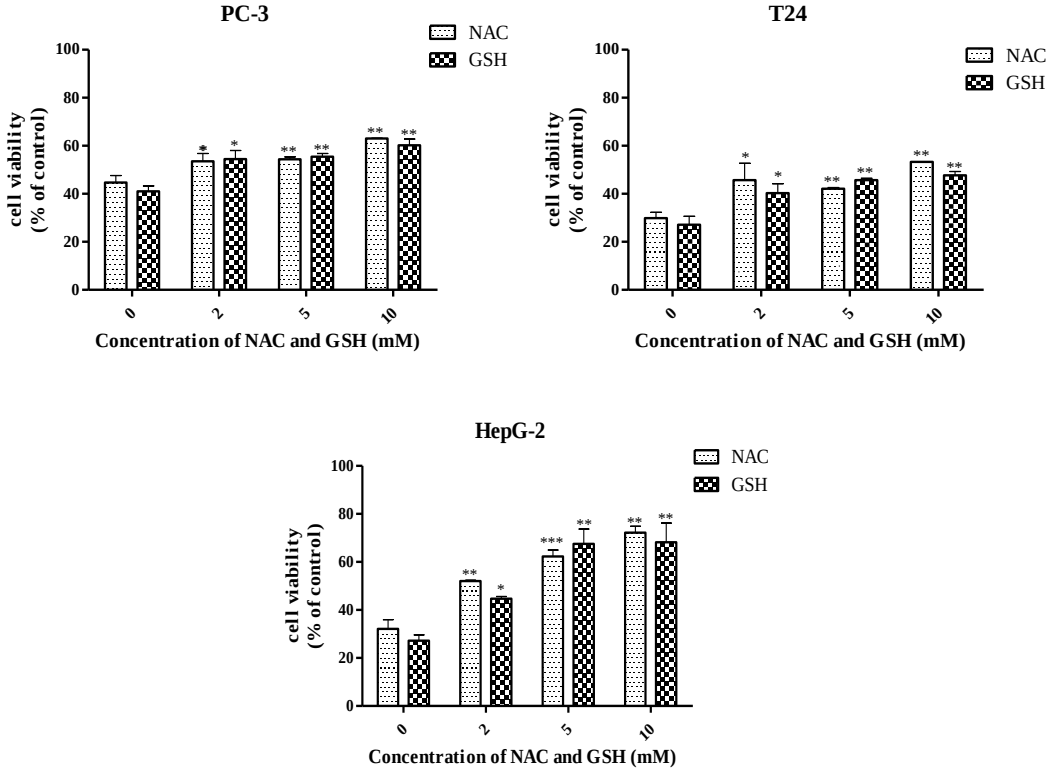

Figure 4.8 The impact of *N*-Acetyl-L-Cystein (NAC) and reduced gluothione (GSH) on the cytotoxicity of complex **III-3c** (1 μM). PC-3, T24 and HepG-2 cells were treated with complex **III-3c** (1 μM) for 24 h in the absence or presence of different concentrations of NAC and GSH. Cell viability was measured by MTT assay. Data are presented as means ± SEM of three independent experiments. *p<0.05, **p<0.005, ***p<0.001, compared with the cell viability of complex **III-3c** alone.

Moreover, the effect of complex **III-3c** on the ROS levels in PC-3 cells was determined by the nitroblue tetrazolium chloride (NBT) and 3,3'-diaminobenzidine (DAB) assays. DAB is oxidized by H_2O_2 in the presence of peroxidases and produces reddish brown precipitate. NBT reacts with $O_2^{-\cdot}$ to form a dark blue insoluble formazan compound.[105] For DAB assays, PC-3 cells were seeded in 24-well plates. After 24 h of incubation at 37 ºC and 5% CO_2, the cell culture medium was replaced by fresh medium containing gold complex **III-3c** (1 μM), and the plates were incubated for different period of time (0 h, 3 h, 6 h and 24 h). 500 μL of 3,3'-diaminobenzidine solution (DAB, 2.5 mM) in potassium phosphate buffer were

added to the plates after removal of medium. After 4 h of incubation, ROS generation was quantified by spectrophotometry with a microplate reader at 405 nm absorbance. For NBT assays, the PC-3 cells were plated in 24-well plates and the tested complex **III-3c** was added at concentration of 1 μM after 24 h of incubation at 37 ºC and 5% CO_2. Then a 0.1% solution of NBT (250 μL per well) in PBS was added to the cells after removal of the medium at different time point (0 h, 3 h, 6 h and 24 h). After another 4 h of incubation, the supernatant NBT solution was discarded and the reduced formazan was dissolved equentially in 360 μL of 2 M KOH followed by 400 μL of DMSO and read at 620 nm using KOH/DMSO as a blank.

As shown in Fig 4.9, after 3 h of incubation in PC-3 cells, complex **III-3c** at concentration of 1 μM induced around 30 % increase of $O_2^{\cdot-}$ levels and 15 % elevation of H_2O_2 production compared with untreated control cells. However, with the increase of time, the ROS production decreased to the same level as the controls perhaps due to cell death.

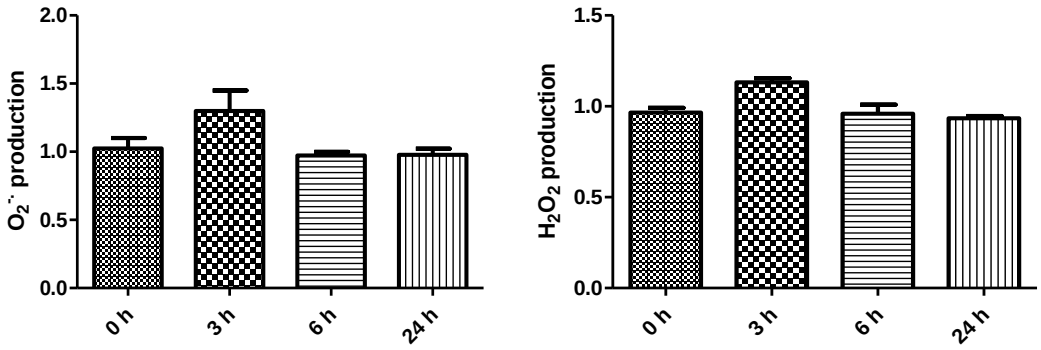

Figure 4.9 ROS levels in PC-3 cells as determined by NBT assays (left) and DAB assays (right).

Furthermore, the effect of gold complex **III-3c** on intracellular ROS levels was detected by fluorometric assays with 2',7'–dichlorofluorescein diacetate (DCFDA), a fluorogenic dye that measures hydroxyl, peroxyl and other ROS production within the cells. After diffusion into the cells, DCFDA is deacetylated by cellular esterases to a non-fluorescent compound, which is later oxidized by ROS into 2',7'-dichloro fluorescin (DCF). DCF is a highly fluorescent compound which can be detected by

fluorescence spectroscopy with maximum excitation and emission wavelengths of 485 nm and 535 nm, respectively.[106] As shown in Fig 4.10, PC-3, T24 and HepG-2 cells treated with auranofin (5 μM) and gold complex **III-3c** (1 μM and 5 μM) significantly triggered the generation of ROS in cells within 6 h. In the case of HepG-2 cells, compared with the control, for cells treated with 1 μM and 5 μM of complex **III-3c**, the mean fluorescence intensity increased by 50 %, which indicated that gold complex **III-3c** can significantly induce elevation of intracellular ROS levels.

Collectively, all these results suggest that ROS play an important role in cell death induced by the two tested complexes **III-3c** and **IV-1**.

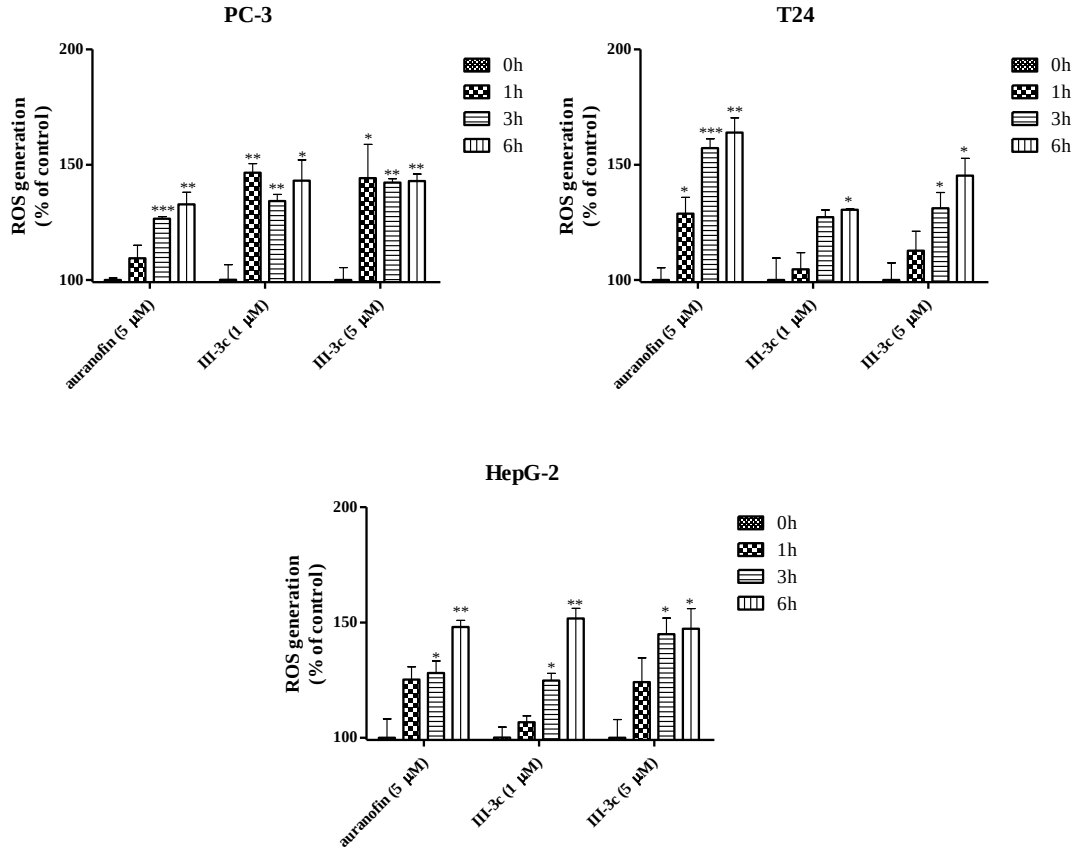

Figure 4.10 Induction of ROS by gold complexes (auranofin and complex **III-3c**) on PC-3, T24 and HepG-2 cells after different times of treatment. *p<0.05, **p<0.005, ***p<0.001, compared with ROS generation at 0 h.

In summary, the mechanistic studies of complexes **III-3c** and **IV-1** showed by monitoring the cellular uptake that these two cationic gold(I) bis(NHC) complexes are

biologically available. In addition, they were inhibitors of TrxR enzyme, a common target for various gold(I) complexes, and the cell death induced by them was ROS-dependent.

5. Gold complexes as antileishmanial agents

5.1. Introduction

Among tropical diseases, leishmaniasis remains one of the most neglected concerning available controls and affects more and more countries. In 2007 this parasitic disease was endemic in 88 countries, in 2012 in 98 countries (mainly in tropical and sub-tropical regions, but also in southern Europe, especially around the Mediterranean area), and the number of cases grows continuously and is still certainly underestimated because reporting of this disease is mandatory in only 33 of the 98 countries involved.[107] The major factors for *Leishmania* propagation are mass migration of non-immune populations, deteriorating of socio-economic conditions and increase of immune-deficient people, leading to a resurgence of leishmaniasis worldwide. Actually, this disease affects approximately 12 million people with approximately 1.3 million new cases every year and is the second most lethal parasitic infection all over the world with about 50,000 deaths per year.[108] The *Leishmania* parasite is transmitted in its promastigote form to the mammalian host by the bite of infected sandflies (Phlebotominae) during their blood meal. Then promastigotes target cells of the immune system, macrophages and dendritic cells, where they differentiate into amastigotes forms, living inside the digestive vacuole of these host cells, responsible for leishmaniasis. The life cycle of *Leishmania* is descripted in more detail in Fig 5.1.

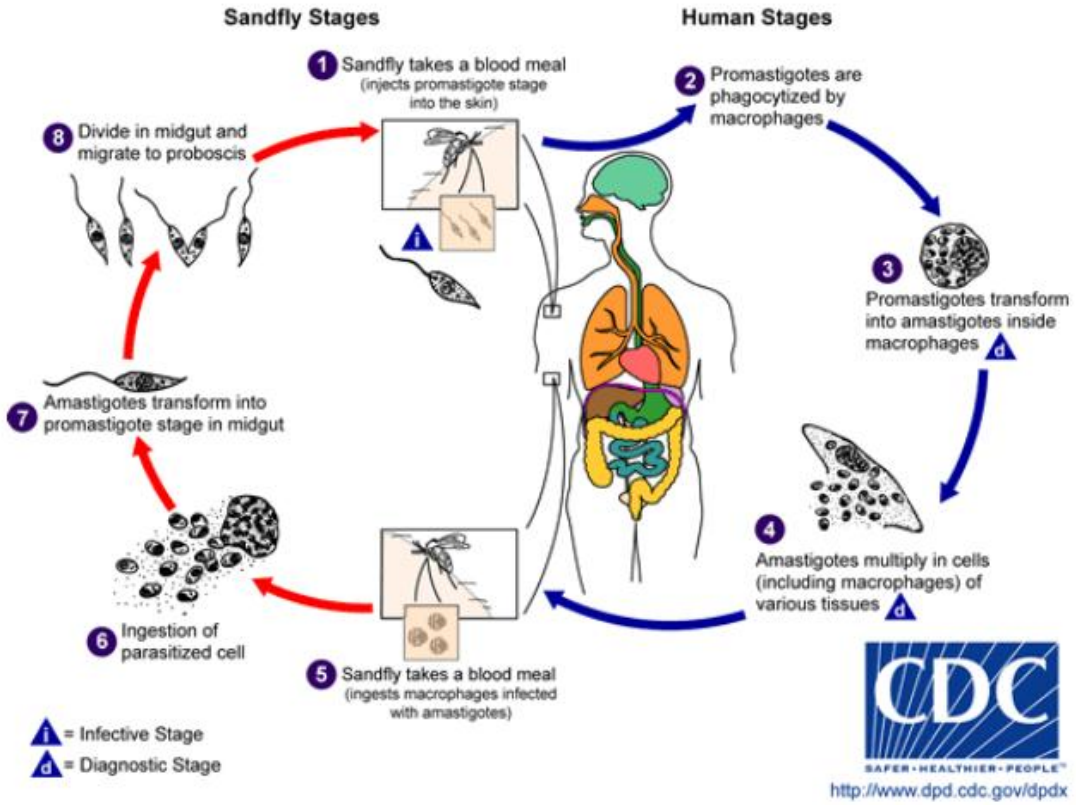

Figure 5.1 Scheme of the life cycle of *Leishmania*.[109]

For many years, treatment of humans has relied on pentavalent antimonials using compounds like sodium stibogluconate and meglumine antimoniate (Fig 5.2), but these antimonials were found to be toxic with life-threatening adverse effects, such as cardiac arrhythmia and acute pancreatitis. Later, antimonials were successfully replaced by antibiotics, amphotericin B (Fig 5.2) and its formulations, paromomycin (Fig 5.2) and the only orally administered drug miltefosine (Fig 5.2).[110] Sitamaquine and fexinidazole (Fig 5.2) are the only new drugs in phase II clinical trial.[111] Nevertheless, none of these drugs are ideal for treatment due to their high toxicity, resistance issues, prohibitive prices, long treatment regimen and mode of administration.[110] Until now, there is no available vaccine for humans, however, dogs can be preventively treated by the CaniLeish® (Europe), Leishmune® or Leish-Tec® (Brazil) vaccines.[112] Therefore, the need for the discovery and development of more efficient drugs with reduced side effects in their treatment against *Leishmania* is in high demand for health researchers.

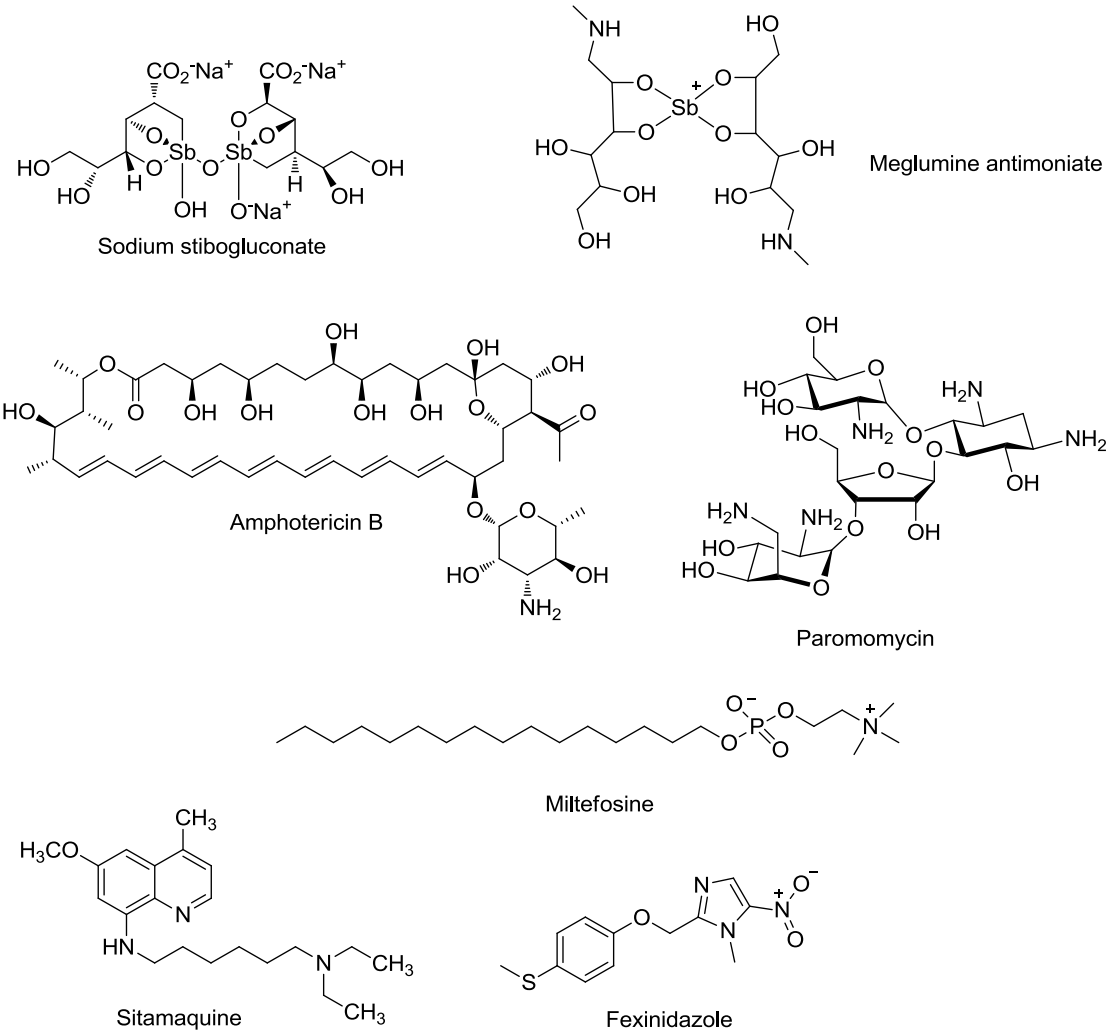

Figure 5.2 Commercial drugs currently used against leishmaniasis.

Recently, besides anticancer activities, we also tested gold(I) NHC complexes for other biomedical applications, in particular the parasite disease leishmaniasis.[113] A series of cationic or neutral gold complexes containing quinoline functionalized NHC ligands (**V-1a** to **V-1e**, Fig 5.3) were designed and prepared by Dr. Catherine Hemmert in our group, and tested for their antileishmanial activities in collaboration with Pr. Alexis Valentin (IRD-Pharma-DEV, Toulouse).[113a] Proligands and their corresponding gold complexes were evaluated *in vitro* towards *Leishmania infantum*. All these complexes showed potent anti-leishmanial activities against *L. infantum* promastigotes (IC_{50} values ranging from 0.39 to 1.86 μM), whereas proligands were inactive. The three most active complexes (**V-1a**, **V-1b** and **V-1d**, Fig 5.3) were also

tested towards *L. infantum* intracellular amastigotes, the relevant form in human cycle, giving low IC_{50} values of 0.40, 0.96 and 0.24 μM, respectively.

Furthermore, cytotoxicity was assessed on the murine J774A.1 macrophages to determine the selectivity of action. The highest selectivity index close to 10 has been observed for the neutral complex **V-1b**. This complex displays an antipromastigotes activity 38 times and 3 times higher than the one of amphotericin B and pentamidine, respectively, but 5.8 times lower than the one of miltefosine, and an antiamatisgotes activity 4.3 times lower than the one of miltefosine also. Overall, SAR can be brought out for this family of gold complexes. Firstly, the results evidenced the key role of the gold cation in antileishmanial activities against *L. infantum* promastigotes and intracellular amastigotes. Secondly, the charge of the complex constitutes an important factor for the selectivity: the neutral gold complex **V-1b** can be considered as the hit molecule in this study.

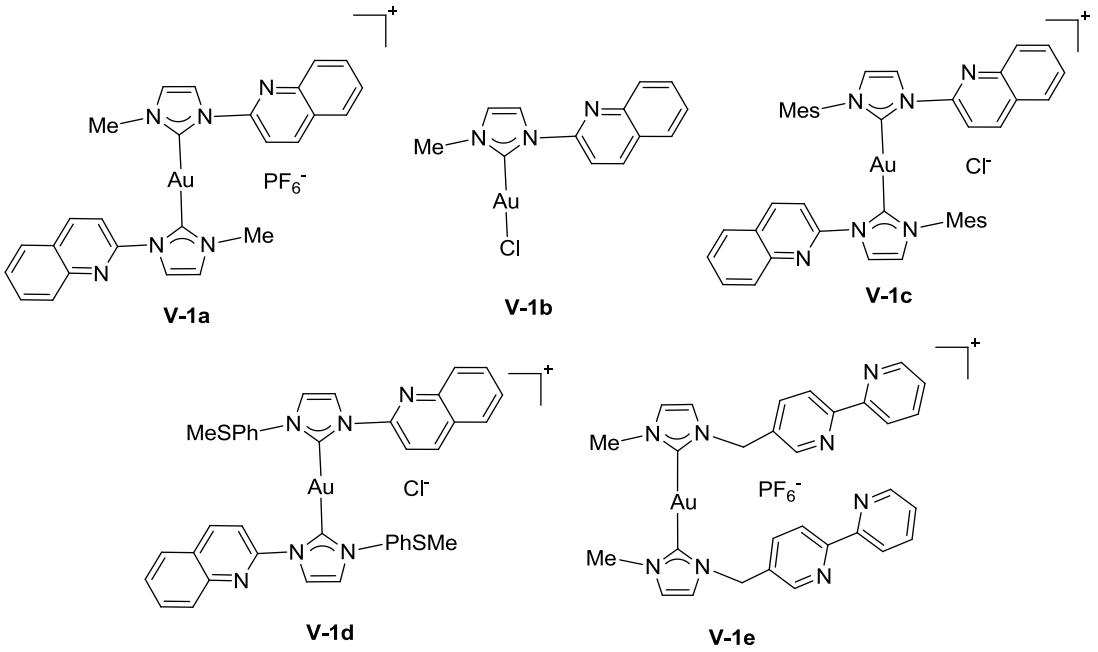

Fig 5.3 NHC-Au(I) complexes as antileishmanial agents (**V-1a** to **V-1e**) reported in our group.

Within this framework, the next step of our work was the pharcomodulation of our lead complex **V-1b** by fine tuning either the non-fuctionalized group (alkyl or aryl) or/and the functionalized entities, in order to improve both activity and selectivity

towards intracellular amatisgote forms of *Leishmania*. Therefore, we investigated the antileishmanial potency of nine mononuclear neutral gold(I) complexes containing NHC ligands (**V-2a to V-2i**, Fig 5.4), including five new complexes.[113b]

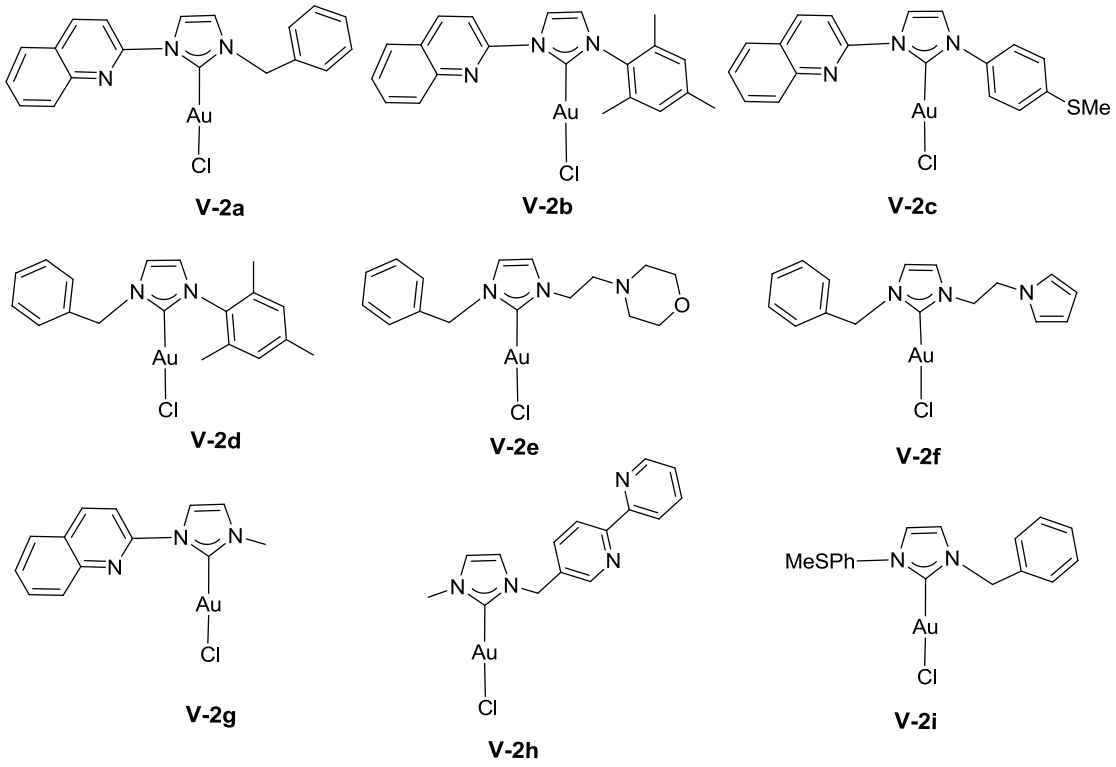

Fig 5.4 Neutral Au(I)-NHC complexes as antileishmanial agents (**V-2a** to **V-2i**) reported from our group.

5.2. Synthesis and Characterization

I participated in this study with the synthesis of complexes **V-2e** and **V-2f**. The synthesis and characterization of proligands **II-2b** and **II-2c** have been mentioned in Chapter 2, Section 2.2.

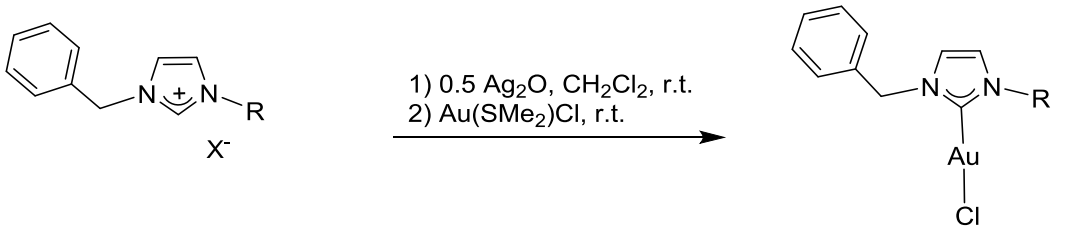

Ligand	R	X	Complex	Yield (%)
II-2c	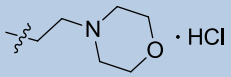	Cl	**V-2e**	90
II-2b	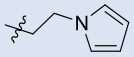	Br	**V-2f**	50

Fig 5.5 Synthesis of gold(I) complexes **V-2e** and **V-2f**.

The neutral gold(I) complexes **V-2e** and **V-2f** were synthesized *via* the transmetalation route (Fig 5.5). Firstly, the silver precursor complexes were prepared by deprotonation of the imidazolium salts **II-2c** and **II-2b**, with one equivalent of the mild base Ag_2O in acetonitrile at room temperature. The carbene transfer reaction was then carried out *in situ*, by adding a little excess (1.2 equivalent) of $Au(SMe_2)Cl$, with respect to the ligands. Gold(I) complexes **V-2e** and **V-2f** were isolated as grey powders with good yields. NMR spectroscopy unequivocally demonstrated the formation of the gold(I) complexes; the ^{13}C NMR spectra show the resonance for the carbene carbon in the range of 170.5 to 170.7 ppm, in good agreement with reported values for NHC-Au-X (X = halide).[97] The elemental analysis of the gold(I) complexes correspond to the general formula AuLCl and the HRMS exhibit the classical peaks corresponding to the cationic fragments $[M\text{-}Cl^-]^+$ for compounds **V-2e** and **V-2f**.

5.3. Molecular structure

Crystals of **V-2e** suitable for X-ray diffraction analysis were obtained by slow evaporation from an acetonitrile solution of this compound (Fig 5.6).

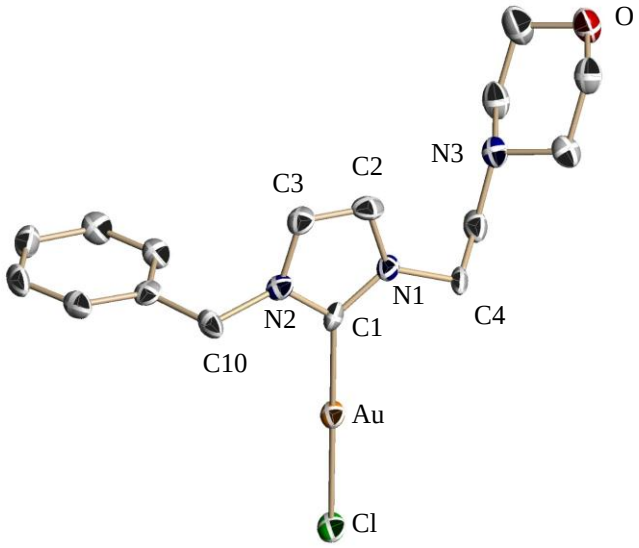

Fig 5.6 Crystal structure of **V-2e** depicted at 50% level. Hydrogen atoms have been omitted for clarity. Selected bond lengths [Å] and angles [°]: Au-C1 1.992(7), Au-Cl 2.284(2), C1-Au-Cl 179.4(2).

Crystals of **V-2f** suitable for X-ray diffraction analysis were obtained by slow evaporation from an acetonitrile solution of this compound (Fig 5.7).

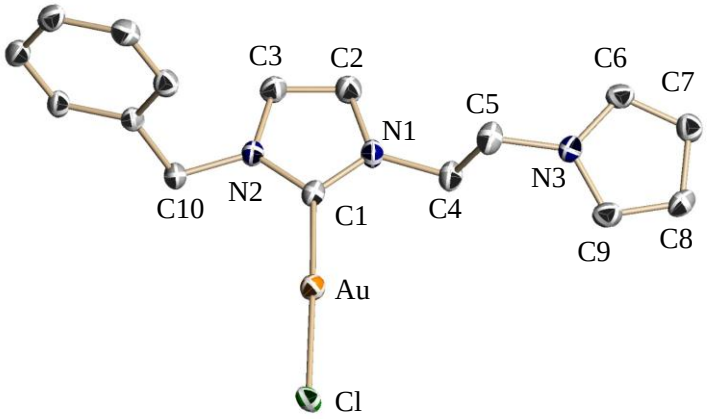

Figure 5.7 Crystal structure of **V-2f** depicted at 50% level. Hydrogen atoms have been omitted for clarity. Selected bond lengths [Å] and angles [°]: Au-C1 1.982(4), Au-Cl 2.309(1), C1-Au-Cl 177.6(2).

In these two complexes gold-carbon distances between 1.98 Å and 2.00 Å and gold-chlorine distances between 2.28 Å and 2.31 Å are in good agreement with other NHC-Au-Cl complexes. The C-Au-Cl angles show a nearly perfect linear

coordination (176 ° to 180 °) which represents the classical geometry for gold in the oxidation state +1. The shortest gold-gold distances of 5.7 Å (**V-2e**) and 4.05 Å (**V-2f**) are too long for aurophilic interactions, so these two complexes present isolated units without strong intermolecular interactions.

5.4. Antileishmanial activity

The antileishmanial activity of complexes **V-2a** to **V-2i** were screened *in vitro* on both the promastigote and the axenic amastigote stages of *L. infantum* by determining their inhibitory concentration 50% (IC_{50}), in collaboration with Pr. Alexis Valentin and Dr. Sandra Bougeade Delmas (IRD-Pharma-DEV, Toulouse). These complexes were also evaluated *in vitro* for their cytotoxicity, measured by cytotoxic concentration 50% (CC_{50}) on J774A.1 macrophages, giving access to selectivity index (SI = CC_{50}/IC_{50}). The results were summarized in Table 5.1. Except complex **V-2e**, all gold(I) complexes were active against promastigote and axenic amatisgote forms of *L. infantum*, with IC_{50} values ranging from 2.52 to 11.16 μM and from 0.19 to 2.17 μM, respectively. In terms of antipromastigote activity, the NHC-Au(I)-Cl complexes were rather toxic for the most part, with SI values between 0.24 to 1.78, except the complex **V-2d** with a SI value of 3.09. Complexes **V-2a** to **V-2d** and **V-2f** to **V-2h** were more efficient than miltefosine (IC_{50} = 20.26 μM) and show the same level of selectivity as that of pentamidine (SI = 0.40) and miltefosine (SI = 2.30). Moreover, the gold(I)-NHC complexes were more active against the axenic amastigote form of *L. infantum* when compared to their antipromastigote activity and five of them were selective against axenic parasites with SI values ranging from 9.14 to 40.29.

Table 5.1 *In vitro* antileishmanial activity and cytotoxicity of complexes **V-2a** to **V-2i**.

Compound	*L. infantum* promastigotes IC_{50} (µM)[a]	*L. infantum* axenic amastigotes IC_{50} (µM)[a]	J774A.1 CC_{50} (µM)[a]	Selectivity index Pro **CC_{50}/IC_{50} (Pro)**	Selectivity index Ama **CC_{50}/IC_{50} (Ama)**	Selectivity index **Pro/Ama IC_{50} (Pro)/IC_{50} (Ama)**
V-2a	11.16 ±0.15	1.17 ±0.21	11.20 ±2.07	1.00	9.60	9.54
V-2b	4.68 ±0.61	0.68 ±0.02	3.69 ±0.73	0.79	5.40	6.88
V-2c	8.27 ±0.15	0.73 ±0.09	6.72 ±0.17	0.81	9.20	11.33
V-2d	2.52 ±0.51	0.19 ±0.04	7.79 ±1.14	3.09	40.29	13.26
V-2e	57.03 ±0.46	11.07 ±1.04	32.39 ±1.22	0.57	2.93	5.15
V-2f	10.32 ±1.29	2.17 ±0.14	9.30 ±076	0.90	4.29	4.76
V-2g	6.05 ±0.17	0.71 ±0.05	10.76 ±2.23	1.78	15.23	8.52
V-2h	2.78 ±0.28	0.40 ±0.13	0.66 ±0.08	0.24	1.64	6.95
V-2i	6.76 ±0.72	0.88 ±0.30	8.04 ±1.14	1.19	9.14	7.68
AmphotericinB[b]	0.04 ±0.01	0.05 ±0.01	1.31 ±0.09	34.47	24.11	0.80
Pentamidine[b]	1.64 ±0.03	1.50 ±0.21	0.65 ±0.17	0.40	0.43	1.09
Miltefosine[b]	20.46 ±0.72	0.66 ±0.03	47.13 ±1.79	2.30	71.78	31.00
Doxorubicin[c]			0.047 ±0.001			

[a] Mean of three independent experiments.

[b] Amphotericin B, Miltefosine and Pentamidine were used as antileishmanial compounds of reference.

[c] Doxorubicin was used as positive control of cytotoxicity.

These complexes can be separated into two families. One family of complexes (**V-2a** to **V-2c**, **V-2g**) used in this study contained a quinoline moiety on one side of the azolium ring and several aliphatic or aromatic groups on the other side, namely methyl (**V-2g**), benzyl (**V-2a**), mesityl (**V-2b**) and thioanisole (**V-2c**). Concerning this series, it should be noted that all these complexes showed strong activities against amatisgotes with IC_{50} values between 0.68 and 1.17 µM. This means that the antiamastigote activity was not affected by the nature of the second subtituent on the NHC. However, it is the second substituent that affects the toxicity against J774A.1

macrophages. The most lipophilic complex of this series, the mesityl substituted **V-2b**, gave the lowest CC_{50} value of 3.69 μM and the lowest selectivity index of 5.4 and the less lipophilic one, the methyl substituted **V-2g**, shows a high CC_{50} value of 10.76 μM giving a selectivity index of 15.23, which represents the second best value of all the complexes tested in this study. Complexes **V-2a** and **V-2c** showed also very good selectivity indexes of 9.60 and 9.20, respectively. As observed for the complex **V-2g**, the bipyridylmethyl substituted complex **V-2h** displayed a low SI value of 1.64, due to its high toxicity against J774A.1 macrophages (CC_{50} value of 0.66 μM).

Another family of complexes (**V-2a**, **V-2d** to **V-2f** and **V-2i**) concerned benzyl substituted ligands with complex **V-2a** being the common point with the quinoline series. From the table 5.1, we can see that both the morpholine containing complex **V-2e** and pyrrole bearing complex **V-2f** showed moderate activities against amatisgotes with IC_{50} values of 11.07 and 2.17 μM and low SI values of 2.93 and 4.29, respectively. Moreover, the thioanisole substituted complex **V-2i** displayed very similar activity (IC_{50} = 0.88 μM) and selectivity (SI = 9.14) as obtained for the quinoline/benzyl complex **V-2a** and the thioanisole/quinoline complex **V-2c**. Interestingly, complex **V-2d** showed the lowest IC_{50} value (0.19 μM) and the highest SI value (40.29) of all the tested complexes and was the lead-complex of this pharmaco-modulation work.

Another important aspect in the development for antileishmanial drug is capacity to differentiate between promastigote and amastigote stages. It should be noted that the reference drugs Amphotericin B and Pentamidine have SI (Pro/Ama) values around 1, and Miltefosine shows a high SI value of 31, due to its low antipromastigote activity. All the tested complexes display high SI (Pro/Ama) values ranging from 4.76 to 13.66, with the best value for the most active complex **V-2d**.

In conclusion, a new family of five neutral gold(I) complexes based on functionalized NHCs has been synthesized and fully characterized. Together with four previously described ones, they were screened *in vitro* against both promatigote and axenic amastigote forms of *L. infantum*. Moreover, their cytotoxicity was evaluated on the murine J774A.1 macrophages in order to determine their selectivity of action.

From this study, 7 of 9 gold(I) NHC complexes displayed good antiamastigote activities with IC_{50} values ranging from 0.19 to 1.17 μM. In particular, the most active one, bearing simple mesityl and benzyl substituents, represents a promising metallodrug showing selectivity of action against the pathological relevant form of *Leishmania*.

6. Iridium(III) NHC complexes as theranostic agents with potential for photodynamic therapy (PDT)

6.1. Introduction

In this chapter, the synthesis and characterization of eight cyclometalated iridium(III) complexes containing NHC ligands, their photophysical properties and related photodynamic anticancer activities will be discussed.

In the literature, only a limited number of iridium(III) bis(NHC) complexes for an application as photosensitizers (PSs) have been reported. Mao and co-workers reported three cyclometalated iridium(III) complexes containing two phenylpyridine ligands and one bis-NHC ligand (**VI-1a** to **VI-1c**, Fig 6.1) as theranostic and photodynamic anticancer agents.[114] All these complexes displayed better cytotoxicity than cisplatin and their precursor $[IrCl(ppy)_2]_2$ against various cancer cells with IC_{50} values ranging from 1.0 to 10.4 μM, and they were less toxic against normal LO2 cells than against cancer cells with IC_{50} values ranging from 8.0 to 17.3 μM. In addition, by measuring the lipophilicity of these complexes, the direct relationship between log P and antiproliferative activity was obtained. Complexes **VI-1a** to **VI-1c** could be taken up into HeLa cells very efficiently, and particularly accumulate in mitochondria. Mechanistic studies demonstrated that complexes **VI-1a** to **VI-1c** induced cell death in HeLa cells through apoptotic pathway involving ROS generation, release of cytochrome c and activation of caspase. Furthermore, the photocytotoxicity of all the complexes were tested against HeLa, A549 and cisplatin-resistant A549R cells upon 365 nm light irradiation. Of note, the cytotoxicity of complexes **VI-1a** to **VI-1c** against various cancer cells was enhanced significantly upon irradiation with PI values ranging from 9 to 3488, which suggests that these iridium(III) complexes have potential to be utilized as photodynamic therapeutic agents.

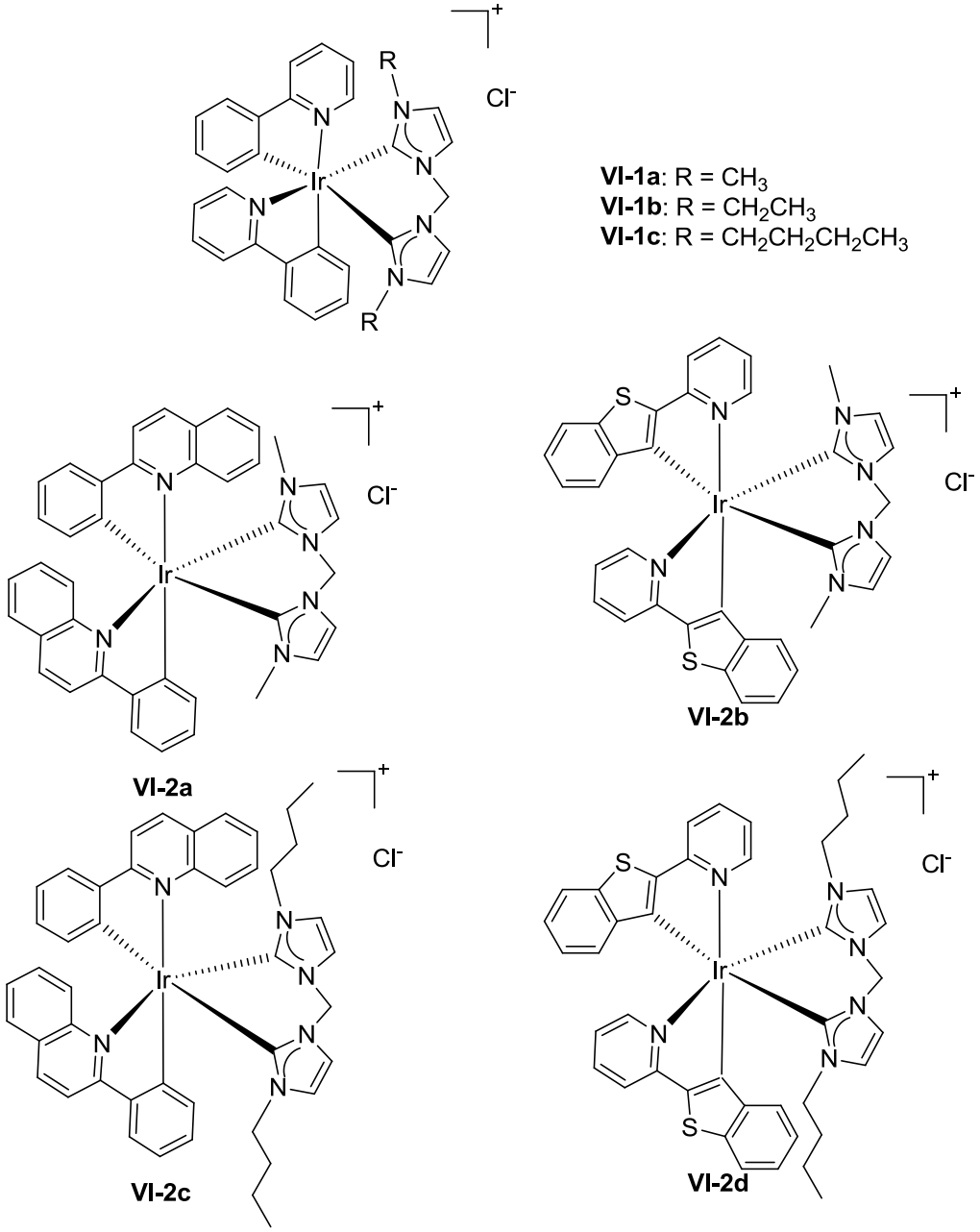

Fig 6.1 Iridium(III)-bisNHC complexes as PSs reported by Mao and co-workers (**VI-1a** to **VI-1c** and **VI-2a** to **VI-2d**).

Following these interesting results, the same group reported four cyclometalated iridium(III) complexes with bisNHC ligands (**VI-2a** to **V-2d**, Fig 6.1) as mitochondria-targeting photodynamic anticancer agents.[115] In this series, they did not change the bisNHC ligands, whereas they did some pharmaco-modulation by using two different kinds of C^N ligands like phenylquinoline and pyridylbenzothiophene. These complexes **VI-2a** to **VI-2d** displayed higher cytotoxicity than cisplatin against

A549 and A549R with IC_{50} values spanning from 1.2 to 5.6 μM. The antiproliferative activities of these complexes were correlated with the lipophilicity and their cellular uptake abilities. Complex **VI-2a** entered A549 cells, and it was localized in mitochondria. Mechanistic studies showed that these complexes can induce a series of events associated with cell death containing mitochondrial depolarization, ROS production, activation of caspase and apoptosis. Due to their high singlet oxygen quantum yields ranging from 0.32 to 0.62, the phototoxic activities of these complexes upon 450 nm LED light irradiation were tested. The IC_{50} values of **VI-2a** to **V-2d** decreased very significantly after irradiation, and the PI values of **VI-2a** were over 500 towards A549 and A549R cells, **VI-2a** being a potential visible light PDT agent.

6.2. Synthesis and characterization

The objective of the project was the preparation of luminescent cyclometalated iridium(III) NHC complexes as theranostic agents with PDT activity. The Fig 6.2 shows schematically three families of iridium complexes that we have designed. The difference between the three families of complexes resides in the NHC ligands. The first two families contain a bis-carbene ligand in which the two NHCs are bridged by a methylene (C1) and an ethylene (C2), giving rise to cationic complexes. The other one (C0) contains only one mono-carbene ligand and one chloride, leading to a neural complex. Moreover, compared to the work of Mao, we introduced different NHC ligands bearing aliphatic or aromatic, nitrogen or sulfur functionalized groups, with the aim of modulating the steric hindrance and the lipophilicty of the resulting complexes.

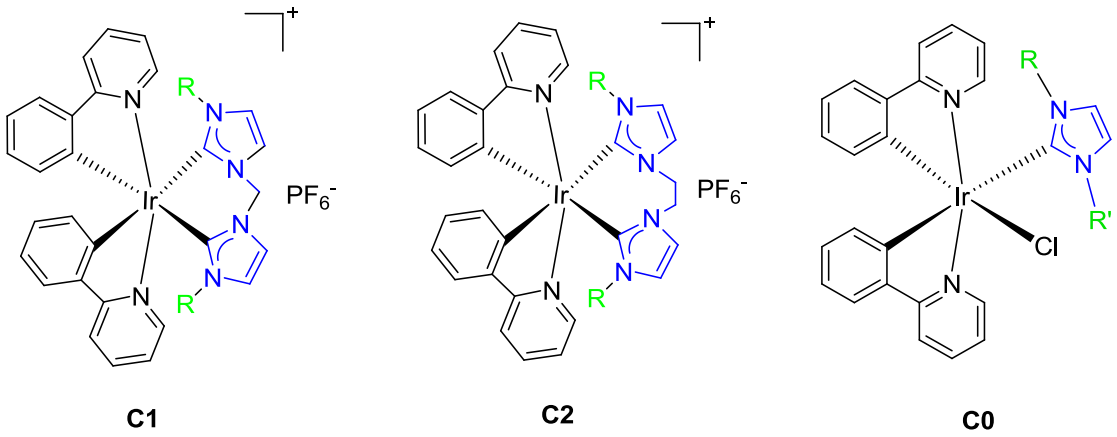

Fig 6.2 Three families of iridium NHC complexes. R and R' will be defined later.

The bis(imidazolium) salts **VI-3a** to **VI-3g** were synthesized by two methods (Fig 6.3). Method 1: firstly, 1,1'-methylene bis(1*H*-imidazole) was obtained using modified protocols of Tejeda.[116] Then it was reacted with 2.2 equivalents of alkyl halides, such as 2-bromopropane (**a**), 1-bromo-2-methylpropane (**b**), benzyl chloride (**c**) and 1-(2-chloroethyl) piperidine hydrochloride (**d**) to obtain the carbene precursors with yields ranging from 34% to 71%. In the case of 4-bromothioanisole, we failed to obtain the carbene precursor using the same conditions. Method 2: the substituted imidazoles were achieved by reacting imidazole with various alkyl and aryl halides like 4-bromothioanisole (**e**), benzyl chloride (**f**) and 1-bromo-2-methylpropane (**g**). Following that, they were reacted with an excess of dibromomethane or dibromoethane to obtain the desired proligands with yields ranging from 44% to 90%.

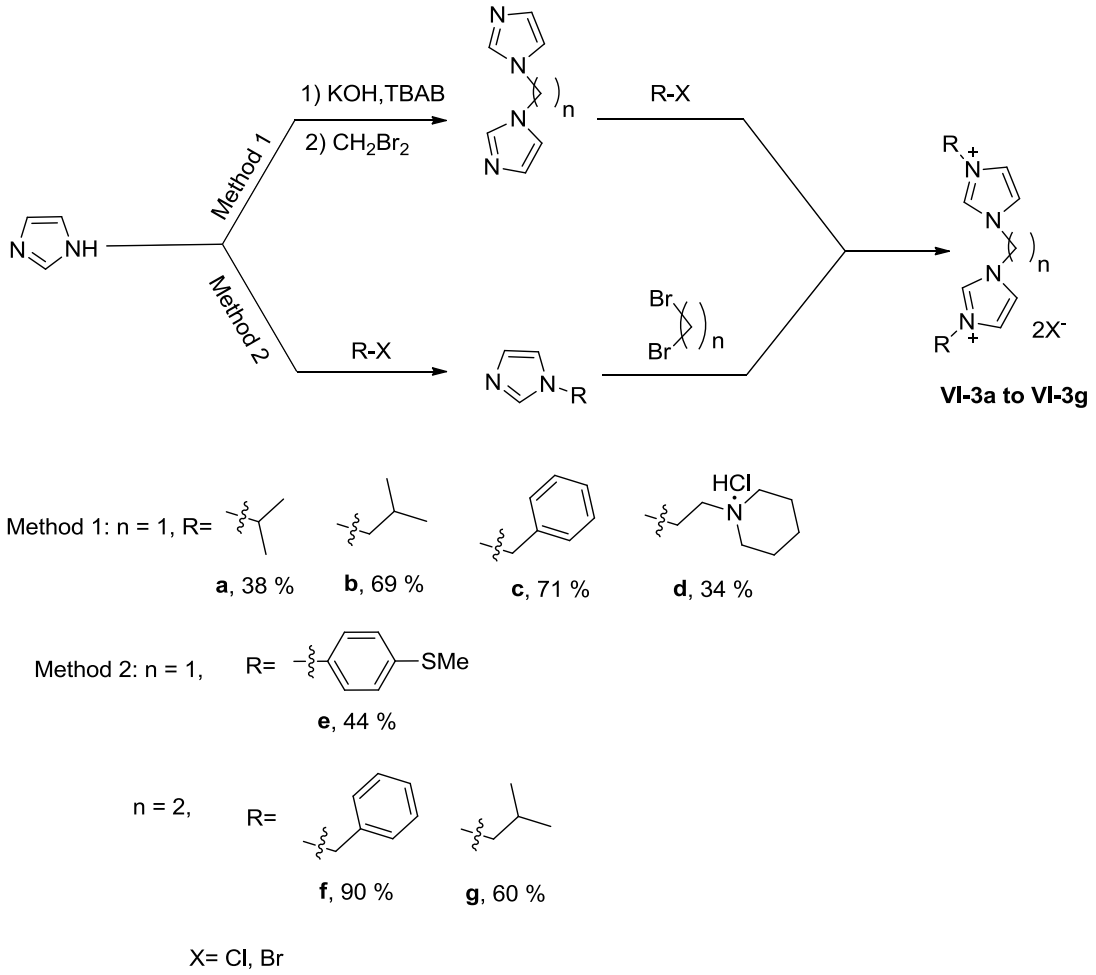

Fig 6.3 Two synthetic approaches to obtain proligands **VI-3a** to **VI-3g**.

The proligands **VI-3a** to **VI-3g** have been characterized by ^{1}H, ^{13}C NMR spectroscopy, elementary analysis and mass spectrometry (MS). The most notable feature in the ^{1}H and ^{13}C NMR spectra of imidazolium salts are the resonances for imidazolium protons (H2) located between 9.06-10.31 ppm and the corresponding imidazolium carbons (C2) in the range of 136.97-139.38 ppm. The mass spectra (MS) of the proligands exhibit the classical peaks corresponding to $[M\text{-}X^{-}]^{+}$ cations.

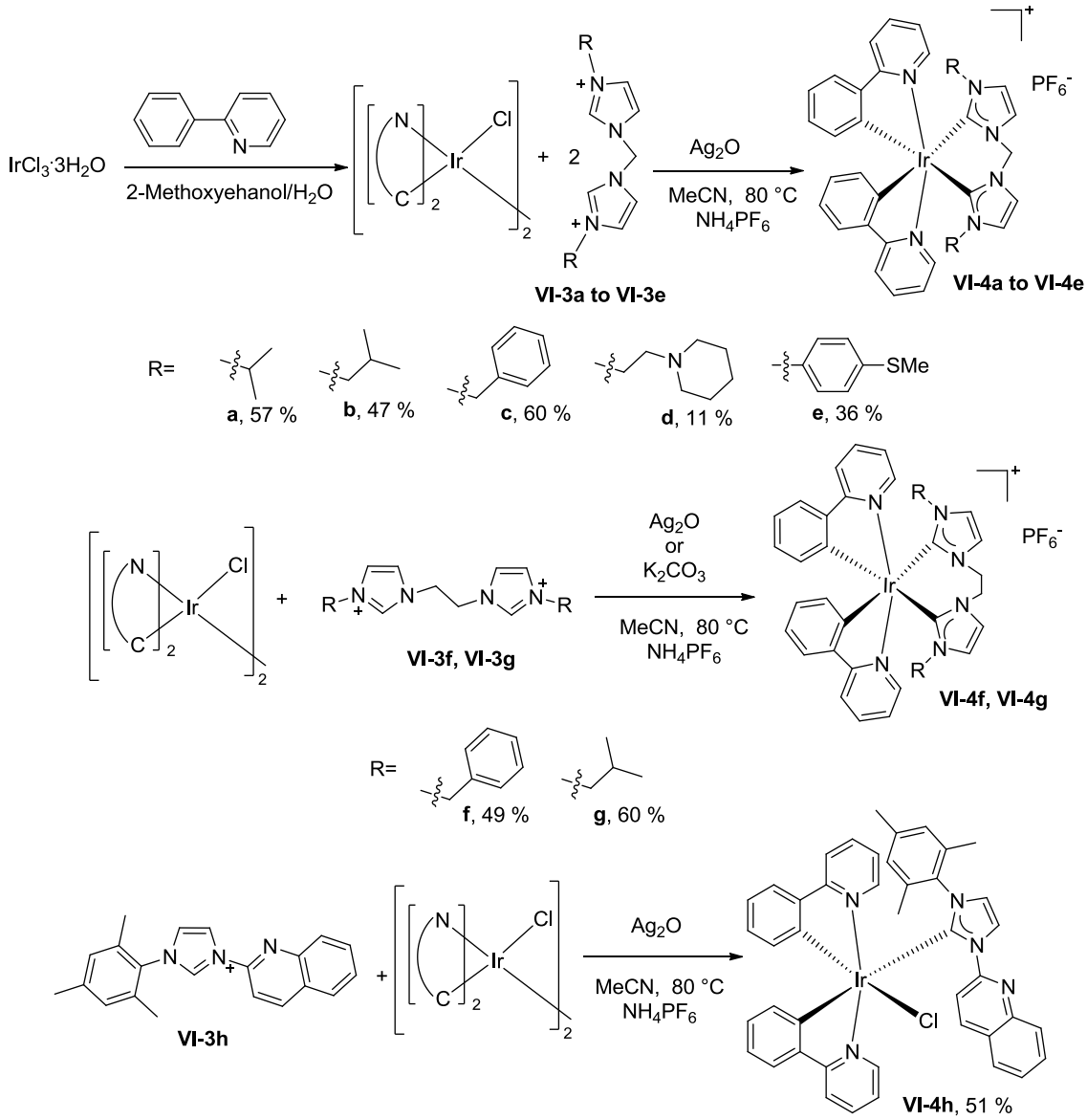

Fig 6.4 Synthesis of iridium(III) NHC complexes **VI-4a** to **VI-4h**.

The iridium precursor $[IrCl(ppy)_2]_2$[117] and the carbene precursor **VI-3h**[113a] were prepared according to literature procedures. The iridium(III) NHC complexes **VI-4a** to **VI-4h** (Fig 6.4) were prepared by reacting $[IrCl(ppy)_2]_2$ with carbene precursors **VI-3a** to **VI-3h** in the presence of Ag_2O or K_2CO_3 in dry acetonitrile at 80 ^oC for 10 h. In the case of complex **VI-4g**, the use of Ag_2O led to some by-products, so we turned to use K_2CO_3 to form the carbene. After cooling to room temperature, an excess of NH_4PF_6 was added to change the anion. Iridium complexes **VI-4a** to **VI-4h** were purified by column chromatography and obtained as yellow powders with moderate

yields ranging from 11% to 60%. All the synthesized iridium complexes are soluble in CH_3CN, MeOH and DMSO and highly stable in the physiological environment. Some ligands (**VI-3f**, **VI-3h**) and corresponding complexes (**VI-4f**, **VI-4h**) were prepared by Clément Sanz (M2R, Université Toulouse 3 Paul Sabatier, 2017), Valentin Boiteau and Yoan Colas (trainees of ENSIACET, 2017), which were supervised by me.

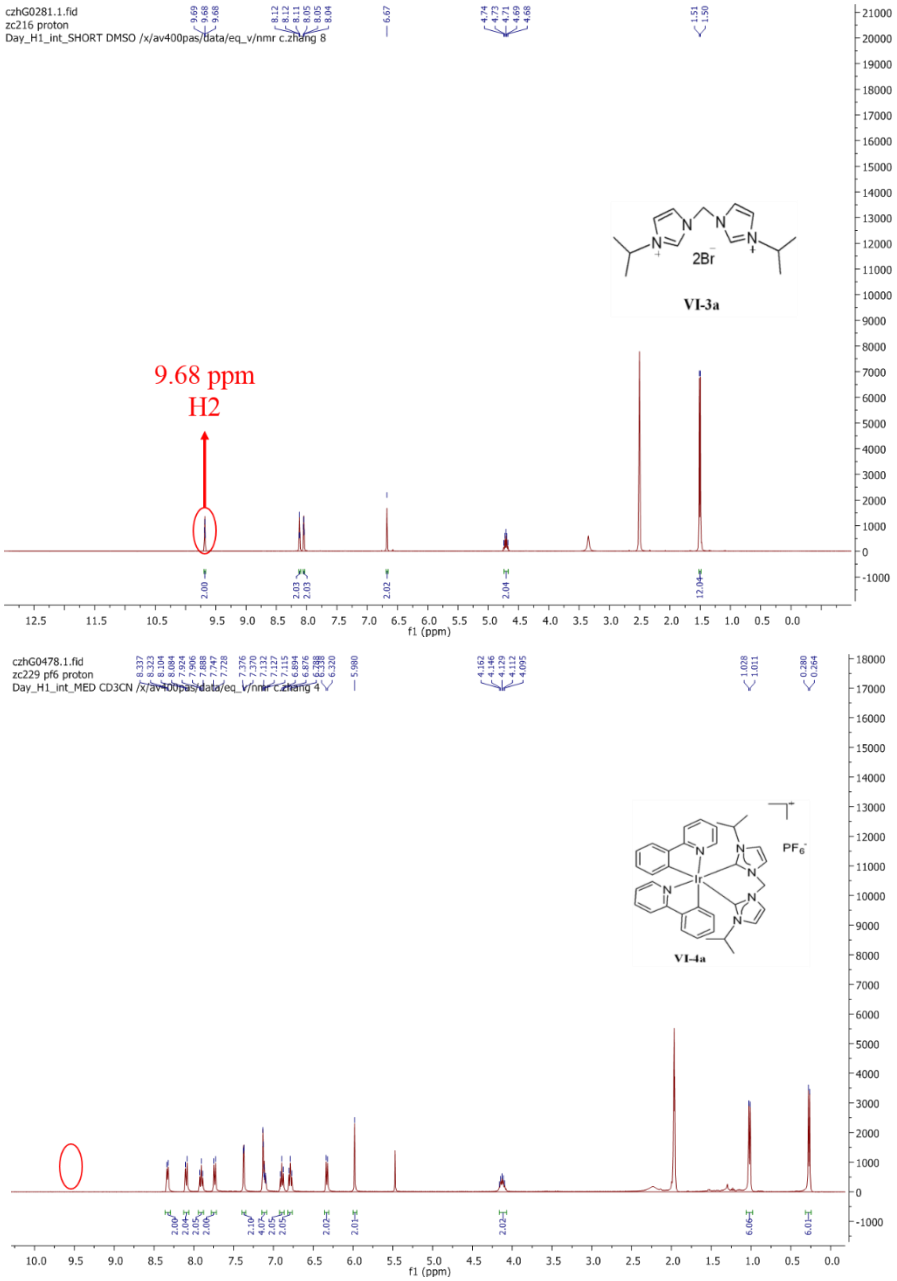

Fig 6.5 ^{1}H NMR spectra of **VI-3a** (top) and **VI-4a** (bottom).

NMR spectroscopy unequivocally manifested the formation of the iridium(III)

complexes with the absence of the proton resonance of the acidic imidazolium (H2, see Fig 6.5); the ^{13}C NMR spectra showed the resonance for the carbene carbon atoms in the range of 162.74-164.87 ppm for complexes **VI-4a** to **VI-4g**, in good agreement with reported values for iridium(III) bisNHC complexes[114] and 180.36 ppm for the complex **VI-4h**, in line with the reported values for iridium monoNHC complexes.[118] Since the structure of complex **VI-4h** is not symmetric, each carbon atom has different attribution (Fig 6.6). The elementary analysis of the iridium complexes correspond to the general $[Ir(ppy)_2L][PF_6]$ formula for **VI-4a** to **VI-4g** and $Ir(ppy)_2(L)Cl$ formula for **VI-4h**. The HRMS displayed the classical peaks corresponding to the cationic fragment $[M\text{-}PF_6^-]^+$ for **VI-4a** to **VI-4g** and the cationic fragment $[M\text{-}Cl^-]^+$ for **VI-4h**. For the configuration of iridium complexes, we obtained two different isomers, such as Λ (lambda) and Δ (delta), which can not be distinguished by NMR spectroscopy.

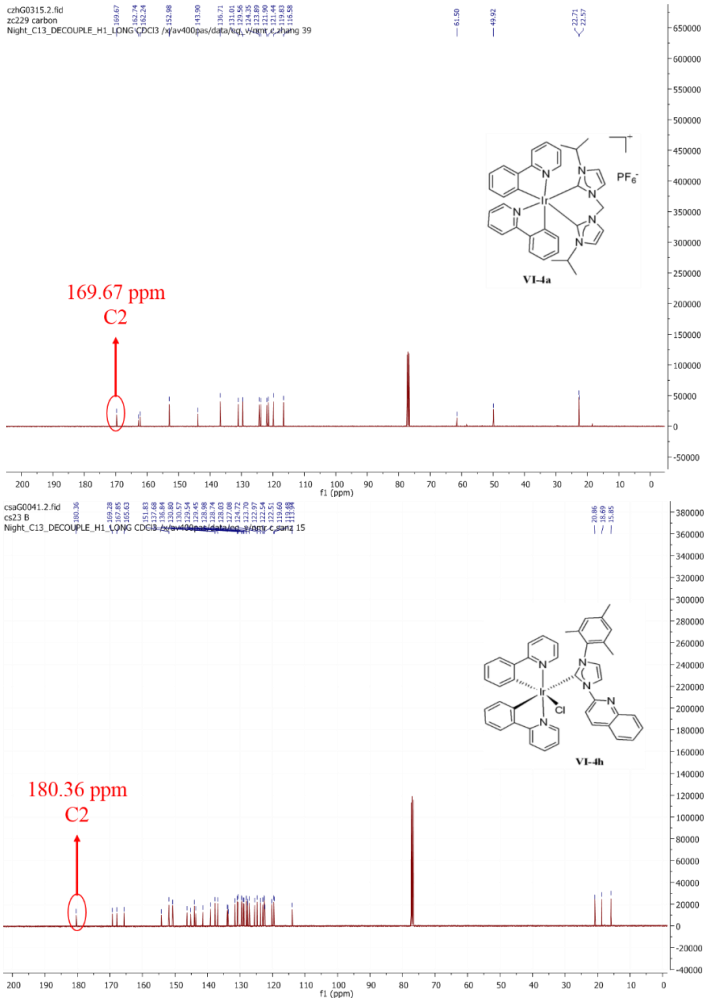

Fig 6.6 ^{13}C NMR spectra of **VI-4a** (top) and **VI-4h** (bottom).

However, we failed to get some bis(imidazolium) salts (**VI-5a** to **VI-5c**, Fig 6.7) and iridium complexes (**VI-7a** and **VI-7b**, Fig 6.7). For the proligands **VI-5a** and **VI-5c**, almost no reaction occurred even under toluene reflux condition. In the case of **VI-5b**, ^{1}H NMR spectra showed some by-products, such as mono and bis-substituted imidazolium salts. In addition, we managed to obtain the bis(imidazolium) salts **VI-6a** and **VI-6b** through the previously described method (Fig 6.3). Nevertheless, we failed to get the two corresponding iridium complexes **VI-7a** and **VI-7b**, probably due to the steric hindrance of the two bulky substituents (mesityl and quinoline) directly connected with the NHCs.

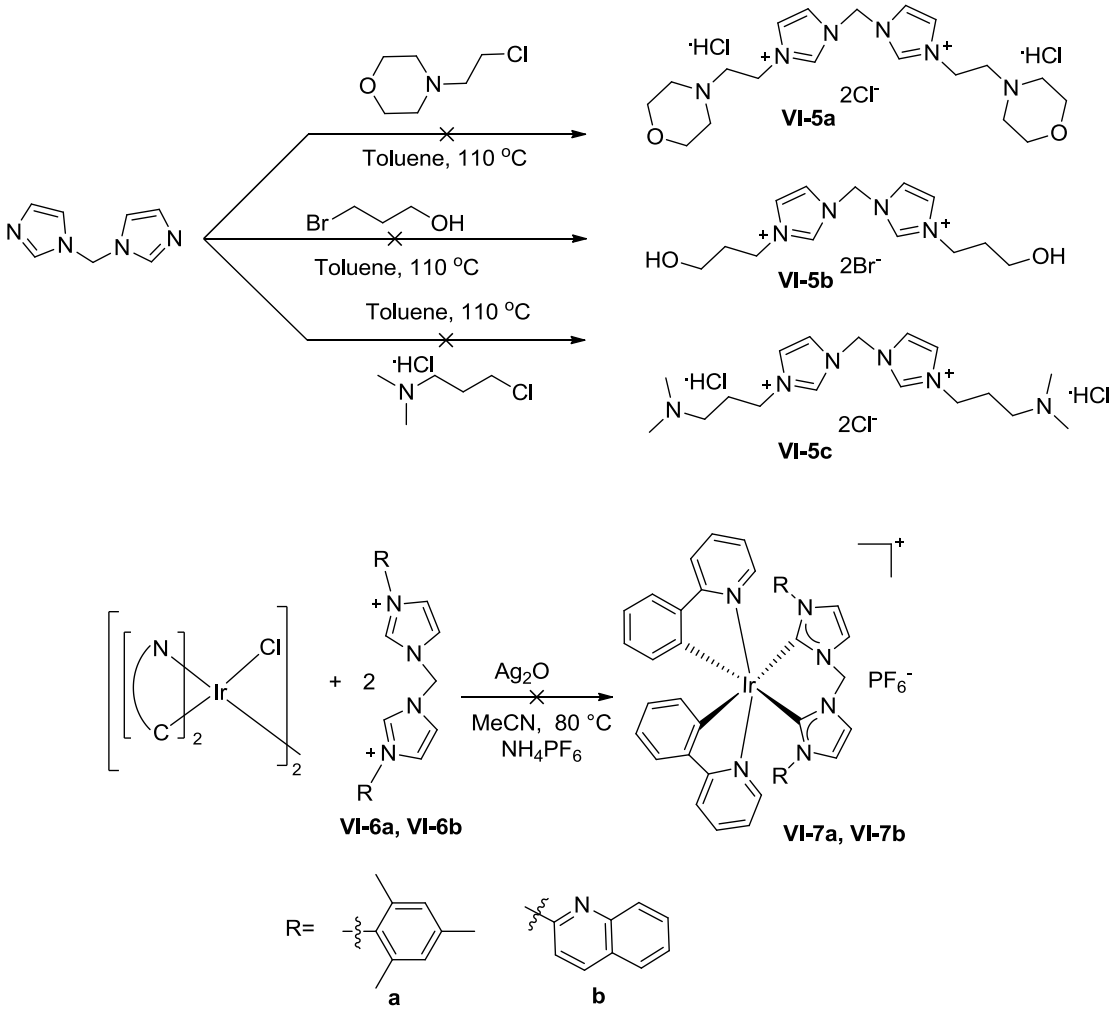

Fig 6.7 Attempts to synthesize the bis(imidazolium) salts (**VI-5a** to **VI-5c**) and the iridium complexes (**VI-7a** and **VI-7b**).

6.3. Molecule structures

Crystals of **VI-4a to VI-4c** and **VI-4f to VI-4g** have been obtained by gas phase diffusion of diethylether in a dichloromethane solution of these complexes.

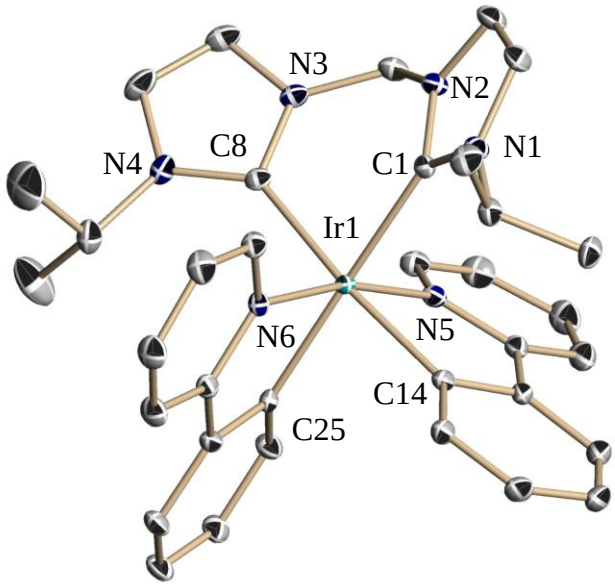

Fig 6.8 Molecule structure of **VI-4a** in the solid state. Hydrogen atoms and non-coordinating anions are omitted for clarity. Selected distances [Å] and angles [°]: Ir-C1 2.120(4), Ir-C8 2.102(4), Ir-C14 2.057(4), Ir-C25 2.049(4), Ir-N5 2.069(3), Ir-N6 2.056(3), C25-Ir1-N6 79.85(11), C25-Ir1-C14 86.27(12), N6-Ir1-C14 91.88(12), C25-Ir1-N5 90.95(12), N6-Ir1-N5 167.82(10), C14-Ir1-N5 79.47(12), C25-Ir1-C8 97.75(12), N6-Ir1-C8 94.16(12), C14-Ir1-C8 173.25(13), N5-Ir1-C8 94.99(12), C25-Ir1-C1 177.74(13), N6-Ir1-C1 98.53(11), C14-Ir1-C1 92.22(12), N5-Ir1-C1 90.43(11), C8-Ir1-C1 83.91(12).

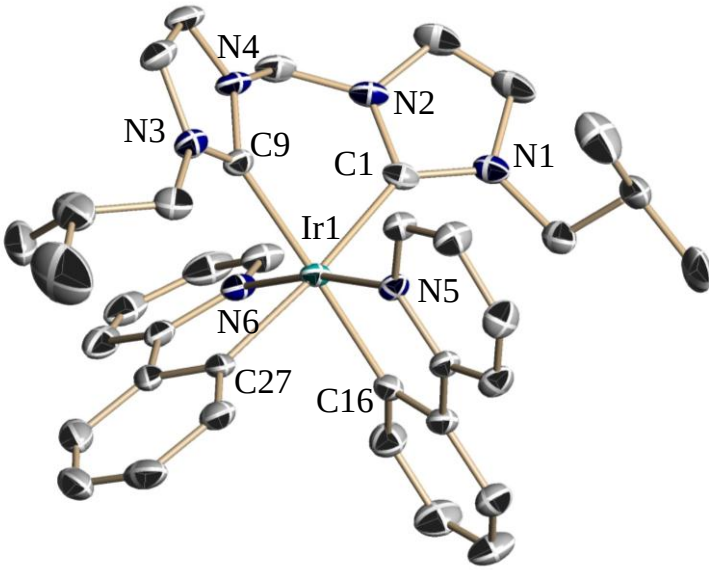

Fig 6.9 Molecule structure of **VI-4b** in the solid state. Hydrogen atoms, disorder of the side arms and non-coordinating anions are omitted for clarity. Selected distances [Å] and angles [ ]:Ir1-C1 2.107(3), Ir1-C9 2.130(3), Ir1-C16 2.049(3), Ir1-C27 2.052(3), Ir1-N5 2.051(2), Ir1-N6 2.058(2), C16-Ir1-N5 80.00(11), C16-Ir1-C27 84.74(11), N5-Ir1-C27 94.39(12), C16-Ir1-N6 91.27(11), N5-Ir1-N6 169.93(10), C27-Ir1-N6 79.69(12), C16-Ir1-C1 98.77(12), N5-Ir1-C1 92.36(11), C27-Ir1-C1 172.84(12), N6-Ir1-C1 93.95(11), C16-Ir1-C9 175.17(12), N5-Ir1-C9 96.41(10), C27-Ir1-C9 92.34(12), N6-Ir1-C9 91.99(10), C1-Ir1-C9 84.56(12).

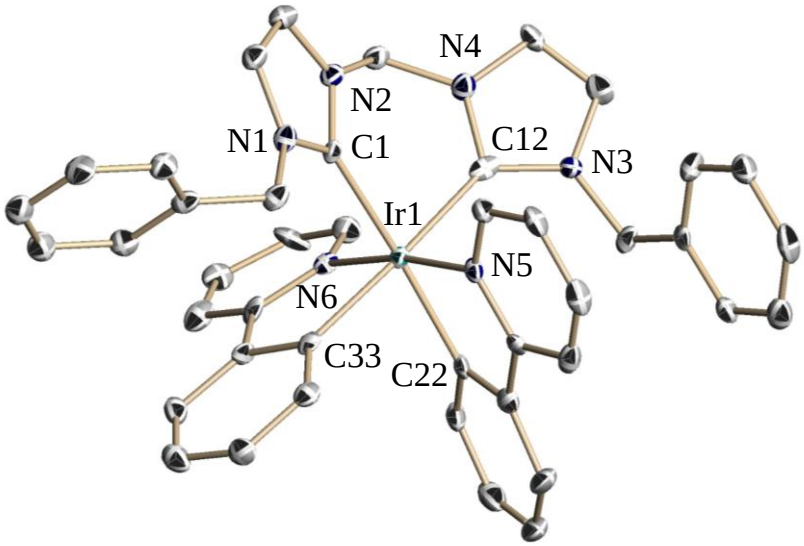

Fig 6.10 Molecule structure of **VI-4c** in the solid state. Hydrogen atoms,

non-coordinating anions and disordered dichloromethane are omitted for clarity. Selected distances [Å] and angles [°]:Ir1-C1 2.113(8), Ir1-C12 2.086(10), Ir1-C22 2.055(8), Ir1-C33 2.066(9), Ir1-N5 2.055(8), Ir1-N6 2.056(7), C22-Ir1-N5 80.2(3), C22-Ir1-N6 92.4(3), N5-Ir1-N6 171.5(3), C22-Ir1-C33 81.1(3), N5-Ir1-C33 95.4(4), N6-Ir1-C33 79.3(3), C22-Ir1-C12 100.4(3), N5-Ir1-C12 89.1(3), N6-Ir1-C12 96.4(3), C33-Ir1-C12 175.5(4), C22-Ir1-C1 172.8(3), N5-Ir1-C1 95.0(3), N6-Ir1-C1 91.9(3), C33-Ir1-C1 94.0(3), C12-Ir1-C1 84.9(3).

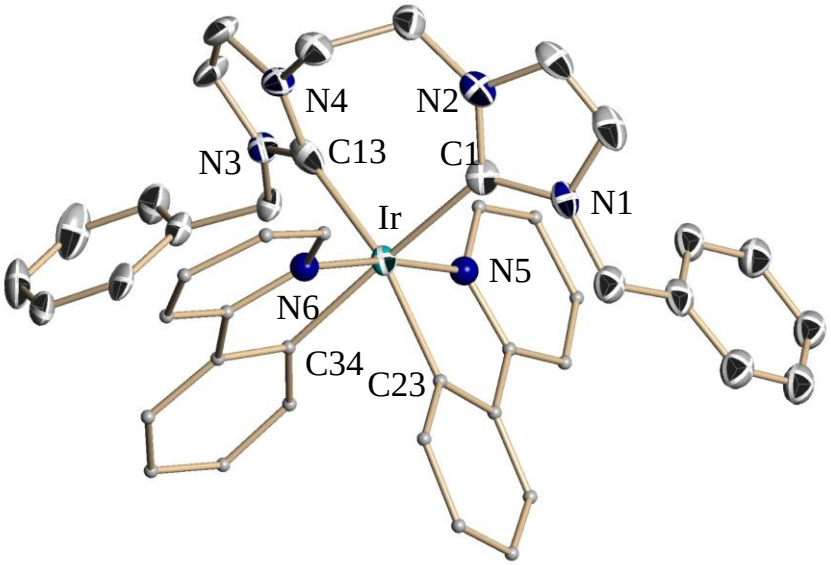

Fig 6.11 Molecule structure of **VI-4f** in the solid state. Only one of two cations presented in the asummetric unit is shown. Hydrogen atoms, anions, disordered ether molecules are omitted and ppy ligands are simplified for clarity. Selected distances [Å] and angles [°]: Ir-C1 2.087(10), Ir-C13 2.161(9), Ir-C23 2.049(8), Ir-C34 2.043(9), Ir-N5 2.041(7), Ir-N62.027(7), N6-Ir1-N5 172.7(3), N6-Ir1-C34 80.4(3), N5-Ir1-C34 92.7(3), N6-Ir1-C23 96.9(3), N5-Ir1-C23 79.1(3), C34-Ir1-C23 77.3(3), N6-Ir1-C1 95.9(3), N5-Ir1-C1 90.1(3), C34-Ir1-C1 165.0(3), C23-Ir1-C1 88.8(3), N6-Ir1-C13 88.7(3), N5-Ir1-C13 94.9(3), C34-Ir1-C13 99.0(3), C23-Ir1-C13 172.7(3), C1-Ir1-C13 95.4(3).

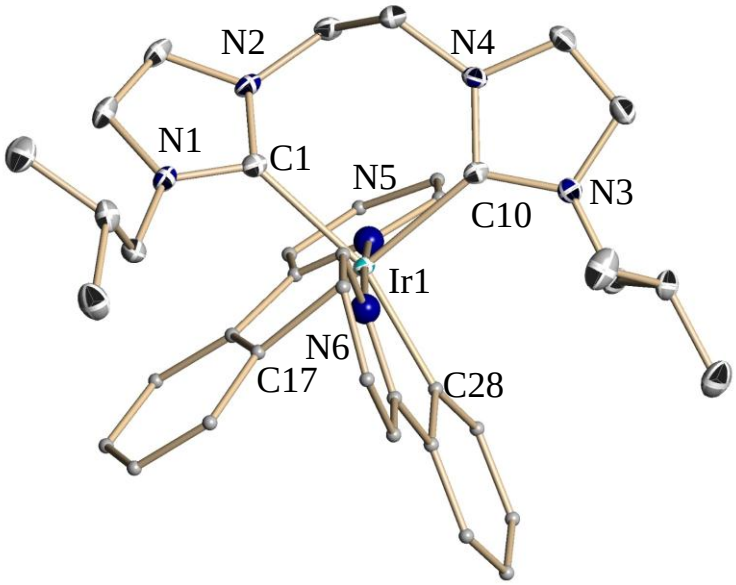

Fig 6.12 Molecule structure of **VI-4g** in the solid state. Hydrogen atoms, anions and a disorder of one side arm are omitted and ppy ligands are simplified for clarity. Selected distances [Å] and angles [°]: Ir-C1 2,145(2), Ir-C10 2,134(2), Ir-C17 2,069(2), Ir-C28 2,043(2), Ir-N5 2,065(2), Ir-N6 2.044(2), C28-Ir1-N6 79.75(9), C28-Ir1-N5 92.85(9), N6-Ir1-N5 172.41(8), C28-Ir1-C17 80.25(9), N6-Ir1-C17 98.14(9), N5-Ir1-C17 78.80(10), C28-Ir1-C10 100.25(9), N6-Ir1-C10 90.65(9), N5-Ir1-C10 92.33(9), C17-Ir1-C10 171.12(10), C28-Ir1-C1 163.02(9), N6-Ir1-C1 98.16(9), N5-Ir1-C1 88.43(9), C17-Ir1-C1 83.40(9), C10-Ir1-C1 96.61(9).

All here presented iridium structures show some common features: the iridium atom is coordinated by a bis-NHC ligand and two phenylpyridine ligands and the four carbon atoms and the two nitrogen atoms linked to iridium form a distorted octahedral geometry. It is notable that the carbene carbon atoms are in trans positions to the deprotonated carbon atoms of the ppy ligands and the two nitrogen atoms are in all cases also in trans positions related to the central iridium. The Ir-C(carbene) distances are in the range of 2.09 and 2.16 Å. The Ir-C distances (2.04 to 2.07 Å) and the Ir-N distances (2.03 to 2.07) of the ppy ligands are nearly the same in all cases. The ppy ligands show in all complexes very similar N-Ir-C bite angles between 78.8 and 80.4 °. The only remarkable differences could only be observed for the bisNHC systems. The C-Ir-C angles in the C1 ligands is between 83.9 and 84.6 °, while it is much more open

for the C2 ligands with angles between 95.4 and 96.6 °, a significant difference of about 10 °between the C1 and the C2 systems.

6.4. Photophysical studies

All complexes have been photophysically investigated at standard pressure and room temperature in solution. Fig 6.13 illustrated the photophysical characterization of the complex **VI-4a** in CH_2Cl_2 solution at 298 K.

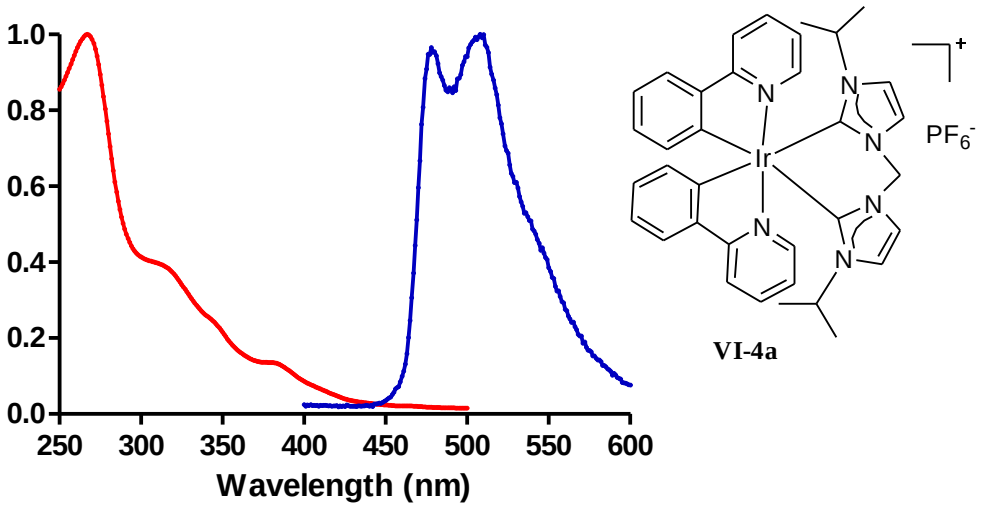

Fig 6.13 Normalized absorption (red) and emission (blue) spectra of complex **VI-4a** in CH_2Cl_2 solution.

The strong absorption bands below 300 nm correspond to spin-allowed $^1\pi\rightarrow\pi^*$ electronic ligand-centered LC transitions. The structureless bands at 300-360 nm were attributed to phenyl-to-pyridine ligand-to-ligand charge transfer (LLCT) and Ir-to-phenylpyridine metal-to-ligand charge transfer (MLCT). The lowest-lying bands in the visible region over 360 nm can be assigned to both singlet and triplet MLCT transitions.[119] No significant difference in the absorption spectra of complexes **VI-4a** to **VI-4h** can be found in CH_2Cl_2 solution.

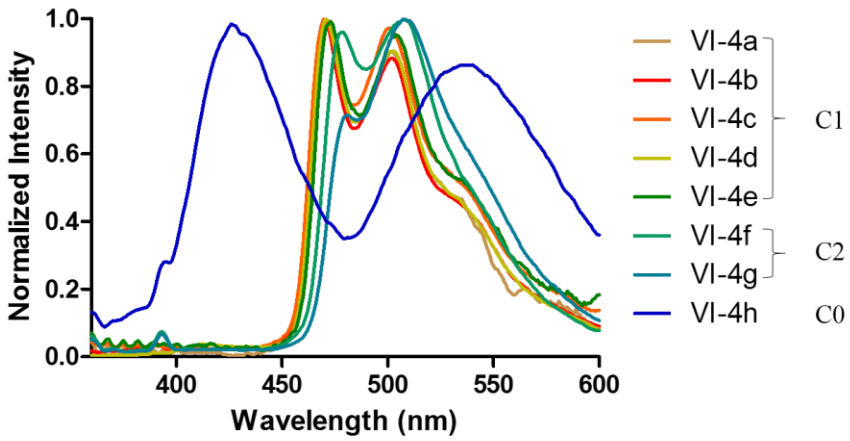

Fig 6.14 Normalized emission spectra of iridium complexes **VI-4a** to **VI-4h** in CH_2Cl_2 solution.

The room temperature luminescence spectra of complexes **VI-4a** to **VI-4h** in CH_2Cl_2 are shown in Fig 6.14. After excitation at 360 nm, all the complexes except **VI-4h** showed similar blue-green emission with a maximum wavelength around 500 nm. The neutral iridium complex **VI-4h** displayed two emission maxima at 425 nm and 535 nm. All the complexes showed vibronically structured phosphorescence spectra in CH_2Cl_2 solution at room temperature, which indicated that the emissive excited state had both LC $\pi\rightarrow\pi^*$ and MLCT characters.[119b]

Table 6.1 Photophysical data of iridium complexes **VI-4a** to **VI-4h**.

Complex	Medium	ε ($M^{-1}cm^{-1}$)	Φ_{PL}(%)	τ_1/ns
VI-4a	CH_2Cl_2	17552	1.2	190.7
VI-4b	CH_2Cl_2	8937	1.6	166.4
VI-4c	CH_2Cl_2	6159	1.6	179.7
VI-4d	CH_2Cl_2	8174	1.6	187.0
VI-4e	CH_2Cl_2	12474	1.1	167.4
VI-4f	CH_2Cl_2	6799	0.2	—
VI-4g	CH_2Cl_2	7381	0.2	—
VI-4h	CH_2Cl_2	10544	0.2	—

The photophysical data are summaried in Table 6.1. The molar attenuation coefficient also known as the molar extinction coefficient (Ɛ) is a measurement of how strongly a compound attenuates light at a certain wavelength. From the table 6.1, it was shown that the molar attenuation coefficients of complexes **VI-4a** to **VI-4h** at 360 nm were ranging from 6159 to 17552 $M^{-1}cm^{-1}$.

In addition, the relative emission quantum yields (Φ_{PL}) of these complexes at room temperature were measured by using quinine sulfate in 1 N H_2SO_4 as a reference standard (Φ_{PL} = 0.55).[120] For the C1 system (**VI-4a** to **VI-4e**), the quantum yields were in the range of Φ_{PL} = 1.1 – 1.6 % in CH_2Cl_2 solution; and for C2 and C0 system (**VI-4f** to **VI-4h**), just 0.2 % (Table 6.1).

The emission lifetime refers to the average time that the compound stays in its excited state before emitting a photon. Table 6.1 showed that the excited-state lifetimes of complexes **VI-4a** to **VI-4e** are in the range of 166.4-190.7 ns.

6.5. *In vitro* cytotoxicity

The *in vitro* cytotoxicity of the tested complexes **VI-4a** to **VI-4h** was evaluated against two cancer cells PC-3 (human prostate), T24 (human bladder) and the non-cancerous NIH3T3 (murine fibroblasts) using colorimetric MTT tests after 48 h of treatment (Table 6.2). The iridium precursor $[IrCl(ppy)_2]_2$ and auranofin were used as references. These results are summarized in Table 6.2. All the complexes except **VI-4d** containing piperidine substituents displayed higher cytotoxicity than auranofin against the two tested cancer cell lines (PC-3 and T24) with GI_{50} values ranging from 0.25 to 0.95 μM. To study the SAR, the lipophilicity of complexes **VI-4a** to **VI-4h** was determined by a shake-flask method (Table 6.2).[100] Unfortunately, no significant relationship between lipophilicity and anticancer activity was found for our iridium(III) complexes. However, the lowest cytotoxicity of complex **VI-4d** could be attributed to its lowest log P value. The two most cytotoxic complexes **VI-4f** and **VI-4h** with GI_{50} values ranging from 0.25 to 0.29 μM against PC-3 and T24 are among the most lipophilic complexes.

Table 6.2 Cytotoxic activity of iridium(III) NHC complexes expressed as GI_{50} (μM) values towards selected cancer and normal cell lines as determined by MTT assay (48 h).

Complex	PC-3	T24	NIH3T3	Log P
VI-4a	0.48	0.31	3.3	-0.063 ±0.032
VI-4b	0.51	0.38	3.5	0.842 ±0.222
VI-4c	0.41	0.43	7.1	0.581 ±0.047
VI-4d	3.8	3.2	> 20	-0.407 ±0.012
VI-4e	0.71	0.95	8.5	0.035 ±0.080
VI-4f	0.25	0.29	2.5	0.847 ±0.116
VI-4g	0.91	0.91	4.1	0.519 ±0.061
VI-4h	0.27	0.25	2.7	0.861 ±0.009
$[IrCl(ppy)_2]_2$	> 20	14.8	>20	
Auranofin	1.2	1.0	1.3	

GI_{50} values correspond to the concentration of complexes causing 50 % inhibition of cell growth. Data were obtained from three independent experiments.

All the iridium(III) complexes were evaluated *in vitro* for their cytotoxicity towards healthy NIH3T3 cells, giving access to the selectivity index (SI, ratio of GI_{50} values towards NIH3T3 to that towards PC-3). From the results (Table 6.2), complexes **VI-4a** to **VI-4h** showed some selectivities for cancer cells since they were found to be less active against non-cancerous NIH3T3 cells than cancer cells (T24 and PC-3). Notably, compared with auranofin (SI value around 1), iridium complexes **VI-4a** to **VI-4h** exhibited better selectivity with SI values ranging from 4.5 to 17.3. The iridium precursor was less cytotoxic than all these complexes against all the tested cell lines. Therefore, comparison the anticancer activity of iridium complexes **VI-4a** to **VI-4h** with that of the precursor showed clearly the importance of the presence of NHC ligands.

6.6. *In vitro* photodynamic activities

Iridium complexes with long-lived excited states can be used as effective singlet oxygen ($^1O_2$) sensitizers.[121] $^1O_2$ is considered to be the main cytotoxic agent in photodynamic therapy (PDT).[122] Subsequently, the photocytotoxicity of complexes **VI-4a** to **VI-4h** was tested against PC-3 and T24 cancer cells. Cells were treated with increasing concentrations of the complexes (from 0.01 μM to 20 μM) for 4 h in the dark. After that, the medium was removed and replaced by fresh culture medium prior to 10 min irradiation at 365 nm light (4 W). Cell viability was determined by MTT assay 44 h after the end of irradiation. The phototoxic index (PI) was calculated as the ratio of GI_{50} values in the dark to those upon light irradiation. The results showed that GI_{50} values of complexes **VI-4a** to **VI-4e** (C1 system) upon light irradiation were decreased by 1.8- to 5.2-fold as compared with the values obtained in the dark except complex **VI-4d** (Table 6.3). However, no significant difference in cytotoxicity was found for cancer cells treated with complex **VI-4f** to **VI-4h** (C2 and C0 systems), iridium precursor and auranofin in the presence and absence of light. Notably, among all the complexes, **VI-4a** displayed the most potent photodynamic anticancer activity with phototoxic index of 5.2 and 2.6 for PC-3 and T24, respectively. These preliminary results suggested that these complexes may be used as potent photodynamic anticancer agents.

Table 6.3 GI_{50} values (μM) and phototoxic indexes of the tested complexes (**VI-4a** to **VI-4h**) towards different cell lines.

Complex	PC-3			T24		
	Dark	Light	PI	Dark	Light	PI
VI-4a	0.48	0.092	5.2	0.31	0.12	2.6
VI-4b	0.51	0.15	3.4	0.38	0.16	2.4
VI-4c	0.41	0.19	2.2	0.43	0.24	1.8
VI-4d	3.8	3.2	1.2	3.2	1.1	3.1
VI-4e	0.71	0.24	3.0	0.95	0.25	3.8
VI-4f	0.25	0.36	n.a.	0.29	0.75	n.a.
VI-4g	0.91	1.3	n.a.	0.91	2.3	n.a.
VI-4h	0.27	0.27	n.a.	0.25	0.37	n.a.
$[IrCl(ppy)_2]_2$	>20	>20	n.a.	14.8	>20	n.a.
Auranofin	1.2	1.2	n.a.	1.1	1.2	n.a.

GI_{50} values correspond to the concentration of complexes causing 50 % inhibition of cell growth. Data were obtained from three independent experiments.

Phototoxic index (PI) is the ratio of GI_{50} values in the dark to those upon light irradiation. Cells were treated with the complexes for 4 h and then irradiated at 365 nm light (4 W) for 10 min.

In addition, the effects of different incubation times on the photocytotoxicity of iridium complexes was evaluated. PC-3 and T24 cells were treated with iridium complexes **VI-4a** and **VI-4e** for 12 h, and then irradiated at 365 nm light for 10 min. Cell viability was determined by MTT assays 36 h after the end of irradiation. From Fig 6.16 and Fig 6.17, it was shown that GI_{50} values of complex **VI-4a** towards PC-3 and T24 cells upon light irradiation were 0.092 μM and 0.17 μM, respectively, which is in the same level as previous measurements obtained for 4 h of incubation. The same phenomenon was found for complex **VI-4e** ($GI_{50} \approx$ 0.20 μM and 0.29 μM towards PC-3 and T24 cells, respectively), suggesting that the different incubation

times had no effects on the photocytotoxicity of our iridium complexes.

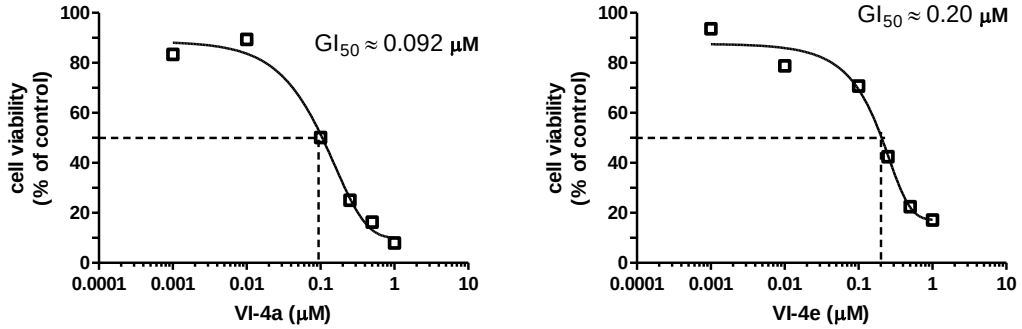

Fig 6.15 Dose- response curves for the *in vitro* photocytotoxicity of iridium complexes (**VI-4a** and **VI-4e**) towards PC-3 cells.

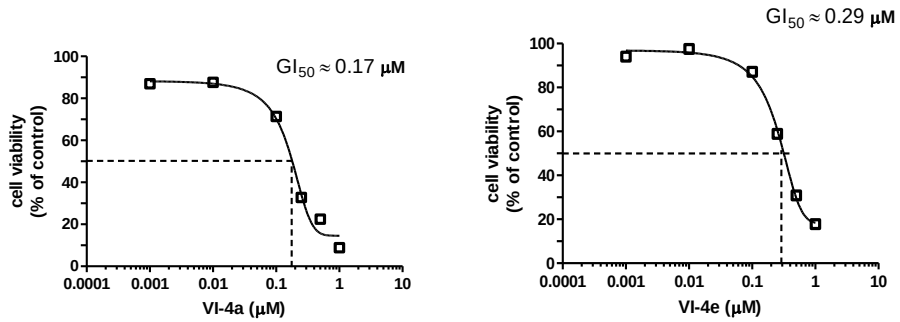

Fig 6.16 Dose- response curves for the *in vitro* photocytotoxicity of iridium complexes (**VI-4a** and **VI-4e**) towards T24 cells.

Furthermore, *in vitro* toxicity of iridium complex **VI-4a** against A549 and HepG-2 cells upon 365 nm irradiation was measured. For this purpose, cells were treated with increasing concentrations of the complexes (from 0.01 μM to 1 μM) for 4 h in the dark. After that, the medium was removed and replaced by fresh culture medium prior to 10 min irradiation at 365 nm light (4 W). Cell viability was determined by MTT assay 44 h after the end of irradiation. In the case of A549 cells, the GI_{50} value in the dark was 0.65 μM, and after light irradiation, the toxicity was increased by four times with a GI_{50} value of 0.16 μM. Nevertheless, the toxicity in the dark and photocytotoxicity towards HepG-2 cells were decreased significantly with GI_{50} values in the micromolar range.

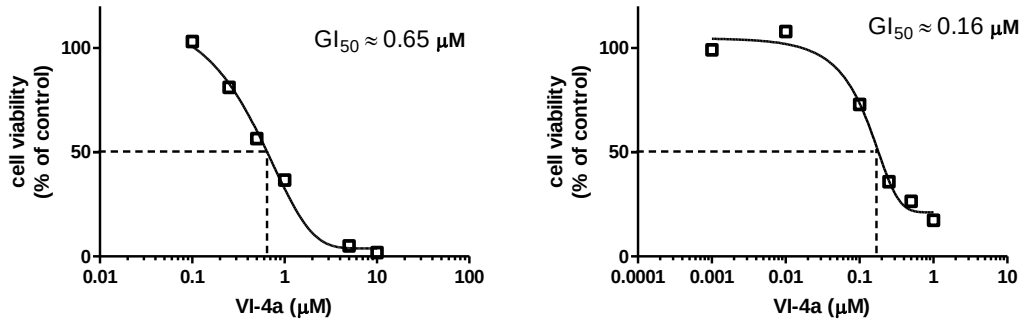

Fig 6.17 Dose- response curves for the *in vitro* photocytotoxicity of iridium complex **VI-4a** towards A549 cells in the dark (left) and upon irradiation (right).

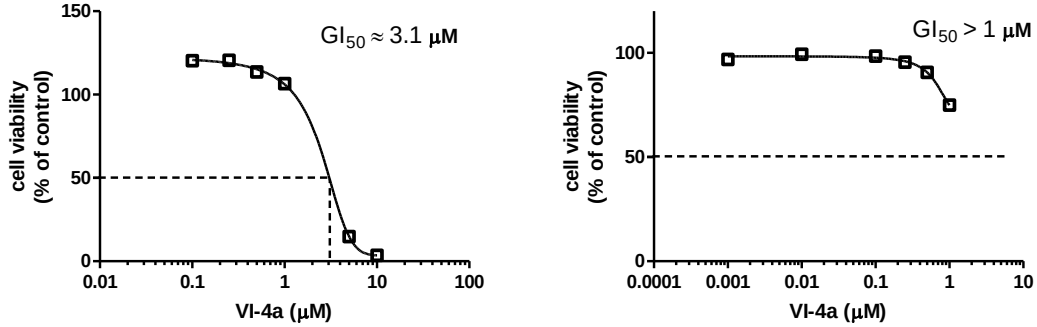

Fig 6.18 Dose- response curves for the *in vitro* photocytotoxicity of iridium complex **VI-4a** towards HepG-2 cells in the dark (left) and upon irradiation (right).

6.7. Cellular localization

Due to the photophysical properties of these iridium complexes, the intracellular distribution can be readily monitored by fluorescent microscopy. This work has been done in collaboration with Dr. Serge Mazères (IPBS, Toulouse).

The most active complex **VI-4a** has been selected for the cellular localization. The photophysical studies showed that complex **VI-4a** had a maximum excitation wavelength at 360 nm. Microscopy imaging experiments were performed with PC-3 cells which were cultured in 6-well plates and on glass slides (180,000 cells per well) for 18 h before treated with complex **VI-4a** at different concentrations (0.25 µM, 0.5 µM and 1 µM). After 24 hours, a MitoTracker deep red probe was incubated on live cells at a final concentration of 200 nM during 15 min at 37 ^{o}C in a 5 % CO_2

humidified incubator and then observed in two channels 440-544 nm for complex **VI-4a** (two-photon excitation at 720 nm) and 644-700 nm for MitoTracker (excitation at 633 nm) at the same time.

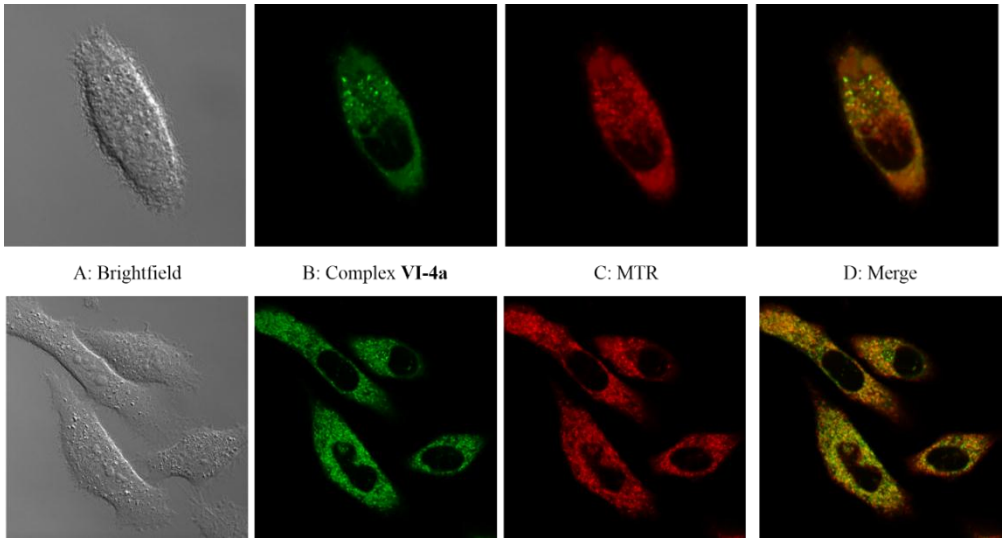

Fig 6.19 Determination of intercellular localization of complex **VI-4a** by confocal microscopy. PC-3 cells were incubated with complex **VI-4a** (0.5 μM) for 24 h, and then co-incubated with MitoTracker Deep Red (200 nM) for 10 min at 37 ºC. The iridium complex **VI-4a** was excited at 720 nm (two photon) and the emission was collected at 440-544 nm. MTR was excited at 633 nm and the emission was collected at 644-700 nm. Full image for zoom 4 (up) was 53.14 μm * 53.14 μm; and 106.27 μm * 106.27 μm for zoom 2 (down).

The fluorescence of the complex **VI-4a** was evaluated using a Zeiss LSM 710 NLO-Meta Confocal microscope. Treatment of PC-3 cells with 0.5 μM of complex **VI-4a** led to development of an intense fluorescence in the cytoplasm (Fig 6.19, B). The specific subcellular location was investigated by staining the organelles with the specific fluorescent probe (Fig 6.19, C). As depicted in Fig 6.19, D, complex **VI-4a** mainly localize into mitochondria which are stained with MitoTracker. Pearson's correlation coefficient for complex **VI-4a** and MitoTracker is 88 %. These results manifested that the cytotoxic properties of iridium complexes may originate from mitochondria mediated cell death.

In conclusion, three families of cyclometalated iridium(III) complexes bearing different NHC ligands have been prepared and characterized. The first two families contain a bis-carbene ligand in which the two NHCs are bridged by a methylene (C1) and an ethylene (C2), giving rise to cationic complexes **VI-4a** to **VI-4g**. The other one (C0) contains only one mono-carbene ligand and one chloride, leading to a neutral complex **VI-4h**. All the iridium complexes, except **VI-4d** with piperidine substituents, displayed higher antiproliferative activity than auranofin against various cancer cells. Moreover, they exhibited better selectivity between cancer cells (PC-3 and T24) and normal cells (NIH3T3) than auranofin. Therefore, the charge on the iridium complexes has no effect on their antiproliferative activity and selevtivity. Notably, complex **VI-4a** can be rapidly and efficiently taken up into PC-3 cells and specifically localize into mitochondria. Interestingly, complexes **VI-4a** to **VI-4e** (C1 system) can act as efficient photosensitizers. The cytotoxicity of **VI-4a** to **VI-4e** against PC-3 and T24 was increased substantially upon irradiation at 365 nm. Therefore, our preliminary studies demonstrated that these iridium(III) complexes had high potential to be mitochondria-targeted theranostic and photodynamic anticancer agents.

7. Conclusions and perspectives

In this work, three series of new *N*-heterocyclic carbene (NHC) gold(I) complexes containing functionalized nitrogen groups bridged to the NHC by aliphatic or aromatic linkers and one series of original cationic and neutral cyclometalated iridium(III) complexes bearing bisNHC ligands or a monoNHC have been synthesized, fully characterized and studied for their anticancer activities.

The first family consists of four cationic $Au^{I}(NHC)_2$ complexes (**II-3a** to **II-3d**) containing nitrogen groups connected to the NHC by aliphatic side arms. These complexes were investigated for their *in vitro* antiproliferative activity towards four human cancer cell lines, including ovarian carcinoma (A2780 and its cisplatin-resistant variant A2780cis), hepatocellular carcinoma (HepG-2 and HepAD38) and the non-cancerous Madin-Darby canine kidney epithelial (MDCK) using MTT assays. Two complexes displayed potent anticancer activity and exhibited higher cytotoxicity against ovarian carcinoma than hepatocellular carcinoma. Notably, they were found to be very effective towards A2780cis, when compared to the reference drug cisplatin. Importantly, these complexes showed low cytotoxicity towards the healthy MDCK cells, demonstrating selectivity for cancer cells. Regarding structure-activity relationship (SAR), the higher lipophilicity found for the complex **II-3b** correlates with the higher cytotoxic activity and selectivity against cancer cells, which is a common feature for delocalized lipophilic cations (DLCs).[11a]

In order to increase the lipophilicity of our complexes, we performed pharmaco-modulation to synthesize a second family of four cationic $Au^{I}(NHC)_2$ complexes (**III-3a** to **III-3d**) containing nitrogen groups linked to the NHC by an aromatic spacer. The *in vitro* cytotoxicity of these lipophilic complexes and their proligands **III-2c** and **III-2d** were evaluated on the representative PC-3 prostate and T24 bladder cancer cell lines and non-cancerous MC3T3 osteoblasts by colorimetric MTT assays. Whereas the carbene precusors were inactive, all the complexes exhibited high cytotoxicity with GI_{50} values in the nanomolar range, but unfortunatedly, less selectivity for cancer cells was found for three of them (**III-3a**,

III-3b and **III-3d**). These results highlight that high lipophilicity of these complexes is in good agreement with the obtained cytotoxic activity, nevertheless too high lipophilicity can also lead to poor selectivity. Accordingly, complex **III-3c** was selected for further *in vitro* screening on six cancer cell lines (prostate PC-3, bladder T24, lung A549, bone U-2 OS, liver HepG-2 and breast MCF-7) and two non-cancerous cell lines (MC3T3 osteoblasts and NIH3T3 fibroblasts). The obtained GI_{50} values of these complexes were in the nanomolar range, suggesting that this complex was highly cytotoxic towards various cancer cells with restricted effects on healthy cells. Clonogenic assays manifested the impressive cytotoxicity of this complex by inhibiting significantly the number of PC-3 and T24 colonies at low concentration.

Taking into account the anticancer activity and selectivity of the two first series, we designed and synthesized an optimized third series of four $Au^{I}(NHC)_2$ complexes (**III-6a** to **III-6d)** with an intermediate lipophilicity between the first two. These complexes were tested *in vitro* for their antiproliferative effects on human prostate cancer cell line PC-3 and non-cancerous NIH3T3 fibroblasts. These four complexes displayed high and specific cytotoxic activity towards cancer cells.

Mechanistic studies on complexes **III-3c** were conducted. Bioavailability has been evidenced by a fast cellular uptake. Moreover, this complex inhibited effectively TrxR, a common target for gold(I) complexes, and its cytotoxicity towards PC-3, T24 and HepG-2 cells was found to be ROS-dependent.

Overall, the biological results showed that some of our lipophilic cationic gold(I) complexes can be considered as good candidates with good prerequisites for *in vivo* tests, in order to provide some conclusive evidence and to pursue the development of gold-based anticancer agents.

Besides anticancer activities, we also tested neutral $Au^{I}(NHC)Cl$ complexes **V-2a** to **V-2i** for other biomedical applications in parasite disease leishmaniasis. These complexes were screened *in vitro* against both promastigote and axenic amastigote forms of *L. infantum*. Moreover, their cytotoxicity was evaluated on the murine J774A.1 macrophages in order to determine their selectivity of action. 7 of 9 gold(I)

complexes displayed good antiamastigote activities with IC_{50} values ranging from 0.19 to 1.17 μM. In particular, the most active complex **V-2d**, bearing simple mesityl and benzyl substituents, represents a promising metallodrug showing selectivity of action against the pathological relevant form of *Leishmania*.

Another axe of research was focused on the synthesis and characterization of new $Ir^{III}(ppy)_2(NHC)$ complexes as theranostic agents with potential for photodynamic therapy (PDT). These complexes can be separated to three families: 1) five cationic $Ir^{III}(ppy)_2$ complexes containing bis(NHC) ligands where the two NHC skeletons are bridged by a CH_2 group (**VI-4a** to **VI-4e**), 2) two cationic $Ir^{III}(ppy)_2$ complexes containing bis(NHC) ligands where the two NHC skeletons are linked by a CH_2CH_2 group (**VI-4f** and **VI-4g**) and 3) one neutral $Ir^{III}(ppy)_2$ complexes containing one NHC ligand and one chloride (**V-4h**). After excitation at 360 nm, the cationic complexes showed similar blue-green emission with a maximum wavelength of around 500 nm, while the neutral complex displayed two emission maxima at 425 nm and 535 nm. The *in vitro* cytotoxicity of these complexes was evaluated on the representative human PC-3 prostate and T24 bladder cancer cell lines and non-cancerous NIH3T3 fibroblasts by colorimetric MTT assays. The iridium precursor $[IrCl(ppy)_2]_2$ was less active than all these complexes against the two tested cancer cells, demonstrating the critical role of NHC ligands. The complexes with Log P values beween -0.06 and 0.86 (**VI-4a** to **VI-4c** and **VI-4e** to **VI-4h**) gave very good GI_{50} values ranging from 0.25 to 0.95 μM for the two cancer cell lines, while one complex **VI-4d** with a Log P value of -0.4 possessed GI_{50} values of 3.8 and 3.2 μM, respectively. The selectivity of the seven active complexes evaluated by the ratio of GI_{50} values of NIH3T3 to those of the two cancer cell lines varies between 4.5 and 17.3, suggesting moderate to good selectivity.

To gain further mechanistic insights, we have performed confocal microscopy experiments by treating PC-3 cells with the most active C1-linked complex **VI-4a**. The results showed that this complex can be quickly and effectively taken up into PC-3 cells and specifically localize into mitochondria. Moreover, these complexes can act as efficient photosensitizers. For this purpose, some preliminary *in vitro*

experiments in the dark and upon UV light irradiation have been made. The cytotoxicity of these complexes was increased substantially upon 365 nm light irradiation, which suggested their potential as a mitochondria-targeting theranostic anticancer agents.

In the near future, it would be interesting to improve iridium complexes to become activable upon two-photon (TP) irradiation in the near IR for deeper penetration of tissues. For this purpose, conjugation of chromophores to the iridium complexes can help to extend π-conjugated systems to achieve NIR emission. Subsequently, the addition of a vector to the PS that target receptors expressed on specific cancer cells will lead to the better selectivity towards cancer cells with limited side effects to normal cells. The vector could be a variety of biomolecules such as antibodies, proteins and peptide etc.

Concerning our cationic $Au^{I}(NHC)_2$ complexes, some of them displayed very interesting anticancer activities and high selectivity. It would be very interesting to modify these complexes by vector-incorporation to become more selective.

Another possibility is the combination of gold and iridium complexes by designing heterobimetallic complexes. Such theranostic complexes with rich photophysical properties of the iridium unit will help to understand some mechanistic aspects, and the activation with the specific wavelength will enable these organometallic complexes to execute dual modes of action, TrxR deactivation by the gold and direct ROS production by the iridium.

Experimental section

General information

Unless stated, all reactions were performed under air. All reagents were used as received from commercial suppliers. Reactions involving silver compounds were performed with the exclusion of light. ^{1}H (300 or 400 MHz) and ^{13}C NMR spectra (75 or 100 MHz) were recorded at 298 K on Bruker AV300 or Bruker AV400 spectrometers in $CDCl_3$, CD_3CN, CD_3OD and DMSO-d_6 as solvants. All chemical shifts for ^{1}H and ^{13}C are relative to TMS using ^{1}H (residual) or ^{13}C chemical shifts of the solvent as a secondary standard. The temperature was set at 298 K. All the ^{1}H and ^{13}C signals were assigned on the basis of chemical shifts, spin-spin coupling constants, splitting patterns and signal intensities, and by using ^{1}H-^{1}H COSY45, ^{1}H-^{13}C HSQC, ^{1}H-^{13}C HMBC, ^{13}C and ^{1}H experiments. Gradient-enhanced ^{1}H COSY45 experiments were realized including 2 scans per increment. ^{1}H-^{13}C correlation spectra using a gradient-enhanced HSQC sequence (delay was optimised for $^{1}J_{CH}$ of 145 Hz) were obtained with 2 scans per increment. Gradient-enhanced HMBC experiments were performed allowing 62.5 ms for long-range coupling evolution (8 scans were accumulated). Typically, 1024 t2 data points were collected for 256 t1 increments. Elemental analyses were carried out by the “Service de Micro-analyse du Laboratoire de Chimie de Coordination (Toulouse)”. Mass spectrometry analysis were performed on a Nermag R1010 (FAB^{+}/meta-nitrobenzylalcohol (MNBA)) spectrometer by the “Plateau technique de GC-LC/MS du Laboratoire de Chimie de Coordination (Toulouse)”. High Resolution Mass Spectrometry (HRMS) analysis were performed with a X évo G2 QTOF Waters spectrometer using electrospray ionization (ESI) by the “Service de Spectrom étrie de Masse de Chimie UPS-CNRS (Toulouse)”.

1. NHC-Au(I) complexes containing aliphatic amino-side arms

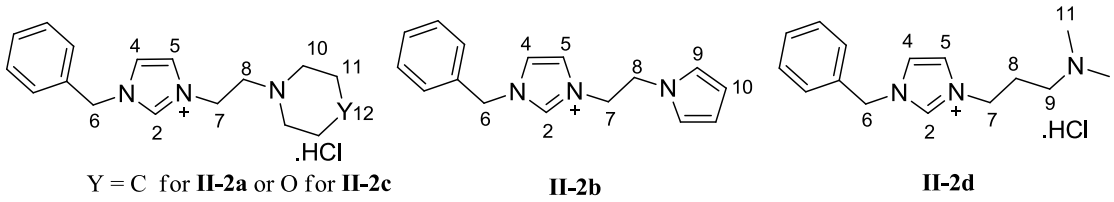

Fig 1.1 General numbering for NMR attribution.

1.1. Preparation of imidazolium salts

1.1.1. 1-Benzyl-3-[2-(piperidine-4-yl)ethyl]-1*H*-imidazol-3-ium chloride hydrochloride (**II-2a**)

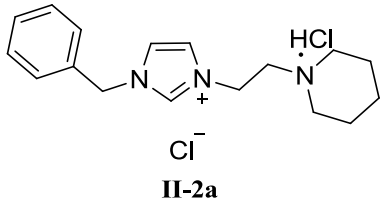

II-2a

In a pressure flask, 1-(2-chloroethyl)piperidine hydrochloride (290 mg, 1.58 mmol) and benzylimidazole (300 mg, 1.9 mmol) were dissolved in 10 mL of dry MeCN. The mixture was stirred at 80 ℃ for 48 h. After cooling to room temperature, the precipitate formed was filtered, washed with Et_2O and dried under vacuum to give a white solid (370 mg, 60% yield). Anal. Calcd. For $C_{17}H_{25}Cl_2N_3$: C, 59.65; H, 7.36; N, 12.28. Found: C, 59.44; H, 7.58; N, 12.18. ^{1}H NMR (300 MHz, DMSO-d_6): δ 11.47 (s, 1H, HCl), 9.50 (s, 1H, H2), 7.92 (s, 1H, H5), 7.82 (s, 1H, H4), 7.49-7.39 (m, 5H, benzyl), 5.44 (s, 2H, H6), 4.73 (t, 2H, *J*= 6 Hz, H7), 3.62-3.40 (m, 4H, H10), 2.97-2.87 (m, 2H, H8), 1.92-1.67 (m, 6H, H11, H12). ^{13}C NMR (75 MHz, DMSO-d_6): δ 137.7 (1C, C2), 135.0 (1C, benzyl), 129.4 (2C, benzyl), 129.2 (1C, benzyl), 128.9 (2C, benzyl), 123.3 (1C, C5), 123.2 (1C, C4), 54.6 (1C, C6), 52.8 (2C, C10), 52.5 (1C, C7), 43.5 (1C, C8), 22.4 (2C, C11), 21.7 (1C, C12). HRMS (ES$^+$): calcd. for $C_{17}H_{24}N_3$ 270.1970; found 270.1975.

1.1.2. 1-Benzyl-3-[2-(1*H*-pyrrol-1-yl)ethyl]-1*H*-imidazol-3-ium bromide (**II-2b**)

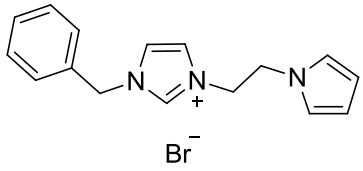

II-2b

In a pressure flask, 1-(2-bromoethyl)-1*H*-pyrrole (220 mg, 1.26 mmol) and benzylimidazole (200 mg, 1.26 mmol) were stirred in 10 mL of dry MeCN at 80 ℃ for 72 h. After cooling to room temperature, the solvent was evaporated to give a brown paste. The paste was dissolved in CH_2Cl_2 and precipitated with Et_2O. The precipitate was filtered, washed with Et_2O and dried under vacuum to give a brown solid (320 mg, 76% yield). Anal. Calcd. For $C_{16}H_{18}BrN_3$: C, 57.84; H, 5.46; N, 12.65. Found: C, 57.70; H, 5.33; N, 12.58. ^{1}H NMR (400 MHz, DMSO-d_6): δ 8.87 (s, 1H, H2), 7.76 (s, 1H, H5), 7.56 (s, 1H, H4), 7.43-7.27 (m, 5H, Bn), 6.61 (t, 2H, J= 2.0 Hz, H10), 5.97 (t, 2H, J= 2.0 Hz, H11), 5.38 (s, 2H, H6), 4.55 (t, 2H, J= 5.2 Hz, H7), 4.36 (t, 2H, J= 5.2 Hz, H8). ^{13}C NMR (100 MHz, DMSO-d_6): δ 136.9 (1C, C2), 135.1 (1C, Bn), 129.4 (2C, Bn), 129.1 (1C, Bn), 128.6 (2C, Bn), 123.3 (1C, C5), 123.0 (1C, C4), 121.0 (2C, C10), 108.8 (2C, C11), 52.2 (1C, C6), 50.6 (1C, C7), 48.4 (1C, C8). HRMS (ES$^+$): calcd. for $C_{16}H_{18}N_3$ 252.1501; found 252.1496.

1.1.3. 1-Benzyl-3-(2-morpholinoethyl)-1*H*-imidazol-3-ium chloride hydrochloride (**II-2c**)

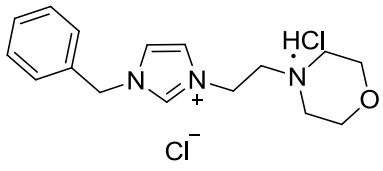

II-2c

In a pressure flask, 4-(2-chloroethyl)morpholine hydrochlodide (585 mg, 3.14 mmol) was suspended in 10 mL of dry MeCN. The mixture was heated at 80 ℃ and stirred until the solid was completely dissolved. Then benzylimidazole (745 mg, 4.71 mmol) was slowly added to the solution. The mixture was stirred for 72 h at 80 ℃. After cooling to room temperature, the precipitate formed was filtered, washed by CH_2Cl_2 and dried under vacuum to give a pale-yellow solid (700 mg, 76% yield). Anal. Calcd. For $C_{16}H_{23}Cl_2N_3O$: C, 55.82; H, 6.73; N, 12.21. Found: C, 55.64; H,

6.87; N, 12.06. ^{1}H NMR (400 MHz, CD_3OD): δ 9.25 (s, 1H, H2), 7.81 (s, 1H, H5), 7.71 (s, 1H, H4), 7.53-7.45 (m, 5H, benzyl), 5.46 (s, 2H, H6), 4.79 (t, 2H, *J*= 6.8 Hz, H7), 4.01 (s, 4H, H11), 3.76 (t, 2H, *J*= 6.8 Hz, H8), 3.50 (s, 4H, H10). ^{13}C NMR (100 MHz, CD_3OD): δ 137.1 (1C, C2), 133.3 (1C, benzyl), 129.1 (2C, benzyl), 129.0 (1C, benzyl), 128.7 (2C, benzyl), 123.0 (1C, C5), 122.7 (1C, C4), 63.3 (2C, C11), 55.0 (1C, C6), 53.1 (1C, C7), 52.2 (2C, C10), 42.9 (1C, C8). HRMS (ES+): calcd. for $C_{16}H_{22}N_3O$ 272.1763; found 272.1771

1.1.4. 1-[2-Dimethyl)propyl]-benzylimidazolium chloride hydrochloride (**II-2d**)

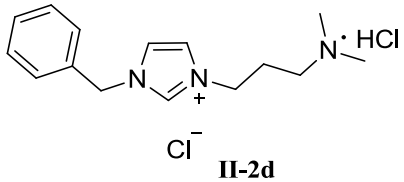

II-2d

In a pressure flask, 3-chloro-*N*,*N*-dimethylpropylamine hydrochloride (300 mg, 1.90 mmol) was suspended in 10 mL of dry MeCN. After the solid was completely dissolved, benzylimidazole (450 mg, 2.85 mmol) was slowly added to the solution. The reaction mixture was stirred for 72 h at 80 ℃. After cooling to room temperature, the solvent was removed under vacuum to give a pale-yellow paste. The paste was dissolved in MeCN and precipitated with Et_2O. The precipitate was filtered, washed with Et_2O and dried under vacuum to give a pale-yellow solid (200 mg, 33% yield). Anal. Calcd. For $C_{15}H_{23}N_3Cl_2$: C, 56.97; H, 7.33; N, 13.29. Found: C, 57.09; H, 7.38; N, 13.31.^{1}H NMR (400 MHz, DMSO-d_6): δ 11.24 (s, 1H, HCl), 9.51 (s, 1H, H2), 7.90 (s, 1H, H5), 7.86 (s, 1H, H4), 7.46-7.40 (m, 5H, benzyl), 5.46 (s, 2H, H6), 4.35 (t, 2H, *J*= 7.2 Hz, H7), 3.06 (t, 2H, *J*= 7.2 Hz, H9), 2.73 (s, 6H, H11), 2.32-2.25 (m, 2H, H8). ^{13}C NMR (100 MHz, DMSO-d_6): δ 137.0 (1C, C2), 135.2 (1C, benzyl), 129.5 (2C, benzyl), 129.2 (1C, benzyl), 128.8 (2C, benzyl), 123.3 (1C, C5), 123.1 (1C, C4), 53.4 (1C, C6), 52.4 (1C, C7), 46.7 (1C, C9), 42.4 (2C, C11), 24.7 (1C, C8). HRMS (ES^+): calcd. for $C_{15}H_{22}N_3$ 244.1814; found 244.1823.

1.2. Preparation of gold(I) bis(NHC) complexes

1.2.1. Complex **II-3a**

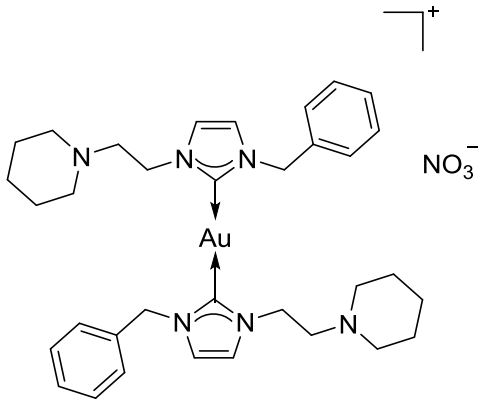

II-3a

In a Schlenk tube 1-benzyl-3-(2-(piperidin-1-yl)ethyl)-1*H*-imidazol-3-ium chloride hydrochloride (100 mg, 0.29 mmol) was suspended in 10 mL of dry MeOH and Ag_2O (69 mg, 0.29 mmol) was added. The mixture was stirred at room temperature for 3 h under nitrogen in the dark. A solution of $AgNO_3$ (25 mg, 0.15 mmol) in 2 mL of MeCN was added and the mixture was stirred for 1 h. Finally, $Au(SMe_2)Cl$ (43 mg, 0.15 mmol) was added and after stirring for 1 h, the mixture was filtered through a pad of celite. The solvent was evaporated under reduced pressure to give a white solid (40 mg, 40% yield). Anal. Calcd. For $C_{34}H_{46}AuN_7O_3$: C, 51.19; H, 5.81; N, 12.29. Found: C, 51.29; H, 5.63; N, 12.31.^{1}H NMR (400 MHz, CD_3CN): δ 7.35-7.23 (m, 14H, benzyl, H4, H5), 5.36 (s, 4H, H6), 4.23 (t, 4H, *J*= 6 Hz, H7), 2.67 (t, 4H, *J*= 6 Hz, H8), 2.36 (t, 8H, *J*= 4.8 Hz, H10), 1.47-1.39 (m, 12H, H11, H12).^{13}C NMR (100 MHz, CD_3CN): δ 184.0 (2C, C2), 136.9 (2C, C2), 128.9 (4C, benzyl), 128.2 (2C, benzyl), 127.1 (4C, benzyl), 122.6 (2C, C5), 121.8 (2C, C4), 58.8 (2C, C6), 54.4 (4C, C10), 54.0 (2C, C7), 48.7 (2C, C8), 25.9 (4C, C11), 24.0 (2C, C12). HRMS (ES^+): calcd. for $C_{34}H_{46}AuN_6$ 735.3449; found 735.3448.

1.2.2. Complex **II-3b**

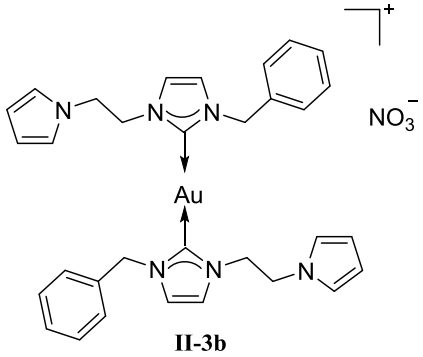

II-3b

In a Schlenk tube 3-(2-(1*H*-pyrrol-1-yl)ethyl)-1-benzyl-1*H*-imidazol-3-ium bromide (100 mg, 0.3 mmol) was suspended in 10 mL of dry MeOH and Ag_2O (67.3 mg, 0.3 mmol) was added. The mixture was stirred at room temperature for 3 h under nitrogen in the dark. A solution of $AgNO_3$ (25 mg, 0.15 mmol) in 2 mL of MeCN was added and the resulting mixture was stirred at room temperature overnight. Then the mixture was filtered through a pad of celite. After that, $Au(SMe_2)Cl$ (44 mg, 0.15 mmol) was added and after stirring for 1 h, the mixture was filtered through a pad of celite. The solvent was evaporated under reduced pressure to give a grey solid (50 mg, 50 % yield). Anal. Calcd. For $C_{32}H_{34}AuN_7O_3$: C, 50.46; H, 4.50; N, 12.87. Found: C, 50.22; H, 4.60; N, 12.80. ^{1}H NMR (300 MHz, CD_3CN): δ 7.37-7.04 (m, 14H, benzyl, H4, H5), 6.39 (t, 4H, *J*= 2.1 Hz, H10), 5.97 (t, 4H, *J*= 2.1 Hz, H11), 5.24 (s, 4H, H6), 4.42 (t, 4H, *J*= 6 Hz, H7), 4.24 (t, 4H, *J*= 6 Hz, H8). ^{13}C NMR (75 MHz, CD_3CN): δ 184.5 (2C, C2), 136.6 (2C, benzyl), 128.8 (4C, benzyl), 128.2 (2C, benzyl), 127.2 (4C, benzyl), 122.4 (2C, C5), 121.8 (2C, C4), 120.7 (4C, C10), 108.5 (4C, C11), 53.9 (2C, C6), 52.3 (2C, C7), 49.4 (2C, C8). HRMS (ES^+): calcd. for $C_{32}H_{34}AuN_6$ 699.2510; found 699.2509.

1.2.3. Complex **II-3c**

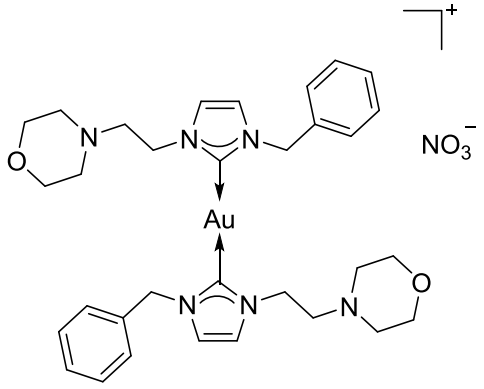

II-3c

In a Schlenk tube 1-benzyl-3-(2-morpholinoethyl)-1*H*-imidazol-3-ium chloride hydrochloride (100 mg, 0.29 mmol) was suspended in 10 mL of dry MeOH and Ag_2O (67.3 mg, 0.29 mmol) was added. The mixture was stirred at room temperature for 3 h under nitrogen in the dark. A solution of $AgNO_3$ (25 mg, 0.15 mmol) in 2 mL of MeCN was added and the mixture was stirred for 1 h. Finally, $Au(SMe_2)Cl$ (43 mg, 0.15 mmol) was added and after stirring for 1 h, the mixture was filtered through a pad of celite. The solvent was evaporated under reduced pressure to give a grey solid (97 mg, 84% yield). Anal. Calcd. For $C_{32}H_{42}AuN_7O_5$: C, 47.94; H, 5.28; N, 12.23. Found: C, 48.08; H, 5.35; N, 12.29. ^{1}H NMR (300 MHz, CD_3CN): δ 7.37-7.22 (m, 14H, benzyl, H4, H5), 5.36 (s, 4H, H6), 4.23 (t, 4H, *J*= 6 Hz, H7), 3.52 (t, 8H, *J*= 4.8 Hz, H10), 2.72 (t, 4H, *J*= 6 Hz, H8), 2.39 (t, 8H, *J*= 4.8 Hz, H9). ^{13}C NMR (75 MHz, CD_3CN): δ 184.0 (2C, C2), 136.9 (2C, benzyl), 128.9 (4C, benzyl), 128.2 (2C, benzyl), 127.1 (4C, benzyl), 122.6 (2C, C5), 121.9 (2C, C4), 66.5 (4C, C11), 58.4 (2C, C6), 54.1 (2C, C7), 53.4 (4C, C10), 48.2 (2C, C8). HRMS (ES^+): calcd. for $C_{32}H_{42}AuN_6O_2$ 739.3035; found 739.3036.

1.2.4. Complex **II-3d**

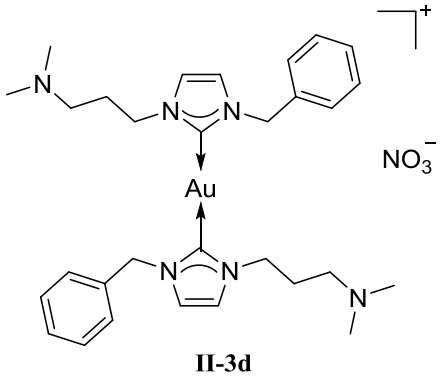

II-3d

In a Schlenk tube 1-benzyl-3-(3-(dimethylamino)propyl)-1*H*-imidazol-3-ium chloride hydrochloride (146 mg, 0.46 mmol) was suspended in 10 mL of dry MeOH and Ag_2O (106 mg, 0.46 mmol) was added. The mixture was stirred at room temperature for 3 h under nitrogen in the dark. A solution of $AgNO_3$ (39 mg, 0.23 mmol) in 2 mL of MeCN was added and the mixture was stirred for 1 h. Finally, $Au(SMe_2)Cl$ (67 mg, 0.23 mmol) was added and after stirring for 1 h, the mixture was filtered through a pad of celite. The solvent was evaporated under reduced pressure to give a grey solid (143 mg, 84% yield). Anal. Calcd. For $C_{30}H_{42}AuN_7O_3$: C, 48.32; H, 5.68; N, 13.15. Found: C, 48.25; H, 5.71; N, 13.28. ^{1}H NMR (400 MHz, CD_3OD): δ 7.45-7.24 (m, 14H, benzyl, H4, H5), 5.41 (s, 4H, H6), 4.27 (t, 4H, *J*= 6.8 Hz, H7), 2.30 (t, 4H, *J*= 6.8 Hz, H9), 2.21 (s, 12H, H10), 2.08-2.01 (m, 4H, H8). ^{13}C NMR (100 MHz, CD_3OD): δ 183.8 (2C, C2), 136.7 (2C, benzyl), 128.7 (4C, benzyl), 128.0 (2C, benzyl), 126.9 (4C, benzyl), 122.2 (2C, C5), 122.0 (2C, C4), 55.6 (2C, C6), 54.0 (2C, C7), 48.8 (2C, C9), 44.0 (4C, C11), 28.7 (2C, C8). HRMS (ES^+): calcd. for $C_{30}H_{42}AuN_6$ 683.3136 found 683.3130.

2. NHC-Au(I) complexes containing aromatic amino-side arms

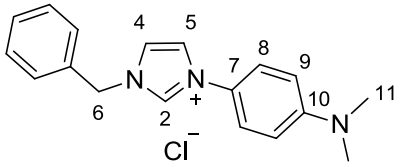

Fig 2.1 General numbering for NMR attribution.

2.1. Preparation of imidazolium salts

2.1.1. 3-Benzyl-1-[4-(dimethylamino)phenyl]-1*H*-imidazol-3-ium chloride (**III-2a**)

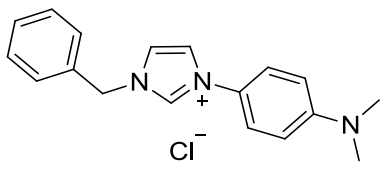

III-2a

Imidazole (3.0 g, 44 mmol), 4-bromo-*N*,*N*-dimethylaniline (4.4 g, 22 mmol), K_2CO_3 (3.04 g, 22 mmol) and a catalytic amount of $CuSO_4$ were stirred in a closed pressure flask at 205 ℃ for 10 h. After cooling to room temperature, the crude product was extracted by dichloromethane, filtered and evaporated to dryness. The resulting residue was purified by column chromatography on silica gel with a mixture of CH_2Cl_2 and MeOH (30:1) as eluent to give 4-(1*H*-imidazol-1-yl)-*N*,*N*-dimethylaniline (**III-1a**) as a yellow solid (3.7 g, 90% yield). ^{1}H NMR (400 MHz, $CDCl_3$): δ 7.79 (s, 1H, H2), 7.28-7.23 (m, 4H, H4/H5/H8), 6.78 (d, 2H, J = 8.8 Hz, H9), 3.02 (s, 6H, H11). A mixture of **III-1a** (400 mg, 2.13 mmol) and benzyl chloride (296 mg, 2.34 mmol) in MeCN was stirred in a closed pressure flask at 80 ℃ for 10 h. After cooling down to room temperature, the solution was evaporated to dryness. The residue was purified by column chromatography on silica gel with a mixture of CH_2Cl_2 and MeOH (10:1) as eluent to give **III-2a** as a highly hydroscopic yellow solid (512 mg, 76 % yield). Anal. Calcd. For $C_{18}H_{20}ClN_3$: C, 68.89; H, 6.42; N, 13.39. Found: C, 68.67; H, 6.38; N, 13.48. ^{1}H NMR (400 MHz, DMSO-d_6): δ 10.02 (s, 1H, H2), 8.22 (s, 1H, H5), 8.02 (s, 1H, H4), 7.59 (d, 2H, J = 9.2 Hz, H8), 7.57-7.54 (m, 2H, benzyl), 7.46-7.40 (m, 3H, benzyl), 6.86 (d, 2H, J = 9.2 Hz, H9), 5.52 (s, 2H, H6), 2.97 (s, 6H, H11). ^{13}C NMR (100 MHz, DMSO- d_6): δ 151.3 (1C, C10), 135.2 (1C, C2), 135.1 (1C, benzyl), 129.4 (2C, benzyl), 129.2 (1C, benzyl), 129.0 (2C, benzyl), 124.0 (1C, C7), 123.3 (1C, C5), 123.1 (2C, C8), 122.1 (1C, C4), 112.7 (2C, C9), 52.1 (2C, C11), 49.0 (1C, C6). HRMS (ES^+): calcd. for $C_{18}H_{20}N_3$ 278.1657; found 278.1658.

2.1.2. 3-Benzyl-1-[4-(diethylamino)phenyl]-1*H*-imidazol-3-ium chloride (**III-2b**)

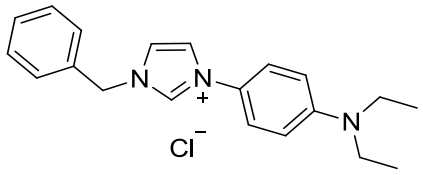

III-2b

Imidazole (1 g, 14.7 mmol), 4-bromo-*N*,*N*-diethylaniline (1.67 g, 7.34 mmol), K_2CO_3 (2.01 g, 7.34 mmol) and a catalytic amount of $CuSO_4$ were stirred in a closed pressure flask at 205 ℃ for 10 h. After cooling to room temperature, the crude product was extracted by CH_2Cl_2, filtered and evaporated to dryness. The resulting residue was purified by column chromatography on silica gel with a mixture of

CH_2Cl_2 and MeOH (30:1) as eluent to give *N*,*N*-diethyl-4-(1*H*-imidazol-1-yl)aniline (**III-1b**) as a brown solid (1.43 g, 90% yield). ^{1}H NMR (400 MHz, $CDCl_3$): δ 7.73 (s, 1H, H2), 7.21 (d, 2H, *J* = 9.2 Hz, H8), 7.18-7.17 (m, 2H, H4/H5), 6.72 (d, 2H, *J* = 9.2 Hz, H9), 3.40 (q, 4H, *J* = 7.2 Hz, H11), 1.21 (t, 6H, *J* = 7.2 Hz, H12). A mixture of **III-1b** (300 mg, 1.39 mmol) and benzyl chloride (194 mg, 1.53 mmol) in MeCN was stirred in a closed pressure flask at 80 ℃ for 10 h. After cooling down to room temperature, the solution was evaporated to dryness. The residue was purified by column chromatography on silica gel with a mixture of CH_2Cl_2 and MeOH (10:1) as eluent to give **III-2b** a highly hydroscopic yellow solid (443 mg, 93% yield). Anal. Calcd. For $C_{20}H_{24}ClN_3$: C, 70.26; H, 7.08; N, 12.29. Found: C, 70.47; H, 7.28; N, 12.48. ^{1}H NMR (400 MHz, DMSO-d_6): δ 9.98 (s, 1H, H2), 8.19 (s, 1H, H5), 8.00 (s, 1H, H4), 7.55-7.51 (m, 4H, benzyl/H8), 7.47-7.40 (m, 3H, benzyl), 6.81 (d, 2H, *J* = 9.2 Hz, H9), 5.50 (s, 2H, H6), 3.40 (q, 4H, *J* = 7.2 Hz, H11), 1.11 (t, 6H, J= 7.2 Hz, H12). ^{13}C NMR (100 MHz, DMSO-d_6): δ 148.5 (1C, C10), 135.2 (1C, C2), 135.1 (1C,benzyl), 129.4 (2C, benzyl), 129.2 (1C, benzyl), 128.9 (2C, benzyl), 123.6 (2C, C8), 123.3 (1C, C7), 123.1 (1C, C5), 122.2 (1C, C4), 112.0 (2C, C9), 52.6 (1C, C6), 44.3 (2C, C11), 12.7 (2C, C12). HRMS (ES^+): calcd. for $C_{20}H_{24}N_3$ 306.1970; found 306.1967.

2.1.3. Benzyl-1-(1*H*-pyrrol-1-yl)-1*H*-imidazol-3-ium chloride (**III-2c**)

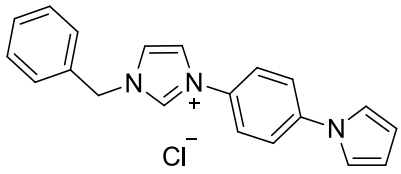

III-2c

Imidazole (268.5 mg, 3.94 mmol), 1-(4-chlorophenyl)-1*H*-pyrrole (500 mg, 2.81 mmol), K_3PO_4 (1.19 g, 5.62 mmol) and CuI (107 mg, 0.56 mmol) in DMF were placed in a closed pressure flask, then stirred at 160 ℃ for 3 days. After cooling to room temperature, distilled water was added to the reaction and the crude was extracted with EtOAc. The organic layer was washed with brine and dried over Na_2SO_4. After filtration and evaporation of the solvent under reduced pressure, the residue was purified by column chromatography on silica gel with a mixture of CH_2Cl_2 and MeOH (30:1) as eluent to give 1-(1*H*-pyrrol-1-yl)-1*H*-imidazole (**III-1c**) as a yellow solid (300 mg, 51% yield). ^{1}H NMR (400 MHz, DMSO-d_6): δ 8.33 (s, 1H,

H2), 7.82 (s, 1H, H5), 7.76-7.71 (m, 4H, H8/H9), 7.45 (t, 2H, *J* = 2.4 Hz, H11), 7.16 (s, 1H, H4), 6.30 (t, 2H, *J* = 2.4 Hz, H12). A mixture of **III-1c** (200 mg, 0.96 mmol) and benzyl chloride (133 mg, 1.05 mmol) in MeCN was stirred in a closed pressure flask at 80 ℃ for 10 h. After cooling down to room temperature, the solution was evaporated to dryness. The residue was purified by column chromatography on silica gel with a mixture of CH_2Cl_2 and MeOH (10:1) as eluent to give **III-2c** as a yellow solid (306 mg, 95% yield). Anal. Calcd. For $C_{20}H_{18}ClN_3$: C, 71.53; H, 5.40; N, 12.51. Found: C, 71.57; H, 5.38; N, 12.48. ^{1}H NMR (400 MHz, DMSO-d_6): δ 10.36 (s, 1H, H2), 8.41 (s, 1H, H5), 8.10 (s, 1H, H4), 7.94-7.89 (m, 4H, H8/H9), 7.59-7.43 (m, 7H, benzyl/H11), 6.33 (s, 2H, H12), 5.56 (s, 2H, H6). ^{13}C NMR (100 MHz, DMSO- d_6): δ 140.9 (1C, C10), 136.1 (1C, C2), 135.0 (1C, benzyl), 131.9 (1C, C7), 129.4 (2C, benzyl), 129.3 (1C, benzyl), 129.0 (2C, benzyl), 123.7 (2C, C8), 123.6 (1C, C5), 122.1 (1C, C4), 120.4 (2C, C9), 119.6 (2C, C11), 112.7 (2C, C12), 52.8 (1C, C6). HRMS (ES$^+$): calcd. for $C_{20}H_{18}N_3$ 300.1501; found 300.1500.

2.1.4. 3-Benzyl-1-[4-(morpholin-4-yl)phenyl]-1*H*-imidazol-3-ium chloride (**III-2d**)

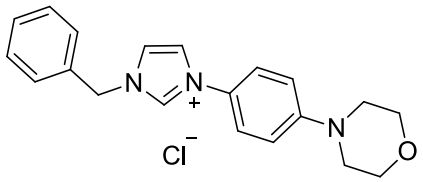

III-2d

To a mixture of 4-phenylmorpholine (816 mg, 5 mmol) and DMSO (429 mg, 5.5 mmol) in EtOAc (20 mL) was added hydrobromic acid (48 %, 1.85 g, 5.5 mmol) at 60 ℃ under air. The mixture was stirred at 60 ℃, then potassium carbonate (1 g) was added to the solution and the mixture was stirred for another 0.5 h. After cooling down to room temperature and evaporation of the solvent under vacuum, the residue was purified by column chromatography on silica gel with a mixture of hexane and EtOAc (10:1) as eluent to give 4-(4-bromophenyl)morpholine as a white solid (1.03 g, 85% yield). ^{1}H NMR (400 MHz, $CDCl_3$): δ 7.37 (d, 2H, *J* = 8.8 Hz), 6.78 (d, 2H, *J* = 8.8 Hz), 3.86 (t, 4H, *J* = 4.8 Hz), 3.12 (t, 4H, *J* = 4.8 Hz). Imidazole (275.6 mg, 4.05 mmol), 4-(4-bromophenyl)morpholine (700 mg, 2.89 mmol), K_3PO_4 (1.2 g, 5.65 mmol) and CuI (110 mg, 0.56 mmol) in DMF were placed to a closed pressure flask, then stirred at 160 ℃ for 3 days. After cooling to room temperature, distilled water

was added to the reaction and the crude was extracted with EtOAc. The organic layer was washed with brine and dried over Na_2SO_4. After filtration and evaporation of the solvent under reduced pressure, the residue was purified by column chromatography on silica gel with a mixture of CH_2Cl_2 and MeOH (30:1) as eluent to give 4-[4-(1*H*-imidazol-1-yl)phenyl]morpholine (**III-1d**) as a yellow solid (200 mg, 30% yield). ^{1}H NMR (400 MHz, DMSO-d_6): δ 8.13 (s, 1H, H2), 7.66 (s, 1H, H5), 7.76-7.71 (d, 2H, J = 8.8 Hz, H8), 7.45 (m, 3H, H4/H9), 3.75 (t, 4H, J = 4.8 Hz, H12), 3.14 (t, 4H, J = 4.8 Hz, H11). HRMS (ES$^+$): calcd. for $C_{13}H_{16}N_3O$ 230.1293; found 230.1293. A mixture of **III-1d** (150 mg, 0.65 mmol) and benzyl chloride (121.5 mg, 0.96 mmol) in MeCN was stirred in a closed pressure flask at 80 ℃ for 10 h. After cooling down to room temperature, the solution was evaporated to dryness. The residue was purified by column chromatography on silica gel with a mixture of CH_2Cl_2 and MeOH (10:1) as eluent to give **III-2d** as a highly hydroscopic yellow solid (200 mg, 91 % yield). Anal. Calcd. For $C_{20}H_{22}ClN_3O$: C, 67.50; H, 6.23; N, 11.81. Found: C, 67.57; H, 6.38; N, 11.58. ^{1}H NMR (400 MHz, DMSO-d_6): δ 10.15 (s, 1H, H2), 8.27 (s, 1H, H5), 8.04 (s, 1H, H4), 7.65 (d, 2H, J = 8.8 Hz, H8), 7.55 (m, 2H, benzyl), 7.47-7.40 (m, 3H, benzyl), 7.15 (d, 2H, J = 8.8 Hz, H9), 5.52 (s, 2H, H6), 3.76 (t, 4H, J = 4.8 Hz, H12), 3.22 (t, 4H, J = 4.8 Hz, H11). ^{13}C NMR (100 MHz, DMSO-d_6): δ 152.1 (1C, C10), 135.4 (1C, C2), 135.2 (1C, benzyl), 129.4 (2C, benzyl), 129.2 (1C, benzyl), 129.0 (2C, benzyl), 126.4 (1C, C7), 123.4 (1C, C5), 123.1 (2C, H8), 122.1 (1C, C4), 115.6 (2C, H9), 66.4 (2C, C12), 52.6 (1C, C6), 48.2 (2C, C11). HRMS (ES$^+$): calcd. for $C_{20}H_{22}N_3O$ 320.1763; found 320.1761.

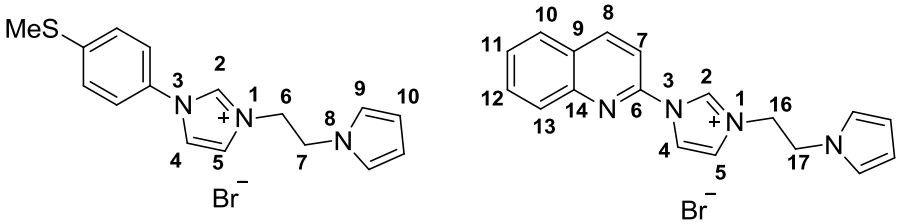

Fig 2.2 General numbering for NMR attribution.

2.1.5. 3-(2-(1*H*-Pyrrol-1-yl)ethyl)-1-(4-(methylthio)phenyl)-1*H*-imidazol-3-ium bromide (**III-5a**)

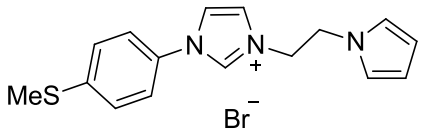

III-5a

Imidazole (3.24 g, 47.6 mmol), 4-bromothioanisole (4.83 g, 23.8 mmol), K_2CO_3 (3.29 g, 23.8 mmol) and a catalytic amount of $CuSO_4$ were stirred in a closed pressure flask at 205 ℃ for 10 h. After cooling to room temperature, the crude product was extracted by CH_2Cl_2, filtered and evaporated to dryness. The resulting residue was washed three times with Et_2O (20 mL) to give 1-(4-methylthiophenyl)-1*H*- imidazole (**III-4a**) as a grey solid (3.6 g, 80% yield). ^{1}H NMR (400 MHz, $CDCl_3$): δ 7.84 (t, 1H, *J*= 1.2 Hz, H2), 7.38-7.32 (m, 4H, H_{SMePh}), 7.27 (t, 1H, *J*= 1.2 Hz, H5), 7.22 (t, 1H, *J*= 1.2 Hz, H4), 2.54 (s, 3H, H_{SMePh}). In a pressure flask, a mixture of **III-4a** (200 mg, 1.05 mmol) and 1-(2-bromoethyl)-1*H*-pyrrole (183 mg, 1.05 mmol) was dissolved in 10 mL of dry MeCN. The mixture was stirred at 80 ℃ for 72 h. After cooling to room temperature, the solvent was removed by vacuum to give a brown paste. The paste was dissolved in CH_2Cl_2 and precipitated with Et_2O. The precipitate was filtered, washed with Et_2O and dried under vacuum to give **III-5a** as a brown solid (154 mg, 40% yield). Anal. Calcd. For $C_{16}H_{18}BrN_3S$: C, 52.75; H, 4.98; N, 11.53. Found: C, 52.82; H, 4.86; N, 11.66. ^{1}H NMR (400 MHz, DMSO-d_6): δ 9.41(s, 1H, H2), 8.25 (s, 1H, H5), 7.66 (s, 1H, H4), 7.62 (d, 2H, *J*= 8.4 Hz, H_{SMePh}), 7.51 (d, 2H, *J*= 8.4 Hz, H_{SMePh}), 6.72 (s, 1H, H9), 6.01 (s, 1H, H10), 4.61 (t, 2H, *J*= 6 Hz, H6), 4.36 (t, 2H, *J*= 6 Hz, H7), 2.55 (s, 3H, H_{SMePh}). ^{13}C NMR (100 MHz, DMSO-d_6): δ 141.5 (1C, C_{SMePh}), 135.8 (1C, C2), 131.8 (1C, C_{SMePh}), 127.2 (2C, C_{SMePh}), 123.7 (1C, C5), 122.7 (2C, C_{SMePh}), 121.5 (1C, C4), 121.2 (2C, C9), 108.9 (2C, C10), 50.9 (1C, C6), 48.4 (1C, C7), 15.0 (1C, C_{SMePh}). HRMS (ES^+): calcd. for $C_{16}H_{18}N_3S$ 284.1221; found 284.1219.

2.1.6. 1-(4-(Methylthio)phenyl)-3-(2-(piperidin-1-yl)ethyl)-1*H*-imidazol-3-ium chloride hydrochloride (**III-5b**)

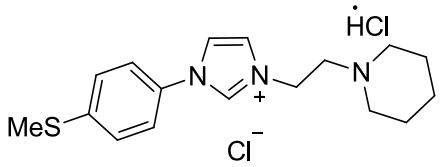

III-5b

In a pressure flask, a mixture of **III-4a** (400 mg, 2.1mmol) and 1-(2-chloroethyl)piperidine hydrochloride (387 mg, 2.1 mmol) was dissolved in 10 mL of dry acetonitrile. The mixture was stirred at 80 ℃ for 72 h. After cooling to room temperature, the precipitate formed was filtered, washed with CH_2Cl_2 and dried under vacuum to obtain **III-5b** as a white solid (205 mg, 26% yield). Anal. Calcd. For $C_{17}H_{25}Cl_2N_3S$: C, 54.54; H, 6.73; N, 11.22. Found: C, 54.23; H, 6.44; N, 11.08. ^{1}H NMR (400 MHz, DMSO-d_6): δ 11.37 (s, 1H, HCl), 10.04 (s, 1H, H2), 8.29 (t, 1H, *J*= 2 Hz, H5), 8.09 (t, 1H, *J*= 2 Hz, H4), 7.75 (d, 2H, *J*= 8.4 Hz, H_{SMePh}), 7.53 (d, 2H, *J*= 8.4 Hz, H_{SMePh}), 4.77 (t, 2H, *J*= 6.4 Hz, H6), 3.70-3.52 (m, 4H, H9), 2.94 (m, 2H, H7), 2.56 (s, 3H, H_{SMePh}), 1.94-1.68 (m, 6H, H10/H11). ^{13}C NMR (100 MHz, DMSO-d_6): δ 141.3 (1C, C_{SMePh}), 137.0 (1C, C2), 132.1 (1C, C_{SMePh}), 127.2 (2C, C_{SMePh}), 123.6 (1C, C5), 123.0 (2C, C_{SMePh}), 121.7 (1C, C4), 54.7 (1C, C6), 52.7 (2C, C9), 43.7 (1C, C7), 22.3 (2C, C10), 21.7 (1C, C11), 15.0 (1C, C_{SMePh}). HRMS (ES^+): calcd. for $C_{17}H_{24}N_3S$ 302.1691; found 302.1683.

2.1.7. 3-(2-(1*H*-Pyrrol-1-yl)ethyl)-1-(quinolin-2-yl)-1*H*-imidazol-3-ium bromide (**III-5c**)

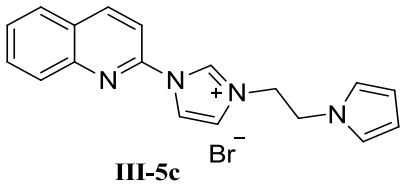

III-5c

Imidazole (2.451 g, 36 mmol), 2-chloroquinoline (3 g, 18 mmol), K_2CO_3 (2.488 g, 18 mmol) and a catalytic amount of $CuSO_4$ were stirred in a closed pressure flask at 205 ℃ for 10 h. After cooling to room temperature, the crude product was extracted by CH_2Cl_2, filtered and evaporated to dryness. The resulting residue was washed three times with Et_2O (20 mL) to give 2-(1*H*-imidazol-1-yl) quinoline (**III-4b**) as a brown solid (2.8 g, 80% yield). ^{1}H NMR (400 MHz, DMSO-d_6): δ 8.74 (t, 1H, *J*= 1.2 Hz,

H2), 8.60 (d, 1H, *J*= 8.8 Hz, H8), 8.14 (t, 1H, *J*= 1.2 Hz, H5), 8.04 (d, 2H, *J*= 8.8 Hz, H7/H10), 7.99 (d, 1H, *J*= 8.8 Hz, H13), 7.84-7.80 (ddd, *J*= 8.4, 6.8, 1.6 Hz, 1H, H12), 7.64-7.60 (ddd, *J*= 8.0, 6.8, 1.2 Hz, 1H, H11), 7.19 (t, 1H, *J*= 1.2 Hz, H4). In a pressure flask, a mixture of **III-4b** (300 mg, 1.54 mmol) and 1-(2-bromoethyl)-1*H*-pyrrole (267.45 mg, 1.54 mmol) was dissolved in 10 mL of dry MeCN. The mixture was stirred at 80 ℃ for 72 h. After cooling to room temperature, the solvent was removed by vacuum to give a brown paste. The paste was dissolved in CH_2Cl_2 and precipitated with Et_2O. The precipitate was filtered, washed with Et_2O and dried under vacuum to give **III-5c** as a yellow solid (180 mg, 32% yield). Anal. Calcd. For $C_{18}H_{17}BrN_4$: C, 58.55; H, 4.64; N, 15.17. Found: C, 58.73; H, 4.36; N, 15.08. ^{1}H NMR (400 MHz, DMSO-d_6): δ 9.98 (t, 1H, *J*= 2 Hz, H2), 8.84 (d, 1H, *J*= 8.8 Hz, H8), 8.64 (t, 1H, *J*= 2 Hz, H5), 8.17 (d, 1H, *J*= 8.0 Hz, H7), 8.11 (d, 1H, *J*= 8.8 Hz, H10), 8.07 (d, 1H, *J*= 8.4 Hz, H13), 7.95 (ddd, 1H, *J*= 8.8, 7.2, 1.6 Hz, H12), 7.77 (ddd, 1H, *J*= 8.4, 7.2, 1.2 Hz, H11), 7.67 (t, 1H, *J*= 2 Hz, H4), 6.76 (t, 2H, *J*= 2 Hz, H19), 6.01 (t, 2H, *J*= 2 Hz, H20), 4.72 (t, 2H, *J*= 6 Hz, H16), 4.49 (t, 2H, *J*= 6 Hz, H17). ^{13}C NMR (100 MHz, DMSO-d_6): δ 145.9 (1C, C6), 145.6 (1C, C14), 141.9 (1C, C8), 136.2 (1C, C2), 132.3 (1C, C12), 128.8 (1C, C13), 128.6 (1C, C10), 128.5 (1C, C9), 128.3 (1C, C11), 124.2 (1C, C5), 121.3 (2C, C19), 119.8 (1C, C4), 112.9 (1C, C7), 109.0 (2C, C20), 51.1 (1C, C16), 48.4 (1C, C17). HRMS (ES^+): calcd. for $C_{18}H_{17}N_4$ 289.1453; found 289.1454.

2.1.8. 3-(2-(Piperidin-1-yl)ethyl)-1-(quinolin-2-yl)-1*H*-imidazol-3-ium chloride hyrdrochloride (**III-5d**)

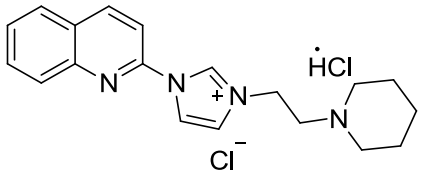

III-5d

In a pressure flask, a mixture of **III-4b** (400 mg, 2.05 mmol) and 1-(2-chloroethyl)piperidine hydrochloride (377 mg, 2.05 mmol) was dissolved in 10 mL of dry MeCN. The mixture was stirred at 80 ℃ for 72 h. After cooling to room temperature, the precipitate formed was filtered, washed with CH_2Cl_2 and dried under vacuum to obtain **III-5d** as a white solid (150 mg, 20% yield). Anal. Calcd. For $C_{19}H_{24}Cl_2N_4$: C, 60.16; H, 6.38; N, 14.77. Found: C, 60.18; H, 6.10; N, 14.92. ^{1}H

NMR (400 MHz, DMSO-d_6): δ 11.26 (s, 1H, HCl), 10.05 (s, 1H, H2), 8.86 (d, 1H, *J*= 8.8 Hz, H8), 8.71 (t, 1H, *J*= 2 Hz, H5), 8.22-8.17 (m, 3H, H4/ H7/H10), 8.09 (d, 1H, *J*= 8.8 Hz, H13), 7.96 (ddd, 1H, *J*= 8.8, 7.2, 1.6 Hz, H12), 7.78 (ddd, 1H, *J*= 8.4, 7.2, 1.2 Hz, H11), 4.86 (t, 2H, *J*= 5.6 Hz, H16), 3.73-3.54 (m, 4H, H19), 2.97 (m, 2H, H17), 1.92-1.69 (m, 6H, H20/H21). ^{13}C NMR (100 MHz, DMSO-d_6): δ 146.0 (1C, C6), 145.8 (1C, C14), 141.8 (1C, C8), 137.3 (1C, C2), 132.3 (1C, C12), 128.9 (1C, C13), 128.6 (1C, C10), 128.5 (1C, C9), 128.3 (1C, C11), 124.1 (1C, C5), 119.9 (1C, C4), 113.1 (1C, C7), 54.7 (1C, C16), 52.8 (2C, C19), 44.1 (1C, C17), 22.4 (2C, C20), 21.7 (1C, C21). HRMS (ES$^+$): calcd. for $C_{19}H_{23}N_4$ 307.1923; found 307.1919.

2.2. Preparation of gold(I) complexes

2.2.1. Complex **III-3a**

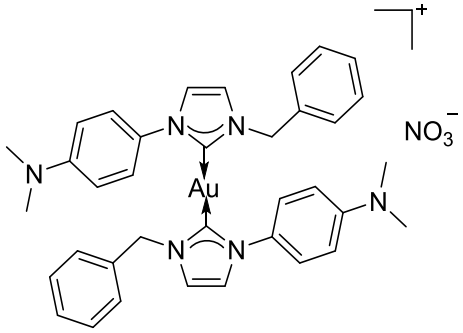

III-3a

In a Schlenk tube, **III-2a** (100 mg, 0.32 mmol) was suspended in 10 mL of dry MeOH and Ag_2O (74 mg, 0.32 mmol) was added. The mixture was stirred at room temperature for 3 h under nitrogen in the dark. A solution of $AgNO_3$ (27 mg, 0.16 mmol) in 2 mL of MeCN was added and the mixture was stirred for 10 h. Finally, $Au(SMe_2)Cl$ (47 mg, 0.15 mmol) was added and after stirring for 1 h, the mixture was filtered through a pad of celite. The solvent was evaporated under reduced pressure and the residue was purified by column chromatography on silica gel with a mixture of CH_2Cl_2 and MeOH (20:1) as eluent to give complex **III-3a** as a yellow solid (52 mg, 40% yield). Anal. Calcd. For $C_{36}H_{38}AuN_7O_3$: C, 53.14; H, 4.71; N, 12.05. Found: C, 53.20; H, 4.58; N, 12.13. ^{1}H NMR (400 MHz, CD_3OD): δ 7.49 (d, 2H, *J* = 2.0 Hz, H5), 7.45 (d, 4H, *J* = 9.2 Hz, H8), 7.43 (d, 2H, *J* = 2.0 Hz, H4), 7.34-7.31 (m, 6H, benzyl), 7.22-7.19 (m, 4H, benzyl), 6.67 (d, 4H, *J* = 9.2 Hz, H9), 5.28 (s, 4H, H6),

2.87 (s, 12H, H11). ^{13}C NMR (100 MHz, CD_3OD): δ 182.8 (2C, C2), 150.9 (2C, C10), 136.0 (2C, benzyl), 128.6 (4C, benzyl), 128.1 (2C, C7), 128.1 (2C, benzyl), 127.5 (4C, benzyl), 125.5 (4C, C8), 123.1 (2C, C5), 121.6 (2C, C4), 111.9 (4C, C9), 54.1 (2C, C6), 39.1 (4C, C11). HRMS (ES^+): calcd. for $C_{36}H_{38}AuN_6$ 751.2823; found 751.2817.

2.2.2. Complex **III-3b**

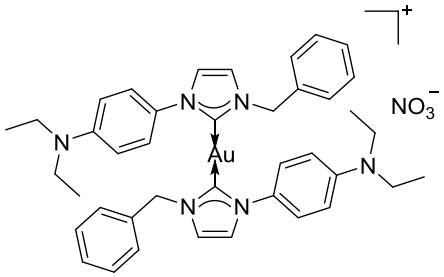

III-3b

In a Schlenk tube, **III-2b** (140 mg, 0.41 mmol) was suspended in 10 mL of dry MeOH and Ag_2O (94 mg, 0.41 mmol) was added. The mixture was stirred at room temperature for 3 h under nitrogen in the dark. A solution of $AgNO_3$ (35 mg, 0.21 mmol) in 2 mL of MeCN was added and the mixture was stirred for 10 h. Finally, $Au(SMe_2)Cl$ (60 mg, 0.21 mmol) was added and after stirring for 1 h, the mixture was filtered through a pad of celite. The solvent was evaporated under reduced pressure and the residue was purified by column chromatography on silica gel with a mixture of CH_2Cl_2 and MeOH (20:1) as eluent to give complex **III-3b** as a yellow solid (110 mg, 62% yield). Anal. Calcd. For $C_{40}H_{46}AuN_7O_3$: C, 55.23; H, 5.33; N, 11.27. Found: C, 55.16; H, 5.34; N, 11.25. ^{1}H NMR (400 MHz, CD_3OD): δ 7.48 (d, 2H, J = 2.0 Hz, H5), 7.46-7.42 (m, 6H, H4/H8), 7.34-7.30 (m, 6H, benzyl), 7.24-7.19 (m, 4H, benzyl), 6.64 (d, 4H, J = 9.2 Hz, H9), 5.27 (s, 4H, H6), 3.30 (q, 8H, J = 7.2 Hz, H11), 1.07 (t, 12H, J = 7.2 Hz, H12). ^{13}C NMR (100 MHz, CD_3OD): δ 182.7 (2C, C2), 148.1 (2C, C10), 136.0 (2C, benzyl), 128.6 (4C, benzyl), 128.1 (2C, benzyl), 127.7 (4C, benzyl), 127.2 (2C, C7), 125.7 (4C, C8), 123.0 (2C, C5), 121.5 (2C, C4), 111.2 (4C, C9), 54.1 (2C, C6), 44.0 (4C, C11), 11.3 (4C, C12). HRMS (ES^+): calcd. for $C_{40}H_{46}AuN_6$ 807.3450; found 807.3447.

2.2.3. Complex **III-3c**

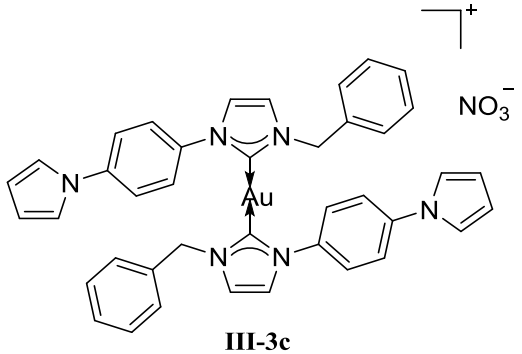

III-3c

In a Schlenk tube, **III-2c** (200 mg, 0.60 mmol) was suspended in 10 mL of dry MeOH and Ag_2O (138 mg, 0.60 mmol) was added. The mixture was stirred at room temperature for 3 h under nitrogen in the dark. A solution of $AgNO_3$ (50 mg, 0.30 mmol) in 2 mL of MeCN was added and the mixture was stirred for 10 h. Finally, $Au(SMe_2)Cl$ (88 mg, 0.30 mmol) was added and after stirring for 1 h, the mixture was filtered through a pad of celite. The solvent was evaporated under reduced pressure and the residue was purified by column chromatography on silica gel with a mixture of CH_2Cl_2 and MeOH (20:1) as eluent to give a yellow solid (150 mg, 60 % yield). Anal. Calcd. For $C_{40}H_{34}AuN_7O_3$: C, 56.01; H, 4.00; N, 11.43. Found: C, 56.12; H, 3.89; N, 11.52. ^{1}H NMR (400 MHz, CD_3CN): δ 7.70 (d, 4H, J = 8.8 Hz, H8), 7.50 (d, 2H, J = 2.0 Hz, H5), 7.45 (d, 4H, J = 8.8 Hz, H9), 7.40 (d, 2H, J = 2.0 Hz, H4), 7.32-7.28 (m, 6H, benzyl), 7.21-7.19 (m, 4H, benzyl), 7.09 (t, 4H, J = 2.4 Hz, H11), 6.34 (t, 4H, J = 2.4 Hz, H12), 5.32 (s, 4H, H6). ^{13}C NMR (100 MHz, CD_3CN): δ 182.7 (2C, C2), 140.7 (2C, C10), 136.1 (2C, benzyl), 136.0 (2C, C7), 128.9 (4C, benzyl), 128.4 (2C, benzyl), 127.5 (4C, benzyl), 126.5 (4C, C8), 123.3 (2C, C5), 122.5 (2C, C4), 120.2 (4C, C9), 119.0 (4C, C11), 111.1 (4C, C12), 54.4 (2C, C6). HRMS (ES^+): calcd. for $C_{40}H_{34}AuN_6$ 795.2510; found 795.2515.

2.2.4. Complex **III-3d**

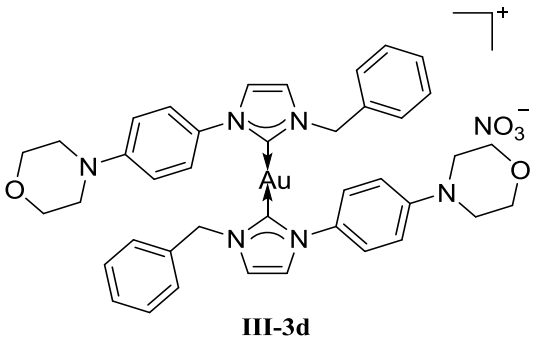

III-3d

In a Schlenk tube, **III-2d** (108 mg, 0.30 mmol) was suspended in 10 mL of dry MeOH and Ag_2O (70 mg, 0.30 mmol) was added. The mixture was stirred at room temperature for 3 h under nitrogen in the dark. A solution of $AgNO_3$ (26 mg, 0.15 mmol) in 2 mL of MeCN was added and the mixture was stirred for 10 h. Finally, $Au(SMe_2)Cl$ (45 mg, 0.30 mmol) was added and after stirring for 1 h, the mixture was filtered through a pad of celite. The solvent was evaporated under reduced pressure and the residue was purified by column chromatography on silica gel with a mixture of CH_2Cl_2 and MeOH (20:1) as eluent to give a yellow solid (70 mg, 52% yield). Anal. Calcd. For $C_{40}H_{42}AuN_7O_5$: C, 53.51; H, 4.72; N, 10.92. Found: C, 53.65; H, 4.70; N, 10.87. ^{1}H NMR (400 MHz, CD_3OD): δ 7.54-7.51 (m, 6H, H5/H8), 7.46 (d, 2H, J = 2.0 Hz, H4), 7.36-7.32 (m, 6H, benzyl), 7.23-7.20 (m, 4H, benzyl), 6.92 (d, 4H, J = 9.2 Hz, H9), 5.28 (s, 4H, H6), 3.78 (t, 8H, J = 4.8 Hz, H12), 3.03 (t, 8H, J = 4.8 Hz, H11). ^{13}C NMR (100 MHz, CD_3OD): δ 182.7 (2C, C2), 151.8 (2C, C10), 135.9 (2C, benzyl), 130.9 (2C, C7), 128.7 (4C, benzyl), 128.2 (2C, benzyl), 127.6 (4C, benzyl), 125.6 (4C, C8), 123.0 (2C, C5), 121.8 (2C, C4), 115.2 (4C, C9), 66.3 (4C, C12), 54.2 (2C, C6), 48.3 (4C, C11). HRMS (ES^+): calcd. for $C_{40}H_{42}AuN_6O_2$ 835.3035; found 835.3055.

2.2.5. Complex **III-6a**

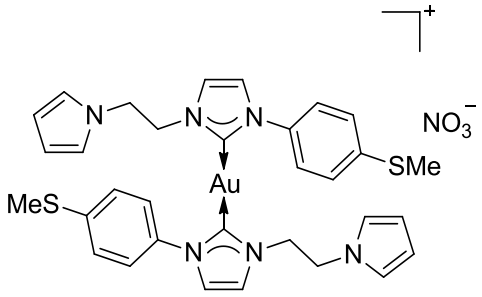

III-6a

In a Schlenk tube **III-5a** (100 mg, 0.27 mmol) was suspended in 10 mL of dry MeOH and Ag_2O (63.6 mg, 0.27 mmol) was added. The mixture was stirred at room temperature for 3 h under nitrogen in the dark. A solution of $AgNO_3$ (23.3 mg, 0.14 mmol) in 2 mL of MeCN was added and the mixture was stirred for 10 h. Finally, $Au(SMe_2)Cl$ (40.4 mg, 0.14 mmol) was added and after stirring for 1 h, the mixture

was filtered through a pad of celite. The solvent was evaporated under reduced pressure and the residue was purified on silica gel with a mixture of CH_2Cl_2 and MeOH (20:1) as eluent to give a pale-yellow solid (32 mg, 28 % yield). Anal. Calcd. For $C_{32}H_{34}AuN_7O_3S_2$: C, 46.54; H, 4.15; N, 11.87. Found: C, 46.36; H, 4.27; N, 11.97. ^{1}H NMR (400 MHz, CD_3OD): δ 7.52 (d, 2H, *J*= 2 Hz, H5), 7.43 (d, 4H, *J*= 8.4 Hz, H_{SMePh}), 7.31 (d, 4H, *J*= 8.4 Hz, H_{SMePh}), 7.26 (d, 2H, *J*= 2 Hz, H5), 6.38 (t, 4H, *J*= 2.0 Hz, H9), 5.97 (t, 4H, *J*= 2.0 Hz, H10), 4.48 (t, 4H, *J*= 5.6 Hz, H6), 4.36 (t, 2H, *J*= 5.6 Hz, H7), 2.55 (s, 6H, H_{SMePh}). ^{13}C NMR (100 MHz, CD_3OD): δ 183.1 (2C, C2), 140.9 (2C, C_{SMePh}), 135.9 (2C, C_{SMePh}), 126.1 (4C, C_{SMePh}), 125.2 (4C, C_{SMePh}), 122.6 (2C, C5), 121.8 (2C, C4), 120.3 (4C, C9), 108.4 (4C, C10), 52.3 (2C, C6), 49.3 (2C, C7), 13.9 (2C, C_{SMePh}). HRMS (ES^+): calcd. for $C_{32}H_{34}N_6S_2Au$ 763.1952; found 763.1962.

2.2.6. Complex **III-6b**

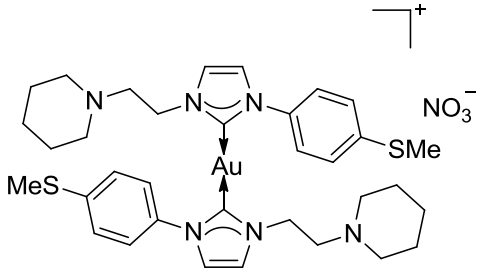

III-6b

In a Schlenk tube **III-5b** (100 mg, 0.27 mmol) was suspended in 10 mL of dry MeOH and Ag_2O (61.9 mg, 0.27 mmol) was added. The mixture was stirred at room temperature for 3 h under nitrogen in the dark. A solution of $AgNO_3$ (22.7 mg, 0.13 mmol) in 2 mL of MeCN was added and the mixture was stirred for 1 h. Finally, $Au(SMe_2)Cl$ (39.3 mg, 0.13 mmol) was added and after stirring for 1 h, the mixture was filtered through a pad of celite. The solvent was evaporated under reduced pressure to give a pale-yellow solid (90 mg, 78% yield). Anal. Calcd. For $C_{34}H_{46}AuN_7O_3S_2$: C, 47.38; H, 5.38; N, 11.38. Found: C, 47.13; H, 5.28; N, 11.50. ^{1}H NMR (400 MHz, CD_3OD): δ 7.61-7.56 (m, 8H, H5/H4/H_{SMePh}), 7.40 (d, 4H, *J*= 8.4 Hz, H_{SMePh}), 4.29 (t, 4H, *J*= 6.4 Hz, H6), 2.69 (t, 4H, *J*= 6.4 Hz, H7), 2.58 (s, 6H, H_{SMePh}), 2.34 (t, 8H, *J*= 4.8 Hz, H9), 1.54-1.49 (m, 8H, H10), 1.46-1.41 (m, 4H, H11). ^{13}C NMR (100 MHz, CD_3OD): δ 182.4 (2C, C2), 140.9 (2C, C_{SMePh}), 136.1 (2C,

C_{SMePh}), 126.3 (4C, C_{SMePh}), 125.2 (4C, C_{SMePh}), 122.5 (2C, C5), 122.3 (2C, C4), 58.9 (2C, C6), 54.2 (4C, C9), 48.1 (2C, C7), 25.4 (4C, C10), 23.7 (2C, C11), 13.9 (2C, C_{SMePh}). HRMS (ES^+): calcd. for $C_{34}H_{46}N_6S_2Au$ 799.2891; found 799.2889.

2.2.7. Complex **III-6c**

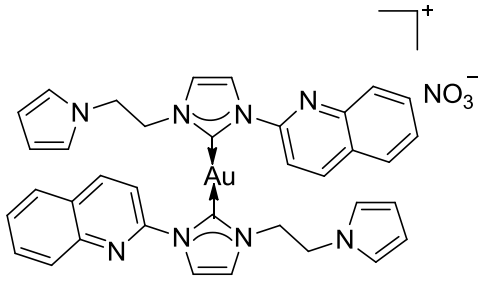

III-6c

In a Schlenk tube **III-5c** (100 mg, 0.27 mmol) was suspended in 10 mL of dry MeOH and Ag_2O (63 mg, 0.27 mmol) was added. The mixture was stirred at room temperature for 3 h under nitrogen in the dark. A solution of $AgNO_3$ (23 mg, 0.14 mmol) in 2 mL of MeCN was added and the mixture was stirred for 10 h. Finally, $Au(SMe_2)Cl$ (40 mg, 0.14 mmol) was added and after stirring for 1 h, the mixture was filtered through a pad of celite. The solvent was evaporated under reduced pressure and the residue was purified on silica gel with a mixture of CH_2Cl_2 and MeOH (20:1) as eluent to give a pale-yellow solid (55 mg, 51% yield). Anal. Calcd. For $C_{36}H_{32}AuN_9O_3$: C, 51.74; H, 3.86; N, 15.09. Found: C, 51.95; H, 3.60; N, 15.18. ^{1}H NMR (400 MHz, CD_3OD): δ 8.03-8.01 (m, 4H, H5/H8), 7.92 (d, 2H, *J*= 8.8 Hz, H7), 7.85 (d, 2H, *J*= 8.4 Hz, H10), 7.74-7.67 (m, 4H, H13/H12), 7.53 (ddd, 2H, *J*= 8.4, 7.2, 1.6 Hz, H11), 7.40 (d, 2H, *J*= 2 Hz, H4), 6.48 (t, 2H, *J*= 2 Hz, H19), 5.91 (t, 2H, *J*= 2 Hz, H20), 4.71 (t, 4H, *J*= 5.6 Hz, H16), 4.49 (t, 4H, *J*= 5.6 Hz, H17). ^{13}C NMR (100 MHz, CD_3OD): δ 183.0 (2C, C2), 149.2 (2C, C6), 146.1 (2C, C14), 139.1 (2C, C8), 130.8 (2C, C12), 128.0 (2C, C13), 127.6 (2C, C10), 127.5 (2C, C9), 127.3 (2C, C11), 122.1 (2C, C5), 121.3 (2C, C4), 120.3 (4C, C19), 115.6 (2C, C7), 108.5 (4C, C20), 53.3 (2C, C17), 49.3 (2C, C18). HRMS (ES^+): calcd. for $C_{36}H_{32}N_8Au$ 773.2415; found 773.2417.

2.2.8. Complex **III-6d**

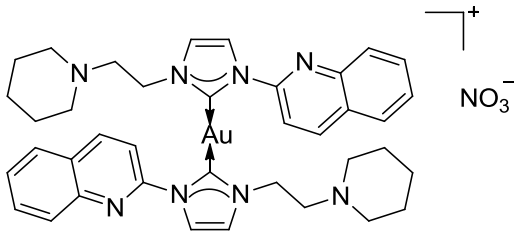

III-6d

In a Schlenk tube **III-5d** (100 mg, 0.26 mmol) was suspended in 10 mL of dry MeOH and Ag_2O (61 mg, 0.26 mmol) was added. The mixture was stirred at room temperature for 3 h under nitrogen in the dark. A solution of $AgNO_3$ (22.4 mg, 0.13 mmol) in 2 mL of MeCN was added and the mixture was stirred for 1 h. Finally, $Au(SMe_2)Cl$ (38.8 mg, 0.13 mmol) was added and after stirring for 1 h, the mixture was filtered through a pad of celite. The solvent was evaporated under reduced pressure to give a pale-yellow solid (88 mg, 77% yield). Anal. Calcd. For $C_{38}H_{44}AuN_9O_3$: C, 52.35; H, 5.09; N, 14.46. Found: C, 52.54; H, 4.97; N, 14.34. ^{1}H NMR (400 MHz, CD_3OD): δ 8.35 (d, 2H, *J*= 8.8 Hz, H8), 8.17 (d, 2H, *J*= 8.8 Hz, H7), 8.08 (d, 2H, *J*= 2 Hz, H5), 7.94-7.88 (m, 4H, H10/H13), 7.76 (ddd, 2H, *J*= 8.4, 7.2, 1.6 Hz, H12), 7.69 (d, 2H, *J*= 2 Hz, H4), 7.61 (ddd, 2H, *J*= 8.4, 7.2, 1.2 Hz, H11), 4.45 (t, 4H, *J*= 6.8 Hz, H16), 2.74 (t, 4H, *J*= 6.8 Hz, H17), 2.26 (t, 8H, *J*= 4.8 Hz, H19), 1.44-1.38 (m, 8H, H20), 1.32-1.28 (m, 4H, H21). ^{13}C NMR (100 MHz, CD_3OD): δ 182.4 (2C, C2), 149.4 (2C, C6), 146.3 (2C, C14), 139.7 (2C, C8), 130.9 (2C, C12), 128.2 (2C, C13), 127.8 (2C, C10), 127.7 (2C, C9), 127.4 (2C, C11), 122.9 (2C, C5), 120.9 (2C, C4), 115.6 (2C, C7), 58.8 (2C, C17), 54.1 (4C, C19), 49.0 (2C, C18), 25.3 (4C, C20), 23.6 (2C, C21). HRMS (ES^+): calcd. for $C_{38}H_{44}N_8Au$ 809.3354; found 809.3338.

3. Neutral gold(I) mono(NHC) complexes

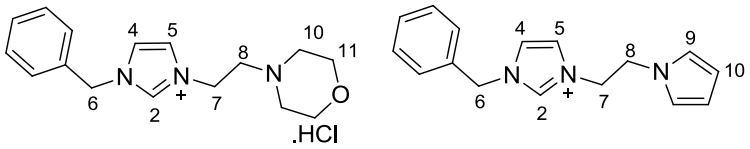

Fig 3.1 General numbering for NMR attribution.

3.1. Complex **V-2e**

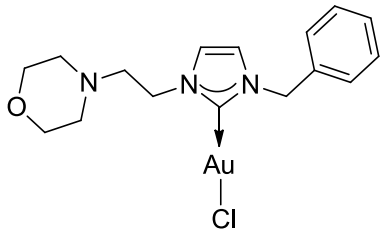

V-2e

Under nitrogen and in the dark, a Schlenk tube was charged with **II-2c** (100 mg, 0.29 mmol) in 6 mL of MeCN and Ag_2O (67.3 mg, 0.29 mmol). The reaction mixture was stirred at 40 ℃ for 24 h. After that, $Au(SMe_2)Cl$ (102.5 mg, 0.348 mmol) was added and the mixture was stirred for 4 h. The solution was filtered through a pad of celite and the solvent was removed under reduced pressure to give a pale-yellow solid (140 mg, 90% yield). Anal. Calcd. For $C_{16}H_{21}AuClN_3O$: C, 38.15; H, 4.20; N, 8.34. Found: C, 38.21; H, 4.26; N, 8.28. ^{1}H NMR (400 MHz, CD_3CN): δ 7.43-7.35 (m, 5H, benzyl), 7.26 (s, 1H, H5), 7.18 (s, 1H, H4), 5.39 (s, 2H, H6), 4.31 (t, 2H, *J*= 5.6 Hz, H7), 3.63 (t, 4H, *J*= 4 Hz, H11), 2.84 (s, 2H, H8), 2.57 (t, 4H, *J*= 4 Hz, H10). ^{13}C NMR (100 MHz, CD_3CN): δ 170.5 (1C, C2), 136.7 (1C, Bn), 128.8 (2C, Bn), 128.2 (1C, Bn), 127.6 (2C, Bn), 122.1 (1C, C5), 121.1 (1C, C4), 66.2 (2C, C11), 58.1 (1C, C6), 54.3 (1C, C7), 53.4 (2C, C10), 47.8 (1C, C8). HRMS (ES^+): calcd. for $C_{16}H_{21}AuN_3O$ 468.1350; found 468.1351.

3.2. Complex **V-2f**

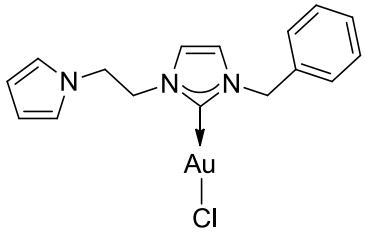

V-2f

Under nitrogen and in the dark, a Schlenk tube was charged with **II-2b** (100 mg, 0.30 mmol) in 6 mL of MeCN and Ag_2O (69.7 mg, 0.30 mmol). The reaction mixture was stirred at 40 ℃ for 24 h. After that, $Au(SMe_2)Cl$ (106.4 mg, 0.36 mmol) was added and the mixture was stirred for 4 h. The solution was filtered through a pad of celite and the solvent was removed under reduced pressure to give a grey solid (105 mg, 72% yield). Anal. Calcd. For $C_{16}H_{17}AuClN_3$: C, 39.73; H, 3.54; N, 8.69. Found: C, 39.81; H, 3.56; N, 8.58. ^{1}H NMR (400 MHz, CD_3CN): δ 7.41-7.36 (m, 3H, benzyl), 7.29-7.27 (m, 2H, benzyl), 7.06 (s, 1H, H5), 6.79 (s, 1H, H4), 6.53 (t, 2H, *J*= 2 Hz, H10), 6.02 (t, 2H, *J*= 2 Hz, H11), 5.33 (s, 4H, H6), 4.49 (t, 2H, *J*= 6 Hz, H7), 4.35 (t, 2H, *J*= 6 Hz, H8). ^{13}C NMR (100 MHz, CD_3CN): δ 170.7 (1C, C2), 136.5 (1C, benzyl), 128.8 (2C, benzyl), 128.2 (1C, benzyl), 127.5 (2C, benzyl), 121.6 (1C, C5), 120.6 (1C, C4), 117.3 (2C, C10), 108.5 (2C, C11), 54.3 (1C, C6), 52.2 (1C, C7), 49.3 (1C, C8). HRMS (ES^+): calcd. for $C_{16}H_{17}AuN_3$ 448.1088; found 448.1097.

4. Iridium(III) NHC complexes

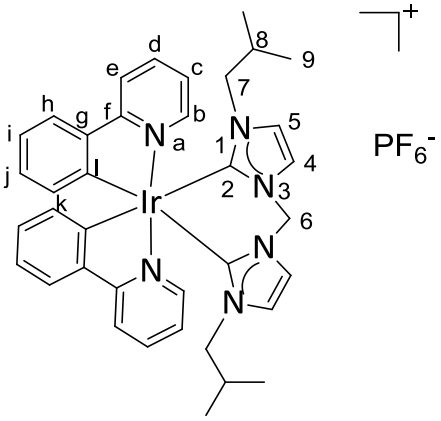

Fig 4.1 General numbering for NMR attribution.

4.1. Preparation of imidazolium salts

4.1.1. 1,1'-Methylenebis(3-isopropyl-1*H*-imidazol-3-ium) bromide (**VI-3a**)

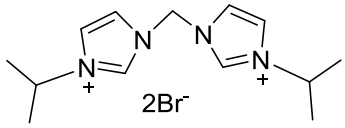

VI-3a

A three-necked flask was charged with a mixture of imidazole (1.36 g, 20 mmol), tetrabutylammonium bromide (193 mg, 0.6 mmol), and powdered potassium hydroxide (2.24 g, 40 mmol) and stirred for 1 h at room temperature. To the resulting liquid was slowly added dibromomethane (0.7 mL, 10 mmol). After 5 hours, a solid was obtained. Purification of the crude product was performed by sublimation at 180 ^{o}C to yield a white product (885 mg, 60 % yield). ^{1}H NMR (400 MHz, $CDCl_3$): δ 7.67 (s, 2H, H_2), 7.14 (s, 2H, H_5), 7.14 (s, 2H, H_4), 6.02 (s, 2H, H_6). 1,1'-Methylene bis(1*H*-imidazole) (50 mg, 0.34 mmol) was dissolved in 2 mL of 2-bromopropane, and the reaction mixture was refluxed for 48 h. After cooling down to room temperature, the precipitate formed was filtered, washed with Et_2O and dried under vacuum to obtain a white solid (50 mg, 38% yield). Anal. Calcd. For $C_{13}H_{22}Br_2N_4$: C, 39.61; H, 5.63; N, 14.21. Found: C, 39.45; H, 5.54; N, 14.05. ^{1}H NMR (400 MHz, DMSO-d_6): δ 9.68 (s, 2H, H_2), 8.12 (s, 2H, H_5), 8.06 (s, 2H, H_4), 6.67 (s, 2H, H_6), 4.74-4.68 (m, 2H, H_7), 1.51 (d, 12H, J= 6.4 Hz, H_8). ^{13}C NMR (100 MHz, DMSO-d_6): δ 137.0 (2C, C_2), 122.9 (2C, C_5), 121.8 (2C, C_4), 58.5 (1C, C_6), 53.3 (2C, C_7), 22.6

(4C, C_8). MS (ES^+): calcd. for $C_{13}H_{22}BrN_4$ 313.10; found m/z = 312.92 $[M\text{-}Br^-]^+$. Calcd. for $C_{13}H_{21}N_4$ 233.18; found 233.17 $[M\text{-}2Br^-\text{-}H^+]^+$.

4.1.2. 1,1'-Methylenebis(3-isobutyl-1*H*-imidazol-3-ium) bromide (**VI-3b**)

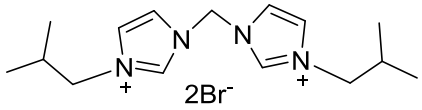

VI-3b

1,1'-Methylene bis(1*H*-imidazole) (100 mg, 0.67 mmol) was dissolved in 2 mL of 1-bromo-2-methylpropane, and the reaction mixture was refluxed for 48 h. After cooling down to room temperature, the precipitate formed was filtered, washed with Et_2O and dried under vacuum to obtain a white solid (195 mg, 69% yield). Anal. Calcd. For $C_{15}H_{26}Br_2N_4$: C, 42.67; H, 6.21; N, 13.27. Found: C, 42.64; H, 6.13; N, 13.10. ^{1}H NMR (400 MHz, DMSO-d_6): δ 9.62 (s, 2H, H_2), 8.11 (s, 2H, H_5), 7.90 (s, 2H, H_4), 6.74 (s, 2H, H_6), 4.09 (d, 4H, J= 7.2 Hz, H_7), 2.16-2.07 (m, 2H, H_8), 0.89 (d, 12H, J= 6.4 Hz, H_9) ^{13}C NMR (100 MHz, DMSO-d_6): δ 138.1 (2C, C_2), 124.0 (2C, C_5), 122.7 (2C, C_4), 58.7 (1C, C_6), 56.4 (2C, C_7), 29.0 (2C, C_8), 19.6 (4C, C_9). MS (ES^+): calcd. for $C_{15}H_{26}BrN_4$ 341.13; found 341.25 $[M\text{-}Br^-]^+$. Calcd. for $C_{15}H_{25}N_4$ 261.21; found 261.25 $[M\text{-}2Br^-\text{-}H^+]^+$.

4.1.3. 1,1'-Methylenebis(3-benzyl-1*H*-imidazol-3-ium) chloride (**VI-3c**)

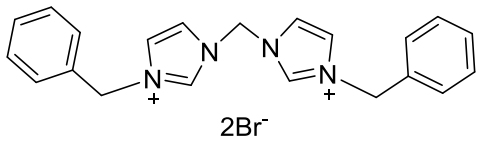

VI-3c

A mixture of 1,1'-methylene bis(1*H*-imidazole) (100 mg, 0.67 mmol) and benzyl chloride (188 mg, 1.48 mmol) was refluxed in 5 ml of MeCN for 10 h. After cooling to room temperature, the precipitate formed was filtered, washed with Et_2O and dried under vacuum to obtain a pale-yellow solid (190 mg, 71% yield). Anal. Calcd. For $C_{21}H_{22}Cl_2N_4$: C, 62.85; H, 5.53; N, 13.96. Found: C, 62.56; H, 5.34; N, 13.72. ^{1}H NMR (400 MHz, DMSO-d_6): δ 9.98 (s, 2H, H_2), 8.26 (s, 2H, H_5), 7.92 (s, 2H, H_4), 7.52-7.34 (m, 10H, benzyl), 6.83 (s, 2H, H_6), 5.51 (s, 4H, H_7). ^{13}C NMR (100 MHz,

DMSO-d_6): δ 138.4 (2C, C_2), 134.7 (2C, benzyl), 129.5 (4C, benzyl), 129.4 (2C, benzyl), 129.0 (4C, benzyl), 123.5 (2C, C_5), 123.1 (2C, C_4), 58.5 (1C, C_6), 52.7 (2C, C_7). MS (ES^+): calcd. for $C_{21}H_{21}N_4$ 329.18; found 329.42 $[M\text{-}2Br^-\text{-}H^+]^+$.

4.1.4. 1,1'-Methylenebis(3-(2-(piperidin-1-yl)ethyl)-1*H*-imidazol-3-ium) chloride hydrochloride (**VI-3d**)

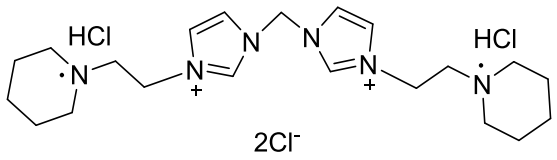

VI-3d

A mixture of 1,1'-methylene bis(1*H*-imidazole) (50 mg, 0.34 mmol) and 1-(2-chloroethyl)piperidine hydrochloride (136.7 mg, 0.74 mmol) was refluxed in 5 ml of toluene for 24 h. After cooling to room temperature, the solvent was evaporated and MeCN was used to make the precipitation. Then the desired solid was filtered off and dried under vaccum to give a yellow solid (60 mg, 34% yield). Anal. Calcd. For $C_{21}H_{38}Cl_4N_6$: C, 48.85; H, 7.42; N, 16.28. Found: C, 48.55; H, 7.34; N, 16.05. ^{1}H NMR (400 MHz, DMSO-d_6): δ 11.03 (s, 2H, HCl), 9.84 (s, 2H, H_2), 8.19 (s, 2H, H_5), 7.95 (s, 2H, H_4), 6.79 (s, 2H, H_6), 4.77 (t, 4H, J= 6 Hz, H_7), 3.63-3.47 (m,8H, H_{10}), 2.97-2.87 (m, 4H, H_8), 1.86-1.66 (m, 12H, H_{11}/H_{12}). ^{13}C NMR (100 MHz, DMSO-d_6): δ 139.4 (2C, C_2), 123.3 (2C, C_5), 123.0 (2C, C_4), 58.6 (1C, C_6), 54.7 (2C, C_7), 52.7 (4C, C_{10}), 43.7 (2C, C_8), 22.3 (4C, C_{11}), 21.7 (2C, C_{12}). MS (ES^+): calcd. for $C_{21}H_{36}ClN_6$ 407.27; found 407.17 $[M\text{-}Cl^-\text{-}2HCl]^+$. Calcd. for $C_{21}H_{35}N_6$ 371.55; found 371.42 $[M\text{-}2Cl^-\text{-}2HCl\text{-}H^+]^+$.

4.1.5. 1,1'-Methylenebis(3-(4-(methylthio)phenyl)-1*H*-imidazol-3-ium) bromide (**VI-3e**)

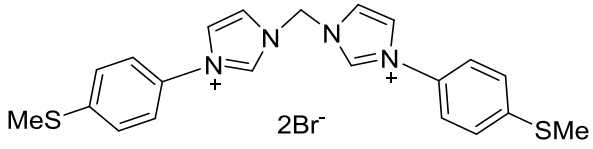

VI-3e

Imidazole (3.24 g, 47.6 mmol), 4-bromothioanisole (4.83 g, 23.8 mmol), K_2CO_3 (3.29 g, 23.8 mmol) and a catalytic amount of $CuSO_4$ were stirred in a closed pressure flask at 205 ℃ for 10 h. After cooling to room temperature, the crude product was extracted by CH_2Cl_2, filtered and evaporated to dryness. The resulting residue was washed three times with Et_2O (20 mL) to give 1-(4-methylthiophenyl)-1*H*-imidazole as a grey solid (3.6 g, 80% yield). ^{1}H NMR (400 MHz, $CDCl_3$): δ 7.84 (t, 1H, *J*= 1.2 Hz, H2), 7.38-7.32 (m, 4H, H_{SMePh}), 7.27 (t, 1H, *J*= 1.2 Hz, H5), 7.22 (t, 1H, *J*= 1.2 Hz, H4), 2.54 (s, 3H, H_{SMePh}). 1-(4-(methylthiophenyl)-1*H*-imidazole (200 mg, 1.05 mmol) was dissolved in 2 mL of dibromomethane, and the reaction mixture was refluxed for 10 h. After cooling down, the precipitate formed was filtered, washed with Et_2O and dried under vacuum to obtain a white solid (255 mg, 44% yield). Anal. Calcd. For $C_{21}H_{22}Br_2N_4S_2$: C, 45.50; H, 4.00; N, 10.11. Found: C, 45.29; H, 3.93; N, 10.50. ^{1}H NMR (400 MHz, DMSO-d_6): δ 10.31 (s, 2H, H_2), 8.42 (s, 2H, H_5), 8.38 (s, 2H, H_4), 7.76 (d, 4H, *J*= 8.8 Hz, H_{SMePh}), 7.56 (d, 4H, *J*= 8.8 Hz, H_{SMePh}), 6.90 (s, 2H, H_6), 2.56 (s, 6H, H_{SMePh}). ^{13}C NMR (100 MHz, DMSO-d_6): δ 141.9 (2C, C_{SMePh}), 137.6 (2C, C_2), 131.6 (2C, C_{SMePh}), 127.2 (4C, C_{SMePh}), 123.4 (2C, C_5), 122.9 (4C, C_{SMePh}), 122.1 (2C, C_4), 58.9 (1C, C_6), 14.9 (2C, C_{SMePh}). MS (ES^+): calcd. for $C_{21}H_{22}BrN_4S_2$ 473.05; found 473.25 $[M\text{-}Br^-]^+$. Calcd. for $C_{21}H_{21}N_4S_2$ 393.12; found 393.33 $[M\text{-}2Br\text{-}H^+]^+$.

4.1.6. 1-Benzyl-3-[3-(3-benzyl-1*H*-imidazol-3-ium-1-yl)propyl]-1*H*-imidazol-3-ium dibromide (**VI-3f**)

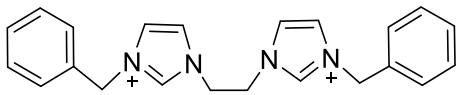

VI-3f

A mixture of imidazole (6.201 g, 91 mmol), K_2CO_3 (15.420 g, 112 mmol) in 60 mL of DMF was strirred for 20 min, then benzyl chloride (12.6 mL, 109 mmol) was slowly added to the solution. The reaction mixture was stirred at 50 ℃ for 2 h. After cooling to room temperature, water (100 mL) was added. The aqueous layer was extracted twice with EtOAc (100 mL) and the combined organic layers were washed with water and brine and dried over Na_2SO_4. The solvent was evaporated to give 1-benzyl-1*H*-imidazole as a beige solid (7.910 g, 55% yield). ^{1}H NMR (400 MHz,

CD_3Cl): δ 7.57 (s, 1H, H_2), 7.40 – 7.33 (m, 3H, H_{Bn}), 7.17 (ddd, J = 7.2, 1.6, 0.8 Hz, 2H, H_{Bn}), 7.11 (dd, J = 1.3, 1.3 Hz, 1H, H_5), 6.92 (dd, J = 1.3, 1.3 Hz, 1H, H_4), 5.14 (s, 2H, H_7). A mixture of 1-benzyl-1*H*-imidazole (105 mg, 0.64 mmol) and 1,2-dibromoethane (63.6 mg, 0.34 mmol) in 5 ml of toluene was stirred under reflux for 24 h. After cooling to room temperature, the solvent was evaporated, the crude was washed with Et_2O, filtered and dried under vacuum to obtain a beige solid (1.027 g, 90% yield). ^{1}H NMR (400 MHz, DMSO-d_6): δ 9.32 (s, 2H, H_2), 7.83 (dd, J = 1.8, 1.8 Hz, 2H, H_5), 7.72 (dd, J = 1.8, 1.8 Hz, 2H, H_4), 7.48 – 7.36 (m, 10H, H_{Bn}), 5.44 (s, 4H, H_6), 4.75 (s, 4H, H_7). ^{13}C NMR (100 MHz, DMSO-d_6): δ 137.2 (2C, C_2), 135.0 (2C, C_{Bn}), 129.5 (4C, C_{Bn}), 129.3 (2C, C_{Bn}), 128.8 (4C, C_{Bn}), 123.4 (2C, C_5), 123.3 (2C, C_4), 52.5 (2C, C_6), 48.9 (2C, C_7). MS (ES^+): calcd. for $C_{22}H_{24}BrN_4$ 423.12; found 423.42 $[M\text{-}Br^-]^+$. Calcd. for $C_{22}H_{23}N_4$ 343.46; found 343.75 $[M\text{-}2Br^-\text{-}H^+]^+$.

4.1.7. 3,3'-(Ethane-1,2-diyl)bis[1-(2-methylpropyl)-1*H*-imidazol-3ium] dihexafluorophosphate (**VI-3g**)

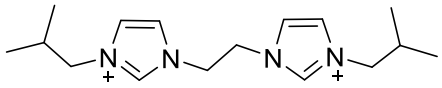

$2PF_6^-$

VI-3g

A mixture of imidazole (500 mg, 7.3 mmol) and potassium hydroxyde (618.4 mg, 11 mmol) was dissolved in 5 ml of DMSO and stirred for 30 min at 19 ℃. Then isobutyl bromide (100.8 mg, 0.7 mmol) was slowly added at 0 ℃. After 2 h stirring at room temperature, the mixture was diluted with water and EtOAc. The organic layer was washed with brine and dried over Na_2SO_4. The solvent was evaporated to give 1-(2-methylpropyl)-1*H*-imidazole as a white solid (547 mg, 60% yield). ^{1}H NMR (400 MHz, $CDCl_3$): δ 7.46 (s, 1H, H_2), 7.09 – 7.05 (dd, J = 1.3, 1.3 Hz, 1H, H_5), 6.89 (dd, J = 1.3, 1.3 Hz, 1H, H_4), 3.74 (d, J = 7.2 Hz, 2H, H_7), 2.04 (dt, J = 13.4, 6.7 Hz, 1H, H_8), 0.93 (d, J = 6.7 Hz, 6H, H_9). A mixture of 1-(2-methylpropyl)-1*H*-imidazole (123.5 mg, 1 mmol) and 1,2-dibromoethane (93.4 mg, 0.5mmol) in 5 ml of toluene was stirred in a closed pressure flask at 110 ℃ for 72 h. After cooling to room temperature, the solvent was evaporated and the crude was dissolved in 10 mL of MeCN. The mixture was filtered and the solvent was removed. The solid was washed with a mixture of MeCN and Et_2O (1:5) and dried under vaccum to afford a white solid. (170

mg, 60% yield). ^{1}H NMR (400 MHz, DMSO-d_6): δ 9.06 (s, 2H, H_2), 7.80 (s, 2H, H_5), 7.70 (s, 2H, H_4), 4.71 (s, 4H, H_6), 3.98 (d, J = 7.1 Hz, 4H, H_7), 2.04 (dt, J = 13.6, 6.8 Hz, 2H, H_8), 0.83 (d, J = 6.6 Hz, 12H, H_9). ^{13}C NMR (100 MHz, DMSO-d_6): δ 137.1 (2C, C_2), 123.8 (2C, C_5), 123.0 (2C, C_4), 56.1 (2C, C_6), 48.9 (2C, C_7), 29.1 (2C, C_8), 19.5 (4C, C_9). MS (ES^+): calcd. for $C_{16}H_{28}F_6N_4P$ 421.20; found 421.17 $[M\text{-}PF_6^-]^+$. Calcd. for $C_{16}H_{27}N_4$; found 275.17 $[M\text{-}2PF_6^-\text{-}H^+]^+$.

4.1.8. 3-Mesityl-1-(quinolin-2-yl)-1*H*-imidazol-3-ium chloride (**VI-3h**)

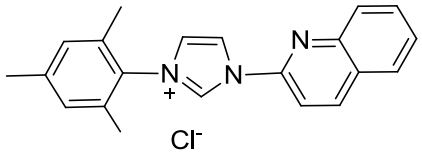

VI-3h

This compound was prepared according to the literature procedure.[113a] ^{1}H NMR (400 MHz, $CDCl_3$): δ 12.15 (s, 1H, H_2), 9.43 (d, J = 8.8 Hz, 1H, H_8), 9.07 (d, J = 1.7 Hz, 1H, H_5), 8.59 (d, J = 8.8 Hz, 1H, H_7), 8.08 (d, J = 8.4 Hz, 1H, H_{13}), 7.97 (d, J = 8.2 Hz, 1H, H_{10}), 7.88 – 7.79 (m, 1H, H_{12}), 7.70 – 7.64 (m, 1H, H_{11}), 7.38 (d, J = 1.7 Hz, 1H, H_4), 7.07 (s, 2H, H_{Mes}), 2.37 (s, 3H, CH_3), 2.24 (s, 6H, CH_3). ^{13}C NMR (100 MHz, $CDCl_3$): δ 146.0 (1C, C_6), 144.9 (1C, C_{14}), 141.8 (1C, C_8), 141.5 (1C, C_{Mes}), 138.0 (1C, C_2), 134.0 (2C, C_{Mes}), 131.3 (1C, C_{12}), 130.7 (2C, C_{Mes}), 130.1 (2C,C_{Mes}), 128.7 (1C, C_{13}), 128.6 (1C, C_9), 128.2 (1C, C_{10}), 128.1 (1C, C_{11}), 123.7 (1C, C_7), 119.8 (1C, C_5), 114.1 (1C, C_4), 21.2 (1C, C_{Mes}), 17.9 (2C, C_{Mes}).

4.2. Synthesis of iridium(III) complexes

The precursor of iridium complex ($[IrCl(ppy)_2]_2$) was prepared according to the literature procedure.[86]

4.2.1. Complex **VI-4a**

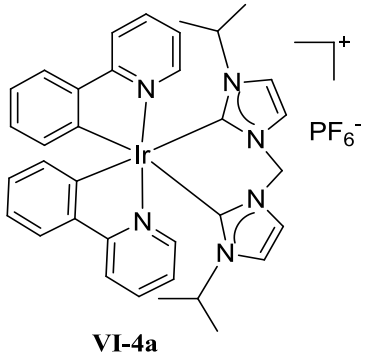

VI-4a

A mixture of **VI-2a** (35 mg, 0.09 mmol), silver oxide (20.6 mg, 0.09 mmol) and $[IrCl(ppy)_2]_2$ (43 mg, 0.04 mmol) in 10 mL of MeCN was refluxed for 10 h. After cooling down to room temperature, an aqueous solution of NH_4PF_6 (200 mg in 10 mL deionized water) was slowly added into the reaction mixture under stirring, resulting in a yellow suspension. The suspension was then filtered and the resulting precipitate was washed with deionized water and dried under vacuum at 70 ^oC for 12 h. The crude product was purified by column chromatography on silica gel with CH_2Cl_2/MeOH (20:1) as the eluent, yielding a yellow solid (40 mg, 57% yield). Anal. Calcd. For $C_{35}H_{36}F_6IrN_6P$: C, 47.89; H, 4.13; N, 9.57. Found: C, 47.45; H, 4.04; N, 9.79. ^1H NMR (400 MHz, CD_3CN): δ 8.33 (d, 2H, J= 5.6 Hz, H_b), 8.09 (d, 2H, J= 7.6 Hz, H_e), 7.91 (ddd, 2H, J= 7.6, 7.6, 1.2 Hz, H_d), 7.74 (d, 2H, J= 7.6 Hz, H_k), 7.37 (d, 2H, J= 2.4 Hz, H_5), 7.13-7.09 (m, 4H, H_c/H_4), 6.89 (ddd, 2H, J= 7.6, 7.6, 1.2 Hz, H_j), 6.79 (ddd, 2H, J= 7.6, 7.6, 1.2 Hz, H_i), 6.30 (d, 2H, J= 7.6 Hz, H_h), 5.98 (s, 2H, H_6), 4.16-4.10 (m, 2H, H_7), 1.02 (d, 6H, J= 6.4 Hz, H_8), 0.27 (d, 6H, J= 6.4 Hz, $H_{8'}$). ^{13}C NMR (100 MHz, $CDCl_3$): δ 169.7 (2C, C_f), 162.7 (2C, C_2), 162.2 (2C, C_l), 153.0 (2C, C_b), 143.9 (2C, C_g), 136.7 (2C, C_d), 131.0 (2C, C_h), 129.6 (2C, C_i), 124.4 (2C, C_5), 123.9 (2C, C_k), 121.9 (2C, C_c), 121.4 (2C, C_4), 119.8 (2C, C_e), 116.6 (2C, C_j), 61.5 (1C, C_6), 49.9 (2C, C_7), 22.7 (2C, C_8), 22.6 (2C, $C_{8'}$). HRMS (ES^+): calcd. for $C_{35}H_{36}N_6Ir$ 731.2607; found 731.2606 $[M\text{-}PF_6^-]^+$.

4.2.2. Complex **VI-4b**

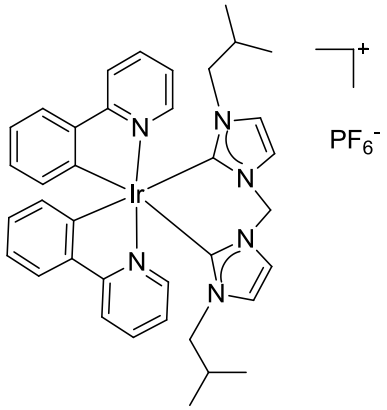

VI-4b

A mixture of **VI-3b** (43.3 mg, 0.10 mmol), silver oxide (23.8 mg, 0.10 mmol) and $[IrCl(ppy)_2]_2$ (50 mg, 0.05 mmol) in 10 mL of MeCN was reluxed for 10 h. After cooling down to room temperature, an aqueous solution of NH_4PF_6 (200 mg in 10 mL deionized water) was slowly added into the reaction mixture under stirring, resulting in a yellow suspension. The suspension was then filtered and the resulting precipitate was washed with deionized water and dried under vacuum at 70 ^oC for 12 h. The crude product was purified by column chromatography on silica gel with CH_2Cl_2/MeOH (30:1) as the eluent, yielding a yellow solid (40 mg, 47% yield). Anal. Calcd. For $C_{37}H_{40}F_6IrN_6P$: C, 49.05; H, 4.45; N, 9.28. Found: C, 49.50; H, 4.14; N, 9.33. ^1H NMR (400 MHz, $CDCl_3$): δ 8.13 (d, 2H, *J*= 6.0 Hz, H_b), 7.95 (d, 2H, *J*= 8.0 Hz, H_e), 7.81 (dd, 2H, *J*= 7.2, 7.2 Hz, H_d), 7.65-7.58 (m, 4H, H_k/H_5), 7.05 (dd, 2H, *J*= 7.2, 7.2 Hz, H_c), 6.89 (dd, 2H, *J*= 7.2, 7.2 Hz, H_j), 6.84 (s, 2H, H_4), 6.78 (dd, 2H, *J*= 7.2, 7.2 Hz, H_i), 6.24 (d, 2H, *J*= 8.0 Hz, H_h), 6.20 (s, 2H, H_6), 3.31 (dd, 2H, *J*= 8.0, 5.2 Hz, H_7), 3.07 (dd, 2H, *J*= 8.0, 5.2 Hz, $H_{7'}$), 1.25-1.20 (m, 2H, H_8), 0.47 (d, 6H, *J*= 6.4 Hz, H_9), 0.12 (d, 6H, *J*= 6.4 Hz, $H_{9'}$). ^{13}C NMR (100 MHz, $CDCl_3$): δ 169.7 (2C, C_f), 163.6 (2C, C_2), 162.8 (2C, C_l), 152.7 (2C, C_b), 143.9 (2C, C_g), 136.7 (2C, C_d), 131.4 (2C, C_h), 129.7 (2C, C_i), 124.6 (2C, C_5), 123.5 (2C, C_k), 122.2 (2C, C_c), 121.5 (2C, C_4), 120.4 (2C, C_e), 119.8 (2C, C_j), 61.5 (1C, C_6), 54.9 (2C, C_7), 28.3 (2C, C_8), 19.1 (2C, C_9), 18.5 (2C, $C_{9'}$). HRMS (ES^+): calcd. for $C_{37}H_{40}N_6Ir$ 759.2920; found 759.2913 $[M\text{-}PF_6^-]^+$.

4.2.3. Complex **VI-4c**

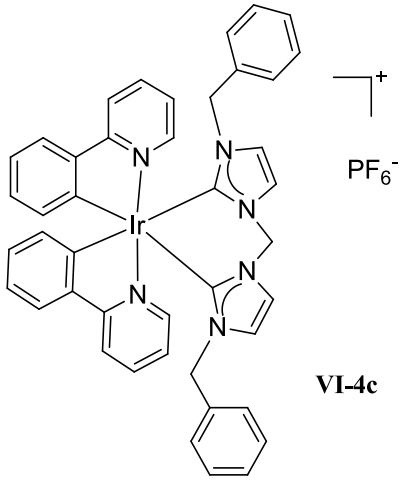

VI-4c

A mixture of **VI-3c** (41.2 mg, 0.10 mmol), silver oxide (23.8 mg, 0.10 mmol) and $[IrCl(ppy)_2]_2$ (50 mg, 0.05 mmol) in 10 mL of MeCN was reluxed for 10 h. After cooling down to room temperature, an aqueous solution of NH_4PF_6 (200 mg in 10 mL deionized water) was slowly added into the reaction mixture under stirring, resulting in a yellow suspension. The suspension was then filtered and the resulting precipitate was washed with deionized water and dried under vacuum at 70 ^oC for 12 h. The crude product was purified by column chromatography on silica gel with CH_2Cl_2/MeOH (20:1) as the eluent, yielding a yellow solid (55 mg, 60% yield). Anal. Calcd. For $C_{43}H_{36}F_6IrN_6P$: C, 53.03; H, 3.73; N, 8.63. Found: C, 53.01; H, 3.49; N, 8.15. ^1H NMR (400 MHz, $CDCl_3$): δ 8.25 (d, 2H, *J*= 5.6 Hz, H_b), 7.68 (d, 2H, *J*= 7.6 Hz, H_e), 7.64-7.58 (m, 4H, H_5/H_d), 7.52 (d, 2H, *J*= 7.6 Hz, H_k), 7.15-7.04 (m, 6H, benzyl), 6.98 (ddd, 2H, *J*= 6.0, 6.0, 1.6 Hz, H_c), 6.79 (ddd, 2H, *J*= 7.2, 7.2, 1.2 Hz, H_j), 6.71 (d, 2H, *J*= 2.0 Hz, H_4), 6.67 (ddd, 2H, *J*= 7.2, 7.2, 1.2 Hz, H_i), 6.34 (d, 4H, *J*= 7.2 Hz, benzyl), 6.30 (s, 2H, H_6), 6.23 (d, 2H, *J*= 7.6 Hz, H_h), 4.81 (d, 2H, *J*= 15.6 Hz, H_7), 4.49 (d, 2H, *J*= 15.6 Hz, $H_{7'}$). ^{13}C NMR (100 MHz, $CDCl_3$): δ 169.3 (2C, C_f), 164.3 (2C, C_2), 161.8 (2C, C_l), 152.4 (2C, C_b), 143.9 (2C, C_g), 136.6 (2C, C_d), 135.9 (2C, benzyl), 131.2 (2C, C_h), 129.6 (2C, C_i), 128.3 (4C, benzyl), 127.3 (2C, benzyl), 126.2 (4C, benzyl), 124.5 (2C, C_5), 124.0 (2C, C_k), 122.2 (2C, C_c), 121.6 (2C, C_4), 121.4 (2C, C_e), 119.8 (2C, C_j), 61.7 (1C, C_6), 52.2 (2C, C_7). HRMS (ES^+): calcd. for $C_{43}H_{36}N_6Ir$ 827.2607; found 827.2606 $[M\text{-}PF_6^-]^+$.

4.2.4. Complex **VI-4d**

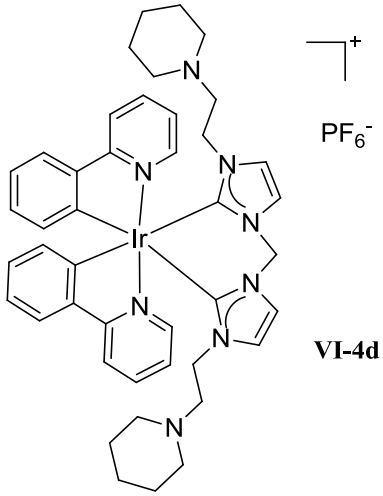

A mixture of **VI-3d** (43 mg, 0.08 mmol), silver oxide (19.3 mg, 0.08 mmol) and $[IrCl(ppy)_2]_2$ (40.6 mg, 0.04 mmol) in 10 mL of MeCN was reluxed for 10 h. After cooling down to room temperature, an aqueous solution of NH_4PF_6 (200 mg in 10 mL deionized water) was slowly added into the reaction mixture under stirring, resulting in a yellow suspension. The suspension was then filtered and the resulting precipitate was washed with deionized water and dried under vacuum at 70 ^oC for 12 h. The crude product was purified by column chromatography on silica gel with CH_2Cl_2/MeOH (10:1) as the eluent, yielding a yellow solid (8 mg, 11% yield). Anal. Calcd. For $C_{43}H_{50}F_6IrN_8P$: C, 50.83; H, 4.96; N, 11.03. Found: C, 50.97; H, 5.07; N, 11.27. ^1H NMR (400 MHz, $CDCl_3$): δ 8.16 (d, 2H, *J*= 5.6 Hz, H_b), 8.13 (d, 2H, *J*= 2.0 Hz, H_5), 7.94 (d, 2H, *J*= 7.6 Hz, H_e), 7.79 (ddd, 2H, *J*= 7.6, 7.6, 1.6 Hz, H_d), 7.62 (d, 2H, *J*= 7.6 Hz, H_k), 7.05-6.98 (m, 4H, H_4/H_c), 6.90 (ddd, 2H, *J*= 7.6, 7.6, 1.6 Hz, H_j), 6.83-6.74 (m, 4H, H_i/H_6), 6.28 (d, 2H, *J*= 7.6 Hz, H_h), 3.56-3.50 (m, 2H, H_7), 3.39-3.34 (m, 2H, $H_{7'}$), 2.12-2.01 (m, 4H, H_{10}), 1.97-1.86 (m, 4H, $H_{10'}$), 1.55-1.32 (m, 16H, H_8/H_{11}/H_{12}). ^{13}C NMR (100 MHz, $CDCl_3$): δ 169.6 (2C, C_f), 162.8 (2C, C_2), 162.7 (2C, C_l), 152.7 (2C, C_b), 143.9 (2C, C_g), 136.7 (2C, C_d), 131.2 (2C, C_h), 129.6 (2C, C_i), 124.5 (2C, C_5), 123.0 (2C, C_k), 122.3 (2C, C_c), 122.1 (2C, C_4), 121.4 (2C, C_e), 112.0 (2C, C_j), 61.7 (1C, C_6), 58.2 (2C, C_7), 54.2 (4C, C_{10}), 46.1 (2C, C_8), 25.6 (4C, C_{11}), 24.0 (2C, C_{12}). HRMS (ES^+): calcd. for $C_{43}H_{50}N_8Ir$ 869.3764; found 869.3741 $[M\text{-}PF_6^-]^+$.

4.2.5. Complex **VI-4e**

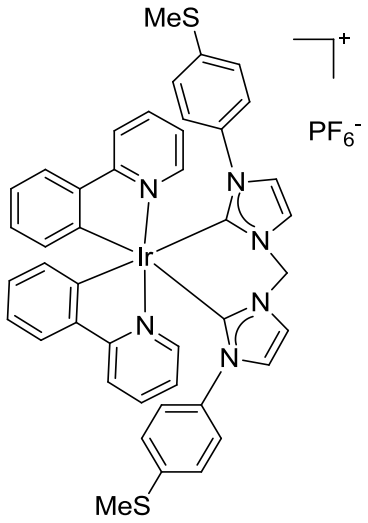

VI-4e

A mixture of **VI-3e** (56.9 mg, 0.10 mmol), silver oxide (23.8 mg, 0.10 mmol) and $[IrCl(ppy)_2]_2$ (50 mg, 0.05 mmol) in 10 mL of MeCN was reluxed for 10 h. After cooling down to room temperature, an aqueous solution of NH_4PF_6 (200 mg in 10 mL deionized water) was slowly added into the reaction mixture under stirring, resulting in a yellow suspension. The suspension was then filtered and the resulting precipitate was washed with deionized water and dried under vacuum at 70 ^oC for 12 h. The crude product was purified by column chromatography on silica gel with CH_2Cl_2/MeOH (20:1) as the eluent, yielding a yellow solid (35 mg, 36% yield). Anal. Calcd. For $C_{43}H_{36}F_6IrN_6PS_2$: C, 49.75; H, 3.50; N, 8.10. Found: C, 50.05; H, 3.42; N, 7.86. ^1H NMR (400 MHz, CD_3CN): δ 8.54 (d, 2H, J= 5.2 Hz, H_b), 7.82 (ddd, 2H, J= 7.2, 7.2, 1.6 Hz, H_d), 7.72 (d, 2H, J= 7.6 Hz, H_e), 7.51 (d, 2H, J= 2.0 Hz, H_5), 7.23 (d, 2H, J= 7.6 Hz, H_k), 7.12 (ddd, 2H, J= 6.4, 6.4, 1.6 Hz, H_c), 6.96 (d, 2H, J= 2.0 Hz, H_4), 6.59 (ddd, 2H, J= 7.2, 7.2, 1.2 Hz, H_j), 6.54 (d, 4H, J= 8.8 Hz, H_{SMePh}), 6.34-6.24 (m, 8H, H_6/H_i/H_{SMePh}), 5.44 (d, 2H, J= 7.6 Hz, H_h), 2.44 (s, 6H, H_{SMePh}). ^{13}C NMR (100 MHz, $CDCl_3$): δ 169.8 (2C, C_f), 164.9 (2C, C_2), 162.9 (2C, C_l), 153.1 (2C, C_b), 142.7 (2C, C_g), 138.4 (2C, C_{SMePh}), 136.6 (2C, C_d), 135.6 (2C, C_{SMePh}), 130.0 (2C, C_h), 129.2 (2C, C_i), 126.2 (4C, C_{SMePh}), 125.3 (4C, C_{SMePh}), 124.6 (2C, C_5), 124.0 (2C, C_k), 122.8 (2C, C_c), 121.5 (2C, C_4), 120.2 (2C, C_e), 119.7 (2C, C_j), 61.8 (1C, C_6), 15.2 (2C, C_{SMePh}). HRMS (ES^+): calcd. for $C_{43}H_{36}N_6S_2Ir$ 891.2049; found 891.2030 $[M\text{-}PF_6^-]^+$.

4.2.6. Complex **VI-4f**

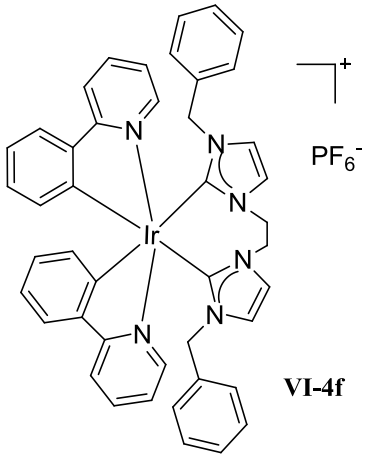

VI-4f

Under a nitrogen atmosphere and protection of the light, a flask was charged with **VI-3f** (52.3mg, 0.10 mmol), $[IrCl(ppy)_2]_2$ (53.5 mg, 0.05 mmol) and Ag_2O (24.5 mg, 0.10 mmol) in 10 mL of MeCN and the mixture was stirred under reflux for 24 h. After cooling to room temperature, NH_4PF_6 (200 mg) was added to the reaction mixture under stirring. The suspension was then filtered over a pad of celite, the resulting precipitate was washed with MeOH and the solvent was evaporated form the filtrate. The crude product was purified by two columns chromatography on silica gel with CH_2Cl_2/MeOH (30:1) and (200:1), respectively, as the eluent. The product was still not pure so it was solubilized in CH_2Cl_2 and precipitated with Et_2O. After drying under vacuum, a yellow solid was obtained (49 mg, 49% yield). Anal. Calcd. for $C_{44}H_{38}F_6IrN_6P$: C, 53.49; H, 3.88; N, 8.51. Found: C, 53.34; H, 3.32; N, 8.77. ^{1}H NMR (500 MHz, $CDCl_3$): δ 8.50 (d, J = 5.5 Hz, 2H, H_b), 7.60-7.57 (m, 4H, H_d/H_e), 7.47 (d, J = 6.5 Hz, 2H, H_h), 7.11 (d, J = 2.0 Hz, 2H, H_4), 7.10 (d, J = 1.5 Hz, 2H, H_{11}), 7.05 (dd, J = 8.5, 6.5 Hz, 6H, H_{10}), 6.97 (ddd, J = 7.0, 7.0, 2.5 Hz, 2H, H_c), 6.76 (ddd, J = 7.0, 7.0, 1.0 Hz, 2H, H_i), 6.55 (d, J = 2.0 Hz, 4H, H_5), 6.53 (dd, J = 7.0, 1.0 Hz, 2H, H_j), 6.21 (d, J = 7.5 Hz, 4H, H_9), 6.13 (d, J = 6.5 Hz, 2H, H_k), 4.80 (d, J = 16.0 Hz, 2H, H_7), 4.61 (s, 4H, H_6), 4.51 (d, J = 16.0 Hz, 2H, H_7). ^{13}C NMR (125 MHz, $CDCl_3$): δ 168.8 (2C, C_f), 164.5 (2C, C_2), 160.7 (2C, C_l), 154.9 (2C, C_b), 143.8 (2C, C_g), 136.8 (2C, C_8), 136.5 (2C, C_d), 131.4 (2C, C_k), 129.1 (2C, C_j), 128.3 (2C, C_{10}), 127.2 (2C, C_{11}), 126.0 (2C, C_9), 125.6 (2C, C_5), 125.1 (2C, C_4), 124.6 (2C, C_h), 122.2 (2C, C_C), 121.3 (2C, C_i), 119.8 (2C, C_e), 53.7 (2C, C_7), 51.3 (2C, C_6). HRMS (ES^+): calcd. for $C_{44}H_{38}N_6Ir$ m/z = 841.2764; found m/z = 841.2783 $[M\text{-}PF_6^-]^+$.

4.2.7. Complex **VI-4g**

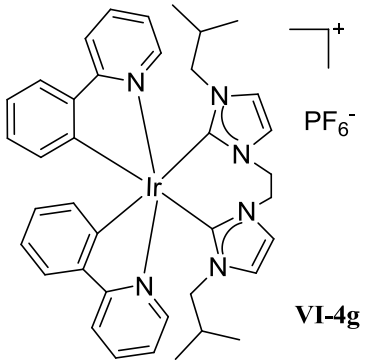

VI-4g

Under a nitrogen atmosphere, a flask was charged with **VI-3g** (52.8 mg, 0.10 mmol), $[IrCl(ppy)_2]_2$ (50 mg, 0.05 mmol) and K_2CO_3 (13 mg, 0.10 mmol) in 10mL of MeCN was stirred under reflux for 24 h. After cooling to room temperature, the solvent was evaporated and the solid was dissolved in CH_2Cl_2. The solution was washed with water and brine, then dried with Na_2SO_4. The solution was filtered and the solvent was evaporated to obtain a yellow solid. The solid was treated with a mixture of CH_2Cl_2/Et_2O (3:20) to give a yellow solid (55 mg, 60% yield). Anal. Calcd. for $C_{38}H_{42}F_6IrN_6P$: C, 49.57; H, 4.57; N, 9.13. Found: C, 49.17; H, 4.27; N, 9.33. ^1H NMR (400 MHz, $CDCl_3$): δ 8.43 (d, J = 5.6 Hz, 2H, H_b), 7.91 (d, J = 8.0 Hz, 2H, H_e), 7.81 (ddd, J = 7.2, 7.2, 1.6 Hz, 2H, H_d), 7.57 (d, J = 8.0 Hz, 2H, H_h), 7.15 (d, J = 2.0 Hz, 2H, H_4), 7.06 (ddd, J = 7.2, 7.2, 1.6 Hz, 2H, H_c), 6.83 (ddd, J = 7.2, 7.2, 1.2 Hz, 2H, H_i), 6.77 (d, J = 2.0 Hz, 2H, H_5), 6.69 (ddd, J = 7.2, 7.2, 1.2 Hz, 2H, H_j), 6.21 (d, J = 8.0 Hz, 2H, H_k), 4.55 (s, 4H, H_6), 3.21 (dd, J = 13.4, 8.4 Hz, 2H, H_7), 2.87 (dd, J = 13.4, 8.4 Hz, 2H, H_7), 1.58 (s, 2H, H_8), 0.49 (d, J = 6.4 Hz, 6H, H_9), 0.17 (d, J = 6.4 Hz, 6H, $H_{9'}$). ^{13}C NMR (100 MHz, $CDCl_3$): δ 169.4 (2C, C_f), 163.7 (2C, C_2), 161.3 (2C, C_l), 154.9 (2C, C_b), 143.9 (2C, C_g), 136.7 (2C, C_d), 134.0 (2C, C_k), 128.9 (2C, C_j), 124.7 (2C, C_h), 124.6 (2C, C_4), 122.2 (2C, C_c), 121.3 (2C, C_i), 120.8 (2C, C_5), 119.7 (2C, C_e), 55.8 (1C, C_7), 50.6 (2C, C_6), 28.3 (2C, C_8), 18.7 (2C, C_9), 18.4 (2C, $C_{9'}$). HRMS (ES^+): calcd. for $C_{38}H_{42}N_6Ir$ 773.3077; found 773.3077 $[M\text{-}PF_6^-]^+$.

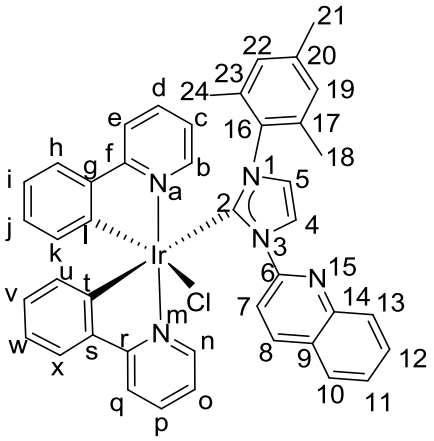

Fig 4.2 General numbering for NMR attribution.

4.2.8. Complex **VI-4h**

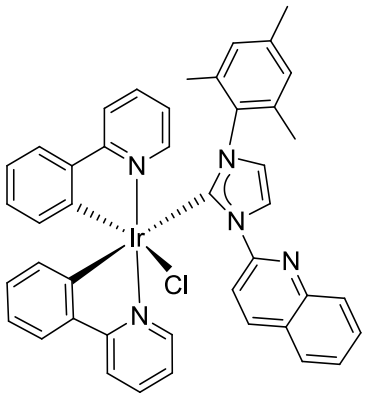

VI-4h

Under a nitrogen atmosphere and protection of the light, a flask was charged with **VI-3h** (51.5mg, 0.15 mmol), $[IrCl(ppy)_2]_2$ (70,8 mg, 0.07 mmol) and Ag_2O (18.8 mg, 0.08 mmol) in 10 mL of MeCN and the resulting mixture was stirred under reflux for 24 h. After cooling to room temperature, the mixture was filtered over a pad of celite and the solvent was evaporated from the filtrate. The product was dissolved in CH_2Cl_2, precipited by Et_2O, filtered and dried under vacuum, yielding a yellow solid (65 mg, 51% yield). Anal. Calcd. for $C_{43}H_{35}IrN_5Cl$: C, 60.74; H, 4.12; N, 8.24. Found: C, 60.54; H, 4.22; N, 8.42. ^{1}H NMR (400 MHz, $CDCl_3$): δ 10.00 (s, 1H, H_5), 9.55 (J = 8.4 Hz, 1H, H_7), 8.72 (d, J = 8.4 Hz, 1H, H_8), 8.09 (d, J = 8.4 Hz, 1H, H_{13}), 8.05 (d, J = 5.6 Hz, 1H, H_b), 7.87 (d, J = 5.6 Hz, 1H, H_n), 7.84 (dd, J = 8.4, 1.6 Hz, 1H, H_{10}), 7.81-7.75 (m, 2H, H_e/H_d), 7.72 (d, J = 8.4 Hz, 1H, H_q), 7.65 (dd, J = 8.0, 8.0 Hz, 1H, H_p), 7.55-7.51 (m, 1H, H_x), 7.41 (ddd, J = 8.0, 8.0, 1.2 Hz, 1H, H_{11}), 7.14 (ddd, J = 8.0, 6.8, 1.2 Hz, 1H, H_{12}), 7.09 (dd, J = 8.0, 1.2 Hz, 1H, H_h), 6.98 (s, 1H, H_4), 6.97-6.90 (m, 4H, H_c/H_v/H_w/H_o), 6.62 (ddd, J = 8.0, 8.0, 1.2 Hz, 1H, H_i), 6.46-6.40 (m,

2H, H_j/H_{20}), 6.27-6.23 (m, 2H, H_u/H_{19}), 5.90 (dd, J = 8.0, 1.2 Hz, 1H, H_k), 1.95 (s, 6H, H_{18}/H_{24}), 0.93 (s, 3H, H_{21}). ^{13}C NMR (100 MHz, $CDCl_3$): δ 180.4 (1C, C_2), 169.3 (1C, C_r), 167.9 (1C, C_f), 165.6 (1C, C_t), 154.2 (1C, C_6), 151.8 (1C, C_n), 150.7 (1C, C_b), 146.3 (1C, C_l), 145.2 (1C, C_{14}), 144.0 (1C, C_8), 143.6 (1C, C_s), 141.4 (1C, C_g), 139.0 (1C, C_{16}), 137.7 (1C, C_p), 136.8 (1C, C_d), 133.9 (1C, C_{23}), 133.7 (1C, C_{12}), 133.6 (1C, C_{19}), 131.5 (1C, C_v), 130.8 (1C, C_j), 130.6 (1C, C_{20}), 129.5 (1C, C_{17}), 129.5 (1C, C_u), 129.0 (1C, C_k), 128.7 (1C, C_{10}), 128.0 (1C, C_{22}), 127.6 (1C, C_9), 127.6 (1C, C_{13}), 127.1 (1C, C_{11}), 125.5 (1C, C_4), 124.7 (1C, C_x), 123.7 (1C, C_h), 123.0 (1C, C_o), 122.5 (1C, C_w), 122.5 (1C, C_c), 122.4 (1C, C_5), 120.2 (1C, C_i), 119.6 (1C, C_q), 119.5 (1C, C_e), 113.9 (1C, C_7), 20.9 (1C, C_{21}), 18.7 (1C, C_{24}), 15.9 (1C, C_{18}). HRMS (ES^+): calcd. for $C_{43}H_{35}N_5Ir$ 812.2498; found 812.2490 $[M\text{-}Cl^-]^+$.

Materials and methods

1. X-ray measurements

All data were collected at low temperature using oil-coated shock-cooled crystals at 100(2) K on a Bruker-AXS APEX II diffractometer with MoKa radiation (λ = 0.71073 Å). The structures were solved by direct methods[123] and all non hydrogen atoms were refined anisotropically using the least-squares method on F^2.[124] The absolute structure parameters have been refined using the Flack-method.[125]

Crystallographic data for **II-3a**, **II-3b**, **II-3c**, **II-3d**, **III-3a**, **III-3b**, **III-3c**, **V-2e**, **V-2f**, **VI-4a**, **VI-4b**, **VI-4c**, **VI-4f** and **VI-4g**:

II-3a: $C_{34}H_{46.5}AuN_7O_{3.5}$, Mr = 806.25, crystal size = 0.40 x 0.10 x 0.02 mm^3, triclinic, space group $P\ \bar{1}$, a = 10.684(2) Å, b = 16.145(2) Å, c = 21.292(2) Å, α = 79.396(3) °, β = 77.511(3) °, γ = 77.607(3) °, V = 3465.6(7) $Å^3$, Z = 4, 48878 reflections collected, 9811 unique reflections (R_{int} = 0.0526), R1 = 0.0538, wR2 = 0.1089 [I>2σ(I)], R1 = 0.0674, wR2 = 0.1140 (all data), residual electron density = 2.641 e $Å^{-3}$.

II-3b: $C_{32}H_{34}AuN_7O_3$, Mr = 761.63, crystal size = 0.20 x 0.10 x 0.05 mm^3, triclinic, space group $P\ \bar{1}$, a = 10.835(1) Å, b = 11.485(1) Å, c = 12.716(1) Å, α = 76.585(4) °, β = 77.134(4) °, γ = 84.412(4) °, V = 1498.7(2) $Å^3$, Z = 2, 48878 reflections collected, 9811 unique reflections (R_{int} = 0.0526), R1 = 0.0491, wR2 = 0.1271 [I>2σ(I)], R1 = 0.0586, wR2 = 0.1338 (all data), residual electron density = 2.345 e $Å^{-3}$.

II-3c: $C_{32}H_{42}AuN_7O_5$, Mr = 801.69, crystal size = 0.30 x 0.30 x 0.20 mm^3, monoclinic, space group $P2_1$, a = 10.984(1) Å, b = 30.847(3) Å, c = 19.590(2) Å, β = 90.277(2) °, V = 6637.4(9) $Å^3$, Z = 8, 110310 reflections collected, 56863 unique reflections (R_{int} = 0.0363), R1 = 0.0538, wR2 = 0.1220 [I>2σ(I)], R1 = 0.0630, wR2 = 0.1265 (all data), absolute structure factor x = 0.245(7), residual electron density = 6.675 e $Å^{-3}$.

II-3d: $C_{30}H_{42}AuN_7O_3$, Mr = 745.67, crystal size = 0.30 x 0.20 x 0.20 mm^3, monoclinic, space group $C2/c$, a = 17.575(1) Å, b = 21.290(1) Å, c = 9.851(1) Å, β = 121.108(2) °, V = 3155.7(2) $Å^3$, Z = 4, 31004 reflections collected, 4798 unique reflections (R_{int} = 0.0480), R1 = 0.0173, wR2 = 0.0359 [I>2σ(I)], R1 = 0.0338, wR2 = 0.0402 (all data), residual electron density = 0.692 e $Å^{-3}$.

III-3a: $C_{36}H_{38}AuN_7O_3$, Mr = 813.7, crystal size = 0.40 x 0.10 x 0.02 mm^3, monoclinic, space group *Cc*, *a* = 17.300(1) Å, *b* = 8.384(1) Å, *c* = 23.168(2) Å, β = 101.883(2) °, V = 3288.2(3) Å^3, Z = 4, 31546 reflections collected, 10626 unique reflections (R_{int} = 0.0511), R1 = 0.0457, wR2 = 0.1095 [I>2σ(I)], R1 = 0.0535, wR2 = 0.1141 (all data), Flack x refined to 0.001(7), residual electron density = 1.553 e Å^{-3}.

III-3b: $C_{40.5}H_{48}AuN_7O_{3.5}$, Mr = 885.82, crystal size = 0.40 x 0.40 x 0.30 mm^3, triclinic, space group $P\ \bar{1}$, *a* = 12.989(1) Å, *b* = 13.120(1) Å, *c* = 22.637(2) Å, α = 89.475(2) °, β = 84.108(2) °, γ = 79.203(2) °, V = 3769.0(4) Å^3, Z = 4, 108465 reflections collected, 22101 unique reflections (R_{int} = 0.0298), R1 = 0.0249, wR2 = 0.0448 [I>2σ(I)], R1 = 0.0384, wR2 = 0.0486 (all data), residual electron density = 1.408 e Å^{-3}.

III-3c: $C_{40}H_{34}AuN_7O_3$, Mr = 857.71, crystal size = 0.50 x 0.30 x 0.05 mm^3, monoclinic, space group *C2/c*, *a* = 15.119(2) Å, *b* = 14.404(2) Å, *c* = 32.326(4) Å, β = 101.172(3) °, V = 6906.1(13) Å^3, Z = 8, 37635 reflections collected, 4910 unique reflections (Rint = 0.0713), R1 = 0.0730, wR2 = 0.1436 [I>2σ(I)], R1 = 0.1020, wR2 = 0.1538 (all data), residual electron density = 3.517 e Å^{-3}.

III-6c: $C_{38}H_{35}AuN_{10}O_{3.5}$, Mr = 884.72, crystal size = 0.30 x 0.30 x 0.20 mm^3, triclinic, space group $P\ \bar{1}$, *a* = 12.2507(8) Å, *b* = 12.4973(8) Å, *c* = 12.9060(7) Å, α = 63.086(3) °, β = 83.924(3) °, γ = 86.093(3) °, V = 1751.55(19) Å^3, Z = 2, 79333 reflections collected, 13932 unique reflections (R_{int} = 0.0460), R1 = 0.0265, wR2 = 0.0514 [I>2σ(I)], R1 = 0.0387, wR2 = 0.0547 (all data), residual electron density = 1.582 e Å^{-3}.

III-6d: $C_{39}H_{48}AuN_9O_4$, Mr = 903.83, crystal size = 0.50 x 0.30 x 0.10 mm^3, triclinic, space group $P\ \bar{1}$, *a* = 12.5761(5) Å, *b* = 12.8909(6) Å, *c* = 13.4962(6) Å, α = 114.471(2) °, β = 100.927(2) °, γ = 98.673(2) °, V = 1889.85(15) Å^3, Z = 2, 39630 reflections collected, 9353 unique reflections (R_{int} = 0.0754), R1 = 0.0416, wR2 = 0.0765 [I>2σ(I)], R1 = 0.0667, wR2 = 0.0855 (all data), residual electron density = 1.588 e Å^{-3}.

V-2e: $C_{16}H_{21}AuClN_3O$, Mr = 503.77, crystal size = 0.20 x 0.20 x 0.05 mm^3, monoclinic, space group $P2_1/n$, *a* = 10.616(2) Å, *b* = 7.603(2) Å, *c* = 21.040(3) Å, β = 102.438(4) °, V = 1658.4(4) Å^3, Z = 4, 21943 reflections collected, 3487 unique reflections (R_{int} = 0.0763), R1 = 0.0413, wR2 = 0.0937 [I>2σ(I)], R1 = 0.0661, wR2 = 0.1074 (all data), residual electron density = 2.673 e Å^{-3}.

V-2f: $C_{16}H_{17}AuClN_3$, Mr = 48374, crystal size = 0.50 x 0.40 x 0.10 mm^3, triclinic, space group $P\ \bar{1}$, a = 9.3339(6) Å, b = 9.4041(6) Å, c = 9.9960(6) Å, α = 104.115(2) °, β = 101.187(2) °, γ = 104.407(2) °, V = 793.3(1) $Å^3$, Z = 2, 15105 reflections collected, 5605 unique reflections (R_{int} = 0.0416), R1 = 0.0308, wR2 = 0.0755 [I>2σ(I)], R1 = 0.0382, wR2 = 0.0794 (all data), residual electron density = 3.468 e $Å^{-3}$.

VI-4a: $C_{35}H_{36}F_6IrN_6P$, Mr = 877.87, crystal size = 0.20 x 0.10 x 0.10 mm^3, orthorhombic, space group $P2_12_12_1$, a = 10.5858(2) Å, b = 17.6393(3) Å, c = 17.8473(3) Å, V = 3332.6(1) $Å^3$, Z = 4, 25742 reflections collected, 15373 unique reflections (R_{int} = 0.0285), R1 = 0.0263, wR2 = 0.0553 [I>2σ(I)], R1 = 0.0303, wR2 = 0.0568 (all data), Flack x refined to -0.021(3), residual electron density = 1.720 e $Å^{-3}$.

VI-4b: $C_{37}H_{41}Br_{0.25}Cl_{0.75}IrN_6O$, Mr = 824.52, crystal size = 0.20 x 0.20 x 0.10 mm^3, monoclinic, space group $C2/c$, a = 39.743(2) Å, b = 8.954(1) Å, c = 22.453(2) Å, β = 121.284(2) °, V = 6827.9(6) $Å^3$, Z = 8, 51077 reflections collected, 8390 unique reflections (R_{int} = 0.0465), R1 = 0.0290, wR2 = 0.0524 [I>2σ(I)], R1 = 0.0421, wR2 = 0.0554 (all data), residual electron density = 0.961 e $Å^{-3}$.

VI-4c: $C_{43.5}H_{37}ClF_6IrN_6O$, Mr = 1016.41, crystal size = 0.40 x 0.30 x 0.20 mm^3, monoclinic, space group $P2_1$, a = 11.03(2) Å, b = 24.53(4) Å, c = 14.32(2) Å, β = 92.13(2) °, V = 3873(10) $Å^3$, Z = 4, 64391 reflections collected, 16738 unique reflections (R_{int} = 0.0314), R1 = 0.0325, wR2 = 0.0694 [I>2σ(I)], R1 = 0.0378, wR2 = 0.0750 (all data), Flack x refined to 0.482(6), residual electron density = 1.360 e $Å^{-3}$.

VI-4f: $C_{47}H_{45.5}F_6IrN_6O_{0.75}P$, Mr = 1043.56, crystal size 0.2 x 0.1 x 0.02 mm^3, triclinic, space group $P\ \bar{1}$, a = 14.94(2) Å, b = 15.06(2) Å, c = 20.52(3) Å, α = 107.64(2) °, β = 107.73(2) °, γ = 94.99(3) °, V = 4108(10) $Å^3$, Z = 4, 53646 reflections collected, 15235 unique, R_{int} = 0.0737, R1 = 0.0522, wR2 = 0.0980 [I > 2σ(I)], R1 = 0.1021, wR2 = 0.1156 (all data), residual electron density = 1.562 eA^{-3}.

VI-4g: $C_{38}H_{42}F_6IrN_6P$, Mr = 919.94, crystal size 0.4 x 0.2 x 0.2 mm^3, orthorhombic, $P2_12_12_1$, a = 10.806(1) Å, b = 17.084(2) Å, c = 19.875(2) Å, V = 3669.1(4) $Å^3$, Z = 4, 54609 reflections collected, 11153 unique, R_{int} = 0.0326, R1 = 0.0142, wR2 = 0.0322 [I > 2σ(I)], R1 = 0.0162, wR2 = 0.0328 (all data), Flack x refined to 0.497(3), residual electron density = 0.635 eA^{-3}.

2. Photophysical measurements

UV/Vis absorption spectra were recorded at RT on solutions contained in quartz cuvettes (optical pathlength 1 cm, Hellma®) with a PerkinElmer®, UV/VIS/NIR spectrophotometer Lambda 950 and a PerkinElmer® ditector; UV/VIS/NIR Accessory 2D Detector Module.

Fluorescence and phosphorescence emission spectra were obtained with a HORIBA JOBIN YVON, fluromax-4 and spectrofluorometer.

Luminescence quantum yields were measured according to the method of Demas and Crosby,[126] on solution samples at RT. The quantum yield is defined as:

$$\Phi_S = \Phi_R * \frac{(A_s)}{(A_r)} * \frac{(\eta_s)^2}{(\eta_r)^2}$$

Where Φ_S is the quantum yield of the sample, Φ_R is the know quantum yield of the reference standard. At the area subtended by the emission band (on a wavelength scale) and η is the refractive index of the solvent used for the preparation of the solution. As (related to the sample) and Ar (related to the reference) must be excitation wavelength. Different standards were selected depending on the spectral region of the interest: POPOP in hexane (Φ = 0.97) and QUININNE in water (Φ = 0.54).

Fluorescence lifetime measurements were performed by an Edinburgh FLS920 spectrofluorimeter equipped with a TCC900 card for data acquisition in time-correlated single-photon counting experiments (0.5 ns time resolution) with a D2 lamp and an LDH-P-C-405 pulsed diode laser. The estimated experimental error is 2 nm on the band maximum. (5% on the lifetime, 10% on the fluorescence quantum yield).

3. Measure of lipophilicity

The octanol-water partition coefficients (*P*) of all the complexes were determined using a shake-flask method.[95] Water (100 mL, distilled after milli-Q purification) and *n*-octanol (100 mL, Sigma Aldrich, ACS spectrophotometric grade, ≥ 99%) were shaken together for 24 h to allow saturation of both phases. Stock solutions of the

compounds (50 µM) were prepared in the aqueous phase. Aliquots (2 mL) of each of these stock solutions were then added to an equal volume of the *n*-octanol phase. The resultant biphasic solution was mixed for 15 min and then centrifuged (3000 tr/min, 5 min) to separate the phases. The concentrations of the complex in the organic and aqueous phases were then determined using UV absorbance spectroscopy (260 nm). The blank is the water saturated to *n*-octanol. Log *P* was defined as logarithm of the ratio of the concentrations of the complex in the organic and aqueous phases (values reported are the means of at least three separated determinations).

$$Log\ P = \frac{[Ir]_{(org)}}{[Ir]_{(aq)}}$$

4. Confocal microscopy

The fluorescence of the complexes was evaluated using a Zeiss LSM 710 NLO-Meta Confocal microscope. PC-3 cells were cultured in 6-well plates and on glass slides (180,000 cells per well) for 18 h before treated with complexes at different concentrations (0.25 µM, 0.5 µM and 1 µM). After 24 hours, a MitoTracker deep red probe was incubated on live cells at a final concentration of 200 nM during 15 min at 37 ºC in a 5 % CO_2 humidified incubator and then observed in two channels 440-544 nm for complex **VI-4a** (two-photon excitation at 720 nm) and 644-700 nm for MitoTracker (excitation at 633 nm) at the same time.

5. Biology

5.1. Cell lines

Human prostate cancer PC-3 and lung carcinoma A549 cell lines were obtained from DSMZ (Braunschweig, Germany). Human bladder cancer T24, osteosarcoma U-2 OS, breast cancer MCF-7, hepatocarcinoma HepG-2, mouse osteoblast MC3T3 and fibroblast NIH3T3 cell lines were from ATCC-LGC Standards (Molsheim, France). PC-3, HepG-2 and A549 cells were cultured in RPMI 1640, T24, MCF-7, U-2 OS and NIH3T3 in DMEM, and MC3T3 in MEM containing 10% fetal bovine

serum and 1% antibiotics (100 U/mL penicillin and 100 μg/mL streotimycin) at 37 ºC in 5% CO_2 humidified incubators.

5.2. Cell viability assay

The MTT reagent (3-(4,5-dimethylthiazol-2-yl)-2,5-diphenyltetrazolium bromide) was used to determine cell death as originally described by Mosmann[93] and modified by Cuvillier et al.[127] Briefly, cells were seeded 5000 cells/well in 24-well plates for various cell lines (PC-3, T24, A549, MCF-7, HepG-2, U-2 OS, MC3T3 and NIH3T3) and allowed to attach overnight. All of the complexes were dissolved in DMSO. The concentration of the complexes was calculated according to the elemental composition of the complexes determined by the elemental analyses. Media in the presence of the tested complexes were added and serially diluted to various concentrations (from 5 μM to 0.01 μM). The maximum concentration of DMSO in media did not exceed 0.5 % (v/v). After 24 h, 48 h or 72 h of treatment, cells were incubated at 37 ºC and 5% CO_2 with 25 μL MTT solution (5 mg/mL; Sigma-Aldrich) in 24-well plates for approximately 3 h. After solubilization with 500 μL of lysis buffer (DMSO), formazan was quantified by spectrophotometry with a microplate reader at 570 nm absorbance. The GI_{50} values corresponding to the concentration that caused 50% inhibition of cell proliferation were calculated from dose-response curves obtained by nonlinear regression analysis (Prism 5, Graphpad Software). All the results were calculated from data obtained in three independent experiments.

5.3. Clonogenic assay

PC-3 and T24 cells were counted and seeded (500 cells/well) to 6-well plates. Cells were allowed to attach overnight and then treated with different concentrations of gold complexes (0.01 μM，0.1 μM, 0.25 μM, 0.5 μM, 1 μM, 5 μM). After incubation for an additional 6 days for T24 and 8 days for PC-3, the cells were washed with PBS (2 mL), fixed with methanol (1 mL) for 20 min and stained with 0.5% crystal violet (2 mL) for 30 min. The relative survival was calculated from the number of single cells that formed colonies of more than 50 cells.

5.4. Cellular uptake studies

The cellular metal uptake was determined as described according to a previously described method.[43] Briefly, for the cellular uptake into HepG-2 human liver cancer cells, the cells were cultured until at least 80% confluence in 75 cm^2 flasks. Stock solutions of gold complexes in sterile DMSO were prepared and diluted with cell culture medium to a final concentration of 2 μM (freshly prepared, final DMSO concentration of 0.1 % v/v). The cell culture medium was replaced by the fresh medium containing the gold complexes, and the flasks were incubated at 37 ℃ and 5% CO_2 for 1, 2 and 4 h. After the desired incubation period, the cellular uptake was stopped by removing the cell culture medium. The cells were washed with PBS (10 mL), and then the pellets were collected after 10 min of trypsinization (0.05% trypsin-EDTA solution (10 mL) and centrifugation (room temperature; 1,500 rpm, 5 min). Cells were resuspended in Mili-Q water (1 mL) and lysed by sonication for 30 s. The protein contents of lysates were determined by the Bradford method. 100 μL of samples were digested in 300 μL of 70 % HNO_3 at 70 ℃ for 2 h and room temperature overnight, then diluted 1:100 in ultrapure water for inductively coupled plasma atomic emission spectroscopy (ICP-AES) analysis. Results were calculated from the data obtained from three independent experiments and are expressed as microgram of gold per milligram of protein.

5.5. Inhibition of mammalian TrxR

To determine the inhibition of mammalian TrxR, an established microplate reader-based assay was performed with minor modifications.[101b] For this propose, commercially available rat liver TrxR (from Sigma-Aldrich) was used and diluted with distilled water to achieve 3.5 U/mL. Gold complexes were freshly dissolved as stock solution in sterile DMSO. 25 μL aliquot of the enzyme and either 25 μL potassium phosphate buffer (pH 7.0) containing gold complexes in graded concentrations or 25 μL buffer without the complex but DMSO (positive control) were added. The resulting solution (final DMSO concentration of 0.5 % v/v) was incubated at 37 ℃ for 75 min with moderate shaking in a 96-well plate. To each well, 225 μL of the reaction mixture (1.0 mL reaction mixture consists of 500 μL 100 mM potassium phosphate buffer pH 7.0, 80 μL 100 mM EDTA solution pH 7.5, 20 μL 0.2 % BSA, 100 μL of a 20 mM NADPH and 300 μL distilled water) was added and the

reaction was initiated immediately by adding 25 µL of 20 mM DTNB solution. After thorough mixing, the formation of TNB was monitored by a microplate reader at 405 nm at 1 min intervals for 10 measurements. The increase of TNB concentration over time followed a linear tendency ($r^2 \geq 0.99$), and the enzymatic activities were calculated as the slopes (increase in absorbance per second) thereof. Non-interference with the assay components was confirmed by a negative control experiment using an enzyme-free test compound. IC_{50} values were calculated as the concentration of the compound decreasing the enzymatic activity of the untreated control by 50%.

5.6. Cellular activity of reducing agents present in cells

The cellular activity of reducing agents present in the cell was determined according to a previously described method.[128] Cells were counted and seeded at $2x10^5$ per well in 6-well plates and incubated for 24 h. Gold complexes were freshly dissolved as stock solution in sterile DMSO, and the stock solution was diluted with cell culture medium to graded concentrations (final DMSO concentration of 1 % v/v). The cell culture medium was replaced by fresh medium containing gold complexes, and the plates were incubated for 1 h at 37 ℃ and 5% CO_2. Afterwards, the cells were washed with PBS for three times, and 100 µL of cold lysis buffer (50 mM phosphate buffer, pH 7.4, 1 mM EDTA, 0.1 % Triton-X 100) were added to the plates. Cell lysis was carried out on ice for 5 min and the cell lysates were collected and stored at -80 ℃. The protein contents of lysates were determined by the Bradford method. Then cell lysates (10 µg) were added to 100 µL of reaction buffer (50 mM phosphate buffer, pH 7.4, 1 mM EDTA and 0.2 mM NADPH). Finally, 5,5'-dithiobis (2-nitrobenzoic acid) (DTNB, final concentration of 3 mM) was added to initiate the reaction and the cellular activity of reducing agents was determined as increases in O.D. 410 nM in 10 min. All the results were calculated from data obtained in three independent experiments.

5.7. Measurement of intracellular reactive oxygen species (ROS)

For *N*-acetyl-cysteine (NAC) and reduced glutathione (GSH) treatment, the cells were pre-treated with different concentrations of NAC and GSH (2, 5 and 10 mM) for 1 h, then gold complexes (1 µM) were added for an additional 24 h. After incubation, cells were incubated at 37 ℃ and 5% CO_2 with 25 µL MTT solution (5 mg/mL;

Sigma-Aldrich) in 24-well plates for approximately 3 h. The cytotoxicity was determined as described above.

The cellular ROS generation was shown by the increase of fluorescence intensity of DCF according to a previously reported protocol.[129] Briefly, PC-3, T24 and HepG-2 cells were seeded at a density of 50,000 cells/well in 24-well plates for 24 h. Cells were washed with PBS buffer and stained with DCFH-DA (final concentration 20 μM) for 45 min. Then cells were washed with PBS buffer and the culture medium without phenol red containing gold complexes was added to the cells. The fluorescence intensity of DCF (excitation/emission, 485/535 nm) was measured by fluorescence microplate reader at different time points. Data are presented as means ± SEM of three independent experiments. *$p<0.05$, **$p<0.005$, ***$p<0.001$, compared with ROS generation at 0 h.

5.8. Measurement of intracellular superoxide anion ($O_2^{-\cdot}$)

To determine reactive oxygen species (ROS) generation, an established microplate-reader-based assay was performed with minor modifications.[130] Cells were counted and seeded at 50,000 per well in 24-well plates. The compounds were freshly dissolved as stock solution in sterile DMSO, and the stock solution was diluted with cell culture medium to graded concentrations. (final DMSO concentration of 0.5 % v/v). After 24 h of incubation at 37 ^{o}C and 5% CO_2, the cell culture medium was replaced by fresh medium containing gold complexes, and the plates were incubated for different period of time (0 h, 3 h, 6 h and 24 h). 250 μL of nitroblue tetrazolium solution (NBT, 1 mg/mL) in PBS were added to the plates after removal of medium. After 4 h of incubation, the supernatant NBT solution was discarded. Then the reduced formazan was dissolved by 360 μL of 2 M KOH followed by 400 μL of DMSO and quantified by spectrophotometry with a microplate reader at 620 nm absorbance using KOH/DMSO as a blank. All the results were calculated from data obtained in three independent experiments.

5.9. Measurement of intracellular hydrogen peroxide (H_2O_2)

Cells were counted and seeded at 50,000 per well in 24-well plates. The compounds were freshly dissolved as stock solution in sterile DMSO, and the stock solution was

diluted with cell culture medium to graded concentrations. (final DMSO concentration of 0.5 % v/v). After 24 h of incubation at 37 ºC and 5% CO_2, the cell culture medium was replaced by fresh medium containing gold complexes, and the plates were incubated for different period of time (0 h, 3 h, 6 h and 24 h). 500 µL of 3,3'-diaminobenzidine solution (DAB, 2.5 mM) in potassium phosphate buffer were added to the plates after removal of medium. After 4 h of incubation, ROS generation was quantified by spectrophotometry with a microplate reader at 405 nm absorbance. All the results were calculated from data obtained in three independent experiments.

5.10. Antileishmanial evaluation

Leishmania species used in this study were *Leishmania infantum* MHOM/MA/67/ITMAP-263 (CNR *Leishmania*, Montpellier, France) expressing luciferase activity.

5.10.1. Antileishmanial activity on promatisgotes

The effects of the tested compounds on the growth of *L. infantum* promastigotes were assessed by Luciferase Assay like previously described.[113a] Briefly, promastigotes in log-phase in RPMI 1640 medium supplemented with 10% fetal calf serum (FCS), 2 mM l-glutamine and antibiotics (100U/mL penicillin, 100 µg/mL streptomycin and 50 µg/mL geneticin), were incubated at a density of 10^6 parasites/mL in sterile 96-well plates with various concentrations of compounds dissolved in DMSO (final concentration less than 0.5% v/v), in duplicate. Appropriate controls treated by DMSO, amphotericin B, miltefosine and pentamidine (reference drugs purchased from Sigma Aldrich) were added to each set of experiments. After a 72 h of incubation period at 24 ℃, each plate-well was then microscope-examined for detecting possible precipitate formation. To estimate the luciferase activity of promastigotes, 80 µl of each well are transferred in white 96-well plates, Steady Glow reagent (Promega) was added according to manufacturer's instructions, and plates were incubated for 2 min. The luminescence was measured in Microbeta Luminescence Counter (PerkinElmer).

Inhibitory concentration 50% (IC_{50}) was defined as the concentration of drug required to inhibit by 50% the metabolic activity of *L. infantum* promastigotes compared to the control. IC_{50} were calculated by non-linear regression analysis processed on dose–response curves, using TableCurve 2D V5 software. IC_{50} values represent the mean value calculated from three independent experiments.

5.10.2. Antileishmanial activity on axenic amastigotes

Here, we described a new method to generate axenic amastigotes. For this, *L. Infantum* promastigotes in logarithmic phase were centrifuged at 900 g for 10 min, the supernatant was removed carefully and was replaced by the same volume of RPMI 1640 complete medium at pH 5.4 and incubated for 24 h at 24 ℃. The acidified promastigotes were incubated 24 h at 37 ℃ in a ventilated flask. Then promastigotes were altered to amastigotes form.

The effects of the tested compounds on the growth of *L. infantum* axenic amastigotes were assessed in the following way. *L. Infantum* amastigotes were incubated at a density of 1.10^6 parasites/mL in sterile 96-well plates with various concentrations of compounds dissolved in DMSO (final concentration less than 0.5% v/v), in duplicate. Appropriate controls treated by DMSO, amphotericin B, miltefosine and pentamidine (reference drugs purchased from Sigma Aldrich) were added to each set of experiments. After a 48 h incubation period at 37 ℃, each plate-well was then microscope-examined for detecting possible precipitate formation. To estimate the luciferase activity of promastigotes, 80 µl of each well are transferred in white 96-well plates, Steady Glow reagent (Promega) was added according to manufacturer's instructions, and plates were incubated for 2 min. The luminescence was measured in Microbeta Luminescence Counter (PerkinElmer). Inhibitory concentration 50% (IC_{50}) was defined as the concentration of drug required to inhibit by 50% the metabolic activity of *L. infantum* amastigotes compared to the control. IC_{50} were calculated by non-linear regression analysis processed on dose–response curves, using TableCurve 2D V5 software. IC_{50} values represent the mean value calculated from three independent experiments.

5.11. Cytotoxicity evaluation

The evaluation of the tested molecules cytotoxicity by MTT assay on the J774A.1 cell line (mouse macrophage cell line, Sigma–Aldrich) was done according like previously described.[113a] Briefly, cells (5×10^4 cells/mL) in 100 μL of complete medium, [DMEM high Glucose supplemented with 10% fetal calf serum (FCS), 2 mM l-glutamine and antibiotics (100 U/mL penicillin and 100 μg/mL streptomycin)] were seeded into each well of 96-well plates and incubated at 37 ℃ and 5% CO_2. After a 24 h incubation, 100 μL of medium with various product concentrations and appropriate controls treated by DMSO, amphotericin B, miltefosine, doxorubicine and pentamidine (reference drugs purchased from Sigma Aldrich) were added and the plates were incubated for 72 h at 37 ℃ and 5% CO_2. Each plate-well was then microscope-examined for detecting possible precipitate formation before the medium was aspirated from the wells. 100 μL of MTT solution (0.5 mg/mL in RPMI) were then added to each well. Cells were incubated for 2 h at 37 ℃ and 5% CO_2. After this time, the MTT solution was removed and DMSO (100 μl/well) was added to dissolve the resulting formazan crystals. Plates were shaken vigorously (300 rpm) for 5 min. The absorbance was measured at 570 nm with a microplate spectrophotometer (Eon BioTek). DMSO was used as blank. CC_{50} were calculated by non-linear regression analysis processed on dose–response curves, using TableCurve 2D V5 software. CC_{50} values represent the mean value calculated from three independent experiments.

5.12. Photodynamic activity

A colormetric assay using MTT was used to compare the cytotoxicity of the complexes in the dark and upon UV irradiation. T24, PC-3 and non-cancerous NIH3T3 cell lines were seeded in 24-well plates at a density of 10,000 cells per well in 500 μL, 24 h prior to treatment. The cells were then treated with increasing concentrations of iridium complexes (from 0.01 μM to 20 μM) for 48 h. For photocytoxicity studies, the cells were treated for 4 h with increasing concentrations of the compounds in the dark. After that, the medium was removed and replaced by

fresh culture medium prior to 10 min irradiation at 365 nm (4 W). After 44 hours of incubation, cells were incubated at 37 °C and 5% CO_2 with 25 µL MTT solution (5 mg/mL; Sigma-Aldrich) in 24-well plates for approximately 3 h. After solubilization with 500 µL of lysis buffer (DMSO), formazan was quantified by spectrophotometry with a microplate reader at 570 nm absorbance. The GI_{50} values corresponding to the concentration that caused 50% inhibition of cell proliferation were calculated from dose-response curves obtained by nonlinear regression analysis (Prism 5, Graphpad Software). All the results were calculated from data obtained in three independent experiments.[131]

Bibliography

1. Martell, A.; Hancock, R., Modern Inorganic Chemistry; ed. JP Fackler jun. Plenum Press, New York: 1996.

2. (a) Berners-Price, S. J.; Sadler, P. J., Coordination chemistry of metallodrugs: insights into biological speciation from NMR spectroscopy. *Coord. Chem. Rev.* **1996**, *151*, 1-40; (b) Stochel, G.; Wanat, A.; Kuliś, E.; Stasicka, Z., Light and metal complexes in medicine. *Coord. Chem. Rev.* **1998**, *171*, 203-220.

3. Bertini, I.; Gray, H. B.; Lippard, S. J.; Valentine, J. S., *Bioinorganic chemistry*. University Science Books: 1994.

4. Rosenberg, B.; Vancamp, L.; Trosko, J. E.; Mansour, V. H., Platinum compounds: a new class of potent antitumour agents. *Nature* **1969**, *222* (5191), 385-386.

5. Wheate, N. J.; Walker, S.; Craig, G. E.; Oun, R., The status of platinum anticancer drugs in the clinic and in clinical trials. *Dalton Trans.* **2010**, *39* (35), 8113-8127.

6. Eastman, A., The formation, isolation and characterization of DNA adducts produced by anticancer platinum complexes. *Pharmacol. Ther.* **1987**, *34* (2), 155-166.

7. Sadler, P. J.; Guo, Z., Metal complexes in medicine: design and mechanism of action. *Pure Appl. Chem.* **1998**, *70* (4), 863-871.

8. (a) Liu, W.; Gust, R., Metal *N*-heterocyclic carbene complexes as potential antitumor metallodrugs. *Chem. Soc. Rev.* **2013**, *42* (2), 755-773; (b) Oehninger, L.; Rubbiani, R.; Ott, I., *N*-Heterocyclic carbene metal complexes in medicinal chemistry. *Dalton Trans.* **2013**, *42* (10), 3269-3284; (c) Aher, S. B.; Muskawar, P. N.; Thenmozhi, K.; Bhagat, P. R., Recent developments of metal *N*-heterocyclic carbenes as anticancer agents. *Eur. J. Med. Chem.* **2014**, *81*, 408-419; (d) Liu, W.; Gust, R., Update on metal *N*-heterocyclic carbene complexes as potential anti-tumor metallodrugs. *Coord. Chem. Rev.* **2016**, *329*, 191-213.

9. Díez-González, S.; Marion, N.; Nolan, S. P., *N*-heterocyclic carbenes in late transition metal catalysis. *Chem. Rev.* **2009**, *109* (8), 3612-3676.

10. Porchia, M.; Pellei, M.; Marinelli, M.; Tisato, F.; Del Bello, F.; Santini, C., New insights in Au-NHCs complexes as anticancer agents. *Eur. J. Med. Chem.* **2018**, *146*, 709-746.

11. (a) Baker, M. V.; Barnard, P. J.; Berners-Price, S. J.; Brayshaw, S. K.; Hickey, J. L.; Skelton, B. W.; White, A. H., Cationic, linear Au(I) *N*-heterocyclic carbene complexes: synthesis, structure and anti-mitochondrial activity. *Dalton Trans.* **2006**, *35* (30), 3708-3715; (b) Arcau, J.; Andermark, V.; Rodrigues, M.; Giannicchi, I.; Pérez‐Garcia, L.; Ott, I.; Rodríguez, L., Synthesis and Biological Activity of Gold(I) *N*-Heterocyclic Carbene Complexes with Long Aliphatic Side Chains. *Eur. J. Inorg. Chem.* **2014**, *2014* (35), 6117-6125; (c) Horvath, U. E.; Bentivoglio, G.; Hummel, M.; Schottenberger, H.; Wurst, K.; Nell, M. J.; van Rensburg, C. E.; Cronje, S.; Raubenheimer, H. G., A cytotoxic bis(carbene) gold(I) complex of ferrocenyl complexes: synthesis and structural characterisation. *New J. Chem.* **2008**, *32* (3), 533-539; (d) Krishnamurthy, D.; Karver, M. R.; Fiorillo, E.; Orru, V.; Stanford, S. M.; Bottini, N.; Barrios, A. M., Gold(I)-mediated inhibition of protein tyrosine phosphatases: a detailed *in vitro* and cellular study. *J. Med. Chem.* **2008**, *51* (15), 4790-4795; (e) Liu, W.; Bensdorf, K.; Proetto, M.; Abram, U.; Hagenbach, A.; Gust, R., NHC gold halide complexes derived from 4,5-diarylimidazoles: synthesis, structural analysis, and pharmacological investigations as potential antitumor agents. *J. Med. Chem.* **2011**, *54* (24), 8605-8615.

12. Zhao, W.; Ferro, V.; Baker, M. V., Carbohydrate-*N*-heterocyclic carbene metal complexes: Synthesis, catalysis and biological studies. *Coord. Chem. Rev.* **2017**, *339*, 1-16.
13. Medici, S.; Peana, M.; Nurchi, V. M.; Lachowicz, J. I.; Crisponi, G.; Zoroddu, M. A., Noble metals in medicine: Latest advances. *Coord. Chem. Rev.* **2015**, *284*, 329-350.
14. Melaiye, A.; Simons, R. S.; Milsted, A.; Pingitore, F.; Wesdemiotis, C.; Tessier, C. A.; Youngs, W. J., Formation of water-soluble pincer silver(I) − carbene complexes: a novel antimicrobial agent. *J. Med. Chem.* **2004**, *47* (4), 973-977.
15. Medvetz, D. A; Hindi, K. M.; Panzner, M. J.; Ditto, A. J.; Yun, Y. H.; Young, W. J., Anticancer activity of Ag(I) *N*-heterocyclic carbene complexes derived from 4,5-dichloro-1*H*-imidazole. *Met. Based Drugs* **2008**, 384010.
16. Siciliano, T. J.; Deblock, M. C.; Hindi, K. M.; Durmus, S.; Panzner, M. J.; Tessier, C. A.; Youngs, W. J., Synthesis and anticancer properties of gold(I) and silver(I) *N*-heterocyclic carbene complexes. *J. Organomet. Chem.* **2011**, *696* (5), 1066-1071.
17. Antonarakis, E. S.; Emadi, A., Ruthenium-based chemotherapeutics: are they ready for prime time? *Cancer Chemother. Pharmacol.* **2010**, *66* (1), 1-9.
18. Oehninger, L.; Stefanopoulou, M.; Alborzinia, H.; Schur, J.; Ludewig, S.; Namikawa, K.; Muñoz-Castro, A.; Köster, R. W.; Baumann, K.; Wölfl, S., Evaluation of arene ruthenium(II) *N*-heterocyclic carbene complexes as organometallics interacting with thiol and selenol containing biomolecules. *Dalton Trans.* **2013**, *42* (5), 1657-1666.
19. Lv, G.; Guo, L.; Qiu, L.; Yang, H.; Wang, T.; Liu, H.; Lin, J., Lipophilicity-dependent ruthenium *N*-heterocyclic carbene complexes as potential anticancer agents. *Dalton Trans.* **2015**, *44* (16), 7324-7331.
20. Oehninger, L.; Spreckelmeyer, S.; Holenya, P.; Meier, S. M.; Can, S.; Alborzinia, H.; Schur, J.; Keppler, B. K.; Wölfl, S.; Ott, I., Rhodium(I) *N*-heterocyclic carbene bioorganometallics as *in vitro* antiproliferative agents with distinct effects on cellular signaling. *J. Med. Chem.* **2015**, *58* (24), 9591-9600.
21. Çetinkaya, B.; Çetinkaya, E.; Küçükbay, H.; Durmaz, R., Antimicrobial activity of carbene complexes of rhodium(I) and ruthenium(II). *Arzneimittel-Forschung* **1996**, *46*, 821-823.
22. Santini, C.; Pellei, M.; Gandin, V.; Porchia, M.; Tisato, F.; Marzano, C., Advances in copper complexes as anticancer agents. *Chem. Rev.* **2013**, *114* (1), 815-862.
23. Streciwilk, W.; Hackenberg, F.; Müller-Bunz, H.; Tacke, M., Synthesis and cytotoxicity studies of p-benzyl substituted NHC-copper(I) bromide derivatives. *Polyhedron* **2014**, *80*, 3-9.
24. Pellei, M.; Gandin, V.; Marinelli, M.; Orsetti, A.; Del Bello, F.; Santini, C.; Marzano, C., Novel triazolium based 11th group NHCs: synthesis, characterization and cellular response mechanisms. *Dalton Trans.* **2015**, *44* (48), 21041-21052.
25. Becker, K.; Gromer, S.; Schirmer, R. H.; Müller, S., Thioredoxin reductase as a pathophysiological factor and drug target. *FEBS J.* **2000**, *267* (20), 6118-6125.
26. Bindoli, A.; Rigobello, M. P.; Scutari, G.; Gabbiani, C.; Casini, A.; Messori, L., Thioredoxin reductase: a target for gold compounds acting as potential anticancer drugs. *Coord. Chem. Rev.* **2009**, *253* (11-12), 1692-1707.
27. Barnard, P. J.; Berners-Price, S. J., Targeting the mitochondrial cell death pathway with gold compounds. *Coord. Chem. Rev.* **2007**, *251* (13-14), 1889-1902.

28. Green, D. R.; Kroemer, G., The pathophysiology of mitochondrial cell death. *Science* **2004**, *305* (5684), 626-629.
29. Green, D. R.; Kroemer, G., Pharmacological manipulation of cell death: clinical applications in sight? *J. Clin. Invest.* **2005**, *115* (10), 2610-2617.
30. Kokoszka, J. E.; Waymire, K. G.; Levy, S. E.; Sligh, J. E.; Cai, J.; Jones, D. P.; MacGregor, G. R.; Wallace, D. C., The ADP/ATP translocator is not essential for the mitochondrial permeability transition pore. *Nature* **2004**, *427* (6973), 461-465.
31. Wei, M. C.; Zong, W.-X.; Cheng, E. H.-Y.; Lindsten, T.; Panoutsakopoulou, V.; Ross, A. J.; Roth, K. A.; MacGregor, G. R.; Thompson, C. B.; Korsmeyer, S. J., Proapoptotic BAX and BAK: a requisite gateway to mitochondrial dysfunction and death. *Science* **2001**, *292* (5517), 727-730.
32. Chen, L. B., Mitochondrial membrane potential in living cells. *Annu. Rev. Cell Biol.* **1988**, *4* (1), 155-181.
33. Hickey, J. L.; Ruhayel, R. A.; Barnard, P. J.; Baker, M. V.; Berners-Price, S. J.; Filipovska, A., Mitochondria-targeted chemotherapeutics: the rational design of gold(I) *N*-heterocyclic carbene complexes that are selectively toxic to cancer cells and target protein selenols in preference to thiols. *J. Am. Chem. Soc.* **2008**, *130* (38), 12570-12571.
34. Shaw, C. F., Gold-based therapeutic agents. *Chem. Rev.* **1999**, *99* (9), 2589-2600.
35. Fung, S. K.; Zou, T.; Cao, B.; Lee, P. Y.; Fung, Y. M. E.; Hu, D.; Lok, C. N.; Che, C. M., Cyclometalated Gold(III) Complexes Containing *N*-Heterocyclic Carbene Ligands Engage Multiple Anti-Cancer Molecular Targets. *Angew. Chem.* **2017**, *129* (14), 3950-3954.
36. Bertrand, B.; Fernandez-Cestau, J.; Angulo, J.; Cominetti, M. M.; Waller, Z. A.; Searcey, M.; O'Connell, M. A.; Bochmann, M., Cytotoxicity of Pyrazine-Based Cyclometalated (C^Npz^C) Au(III) Carbene Complexes: Impact of the Nature of the Ancillary Ligand on the Biological Properties. *Inorg. Chem.* **2017**, *56* (10), 5728-5740.
37. Haque, R. A.; Ghdhayeb, M. Z.; Budagumpi, S.; Ahamed, M. B. K.; Majid, A. M. A., Synthesis, crystal structures, and *in vitro* anticancer properties of new *N*-heterocyclic carbene (NHC) silver(I)- and gold(I)/(III)-complexes: a rare example of silver(I)-NHC complex involved in redox transmetallation. *RSC Adv.* **2016**, *6* (65), 60407-60421.
38. Sivaram, H.; Tan, J.; Huynh, H. V., Syntheses, characterizations, and a preliminary comparative cytotoxicity study of gold(I) and gold(III) complexes bearing benzimidazole-and pyrazole-derived *N*-heterocyclic carbenes. *Organometallics* **2012**, *31* (16), 5875-5883.
39. Barnard, P. J.; Baker, M. V.; Berners-Price, S. J.; Day, D. A., Mitochondrial permeability transition induced by dinuclear gold(I)–carbene complexes: potential new antimitochondrial antitumour agents. *J. Inorg. Biochem.* **2004**, *98* (10), 1642-1647.
40. Sanchez, O.; Gonz âlez, S.; Fern ández, M.; Higuera-Padilla, A. R.; Leon, Y.; Coll, D.; Vidal, A.; Taylor, P.; Urdanibia, I.; Goite, M. C., Novel silver(I)–and gold(I)-*N*-heterocyclic carbene complexes. Synthesis, characterization and evaluation of biological activity against tumor cells. *Inorg. Chim. Acta* **2015**, *437*, 143-151.
41. Zou, T.; Lum, C. T.; Lok, C. N.; To, W. P.; Low, K. H.; Che, C. M., A Binuclear Gold(I) Complex with Mixed Bridging Diphosphine and Bis(*N*-Heterocyclic Carbene) Ligands Shows Favorable Thiol Reactivity and Inhibits Tumor Growth and Angiogenesis *In Vivo*. *Angew. Chem. Int. Ed.* **2014**, *53* (23), 5810-5814.
42. Sun, R. W. Y.; Zhang, M.; Li, D.; Zhang, Z. F.; Cai, H.; Li, M.; Xian, Y. J.; Ng, S. W.;

Wong, A. S. T., Dinuclear Gold(I) Pyrrolidinedithiocarbamato Complex: Cytotoxic and Antimigratory Activities on Cancer Cells and the Use of Metal-Organic Framework. *Chem. Eur. J.* **2015**, *21* (51), 18534-18538.

43. Rubbiani, R.; Can, S.; Kitanovic, I.; Alborzinia, H.; Stefanopoulou, M.; Kokoschka, M.; Mönchgesang, S.; Sheldrick, W. S.; Wölfl, S.; Ott, I., Comparative *in vitro* evaluation of *N*-heterocyclic carbene gold(I) complexes of the benzimidazolylidene type. *J. Med. Chem.* **2011**, *54* (24), 8646-8657.

44. Holenya, P.; Can, S.; Rubbiani, R.; Alborzinia, H.; Jünger, A.; Cheng, X.; Ott, I.; Wölfl, S., Detailed analysis of pro-apoptotic signaling and metabolic adaptation triggered by a *N*-heterocyclic carbene-gold(I) complex. *Metallomics* **2014**, *6* (9), 1591-1601.

45. Rubbiani, R.; Salassa, L.; de Almeida, A.; Casini, A.; Ott, I., Cytotoxic Gold(I) *N*-heterocyclic Carbene Complexes with Phosphane Ligands as Potent Enzyme Inhibitors. *ChemMedChem* **2014**, *9* (6), 1205-1210.

46. Rubbiani, R.; Schuh, E.; Meyer, A.; Lemke, J.; Wimberg, J.; Metzler-Nolte, N.; Meyer, F.; Mohr, F.; Ott, I., TrxR inhibition and antiproliferative activities of structurally diverse gold *N*-heterocyclic carbene complexes. *MedChemComm* **2013**, *4* (6), 942-948.

47. Turek, J.; Růžičková, Z.; Tloušťová, E.; Mertlíková-Kaiserová, H.; Günterová, J.; Rulíšek, L.; Růžička, A., 1, 2, 4-Triazole-based *N*-heterocyclic carbene complexes of gold(I): synthesis, characterization and biological activity. *Appl. Organomet. Chem.* **2016**, *30* (5), 318-322.

48. Citta, A.; Schuh, E.; Mohr, F.; Folda, A.; Massimino, M. L.; Bindoli, A.; Casini, A.; Rigobello, M. P., Fluorescent silver(I) and gold(I)-*N*-heterocyclic carbene complexes with cytotoxic properties: mechanistic insights. *Metallomics* **2013**, *5* (8), 1006-1015.

49. Ibrahim, H.; Gibard, C.; Hesling, C.; Guillot, R.; Morel, L.; Gautier, A.; Cisnetti, F., 'Auto-click' functionalization for diversified copper(I) and gold(I) NHCs. *Dalton Trans.* **2014**, *43* (19), 6981-6989.

50. Visbal, R.; Fernández-Moreira, V.; Marzo, I.; Laguna, A.; Gimeno, M. C., Cytotoxicity and biodistribution studies of luminescent Au(I) and Ag(I) *N*-heterocyclic carbenes. Searching for new biological targets. *Dalton Trans.* **2016**, *45* (38), 15026-15033.

51. Cucciolito, M. E.; Trinchillo, M.; Iannitti, R.; Palumbo, R.; Tesauro, D.; Tuzi, A.; Ruffo, F.; D'Amora, A., Sugar-Incorporated *N*-Heterocyclic-Carbene-Containing Gold(I) Complexes: Synthesis, Characterization, and Cytotoxic Evaluation. *Eur. J. Inorg. Chem.* **2017**, *2017* (42), 4955-4961.

52. Longevial, J.-F.; El Cheikh, K.; Aggad, D.; Lebrun, A.; van der Lee, A.; Tielens, F.; Clément, S.; Morère, A.; Garcia, M.; Gary-Bobo, M., Porphyrins Conjugated with Peripheral Thiolato Gold(I) Complexes for Enhanced Photodynamic Therapy. *Chem. Eur. J.* **2017**, *23* (56), 14017-14026.

53. Liu, W.; Bensdorf, K.; Proetto, M.; Hagenbach, A.; Abram, U.; Gust, R., Synthesis, characterization, and *in vitro* studies of bis [1,3-diethyl-4,5-diarylimidazol-2-ylidene] gold(I/III) complexes. *J. Med. Chem.* **2012**, *55* (8), 3713-3724.

54. Sivaram, H.; Tan, J.; Huynh, H. V., Cationic gold(I) heteroleptic complexes bearing a pyrazole-derived *N*-heterocyclic carbene: syntheses, characterizations, and cytotoxic activities. *Dalton Trans.* **2013**, *42* (34), 12421-12428.

55. Li, Y.; Liu, G.-F.; Tan, C.-P.; Ji, L.-N.; Mao, Z.-W., Antitumor properties and mechanisms

of mitochondria-targeted Ag(I) and Au(I) complexes containing *N*-heterocyclic carbenes derived from cyclophanes. *Metallomics* **2014**, *6* (8), 1460-1468.

56. Messori, L.; Marchetti, L.; Massai, L.; Scaletti, F.; Guerri, A.; Landini, I.; Nobili, S.; Perrone, G.; Mini, E.; Leoni, P., Chemistry and biology of two novel gold(I) carbene complexes as prospective anticancer agents. *Inorg. Chem.* **2014**, *53* (5), 2396-2403.

57. Boselli, L.; Ader, I.; Carraz, M.; Hemmert, C.; Cuvillier, O.; Gornitzka, H., Synthesis, structures, and selective toxicity to cancer cells of gold(I) complexes involving *N*-heterocyclic carbene ligands. *Eur. J. Med. Chem.* **2014**, *85*, 87-94.

58. Serebryanskaya, T.; Zolotarev, A.; Ott, I., A novel aminotriazole-based NHC complex for the design of gold(I) anti-cancer agents: synthesis and biological evaluation. *MedChemComm* **2015**, *6* (6), 1186-1189.

59. Nandy, A.; Samanta, T.; Mallick, S.; Mitra, P.; Seth, S. K.; Saha, K. D.; Al-Deyab, S. S.; Dinda, J., Synthesis of gold(III)←gold(I)-NHC through disproportionation: the role of gold(I)-NHC in the induction of apoptosis in HepG-2 cells. *New J. Chem.* **2016**, *40* (7), 6289-6298.

60. Arambula, J. F.; McCall, R.; Sidoran, K.; Magda, D.; Mitchell, N.; Bielawski, C. W.; Lynch, V. M.; Sessler, J. L.; Arumugam, K., Targeting antioxidant pathways with ferrocenylated *N*-heterocyclic carbene supported gold(I) complexes in A549 lung cancer cells. *Chem. Sci.* **2016**, *7* (2), 1245-1256.

61. Bertrand, B.; Stefan, L.; Pirrotta, M.; Monchaud, D.; Bodio, E.; Richard, P.; Le Gendre, P.; Warmerdam, E.; de Jager, M. H.; Groothuis, G. M., Caffeine-based gold(I) *N*-heterocyclic carbenes as possible anticancer agents: synthesis and biological properties. *Inorg. Chem.* **2014**, *53* (4), 2296-2303.

62. Papi, F.; Bazzicalupi, C.; Ferraroni, M.; Massai, L.; Bertrand, B.; Gratteri, P.; Colangelo, D.; Messori, L., The $[Au(9\text{-methylcaffein-8-ylidene})_2]^+$/DNA Tel23 System: Solution, Computational and Biological Studies. *Chem. Eur. J.* **2017**, *23* (55), 13784-13791.

63. Schmidt, C.; Karge, B.; Misgeld, R.; Prokop, A.; Brönstrup, M.; Ott, I., Biscarbene gold(I) complexes: structure-activity-relationships regarding antibacterial effects, cytotoxicity, TrxR inhibition and cellular bioavailability. *MedChemComm* **2017**, *8* (8), 1681-1689.

64. McCall, R.; Miles, M.; Lascuna, P.; Burney, B.; Patel, Z.; Sidoran, K.; Sittaramane, V.; Kocerha, J.; Grossie, D.; Sessler, J., Dual targeting of the cancer antioxidant network with 1,4-naphthoquinone fused Gold(I) *N*-heterocyclic carbene complexes. *Chem. Sci.* **2017**, *8* (9), 5918-5929.

65. Barnard, P. J.; Wedlock, L. E.; Baker, M. V.; Berners‐Price, S. J.; Joyce, D. A.; Skelton, B. W.; Steer, J. H., Luminescence Studies of the Intracellular Distribution of a Dinuclear Gold(I) *N*-Heterocyclic Carbene Complex. *Angew. Chem. Int. Ed.* **2006**, *45* (36), 5966-5970.

66. Boselli, L.; Carraz, M. l.; Mazères, S.; Paloque, L.; Gonzalez, G.; Benoit-Vical, F.; Valentin, A.; Hemmert, C.; Gornitzka, H., Synthesis, Structures, and Biological Studies of Heterobimetallic Au(I)–Ru(II) Complexes Involving *N*-Heterocyclic Carbene-Based Multidentate Ligands. *Organometallics* **2015**, *34* (6), 1046-1055.

67. Zou, T., A binuclear gold(I) complex with mixed bridging diphosphine and bis(*N*-heterocyclic carbene) ligands shows favorable thiol reactivity and effectively inhibits tumor growth and angiogenesis *in vivo*. In *Anti-Cancer N-Heterocyclic Carbene Complexes of Gold(III), Gold(I) and Platinum(II)*, Springer: 2016; pp 101-134.

68. Muenzner, J. K.; Biersack, B.; Kalie, H.; Andronache, I. C.; Kaps, L.; Schuppan, D.; Sasse, F.; Schobert, R., Gold(I) Biscarbene Complexes Derived from Vascular-Disrupting Combretastatin A-4 Address Different Targets and Show Antimetastatic Potential. *ChemMedChem* **2014**, *9* (6), 1195-1204.

69. Nandy, A.; Dey, S. K.; Das, S.; Munda, R. N.; Dinda, J.; Saha, K. D., Gold(I) *N*-heterocyclic carbene complex inhibits mouse melanoma growth by p53 upregulation. *Mol. Cancer Res.* **2014**, *13* (1), 57-70.

70. Walther, W.; Dadac, O.; Beirnec, C.; Ott, I.; Sanchez-Sanz, G.; Schmidt, C.; Werner, C.; Zhu, X.; Tacke, M., *In vitro* and *in vivo* investigations into the carbene gold chloride and thioglucoside anticancer drug candidates NHC-AuCl and NHC-AuSR. *Lett. Drug Des. Discov.* **2017**, *14* (2), 125-134.

71. Moan, J.; Peng, Q., An outline of the hundred-year history of PDT. *Anticancer Res.* **2003**, *23* (5A), 3591-3600.

72. Dolmans, D. E.; Fukumura, D.; Jain, R. K., Photodynamic therapy for cancer. *Nat. Rev. Cancer* **2003**, *3* (5), 380-387.

73. Agostinis, P.; Berg, K.; Cengel, K. A.; Foster, T. H.; Girotti, A. W.; Gollnick, S. O.; Hahn, S. M.; Hamblin, M. R.; Juzeniene, A.; Kessel, D., Photodynamic therapy of cancer: an update. *CA Cancer J. Clin.* **2011**, *61* (4), 250-281.

74. Yoon, I.; Li, J. Z.; Shim, Y. K., Advance in photosensitizers and light delivery for photodynamic therapy. *Clin. Endosc.* **2013**, *46* (1), 7-23.

75. de Visscher, S. A.; Dijkstra, P. U.; Tan, I. B.; Roodenburg, J. L.; Witjes, M. J., mTHPC mediated photodynamic therapy (PDT) of squamous cell carcinoma in the head and neck: a systematic review. *Oral Oncol.* **2013**, *49* (3), 192-210.

76. Azzouzi, A. R.; Barret, E.; Moore, C. M.; Villers, A.; Allen, C.; Scherz, A.; Muir, G.; de Wildt, M.; Barber, N. J.; Lebdai, S.; Emberton, M., TOOKAD® Soluble vascular-targeted photodynamic (VTP) therapy: determination of optimal treatment conditions and assessment of effects in patients with localised prostate cancer. *BJU Int.* **2013**, *112* (6), 766-74.

77. Jocham, D.; Witjes, F.; Wagner, S.; Zeylemaker, B.; Van Moorselaar, J.; Grimm, M.-o.; Muschter, R.; Popken, G.; König, F.; Knüchel, R., Improved detection and treatment of bladder cancer using hexaminolevulinate imaging: a prospective, phase III multicenter study. *J. Urol.* **2005**, *174* (3), 862-866.

78. D'hallewin, M.-A.; De Witte, P. A.; Waelkens, E.; Merlevede, W.; Baert, L., Fluorescence detection of flat bladder carcinoma in situ after intravesical instillation of hypericin. *J. Urol.* **2000**, *164* (2), 349-351.

79. (a) Mari, C.; Pierroz, V.; Ferrari, S.; Gasser, G., Combination of Ru(II) complexes and light: new frontiers in cancer therapy. *Chem. Sci.* **2015**, *6* (5), 2660-2686; (b) Bolze, F.; Jenni, S.; Sour, A.; Heitz, V., Molecular photosensitisers for two-photon photodynamic therapy. *Chem. Commun.* **2017**, *53* (96), 12857-12877.

80. Stephenson, M.; Reichardt, C.; Pinto, M.; Wächtler, M.; Sainuddin, T.; Shi, G.; Yin, H.; Monro, S.; Sampson, E.; Dietzek, B., Ru(II) Dyads Derived from 2-(1-Pyrenyl)-1*H*-imidazo[4,5-f][1,10]phenanthroline: Versatile Photosensitizers for Photodynamic Applications. *J. Phys. Chem. A* **2014**, *118* (45), 10507-10521.

81. Frei, A.; Rubbiani, R.; Tubafard, S.; Blacque, O.; Anstaett, P.; Felgenträger, A.; Maisch, T.; Spiccia, L.; Gasser, G., Synthesis, characterization, and biological evaluation of new Ru(II)

polypyridyl photosensitizers for photodynamic therapy. *J. Med. Chem.* **2014**, *57* (17), 7280-7292.

82. Liu, J.; Chen, Y.; Li, G.; Zhang, P.; Jin, C.; Zeng, L.; Ji, L.; Chao, H., Ruthenium(II) polypyridyl complexes as mitochondria-targeted two-photon photodynamic anticancer agents. *Biomaterials* **2015**, *56*, 140-153.

83. He, L.; Li, Y.; Tan, C.-P.; Ye, R.-R.; Chen, M.-H.; Cao, J.-J.; Ji, L.-N.; Mao, Z.-W., Cyclometalated iridium(III) complexes as lysosome-targeted photodynamic anticancer and real-time tracking agents. *Chem. Sci.* **2015**, *6* (10), 5409-5418.

84. Zheng, Y.; He, L.; Zhang, D.-Y.; Tan, C.-P.; Ji, L.-N.; Mao, Z.-W., Mixed-ligand iridium(III) complexes as photodynamic anticancer agents. *Dalton Trans.* **2017**, *46* (34), 11395-11407.

85. Lv, W.; Zhang, Z.; Zhang, K. Y.; Yang, H.; Liu, S.; Xu, A.; Guo, S.; Zhao, Q.; Huang, W., A Mitochondria-Targeted Photosensitizer Showing Improved Photodynamic Therapy Effects Under Hypoxia. *Angew. Chem. Int. Ed.* **2016**, *55* (34), 9947-9951.

86. Nam, J. S.; Kang, M.-G.; Kang, J.; Park, S.-Y.; Lee, S. J. C.; Kim, H.-T.; Seo, J. K.; Kwon, O.-H.; Lim, M. H.; Rhee, H.-W., Endoplasmic Reticulum-localized iridium(III) complexes as efficient photodynamic therapy agents via protein modifications. *J. Am. Chem. Soc.* **2016**, *138* (34), 10968-10977.

87. Liu, J.; Jin, C.; Yuan, B.; Liu, X.; Chen, Y.; Ji, L.; Chao, H., Selectively lighting up two-photon photodynamic activity in mitochondria with AIE-active iridium(III) complexes. *Chem. Commun.* **2017**, *53* (12), 2052-2055.

88. Liu, J.; Jin, C.; Yuan, B.; Chen, Y.; Liu, X.; Ji, L.; Chao, H., Enhanced cancer therapy by the marriage of metabolic alteration and mitochondrial-targeted photodynamic therapy using cyclometalated Ir(III) complexes. *Chem. Commun.* **2017**, *53* (71), 9878-9881.

89. McKenzie, L. K.; Sazanovich, I. V.; Baggaley, E.; Bonneau, M.; Guerchais, V.; Williams, J.; Weinstein, J. A.; Bryant, H. E., Metal Complexes for Two-Photon Photodynamic Therapy: A Cyclometallated Iridium Complex Induces Two-Photon Photosensitization of Cancer Cells under Near-IR Light. *Chem. Eur. J.* **2017**, *23* (2), 234-238.

90. Tian, X.; Zhu, Y.; Zhang, M.; Luo, L.; Wu, J.; Zhou, H.; Guan, L.; Battaglia, G.; Tian, Y., Localization matters: a nuclear targeting two-photon absorption iridium complex in photodynamic therapy. *Chem. Commun.* **2017**, *53* (23), 3303-3306.

91. Palao, E.; Sola-Llano, R.; Tabero, A.; Manzano, H.; Agarrabeitia, A. R.; Villanueva, A.; Lopez-Arbeloa, I.; Martinez-Martinez, V.; Ortiz, M. J., Acetylacetonate BODIPY-Biscyclometalated Iridium(III) Complexes: Effective Strategy towards Smarter Fluorescent Photosensitizer Agents. *Chem. Eur. J.* **2017**, *23* (42), 10139-10147.

92. Pracharova, J.; Vigueras, G.; Novohradsky, V.; Cutillas, N.; Janiak, C.; Kostrhunova, H.; Kasparkova, J.; Ruiz, J.; Brabec, V., Exploring the Effect of the Polypyridyl Ligands on Anticancer Activity of Phosphorescent Iridium(III) Complexes: From Proteosynthesis Inhibitors to Photodynamic Therapy Agents. *Chem. Eur. J.* **2018**, *24* (18), 4607-4619.

93. Mosmann, T., Rapid colorimetric assay for cellular growth and survival: application to proliferation and cytotoxicity assays. *J. Immunol. Methods* **1983**, *65* (1-2), 55-63.

94. Rangwala, F.; Williams, K. P.; Smith, G. R.; Thomas, Z.; Allensworth, J. L.; Lyerly, H. K.; Diehl, A. M.; Morse, M. A.; Devi, G. R., Differential effects of arsenic trioxide on chemosensitization in human hepatic tumor and stellate cell lines. *BMC cancer* **2012**, *12* (1),

402-412.
95. Albert, A., The Physico-Chemical Basis of Therapy: Selective Toxicity. *Chapman and Hall, London* **1979**.
96. Zhang, C.; Hemmert, C.; Gornitzka, H.; Cuvillier, O.; Zhang, M.; Sun, R. W. Y., Cationic and Neutral *N*-Heterocyclic Carbene Gold(I) Complexes: Cytotoxicity, NCI-60 Screening, Cellular Uptake, Inhibition of Mammalian Thioredoxin Reductase, and Reactive Oxygen Species Formation. *ChemMedChem* **2018**, *13*, 1-13.
97. Lin, J. C. Y.; Huang, R. T. W.; Lee, C. S.; Bhattacharyya, A.; Hwang, W. S.; Lin, I. J. B., Coinage Metal-*N*-Heterocyclic Carbene Complexes. *Chem. Rev.* **2009**, *109* (8), 3561-3598.
98. Schmidbaur, H., Ludwig Mond Lecture. High-carat gold compounds. *Chem. Soc. Rev.* **1995**, *24* (6), 391-400.
99. Franken, N. A.; Rodermond, H. M.; Stap, J.; Haveman, J.; Van Bree, C., Clonogenic assay of cells *in vitro*. *Nat. Protoc.* **2006**, *1* (5), 2315-2319.
100. McKeage, M. J.; Berners-Price, S. J.; Galettis, P.; Bowen, R. J.; Brouwer, W.; Ding, L.; Zhuang, L.; Baguley, B. C., Role of lipophilicity in determining cellular uptake and antitumour activity of gold phosphine complexes. *Cancer Chemother. Pharmacol.* **2000**, *46* (5), 343-350.
101. (a) Ott, I., On the medicinal chemistry of gold complexes as anticancer drugs. *Coord. Chem. Rev.* **2009**, *253* (11-12), 1670-1681; (b) Rubbiani, R.; Kitanovic, I.; Alborzinia, H.; Can, S.; Kitanovic, A.; Onambele, L. A.; Stefanopoulou, M.; Geldmacher, Y.; Sheldrick, W. S.; Wolber, G., Benzimidazol-2-ylidene gold(I) complexes are thioredoxin reductase inhibitors with multiple antitumor properties. *J. Med. Chem.* **2010**, *53* (24), 8608-8618.
102. Holmgren, A.; Lu, J., Thioredoxin and thioredoxin reductase: current research with special reference to human disease. *Biochem. Biophys. Res. Commun.* **2010**, *396* (1), 120-124.
103. Pratesi, A.; Gabbiani, C.; Ginanneschi, M.; Messori, L., Reactions of medicinally relevant gold compounds with the C-terminal motif of thioredoxin reductase elucidated by MS analysis. *Chem. Commun.* **2010**, *46* (37), 7001-7003.
104. (a) Rana, B. K.; Nandy, A.; Bertolasi, V.; Bielawski, C. W.; Das Saha, K.; Dinda, J., Novel Gold(I)- and Gold(III)-*N*-Heterocyclic Carbene Complexes: Synthesis and Evaluation of Their Anticancer Properties. *Organometallics* **2014**, *33* (10), 2544-2548; (b) Dinda, J.; Nandy, A.; Rana, B. K.; Bertolasi, V.; Saha, K. D.; Bielawski, C. W., Cytotoxicity of silver(I), gold(I) and gold(III) complexes of a pyridine wingtip substituted annelated *N*-heterocyclic carbene. *RSC Adv.* **2014**, *4* (105), 60776-60784.
105. Kumar, D.; Yusuf, M. A.; Singh, P.; Sardar, M.; Sarin, N. B.; Biosciences, J. M. I., Histochemical detection of superoxide and H_2O_2 accumulation in Brassica juncea seedlings. *Bio-protocol* **2014**, *4* (8), 1108-1112.
106. Rastogi, R. P.; Singh, S. P.; Häder, D.-P.; Sinha, R. P., Detection of reactive oxygen species (ROS) by the oxidant-sensing probe 2',7'-dichlorodihydrofluorescein diacetate in the cyanobacterium Anabaena variabilis PCC 7937. *Biochem. Biophys. Res. Commun.* **2010**, *397* (3), 603-607.
107. Paloque, L.; Verhaeghe, P.; Casanova, M.; Castera-Ducros, C.; Dumètre, A.; Mbatchi, L.; Hutter, S.; Kraiem-M'Rabet, M.; Laget, M.; Remusat, V., Discovery of a new antileishmanial hit in 8-nitroquinoline series. *Eur. J. Med. Chem.* **2012**, *54*, 75-86.
108. World Health Organization. http://whqlibdoc.who.int/trs/WHO_TRS_949_eng.pfd.

109. Laboratory Identification of Parastic Diseases of Public Healthe Concer http://www.dpd/cdc/gov/dpdx.
110. Singh, K.; Garg, G.; Ali, V., Current therapeutics, their problems and thiol metabolism as potential drug targets in leishmaniasis. *Curr. Drug Metab.* **2016**, *17* (9), 897-919.
111. (a) A Reynolds, K.; A Loughlin, W.; J Young, D., Quinolines as chemotherapeutic agents for leishmaniasis. *Mini-Rev. Med. Chem.* **2013**, *13* (5), 730-743; (b) Sundar, S.; Chakravarty, J., Investigational drugs for visceral leishmaniasis. *Expert Opin. Investig. Drugs* **2015**, *24* (1), 43-59.
112. (a) Evans, K. J.; Kedzierski, L., Development of vaccines against visceral leishmaniasis. *J. Trop. Med.* **2012**, *2012*, 892817-892830; (b) Palatnik-de-Sousa, C. B., Vaccines for canine leishmaniasis. *Front. Immunol.* **2012**, *3*, 69-83.
113. (a) Paloque, L.; Hemmert, C.; Valentin, A.; Gornitzka, H., Synthesis, characterization, and antileishmanial activities of gold(I) complexes involving quinoline functionalized *N*-heterocyclic carbenes. *Eur. J. Med. Chem.* **2015**, *94*, 22-29; (b) Zhang, C.; Delmas, S. B.; Álvarez, Á. F.; Valentin, A.; Hemmert, C.; Gornitzka, H., Synthesis, characterization, and antileishmanial activity of neutral *N*-heterocyclic carbenes gold(I) complexes. *Eur. J. Med. Chem.* **2018**, *143*, 1635-1643.
114. Li, Y.; Tan, C.-P.; Zhang, W.; He, L.; Ji, L.-N.; Mao, Z.-W., Phosphorescent iridium(III)-bis-*N*-heterocyclic carbene complexes as mitochondria-targeted theranostic and photodynamic anticancer agents. *Biomaterials* **2015**, *39*, 95-104.
115. Li, Y.; Liu, B.; Lu, X.-R.; Li, M.-F.; Ji, L.-N.; Mao, Z.-W., Cyclometalated iridium(III) *N*-heterocyclic carbene complexes as potential mitochondrial anticancer and photodynamic agents. *Dalton Trans.* **2017**, *46* (34), 11363-11371.
116. Diez-Barra, E.; De la Hoz, A.; Sanchez-Migallon, A.; Tejeda, J., Phase-Transfer Catalysis without Solvent. Synthesis of Bisazolylalkanes. *ChemInform* **1992**, *23* (46), 1365-1373.
117. King, K.; Watts, R., Dual emission from an ortho-metalated iridium (III) complex. *J. Am. Chem. Soc.* **1987**, *109* (5), 1589-1590.
118. Yvonne, G.; Isolda, R. C.; Tiziano, M.; J., S. P.; Luigi, M.; Nils, M. N., Synthesis and Mode of Action Studies on Iridium(I)-NHC Anticancer Drug Candidates. *Eur. J. Inorg. Chem.* **2018**, *2018* (20-21), 2461-2470.
119. (a) Monti, F.; Kessler, F.; Delgado, M.; Frey, J.; Bazzanini, F.; Accorsi, G.; Armaroli, N.; Bolink, H. J.; Ort ́ E.; Scopelliti, R., Charged bis-cyclometalated iridium(III) complexes with carbene-based ancillary ligands. *Inorg. Chem.* **2013**, *52* (18), 10292-10305; (b) Yang, C.-H.; Beltran, J.; Lemaur, V.; Cornil, J.; Hartmann, D.; Sarfert, W.; Fröhlich, R.; Bizzarri, C.; De Cola, L., Iridium metal complexes containing *N*-heterocyclic carbene ligands for blue-light-emitting electrochemical cells. *Inorg. Chem.* **2010**, *49* (21), 9891-9901.
120. Drobnik, J.; Yeargers, E., On the use of quinine sulfate as a fluorescence standard. *J. Mol. Spectrosc.* **1966**, *19* (1-4), 454-455.
121. Gao, R.; Ho, D. G.; Hernandez, B.; Selke, M.; Murphy, D.; Djurovich, P. I.; Thompson, M. E., Bis-cyclometalated Ir(III) complexes as efficient singlet oxygen sensitizers. *J. Am. Chem. Soc.* **2002**, *124* (50), 14828-14829.
122. Ethirajan, M.; Chen, Y.; Joshi, P.; Pandey, R. K., The role of porphyrin chemistry in tumor imaging and photodynamic therapy. *Chem. Soc. Rev.* **2011**, *40* (1), 340-362.
123. Sheldrick, G. M., Phase annealing in SHELX-90: direct methods for larger structures.

Acta Crystallogr. Sect. A **1990**, *46* (6), 467-473.

124. Sheldrick, G. M., Crystal structure refinement with SHELXL. *Acta Crystallogr. Sect. C* **2015**, *71* (1), 3-8.

125. Parsons, S.; Flack, H. D.; Wagner, T., Use of intensity quotients and differences in absolute structure refinement. *Acta Crystallogr. Sect. B* **2013**, *69* (3), 249-259.

126. Crosby, G. A.; Demas, J. N., Measurement of photoluminescence quantum yields. Review. *J. Phys. Chem.* **1971**, *75* (8), 991-1024.

127. Cuvillier, O.; Nava, V.; Murthy, S.; Edsall, L.; Levade, T.; Milstien, S.; Spiegel, S., Sphingosine generation, cytochrome c release, and activation of caspase-7 in doxorubicin-induced apoptosis of MCF7 breast adenocarcinoma cells. *Cell Death Differ.* **2001**, *8* (2), 162-171.

128. Zou, T.; Lum, C. T.; Chui, S. S. Y.; Che, C. M., Gold(III) Complexes Containing *N*-Heterocyclic Carbene Ligands: Thiol "Switch-on" Fluorescent Probes and Anti-Cancer Agents. *Angew. Chem. Int. Ed.* **2013**, *52* (10), 2930-2933.

129. Zhao, Z.; Gao, P.; You, Y.; Chen, T., Cancer-Targeting Functionalization of Selenium-Containing Ruthenium Conjugate with Tumor Microenvironment-Responsive Property to Enhance Theranostic Effects. *Chem. Eur. J.* **2018**, *24* (13), 3289-3298.

130. Tabrizi, L.; Chiniforoshan, H., The cytotoxicity and mechanism of action of new multinuclear Scaffold Au^{III}, Pd^{II} pincer complexes containing a bis(diphenylphosphino) ferrocene/non-ferrocene ligand. *Dalton Trans.* **2017**, *46* (41), 14164-14173.

131. Quental, L.; Raposinho, P.; Mendes, F.; Santos, I.; Navarro-Ranninger, C.; Alvarez-Valdes, A.; Huang, H.; Chao, H.; Rubbiani, R.; Gasser, G., Combining imaging and anticancer properties with new heterobimetallic Pt(II)/M(I) (M = Re, ^{99m}Tc) complexes. *Dalton Trans.* **2017**, *46* (42), 14523-14536.